https://ntrs.nasa.gov/search.jsp?R=19820016894 2020-03-21T09:05:29+00:00Z

General Disclaimer

One or more of the Following Statements may affect this Document

- This document has been reproduced from the best copy furnished by the organizational source. It is being released in the interest of making available as much information as possible.

- This document may contain data, which exceeds the sheet parameters. It was furnished in this condition by the organizational source and is the best copy available.

- This document may contain tone-on-tone or color graphs, charts and/or pictures, which have been reproduced in black and white.

- This document is paginated as submitted by the original source.

- Portions of this document are not fully legible due to the historical nature of some of the material. However, it is the best reproduction available from the original submission.

Produced by the NASA Center for Aerospace Information (CASI)

UNIVERSITY OF ILLINOIS
URBANA

AERONOMY REPORT NO. 100

INVESTIGATION OF THE WINDS AND ELECTRON CONCENTRATION VARIABILITY IN THE D REGION OF THE IONOSPHERE BY THE PARTIAL-REFLECTION RADAR TECHNIQUE

by
R. M. Weiland
S. A. Bowhill

December 1, 1981

MAY 1982
RECEIVED
NASA STI FACILITY
ACCESS DEPT.

Library of Congress ISSN 0568-0581

(NASA-CR-168943) INVESTIGATION OF THE WINDS AND ELECTRON CONCENTRATION VARIABILITY IN THE D REGION OF THE IONOSPHERE BY THE PARTIAL-REFLECTION RADAR TECHNIQUE (Illinois Univ.) 237 p HC A11/MF A01 N82-24770
Unclas
G3/46 21407

Aeronomy Laboratory
Department of Electrical Engineering
University of Illinois
Urbana, Illinois

Supported by
National Aeronautics and Space Administration

UILU ENG-81 2506

AERONOMY REPORT

NO. 100

INVESTIGATION OF THE WINDS AND ELECTRON CONCENTRATION VARIABILITY IN THE D REGION OF THE IONOSPHERE BY THE PARTIAL-REFLECTION RADAR TECHNIQUE

by

R. M. Weiland
S. A. Bowhill

December 1, 1981

Supported by
National Aeronautics and
Space Administration
Grant NGR 14-005-181

Aeronomy Laboratory
Department of Electrical Engineering
University of Illinois
Urbana, Illinois

PRECEDING PAGE BLANK NOT FILMED

ABSTRACT

The development and first observations of the partial-reflection drifts experiment at Urbana, Illinois (40°N) are described. The winds data from the drifts experiment are compared with electron concentration data obtained by the differential-absorption technique to study the possible meteorological causes of the winter anomaly in the mesosphere at midlatitudes. Winds data obtained by the meteor-radar experiment at Urbana are also compared with electron concentration data measured at Urbana. A significant correlation is shown in both cases between southward winds and increasing electron concentration measured at the same location during winter.

The possibility of stratospheric/mesospheric coupling is investigated by comparing satellite-measured 0.4 mbar geopotential data with mesospheric electron concentration data. No significant coupling was observed.

The winds measured at Saskatoon, Saskatchewan (52°N) are compared with the electron concentrations measured at Urbana in an effort to establish a transport path from the auroral zone to Urbana. No constant fixed relationship is shown, but significant correlations are shown for short segments of the winter. A significant coherence is observed at discrete frequencies during segments of the winter.

TABLE OF CONTENTS

LIST OF TABLES

LIST OF FIGURES

1. INTRODUCTION

1.1 *The Winter Anomaly in the D Region*

The D region of the ionosphere extends from 60 to 90 km in altitude. The D region is the most complex, and least understood region of the ionosphere. The relatively high atmosphere pressure in the D region is responsible for the complexity of the ion chemistry. It is the only atmospheric region where both positive and negative ions are present in significant concentrations. Efficient three-body reactions may occur and large water cluster ions may form. Also, negative ions are present mainly in the lower D region because the relatively high neutral gas density allows rapid three-body attachment of electrons to molecular oxygen. Consequently, O_2^- ions are formed and these react with various minor neutral gases to form other negative ions. The positive ion reaction scheme in the D region, and therefore the electron loss processes are not yet understood.

The undisturbed daytime upper D region ionization is produced mainly by the photoionization of nitric oxide by solar Lyman-α radiation (STROBEL, 1971). Other sources of ionization include the solar X-radiation of major D-region constituents (O_2 and N_2), galactic cosmic radiation of constituents in the lower D region (60 to 70 km), and extreme ultraviolet radiation of metastable molecular oxygen $O_2(^1\Delta)$ (WHITTEN and POPPOFF, 1971). Also, precipitating energetic electrons may be a significant source of ionization in midlatitudes during geomagnetic storms. Because the ionization in the D region is formed mainly by solar radiation, it almost completely disappears at night. The solar zenith angle has a seasonal effect on the ionization, with slightly higher electron concentrations in the summer than in the winter months, due to the lower solar zenith angle. The dynamical processes in the D region are not well understood either, because of the difficulty in

making measurements in the region.

The day-to-day variation in electron concentration in the D region is much greater in the winter months than it is in the summer months. Enhancements in the electron concentration above 80 km cause an abnormally large absorption of high and medium frequency radio waves during particular days in the winter months. This phenomenon has been called the winter anomaly. Figure 1.1 shows rocket electron-density profiles comparing summer values with normal and anomalous winter electron densities (from SECHRIST et al. (1969)). The rocket data were obtained at midlatitudes (Wallops Island, Virginia) during 1965-1967. Profile number 2 is a normal winter profile and profile number 3 is a profile that was measured on a winter day of anomalous absorption. The electron concentrations are about four or five times higher on the anomalous day than on the normal winter day, throughout almost the entire D region.

The winter anomaly is probably the result of many causes, and the relative importance of each on a particular day is unknown. Enhancements can be due to an increase in the electron production rate or a decrease in the electorn loss rate. Both of these effects may occur as a result of horizontal or vertical transport of neutral constituents that are easily ionized, or because of a variation in the temperature in the region.

SECHRIST (1967) theorized that a temperature increase in the D region would cause an increase in the photochemical equilibrium concentration of NO, which would be ionized, increasing the electron concentration. GEISLER and DICKINSON (1968) demonstrated that NO is not in photochemical equilibrium in the D region due to an insufficient supply of atomic nitrogen. They concluded that NO is produced in the E region, and is transported downwards by the vertical movements accompanying planetary-scale waves. Vertical

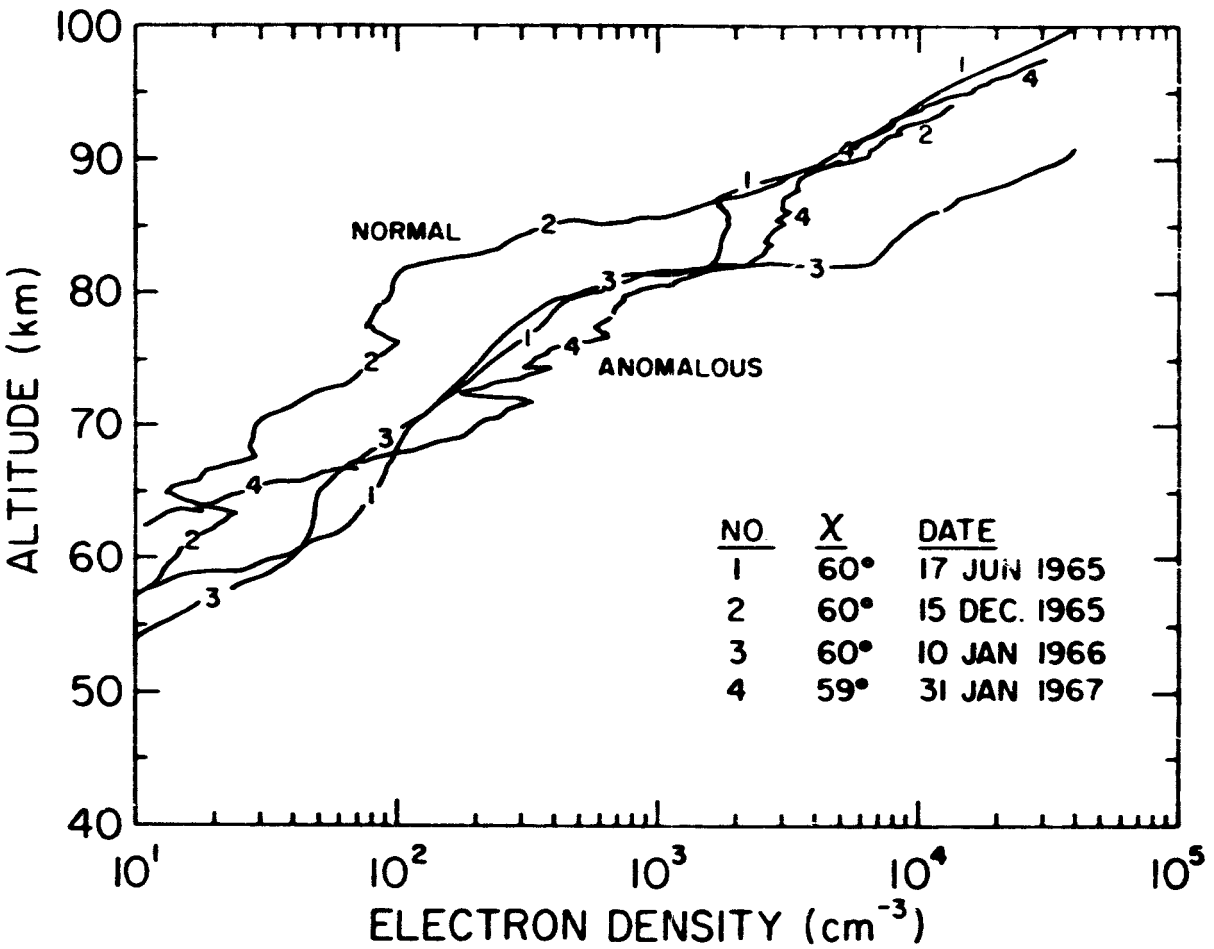

Figure 1.1 Rocket electron-density profiles comparing summer values with normal and anomalous winter electron densities (from SECHRIST et al., 1969).

transport of NO may also result from enhanced turbulent diffusion due to a basic state of temperature and wind that is less stable (ZIMMERMAN and NARCISI, 1970), or due to gravity wave instabilities (GELLER and SECHRIST, 1971). SECHRIST (1970) suggested that an increase in the upward transport of water vapor would alter the water cluster ion concentration, and thus the electron loss rate, resulting in a change in the electron concentration.

Another possible cause is the effect of precipitating energetic electrons originating in the radiation belts of the magnetosphere. It has been theorized that, following certain geomagnetic storms there is precipitation of energetic electrons into the midlatitude D region (MAEHLUM, 1967). This magnetic storm aftereffect may persist for several days or weeks.

MANSON (1971) suggested that during winter periods of enhanced equatorward flow, the increased transport of NO from the auroral zone would result in higher D region electron concentrations at midlatitudes. The concentration of NO in the auroral zone is enhanced by the dissociation of molecular nitrogen by precipitating energetic particles. The auroral zone at 90°W longitude extends from about 52° to 65°N latitude (VOSS and SMITH, 1977, Figure 7.16). The peak NO concentration in the auroral zone is two or three times the value at the equator in the E region (CRAVENS and STEWART, 1978).

Cravens and Stewart presented measurements of NO concentration made by the Atmosphere Explorer C satellite, at an altitude of 105 km. Figure 1.2a shows a map of NO concentration measured during August 1974. The NO concentration in the auroral zones is enhanced, and the effect of transport in the southern (winter) hemisphere is shown with a wider latitudinal distribution of NO concentration as compared with the northern (summer) hemisphere. Figure 1.2b shows a map of NO concentration in the northern hemisphere during mid-January through mid-February. The effect of horizontal transport

ORIGINAL PAGE
BLACK AND WHITE PHOTOGRAPH

(a)

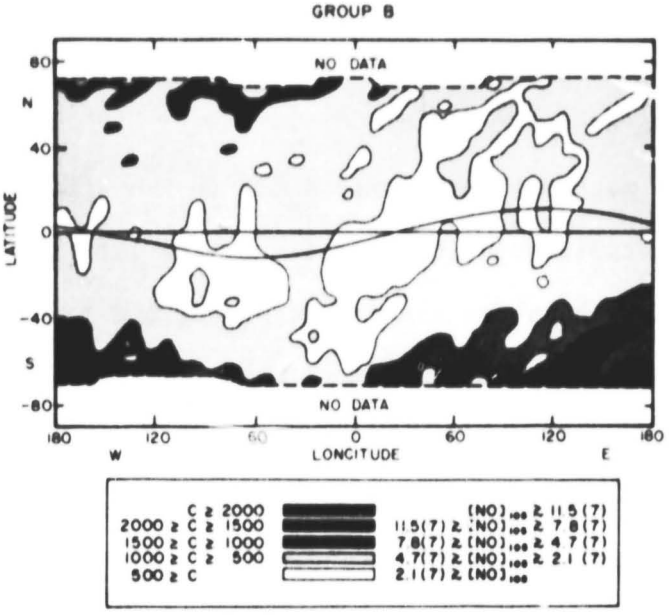

(b)

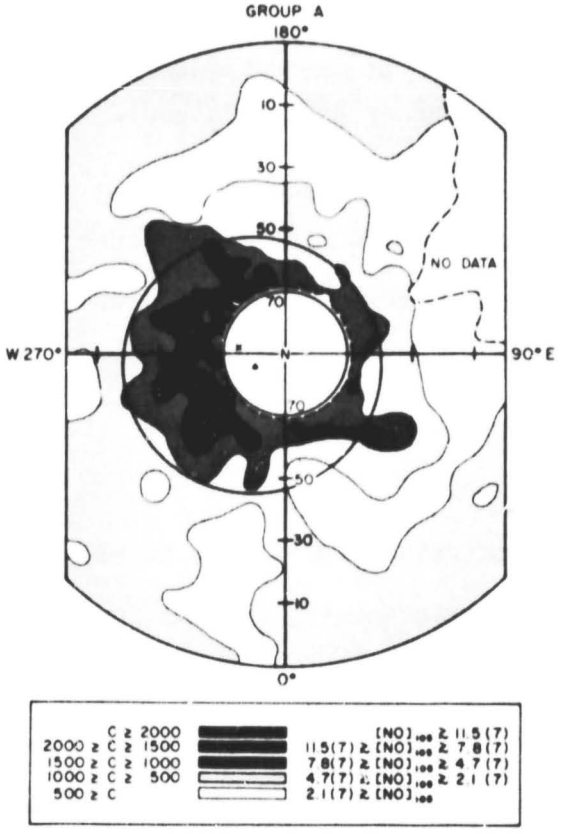

Figure 1.2 (a) Map of nitric oxide concentration measured during August 1974 (b) Map of nitric oxide during mid-January through mid-February 1974 (CRAVENS and STEWART, 1978).

during winter is shown in the distribution of NO that extends down to about 40°N at a longitude of 90°W.

The main loss mechanism of nitric oxide in the upper D region and lower E region is the photodissociation process, so the lifetime of nitric oxide is significantly longer in the winter because of the lower solar zenith angle. OGAWA and KONDO (1977) estimated that the lifetime of nitric oxide below about 105 km is about 10 hours during daytime, and about 1000 hours at night. The longer lifetime during winter will allow the longer transport of NO during winter. The region of peak auroral activity is about 2000 km north of Urbana. Thus a likely time scale for the transport of NO from the auroral zone to Urbana by winds of the order of 10 m/s would be about 2.3 days. A wind speed of the order of 10 m/s could be expected from planetary wave activity in the mesosphere during winter.

It is generally accepted that the major cause of the anomalously high electron concentrations is a result of the redistribution of minor constituents by the vertical and/or horizontal transport processes present during the winter in the mesosphere at midlatitudes.

1.2 *Experimental Techniques*

The D region is particularly difficult to obtain measurements from. It is too high for balloon measurements, and too low for effective satellite measurements. Rocket measurements can be made in the region, but because of the high cost and restrictions on locations where launches can be made, are not practical. The best alternative for the long-term study of the region is the use of ground-based radio-wave probing. Several radio-wave probing methods have been developed for the measurement of electron concentration. These include absorption measurements, the ionosonde experiment, the wave-interaction experiment, and the partial-reflection experiment.

The absorption experiment measures the absorption (loss) of a radio wave along an ionospheric path, and this can be done in several ways. One method is to transmit a pulse vertically, which is then nearly totally reflected by a layer in the E region. The absorption due to the D region can thus be determined.

The ionosonde experiment sweeps through a range of frequencies, transmitting a signal vertically. The height where total reflection occurs is measured, and this reflection height versus frequency data can be inverted to obtain an electron concentration profile.

The wave interaction experiment (FEJER, 1955) uses a high-power transmitter to heat the ionosphere. A second transmitter is used in probing the heated region. The heating causes a change in the electron-neutral collision frequency. The probing signal returns for the heated and nonheated are then used in calculating the electron concentration profile.

In the partial reflection differential-absorption experiment, ordinary and extraordinary mode signals are alternately transmitted vertically into the ionosphere. The modes are the characteristic modes which by definition propagate through the medium without a change in polarization, but experience a different attenuation. As the signals pass through the D region, irregularities cause the signals to be partially reflected. By measuring the ratio of the amplitudes of the two modal returns as a function of altitude, an electron-concentration profile can be calculated.

Ground-based radio-wave techniques for measuring winds in the mesosphere include incoherent scatter, meteor radar, and partial reflection drifts. In the incoherent scatter technique, the Doppler shift due to ions can be determined from the spectrum of received pulses, and up to an altitude of about 115 km the collision frequency is high enough that the ions

should travel with the neutral air (EVANS, 1969). One component of wind can be measured along the antenna pointing direction, and a steerable antenna is used for measurements of wind in two dimensions.

In the meteor radar technique, the velocity of the neutral air is measured by measuring the Doppler shift of radio-frequency signals scattered off of the ionized trails left by meteors in the upper atmosphere. The meteor radar technique is further described in Chapter 7.

Winds are calculated in the partial reflection drifts technique by vertically transmitting signals and correlating the fading patterns measured at three or more spaced receiving antennas. The drifts technique is fully described in Chapter 2.

1.3 *Unique Aspects of the Partial-Reflection System at Urbana*

The partial reflection system at Urbana has two large antenna arrays (see Chapter 2), with a separate large antenna array used in transmitting. The receiving array was modified to form four separate spaced antennas for making drifts measurements. Each quadrant consists of 12 half-wave antenna elements, providing a better antenna gain and greater directivity than other similar experiments. The separate high gain antenna array used in transmitting results in a high level transmitted signal, providing a good signal-to-noise ratio. The on-site computer provides full-correlation analysis in near real time. The availability of electron concentration data, and the location of the station at the low latitude cutoff of winter anomaly effects are also unique.

1.4 *Scope and Purpose of This Study*

In this work, the design of the partial reflection drifts system at Urbana will be described. The wind and electron concentration data obtained during three winter seasons (1978/1979, 1979/1980, and 1980/1981) will be

analyzed to test the theory that horizontal equatorward transport is a major cause of the winter anomaly at midlatitudes. Winds measured by the meteor-radar technique at Urbana will also be used in this test. Satellite stratospheric geopotential data will be compared with mecospheric data in Chapter 8 to obtain evidence of stratospheric/mesospheric coupling. In Chapter 9, winds measured at Saskatoon, Saskatchewan will be compared with Urbana data to establish evidence of transport from the auroral zone to Urbana, and to verify the existence of Rossby waves in the mesosphere.

2. THEORY OF THE PARTIAL-REFLECTION EXPERIMENT

The partial-reflection experiment for electron concentration and winds both rely on weak reflections from irregularities in the ionosphere. A pulse is transmitted vertically upward, and after a suitable time delay determined by the propagation characteristics of the medium, the amplitude of the ionospheric return is recorded versus time. Knowing the wave propagation speed through the medium (assumed to be the speed of light) the return signal amplitude versus altitude can be obtained. In the differential-absorption experiment the average return signal amplitude from two orthogonal circular polarization transmitted signals will be equated to obtain an electron concentration profile. In the drifts experiment return signal amplitude versus altitude profiles are obtained at four spaced receiving antennas. A time series which is a fading pattern at each antenna for several altitudes is formed. Time series from pairs of antennas are correlated to find the time shift in the fading patterns and hence the velocity of the ionospheric irregularities moving through the scattering region.

2.1 *Generalized Magnetoionic Theory*

In an ionized medium in the presence of a magnetic field the two characteristic modes (modes which propagate through the medium without changing polarization) are in general elliptical. If a characteristic mode signal is vertically transmitted it will propagate, be reflected, and return with the same polarization. The attenuation and phase change that occurs during the propagation of that wave can be predicted by magnetoionic theory.

The original partial-reflection experiment was performed by GARDNER and PAWSEY (1953) using the Appleton-Hartree formula (BUDDEN, 1961) for the refractive index of the medium. This theory assumed that the electron-neutral

collision frequency was proportional to the electron velocity. By laboratory experiments PHELPS and FACK (1959) established that the electron-neutral collision frequency of an electron in nitrogen gas is proportional to the square of its velocity. SEN and WYLLER (1960) derived the formula for the refractive index of the medium using a coordinate system with oblique axes, allowing for the harmonic time variation of the radio-wave fields with real factors of $\cos\omega t$ and $\sin\omega t$. BUDDEN (1965) derived the same formula using orthogonal axes and a complex time factor $e^{j\omega t}$, giving a simplified approach. The Sen-Wyller expression for the refractive index of the medium is shown in Appendix I.

When the Earth's magnetic field is nearly aligned with the radio wave normal, the expression for the refractive index can be greatly simplified. This is the quasi-longitudinal approximation, which is valid for small values of θ, which makes the expression from Appendix I:

$$\eta_{o,x} = \left[\frac{A \pm (-C^2 \cos^2\theta)^{\frac{1}{2}}}{D}\right]^{\frac{1}{2}} \tag{2.1}$$

or:

$$\eta_{o,x}^2 = 1 - \left[\frac{\omega_o^2(\omega \pm \omega_L)}{\omega\nu_m^2}\right]\mathfrak{C}_{3/2}\left(\frac{\omega \pm \omega_L}{\nu_m}\right)$$

$$- j\left(\frac{5\,\omega_o^2}{2\,\omega\nu_m}\right)\mathfrak{C}_{5/2}\left(\frac{\omega \pm \omega_L}{\nu_m}\right) \tag{2.2}$$

where: η = complex refractive index of the medium

ω = operating frequency

$\omega_L = \omega_H \cos\theta$

ω_H = angular gyro frequency $\equiv \frac{eB}{m}$

ω_o = plasma frequency $\equiv \frac{Ne^2}{m\,\epsilon_o}$

θ = angle between the wave normal and the Earth's magnetic field

ν_m = electron-neutral collision frequency.

The quasi-longitudinal approximation is valid for Urbana (PIRNAT and BOWHILL, 1968) and is used in the measurements of electron concentrations in this work.

2.2 *Differential-Absorption Theory*

The differential-absorption experiment is based on the fact that the two characteristic modes of propagation through the ionospheric medium (right-handed and left-handed circular polarizations, at this latitude) have different attenuations during propagation and reflection. The two-way absorption (up to the reflection point and back) is given by BUDDEN, 1961):

$$\exp\left(-2\int_o^h k_{o,x}\,dh\right) \tag{2.3}$$

where $k_{o,x}$ is the absorption coefficient defined as $(\frac{\omega}{C})x_{o,x}$, where $x_{o,x}$ is the imaginary part of the refractive index. The received amplitude on the ground after reflection is then given by:

$$A_{o,x} \propto R_{o,x} \exp\left(-2\int_o^h k_{o,x}\,dh\right) \tag{2.4}$$

where $R_{o,x}$ is the reflection coefficient. The ratio of the two return mode signals can be written as:

$$\frac{A_x}{A_o} = \frac{|R_x|}{|R_o|} \exp\left[-2\int_o^h (k_x - k_o)\,dh\right] \tag{2.5}$$

taking the logarithm of both sides gives the following:

$$\ln\left(\frac{A_x}{A_o}\right) = \ln\left(\frac{|R_x|}{|R_o|}\right) - 2\int_o^h (k_x - k_o)\,dh \tag{2.6}$$

If the A_x/A_o ratio is measured at two closely spaced altitudes h_1 and h_2, $k_{o,x}$ is approximately constant in that interval of altitude so that the

difference of the logarithms of the A_x/A_o ratio at two altitudes can be written as

$$\ln\left(\frac{A_x}{A_o}\right)\Big|_{h_2} - \ln\left(\frac{A_x}{A_o}\right)\Big|_{h_1} = \ln\left(\frac{R_x}{R_o}\right)\Big|_{h_2} - \ln\left(\frac{R_x}{R_o}\right)\Big|_{h_1} - 2(k_x - k_o)\Delta h \qquad (2.7)$$

where $\Delta h = h_2 - h_1$.

There are two theories on the type of reflection model that is responsible for the ionospheric reflections. The two models are the single reflector (Fresnel) model and the volume scattering model (FLOOD, 1968; COHEN, 1971; COHEN and FERRARO, 1973). There has been a good deal of discussion over which model is most appropriate (HOLT 1969; FLOOD, 1969). Studies of the statistical distribution of individual pulses reflected from the ionosphere have been made by many investigators. Scattering from a single reflector would result in a distribution with a Rician probability density. Scattering from a volume of scatterers would result in a distribution with a Rayleigh probability density. VON BIEL (1977) using this analysis found that the distributions were predominantly Rayleigh below 60 km, and Rician above 80 km. This would predict volume scattering below 80 km, and single reflector scattering above 80 km. MATHEWS et al. (1973) did a similar but more extensive analysis and found similar retuls. NEWMAN (1974) also did this analysis on his data and found similar results with the shift to the single reflector model above 85 km. FRASER and VINCENT (1970), and CHANDRA and VINCENT (1977), using a similar analysis concluded that the reflection mechanism throughout the D region was predominantly a single reflector. Further work by BELROSE (1970) lead him to conclude that in general, the reflection process was a combination of the two models, and that the altitudes where each model applied varied from day to day, by season, and with

changes in latitude. AUSTIN and MANSON (1969) concluded that the reflection process was a result of several reflectors distributed so that they did not fill a significant amount of the scattering volume (which was 3 km in altitude in their case). They also concluded that the error in calculated electron concentrations when assuming a single reflector model was only a few percent below about 84 km. WRATT (1974) computed the maximum error in computed electron concentrations when assuming a single reflector model for a pulse width of 25 μs, and found that for an average electron-concentration profile that the error would be less than 5 percent for the altitude range of 70 to 87.5 km. HOLT (1969) did a similar analysis also for a 25 μs pulse and found that the error would be less than 10 percent throughout the D region. In view of the uncertainty in the reflection process, the amount of extra computation involved in using a volume scattering model, and the small possible error in assuming a single reflector with our pulse width (23 μs), the single reflector model is used in this work.

The reflection model for a single reflector is given by

$$R = \frac{\eta_2 - \eta_1}{\eta_2 + \eta_1} \tag{2.8}$$

Since the reflections are weak, the gradient in index of refraction is small and $\eta_2 \cong \eta_1 \cong \eta \cong 1$ for both modes, so the reflection coefficient can be approximated as

$$R_{o,x} \cong \frac{\delta \eta_{o,x}}{2 \eta_{o,x}} \tag{2.9}$$

so that

$$\frac{R_x}{R_o} = \frac{\delta\eta_x \, \eta_o}{\eta_x \, \delta\eta_o} \tag{2.10}$$

By using the quasi-longitudinal approximation, the electron concentration can now be solved for explicitly. The value for the refractive index can be found by expanding equation 2.2 by the binomial theorem, and neglecting the small higher order terms. The real part is

$$\mu_{o,x} = \left[1 - \frac{\omega_o^2}{\omega\nu_m}\left(\frac{\omega \pm \omega_L}{\nu_m}\right)\text{ç}_{3/2}\left(\frac{\omega \pm \omega_L}{\nu_m}\right)\right]^{\frac{1}{2}} \tag{2.11}$$

and the imaginary part is

$$\chi_{o,x} = \frac{5}{4}\frac{\omega_o^2}{\omega\nu_m}\text{ç}_{5/2}\left(\frac{\omega \pm \omega_L}{\nu_m}\right) = \frac{5}{4}\frac{Ne^2}{m\epsilon_o\,\omega\nu_m}\text{ç}_{5/2}\left(\frac{\omega \pm \omega_L}{\nu_m}\right) \tag{2.12}$$

The real part can be expanded by the binomial theorem to yield

$$\mu_{o,x} = 1 - \frac{\omega_o^2}{2\omega\nu_m}\left(\frac{\omega \pm \omega_L}{\nu_m}\right)\text{ç}_{3/2}\left(\frac{\omega \pm \omega_L}{\nu_m}\right) \tag{2.13}$$

Assuming ν_m is constant across the discontinuity (BELROSE and BURKE, 1964), η^2 is a function of electron concentration, N alone. Differentiating equation (2.2) with respect to N yields

$$2\eta\frac{\delta\eta}{\delta N} = -\frac{e^2}{m\epsilon_o\,\omega\nu_m}\left[\left(\frac{\omega \pm \omega_L}{\nu_m}\right)\text{ç}_{3/2}\left(\frac{\omega \pm \omega_L}{\nu_m}\right) + j\frac{5}{2}\text{ç}_{5/2}\left(\frac{\omega \pm \omega_L}{\nu_m}\right)\right] \tag{2.14}$$

Assuming that $\eta_o \doteq \eta_x \doteq 1$ the magnitude of the ratio of reflection coefficients becomes

$$\frac{|R_x|}{|R_o|} = \frac{\left[\left(\frac{\omega - \omega_L}{\nu_m}\right)\text{ç}_{3/2}\left(\frac{\omega - \omega_L}{\nu_m}\right)\right]^2 + \left[\frac{5}{2}\text{ç}_{5/2}\left(\frac{\omega - \omega_L}{\nu_m}\right)\right]^2}{\left[\left(\frac{\omega + \omega_L}{\nu_m}\right)\text{ç}_{3/2}\left(\frac{\omega + \omega_L}{\nu_m}\right)\right]^2 + \left[\frac{5}{2}\text{ç}_{5/2}\left(\frac{\omega + \omega_L}{\nu_m}\right)\right]^2} \tag{2.15}$$

Substituting $k_{o,x} = \frac{\omega}{c}\chi_{o,x}$, with $\chi_{o,x}$ from equation (2.12) into equation (2.7) results in the expression for electron concentration.

$$N = \frac{\Delta \ln \frac{|R_x|}{|R_o|} - \Delta \ln \frac{A_x}{A_o}}{\frac{5\,\Delta h\, e^2}{2\, cm\, \epsilon_o\, \nu_m}\left[\mathcal{C}_{5/2}\left(\frac{\omega - \omega_L}{\nu_m}\right) - \mathcal{C}_{5/2}\left(\frac{\omega + \omega_L}{\nu_m}\right)\right]} \qquad (2.16)$$

The collision-frequency ν_m profile assumed is given in Appendix III, which includes seasonal variations. An electron-concentration profile can thus be calculated from the measured signal returns for two polarization modes.

2.3 *Drifts Experiment Theory*

When the ionosphere is illuminated from below by a single radio-wave point source, the resultant reflected energy from a given altitude will create a two-dimensional diffraction pattern on the ground. If the amplitude of the returned pattern is measured at a fixed point on the ground, variations in the signal strength, known as fading, will be observed. This phenomenon has been attributed to the turbulent horizontal movement of ionized irregularities (BRIGGS et al., 1950; FEDOR, 1967; WRIGHT, 1974). In the D region above 70 km the collision frequency is larger than the gyrofrequency for ions, but the collision frequency is smaller than the gyrofrequency for electrons. Therefore, the ions will move with the neutral air, but the electrons will be controlled by magnetic forces. However, ionized irregularities will move with the neutral air because they would become polarized, and are held together by space charge. The model has also been proposed (HINES and RAO, 1968; PFISTER, 1971) that the fading could be attributed to the superposition of atmospheric waves. It is possible that both processes could be operative in practice. The difference in models may also arise from the differing ionospheric conditions at the different locations.

Assuming a steady horizontal ionospheric drift with a superimposed random motion of the irregularities, the ground diffraction pattern would

also have a related steady velocity and would also have a random change as it moved. The fading recorded at two spaced receivers, separated in the direction of motion, would be similar but displaced in time, provided their separation distance was not excessive. The similarity between fading records would diminish and then vanish with increasing receiver separation. GOLLEY and ROSSITER (1970) investigated the receiver separation question and found that the drift velocity estimates diminished in magnitude with decreasing receiver separation. A receiver separation of about 160 meters was found to be optimum for D-region measurements. The receiving antenna separation for the Urbana drifts experiment is 169 meters for the shorter sides of the triangle forming the receiving array, and 240 meters for the hypotenuse side.

In order to estimate the time lag between fading patterns of a pair of antennas, and therefore the apparent velocity in that direction, it is necessary to statistically correlate the fading time series at the two antennas. A minimum of three spaced antennas are required to measure the horizontal wind in two dimensions.

The first method of analyzing drifts records, which was used before computers were available, was the method of similar fades (MITRA, 1949). In this method, the fading sequences at three antennas were recorded on film and examined for similar features. The time delays for the occurrence of these features was measured and knowing the antenna spacing, the drift velocity was directly calculated. In this analysis it is assumed that there is no random change in the pattern during the experiment, and that the amplitude contours are isotropic (the mean change in amplitude for the average of many irregularities is independent of the direction of travel of the irregularities). These assumptions do not often hold for individual pattern

maxima, but may hold when the average for many fades is used (SPRENGER and SCHMINDER, 1969).

The most widely accepted method of analysis of data from the three-antenna drifts experiment is the full correlation analysis (BRIGGS et al., 1950). In this analysis, the fading records at the three antennas are correlated. To use this method, care must be taken when collecting the data to avoid saturating the receiver which would alter the correlation functions. It is assumed that the ionosphere is in turbulent motion with small scale irregularities of equal statistical shape and orientation in a medium with a constant drift. The auto-correlation functions of the three fading records, and the cross-correlation functions of the fading records taken in pairs are calculated. The assumption is made that there is sufficient information in these correlation functions to describe a correlation surface of concentric ellipsoids in two space, and time coordinates. The object of the correlation analysis is to find the parameters of a particular ellipse and translate them to parameters that describe the drift and random motion of the ionosphere. These drift parameters are the velocity and direction of drift, the size, shape, and orientation of the characteristic ellipse (which represents an average pattern irregularity) and the quantity V_c which has the dimensions of velocity and is a measure of the random change in the pattern.

The arrangement of receiving antennas is shown in Figure 2.1. The degree of association between two fading series for a spatial antenna separation d and temporal separation τ can be expressed by the discrete cross-correlation function:

$$\rho(d,t) = \frac{\Sigma[A(x,t) - \bar{A}][A(x+d,\ t+\tau) - \bar{A}]}{\Sigma[A(x,t) - \bar{A}]^2} \qquad (2.17)$$

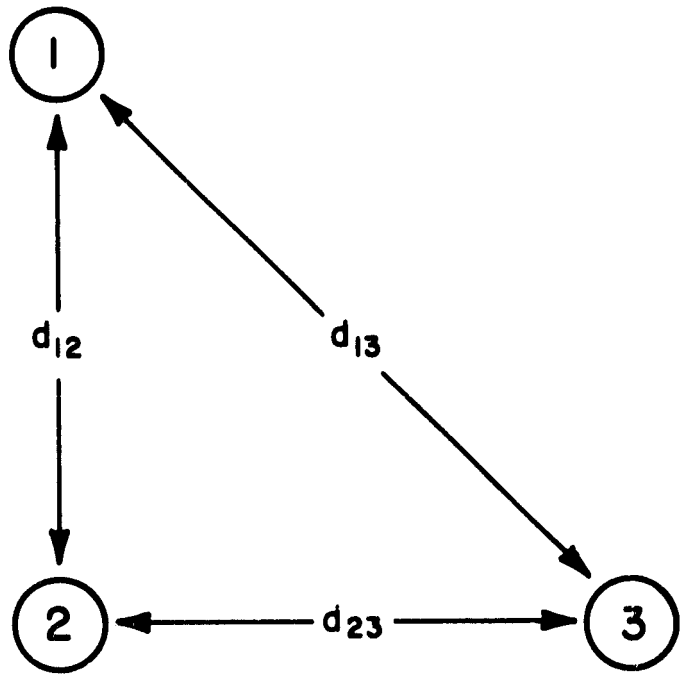

Figure 2.1 Arrangement of receiving antennas.

In practice $\rho(d,t)$ can only be approximated because of the finite observation period possible of a statistical process which should ideally be both infinite and stationary. The autocorrelation of the time series is calculated, and the three cross correlations of the fading records taken in pairs are calculated. The next step is to calculate the parameters of the characteristic ellipse.

The dynamics of the ground diffraction pattern can be described by four velocity-type parameters (BRIGGS et al., 1950):

(1) Fading velocity V'_c: This is a measure of the space shift to time shift needed to produce, on average, the same change in the value of the pattern amplitude, A.

$$V'_c = \frac{x_o}{t_o}, \quad \text{where } \rho(x_o,0) = \rho(o,\ t_o) \tag{2.18}$$

Thus V'_c is the velocity of drift necessary to explain the fading in terms of the drifting pattern with no random changes.

(2) Drift (or true) velocity V: This is the velocity of an observer who has adjusted his motion to observe the slowest possible fading speed. If the observer compares amplitudes at time τ_1 apart, his displacement d_1 during this time must be adjusted until $\rho(d_1,\ \tau_1)$ maximizes, and then

$$V = \frac{d_1}{\tau_1} \tag{2.19}$$

(3) Characteristic velocity V_c: This parameter gives an estimate of the amount of random change taking place within the pattern. An observer moving at velocity V would observe this velocity of fading (V'_c). To this observer the ratio of space shift to time shift needed to produce a similar change in amplitude is;

$$V_c = \frac{x_o}{\tau_1} \tag{2.20}$$

where

$$\rho(x_o, o) = \rho(V\tau_1, \tau_1) = \rho(d_1, \tau_1) \tag{2.21}$$

(4) Apparent velocity V': For a spatial separation d_o of two points on a one-dimensional ground, τ_o is the time separation that maximizes $\rho(d_o, \tau_o)$.

$$V' = \frac{d_o}{\tau_o} \tag{2.22}$$

For a frozen pattern ($V_c = 0$) the apparent velocity V' is the same as V. With increasing V_c it can be seen that V' will be greater than V by an increasing amount.

Assuming that the contours of amplitude over a continuous line of points and with time are known, the amplitude contours would look something like Figure 2.2a (from BRIGGS et al., 1951). There is a tendency for the contours to be elongated along a line whose slope depends on the velocity at which the maxima and minima of the fading pattern A drift over the ground. If the origin of the x-axis is moved along with a velocity V, Figure 2.2b is obtained by an observer moving with velocity V, who experiences the minimum amount of fading. From the definition of the characteristic velocity, V_c, the ratio of the space shift to time shift which on average have an equal effect on A is V_c. Therefore by scaling the vertical axis of Figure 2.2b by the factor V_c, we get Figure 2.2c with equal average gradients in the contours along each axis. The average change (or expected correlation) between two points on this diagram depends only on their distance apart. A correlation surface corresponding to this surface would have contours in the form of circles centered at the origin.

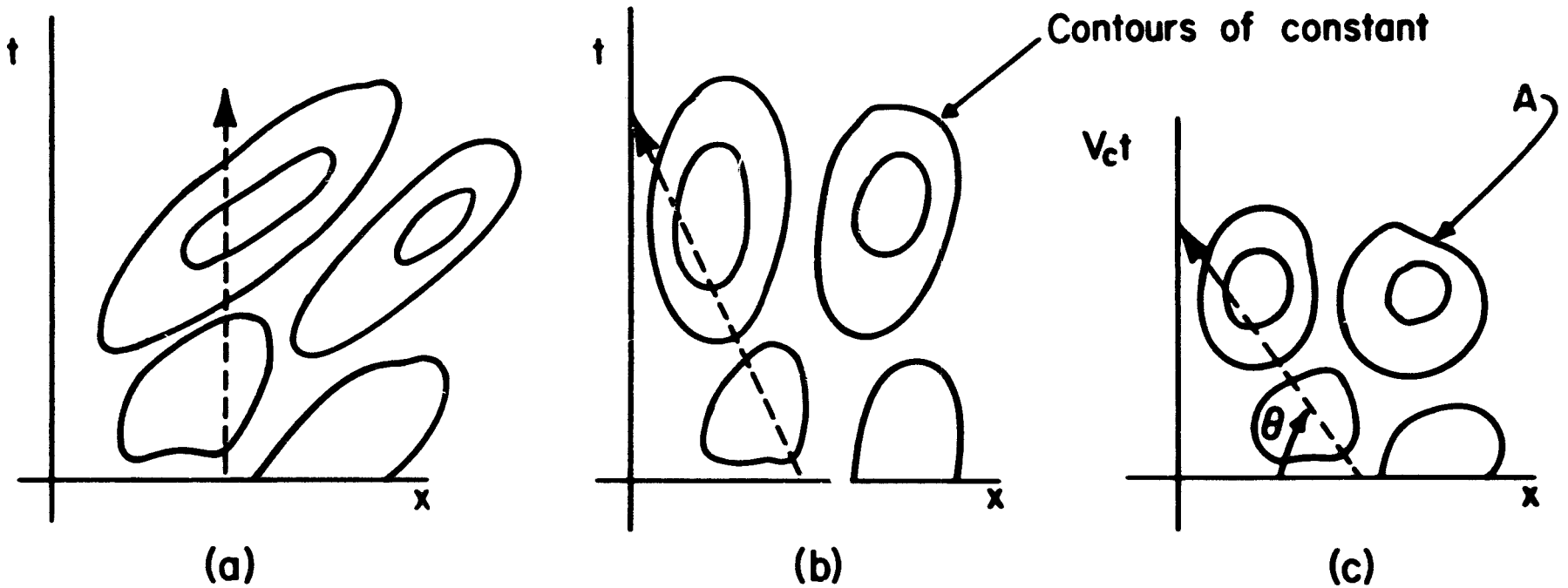

Figure 2.2 Contours of constant A. (a) Within x and t coordinates. (b) Within x and t coordinates but origin moved along with velocity V. (c) Within x and $V_c t$ coordinates (from BRIGGS et al., 1950).

A fixed point on the ground would have a velocity $-V$ relative to the axes of Figure 2.2c, and would traverse a line sloping backwards at an angle θ where

$$\cot\theta = \frac{x}{V_c t} = \frac{V}{V_c} \tag{2.23}$$

The values of A along this line are those of a fixed point on the ground. The $(x, V_c t)$ diagram of Figure 2.2c is redrawn in Figure 2.3a without the fading contours. Define the speed of fading as

$$S = \frac{\left|\frac{\partial A}{\partial t}\right|}{A} \tag{2.24}$$

From Figure 2.3a we get

$$S = \frac{S_c}{\sin\theta} \tag{2.25}$$

Since for a given time interval the distance along line OC is greater than the corresponding distance along the $V_c t$ axis by a factor of $1/\sin\theta$, and using the identity $\cot\theta = V/V_c$ we get

$$S = S_c\left[1 + \left(\frac{V}{V_c}\right)^2\right]^{\frac{1}{2}} \tag{2.26}$$

Similarly, for the measures of the speed of fading V_c' and V_c

$$V_c' = V_c\left[1 + \left(\frac{V}{V_c}\right)^2\right]^{\frac{1}{2}} \tag{2.27}$$

which may be written as

$$V_c'^2 = V_c^2 + V^2 \tag{2.28}$$

A second receiver at a distance d_o from the first receiver would measure a fading record represented by line AD, parallel to line OC, on Figure 2.3a. The point along AD that is most correlated with the receiver at point O is the closest point (point M). The height of M along the $V_c t$ axis will

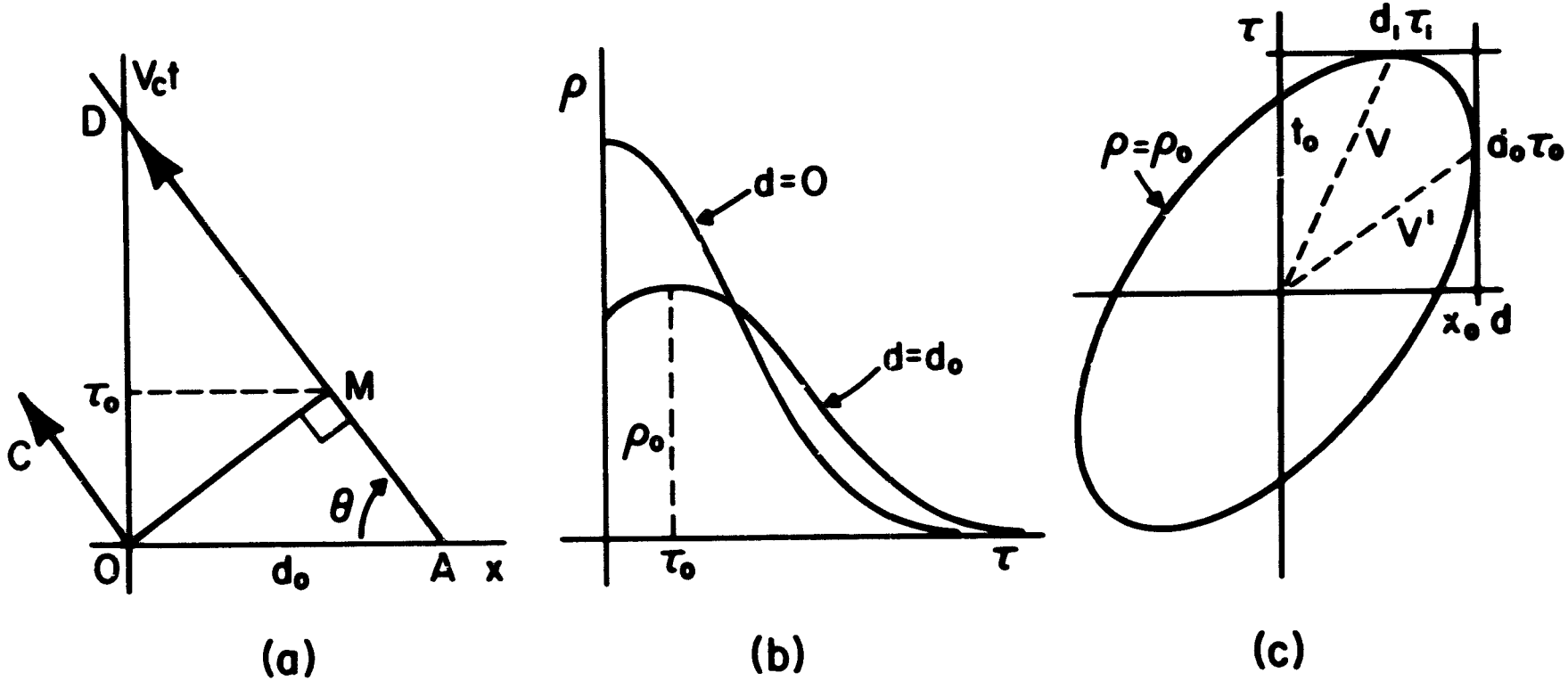

Figure 2.3 (a) $(x, V_c t)$ diagram after omitting the contours. (b) Auto- and cross correlation functions. (c) Correlation ellipse in the (d,τ) plane (from BRIGGS et al., 1950).

give τ_o, the time lag corresponding to maximum cross correlation. From the geometry of Figure 2.3a

$$V_c \tau_o = d_o \sin\theta \cos\theta \tag{2.29}$$

or
$$V_c \tau_o = \frac{d_o V_c V}{V_c^2 + V^2} \tag{2.30}$$

Using equation (2.23) to eliminate θ,

$$V' = \frac{d_o}{\tau_o} = \frac{V_c^2 + V^2}{V} \tag{2.31}$$

or
$$V'V = V_c^2 + V^2 \tag{2.32}$$

and using equation (2.28)

$$V'V = V_c'^2 \tag{2.33}$$

V' can be determined from τ_o using the relation $V' = d_o/\tau_o$. To find the true velocity V, we need to find V_c' as follows: The cross correlation $\rho(d_o, o)$ between the two records gives a measure of the effect of a space shift of d_o. If we find the time lag τ_s which gives the same value of the correlation coefficient $\rho(o, \tau_s)$ measured on one fading record, then using the definition of V_c' we can get the value of V_c'.

$$V_c' = \frac{d_o}{\tau_o} \tag{2.34}$$

Thus the drift velocity along one dimension can be calculated. The time lag τ_o for the maximum cross-correlation between the fading records from two receivers separated by a distance d_o can be found by drawing a line on Figure 2.3c through the point (d_o, τ_o) parallel to the τ axis, and finding the value of τ_o where it touches the elliptical contour of ρ_o. This value of ρ_c is the maximum value of cross-correlation. Let t_o be the value

of τ where the ρ_o ellipse intersects the τ-axis. t_o is the time lag for the autocorrelation required to give a value of correlation equal to this maximum cross-correlation corresponding to a lag τ_o. If x_o is the intercept of the d axis and (d_1, τ_1) is the point at which the tangent parallel to the d axis touches the ellipse, the notation is the same as that used in equations (2.18), (2.19), (2.20), and (2.22), for the four velocity parameters ($V'_o = x_o/t_o$, $V = d_1/\tau_1$, $V_o = x_o/\tau_1$, $V' = d_o/\tau_o$). The equation of the ellipse can be written as

$$Ad^2 + B\tau^2 + 2Hd\tau = 1 \tag{2.35}$$

If the ellipse has a vertical tangent at (d_o, τ_o) and intersects the τ-axis at (o, t_o), then

$$A = \frac{t_o^2 + \tau_o^2}{t_o^2 d_o^2}, \quad B = \frac{1}{t_o^2}, \quad H = \frac{-\tau_o}{t_o^2 d_o} \tag{2.36}$$

If the ellipse also has a horizontal tangent at (d_1, τ_1) and intersects the d axis at (x_o, o), then

$$\tau_1^2 = \frac{A}{AB - H^2}, \quad d_1 = \frac{-H\tau_1}{A}, \quad x_o^2 = \frac{1}{A} \tag{2.37}$$

Now writing the various velocity parameters in terms of A, B, H, d_o, τ_o, and t_o:

$$V'_o = \left(\frac{B}{A}\right)^{\frac{1}{2}} = \frac{d_o}{(t_o^2 + \tau_o^2)^{\frac{1}{2}}} \tag{2.38}$$

$$V = -\frac{H}{A} = \frac{d_o t_o}{t_o^2 + \tau_o^2} \tag{2.39}$$

$$V_o = \frac{(AB - H^2)^{\frac{1}{2}}}{A} = \frac{d_o \tau_o}{t_o^2 + \tau_o^2} \tag{2.40}$$

$$V' = -\frac{B}{H} = \frac{d_o}{\tau_o} \tag{2.41}$$

$$VV' = V_c'^2 = V_o^2 + V^2 \tag{2.42}$$

Equation (2.42) is the same as equation (2.32) shown earlier by another method. The connection with the previous derivation method is

$$\tau_s^2 = t_o^2 + \tau_o^2 \tag{2.43}$$

These derivations are for a one-dimensional ground, and the extension to a two-dimensional ground is straightforward. The concentric ellipses of constant correlation in two dimensions becomes concentric ellipsoids of constant correlation in three dimensions, centered on the origin. Velocity components are calculated along the directions defined by the lines forming the sides of the triangle formed by the three spaced receivers.

The method of implementing the Briggs full correlation analysis on a digital computer was worked out by FOOKS (1965). In his notation the maximum cross correlation (τ_o) is (τ') and the corresponding time displacement from the autocorrelation function for the same value of correlation (t_o) is (τ_m). So equation (2.43) becomes

$$\tau_{12}^2 = (\tau')_{12}^2 + (\tau_m)_{12}^2 \tag{2.44}$$

where subscripts have been added to denote the pair of antennas (and the direction) being correlated. The geometry of the full correlation analysis is shown in Figure 2.4. First, the characteristic ellipse is determined by the three endpoints of the vectors V_c' from equation (2.38) plotted along the compass direction of that receiver pair. The orientation of the characteristic ellipse (θ_o) and the semi-major and semi-minor axes (a and b) can

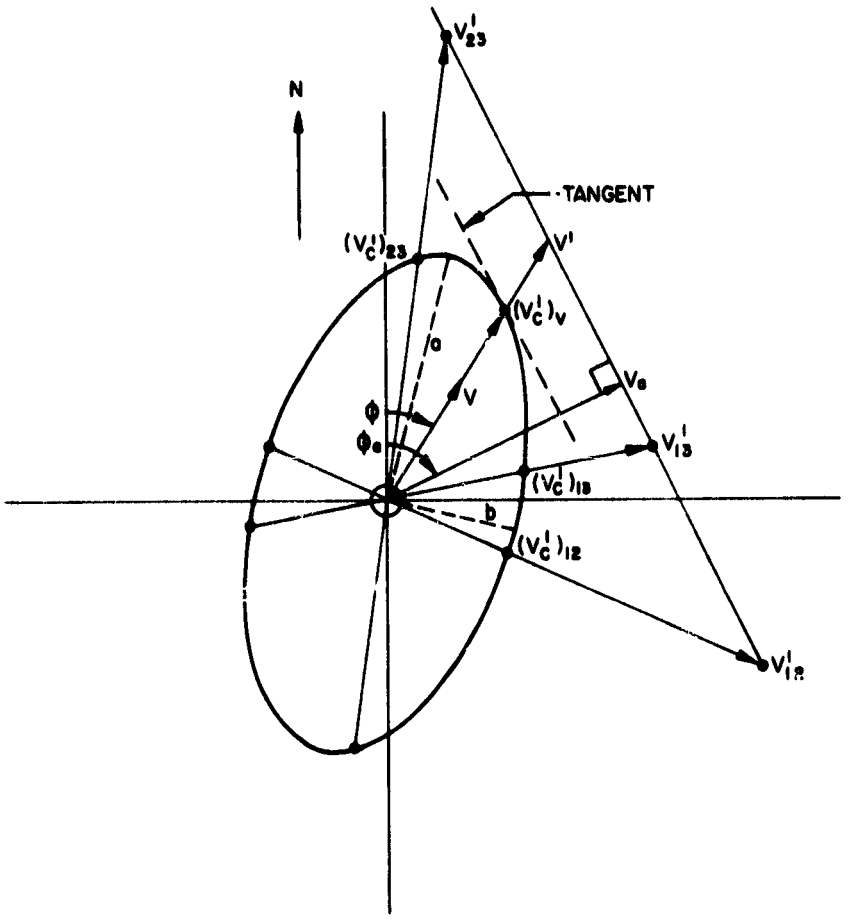

Figure 2.4 Geometry of full correlation analysis.

be calculated by simultaneous equations. Dimensions on the ellipse are in units of velocity and must be multiplied by $\tau_{0.5}$ (the value of time displacement or the mean autocorrelation function with $\rho = 0.5$) to convert them to units of distance.

The next step is to calculate the apparent velocity (V'). The three vectors $V'_{12} = d_{12}/\tau'_{12}$ are plotted, and their endpoints should lie on a straight line. In the computer analysis, a least-squares line is fitted to the three points. Two parameters of the perpendicular from the origin to this line are V_a, the length, and θ_a, the direction which is the apparent velocity. Now draw a tangent to the ellipse parallel to the V' line. The point of contact is $(V'_c)_v$. The angle of the radius to that point is ϕ, which is the angle of the true velocity, V. The length of the radius is $(V'_c)_v$. The length of the vector along this radius to the V' line is V'. The true velocity is given by

$$V = \frac{(V'_c)_v^2}{V'} \tag{2.45}$$

from equation (2.42).

It is then assumed that the amplitude pattern observed by spaced receivers on the ground is moving at twice the velocity of the irregularities in the ionosphere. This factor arises because the ionosphere is illuminated by a point source. If a plane wave source were used this factor would not occur. This factor has been experimentally investigated by FELGATE (1970) and WRIGHT (1972) using ionospheric reflections. The factor has also been studied by computer simulation by PITTEWAY et al. (1971). All of these studies concluded that the point source factor was valid, and calculated velocities should be divided by two for the correct ionospheric velocity.

3. SYSTEM DESCRIPTION

3.1 *System Requirements*

The reflection coefficient in the D region is on the order of 10^{-6} in the lower D region, and on the order of 10^{-3} in the upper D region (DA SILVA and BOWHILL, 1974). The attenuation experienced by the ordinary and extraordinary signals during propagation is different. The extraordinary mode signal undergoes a much higher attenuation as it propagates through the ionosphere, though it usually has a larger reflection coefficient than does the ordinary mode signal. The result is that in the lower part of the D region the extraordinary mode signal is higher in amplitude by a factor of about 2, and as propagation progresses through some ionization at higher altitudes, the ordinary mode return signal becomes relatively larger than the extraordinary mode return signal. At about 78 km, on average, the ordinary model return signal will be about twice that of the extraordinary mode return signal. This trend will continue as the altitude increases, and at 90 km the ordinary mode will be larger by a factor of about ten. The ordinary mode reflection cofficient is so large at the upper D region that the receiver will usually saturate at about 85 km, when operating at full sensitivity. The signals are also affected by fading which will cause signal levels to vary by about 10 dB in a time scale of a few seconds. These signal levels set the difficult requirement that the receiver must be linear within a tolerance of a few percent over a range of at least 40 dB.

Noise in this frequency range can arise from atmospheric and man-made sources. The signal-to-noise ratio in the lowest part of the D region when the noise is due to background atmospheric noise is about 1.5 or 2, on average. Lightning and static discharge noises can be quite large (several times that of the return signal) when a storm is near, and noise rejection

techniques which will be discussed later in Section 3.5 are necessary.

3.2 *Partial-Reflection System at Urbana*

A block diagram of the Urbana partial-reflection system is shown in Figure 3.1. The transmitter output is split between two 50-ohm coaxial cables. One line is phase shifted by 90° by a quarter wavelength of coaxial cable to allow a circularly polarized wave to be radiated. Attenuators are inserted in each feedline, and a phase shift network is inserted in one feedline, so that the relative level of signal feed to each of the orthogonal linear dipole arrays (N-S and E-W directed) can be adjusted to set the polarization at circular. Coaxial cables run the distance (about 1000 feet) to the transmitting antenna array where matching networks match the feedlines to the 600 ohm balanced antenna arrays. Switching from ordinary mode (right-hand circular) to extraordinary mode (left-hand circular) is accomplished by reversing the balanced line to one linear array.

The receiving array is broken up into four quadrants. Each of the four quadrants of the receiving array consists of sets of orthogonal linear dipoles (N-S and E-W directed). There are eight coaxial cables running into the field station building where the quadrant switching relays switch the desired receiving quadrant. All quadrants are combined during differential-absorption measurements of electron concentration. Switching the antenna quadrant ahead of the receiver eliminates the need for four separate receivers in the system when making drifts measurements. There are two coaxial cables from the quadrant switching box (N-S and E-W dipoles) which are fed to attenuators, a phase 90° shifter, and a 180° phase shifter, as in the transmitter feeders, to adjust and switch the antenna polarization. The signals are then combined and fed to a computer-controlled digital attenuator. This attenuator can switch in attenuation ahead of the receiver under computer control, which is useful in calibrating the receiver and in

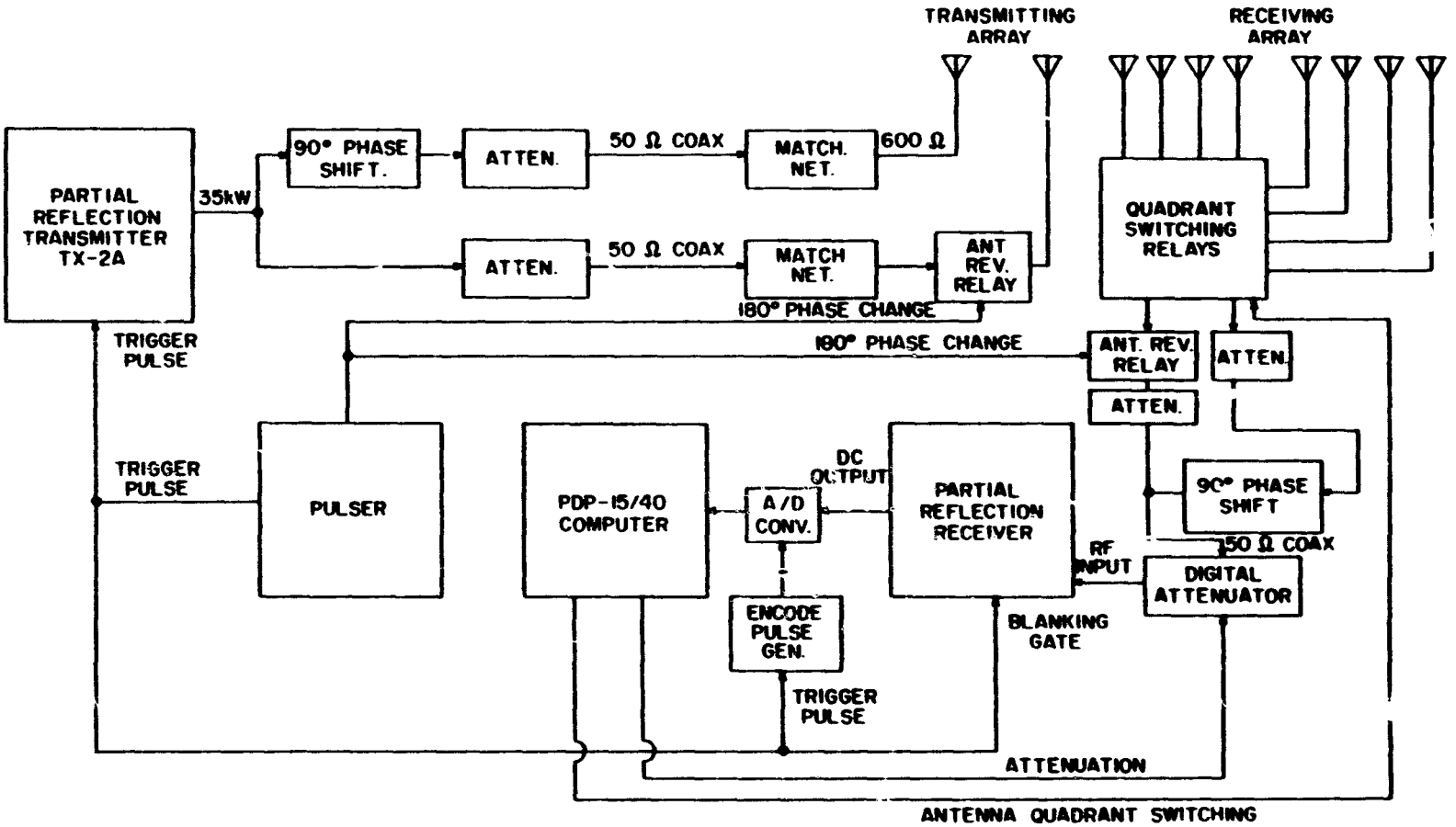

Figure 3.1 Block diagram of the partial-reflection system.

preventing receiver saturation which occurs at the higher altitudes. The receiver output is fed to the A/D converter which samples continuously in 10 μs intervals in the altitude range of interest. The pulser supplies all the timing and control signals for the system. Two pulsers are available now, a hardwired logic unit and a versatile microprocessor-based system.

3.2.1 *Transmitting equipment.* The low signal-to-noise ratio at the lowest point in the D region sets the requirement of a large transmitted power and a high-gain antenna array. The transmitter is a multi-stage tube type, and is fully desribed by HENRY (1966), and by PIRNAT and BOWHILL (1968). Its characteristics are listed below.

Peak power: 35 kW

Frequency: 2.66 MHz

Pulse width: Normally 25 μs. (Can be set at 10, 15, 25, or 50 μs with the microprocessor timing and control equipment.)

Output impedance: 50 ohms, unbalanced

3.2.2 *Receiving equipment.* To accurately measure the return signals which vary greatly in amplitude, an extremely linear receiver is required. The original receiver (HENRY, 1966) was modified later (Henry in EDWARDS, 1973) to achieve a total range of 55 dB for a 1 dB deviation in linearity. The characteristics of the receiver are listed below.

Center frequency: 2.66 MHz

Bandwidth: 40 kHz between -3 dB points

Noise figure: 3 dB MAX, 15° to 35°C

Recovery time: 200 μs after removing 0.1 V RMS input

RF input impedance: 50 ohms, unbalanced

Output impedance: 10 k ohms, unbalanced

Output response: DC to 50 kHz, 10 V MAX

Linearity: 55 dB for 1 dB deviation

Only one receiver is used in the system during drifts measurements by using a four-pulse frame and switching the antenna input for each pulse.

3.2.3 *Antenna system.* The original partial-reflection antenna system consisted of two identical square dipole arrays of 60 half-wave dipoles each. One array is used for transmitting and the other for receiving, to eliminate the need for a transmit-receive switch. The layout of the antenna arrays is shown in Figure 3.2. The array to the west of the field station building is used for transmitting. The calculated gain of this array is 22 dB, with a 3 dB beamwidth of 14 degrees. The north-south and east-west directed dipoles are matched to separate feedlines and brought into the field station building.

3.2.3.1 *Modifications made to the receiving array to implement the drifts experiment.* To implement a partial-reflection drifts experiment, the receiving array was divided into four quadrants. Having four antennas instead of the minimum of three antennas in the drifts experiment results in a four-fold redundancy in the velocity estimates than can be made, allowing winds estimates to be made even with one antenna not functioning. The $\lambda/4$ matching stubs of the original antenna matching system at the end of the $\lambda/2$ dipole sections (shown at the Xs on Figure 3.2) were disconnected, so the array now consists of four isolated quadrants and a center cross-shaped section. The dimensions and orientation of the drifts antenna layout are shown in Figure 3.3. The original antenna array matching is described by KNECHT (1966). The cross-shape center section which still has the balanced line feeder connecting the dipole could be used as a separate polarized array, but for now has been grounded. The quadrants, as shown in Figure 3.4, each consist of three north-south directed center-fed λ dipoles and

ORIGINAL PAGE IS
OF POOR QUALITY

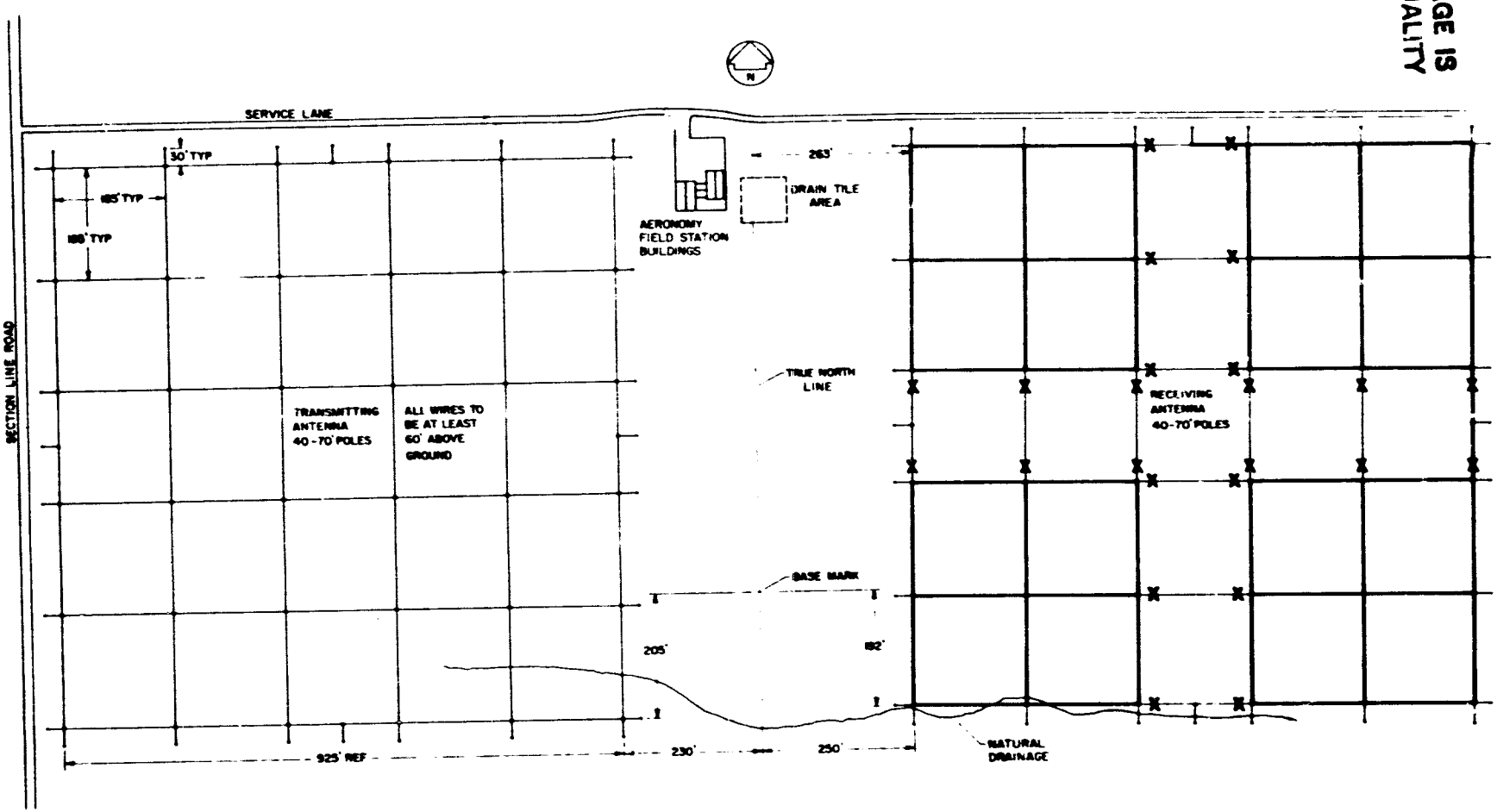

Figure 3.2 Partial-reflection antenna arrays at the Aeronomy Laboratory Field Station.

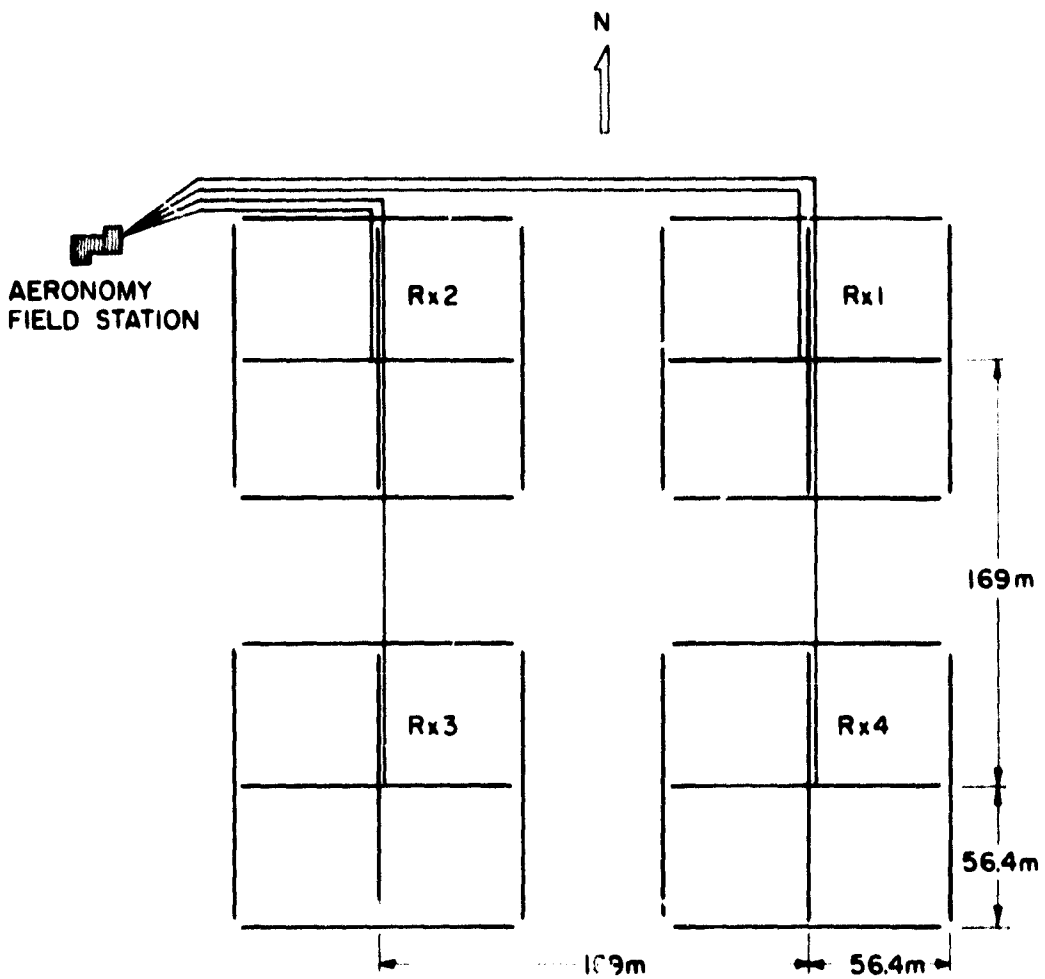

Figure 3.3 Intended antenna quadrant arrangement of the partial-reflection drifts antenna.

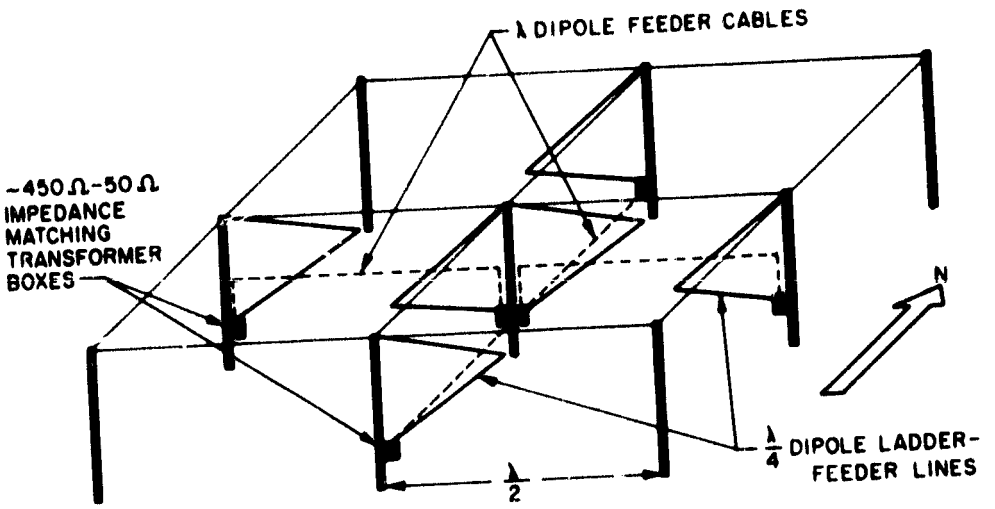

Figure 3.4 Physical arrangement of typical quadrant of 'drift' receiving antenna. Dashed lines indicate 50 Ω coaxial feeder lines. Center box contains two matching transformers for two center dipoles as well as two power combiners.

three east-west directed center fed λ dipoles. The existing λ/4 matching stub at the feed point of each λ dipole was used in the new matching system. The matching stubs are angled away from the utility pole and terminate at the utility pole at about ten feet off the ground. The short circuit at the bottom of the stub was removed, providing a driving impedance of about 450 ohms for the λ dipole. The antenna matching arrangement is shown in Figure 3.5. The 1200-ohm impedance of the λ dipole is matched to 450 ohms by the λ/4 section of 600 ohm balanced line, and the 450 ohms is matched to a 50 ohm coaxial cable by a small Ferrite transformer. A three-way hybrid power combiner is used to combine the signals from the three parallel dipoles, with -length coaxial cables running from the outer dipoles to the center. A coaxial feedline from these three parallel dipoles is run into the field station building. Because the land under the array is cultivated, cables running east-west were suspended about 20 feet to allow clearance for farm implements. The λ coaxial cables running from the outer dipoles to the center in the south-east quadrant are RG-8 coaxial cable, while the sections in the other quadrants are RG-58 coaxial cable. This gives a slight gain advantage to the quadrant farthest from the field station to partially offset the additional feedline loss along the route to the field station building. Cables running north-south are suspended about four feet above the ground over strips of land along the utility poles that are not cultivated. The calculated gain of each quadrant antenna is 12 dB.

In order to use the four quadrants together during differential-absorption measurements of electron concentration the signals from each quadrant must arrive at the receiver with the same phase. All of the eight feedlines from the quadrants had to be matched in phase delay at 2.66 MHz. This was accomplished by inserting a 2.66 MHz reference signal into the ends of two

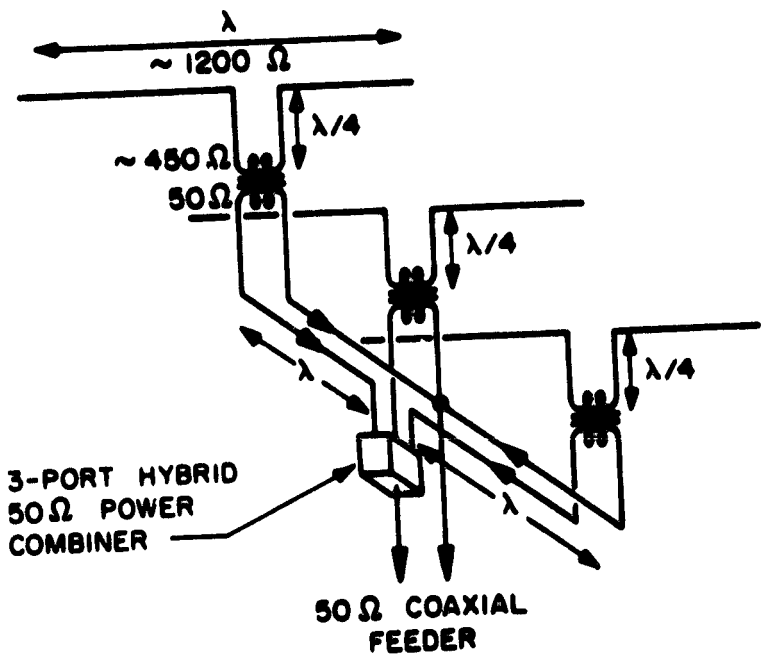

Figure 3.5 First system of matching and combining of in-phase signal components from parallel quadrant dipoles. The λ feeder line sections correspond to the dashed (coaxial) lines in Figure 3.4.

feedlines in the field, and measuring the phase difference at the other end of the cables using a vector voltmeter. One of the eight feedlines was used as a reference, and the remaining seven were matched in phase to it, by cutting out or adding cable. Adjustment of the cable lengths was facilitated by being able to introduce a 180° phase shift at any quadrant requiring more than $\lambda/2$ of additional cable to match its phase, by reversing the balanced line $\lambda/4$ matching lines at that quadrant's dipoles. The tolerance of these phase-length adjustments is estimated to be about one degree, well within the precision necessary to ensure effective in-phase summation of the signals from the four quadrants.

The small dipole impedance matching Ferrite transformers though protected from static discharge by leakage resistors and neon gas discharge tubes did not survive a storm that occurred shortly after the completion of the antenna modifications. Lightning struck one of the antenna support poles in the southwest corner of the array, destroying most of the matching transformers in the entire array. It was decided to redesign the matching system using larger transformers so that in the event of another lightning strike only a small portion of the array would be damaged. Figure 3.6 shows the new matching system. The small Ferrite dipole matching transformers were replaced with two-inch Ferrite torroidal core transformers wound with 14-gauge wire. The three-port hybrid power combiners were replaced by paralleling the three dipole feeders and matching this impedance to 50 ohms using a 3:1 transformer. These transformers were also wound on Ferrite toroidal cores with large diameter wire. After more than two years of operation, none of these transformers have been damaged.

3.2.3.2 *The drifts experiment quadrant switching circuitry.* The functional schematic of the quadrant switching unit is shown in Figure 3.7.

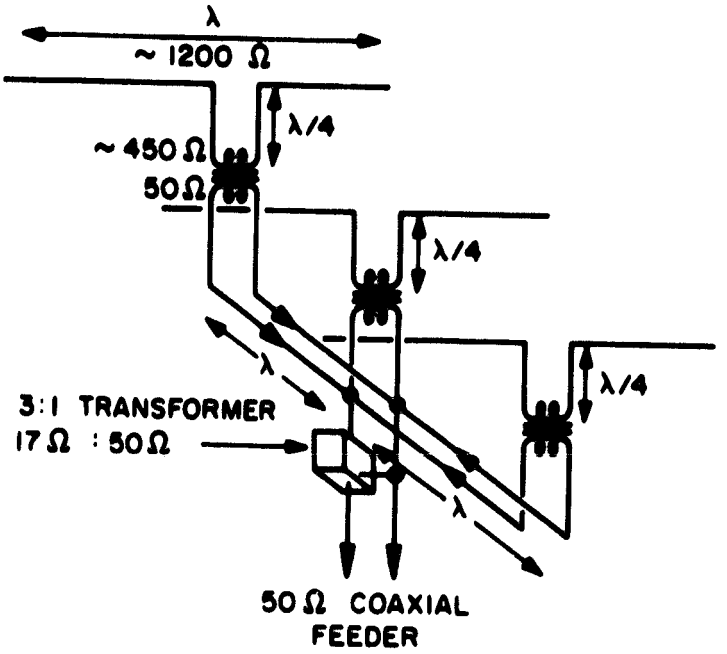

Figure 3.6 Final system of matching and combining of in-phase signal components from parallel quadrant dipoles. The λ feeder line sections correspond to the dashed (coaxial) lines in Figure 3.4.

ORIGINAL PAGE IS
OF POOR QUALITY

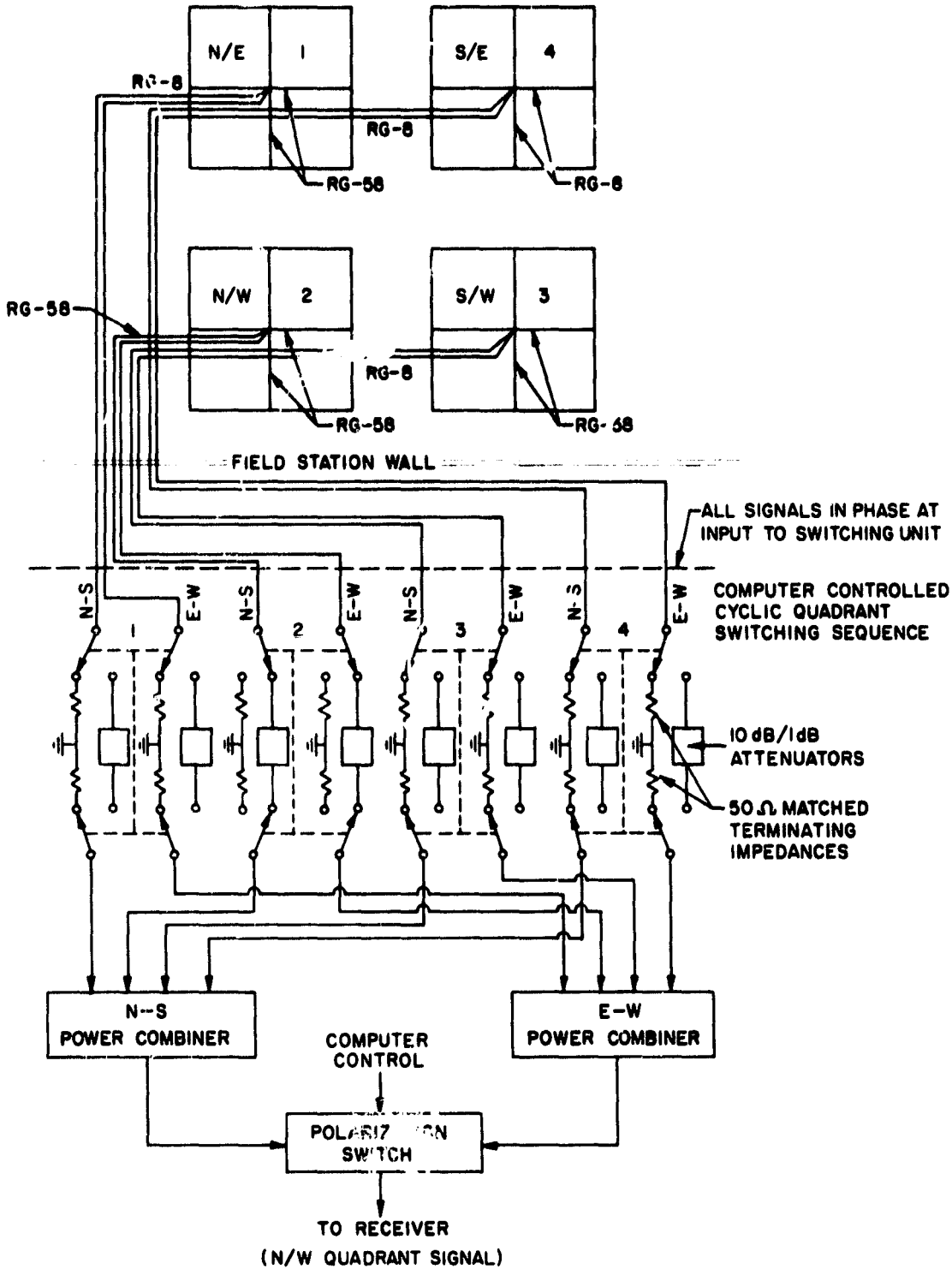

Figure 3.7 Functional schematic of quadrant switching of receiving antennas for drift experiment. Computer-controlled switching can combine four quadrants (in-phase and closely equal signal amplitude) to render combined high-gain antenna for conventional partial-reflection experiment.

The unit can be commanded to feed the signal from any one of the antenna quadrants to the receiver, or the summation of all the signals can be fed to the receiver. All unused antennas are terminated at 50 ohms to minimize re-radiation effects. Reed relays with a switching time of about 2 ms were used instead of solid-state devices because of their tolerance of over voltage that might occur when storms are nearby. To prevent damage to the unit when the equipment is not in use, jumper plugs were included in each antenna feedline coming into the unit so that they could be disconnected and grounded.

Control of the switching unit can be provided by either the PDP-15 computer or the PET microcomputer. When switching is under control of the PDP-15, the switching command signals are taken from the PDP-15 digital input/output interface. The interface is described in Section 3.3. Switching can also be done under the control of the PET microcomputer.

3.2.4 *Microprocessor timing and control equipment.* The original timing and control system consisted of a hard-wired logic unit with a fixed pulse width of 25 μs, and frames of 2 or 4 pulses, at a fixed pulse repetition frequency of 2.5 frames per second. To allow more versatile pulse timing, a microcomputer has been interfaced to the system. Figure 3.8 shows the timing of the control signals needed to control the system. A Commodore Business Machine PET model 2001-8 is used as the controller. The program TIMOD (listed in Appendix V) is used to output the user-controlled timing pulses to the parallel user port J2. The TTL level signals from this port must be modified to control the experiment. Figure 3.9 shows the PET interface circuitry. The four antenna quadrant switching signals which remain high during the time that the desired quadrant is selected must be inverted (the quadrant switching box is designed to sum all quadrant signals in the

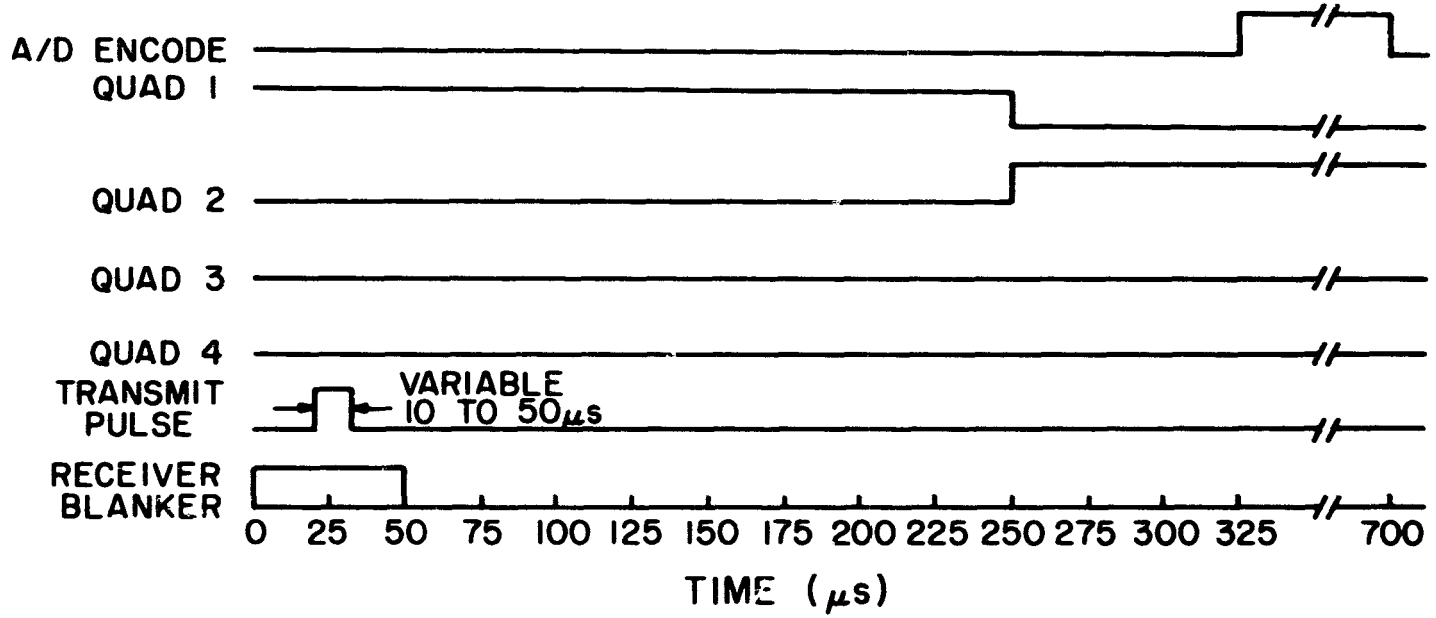

Figure 3.8 Timing diagram of signals required to control partial-reflection system (shown sampling first quadrant).

ORIGINAL PAGE IS
OF POOR QUALITY

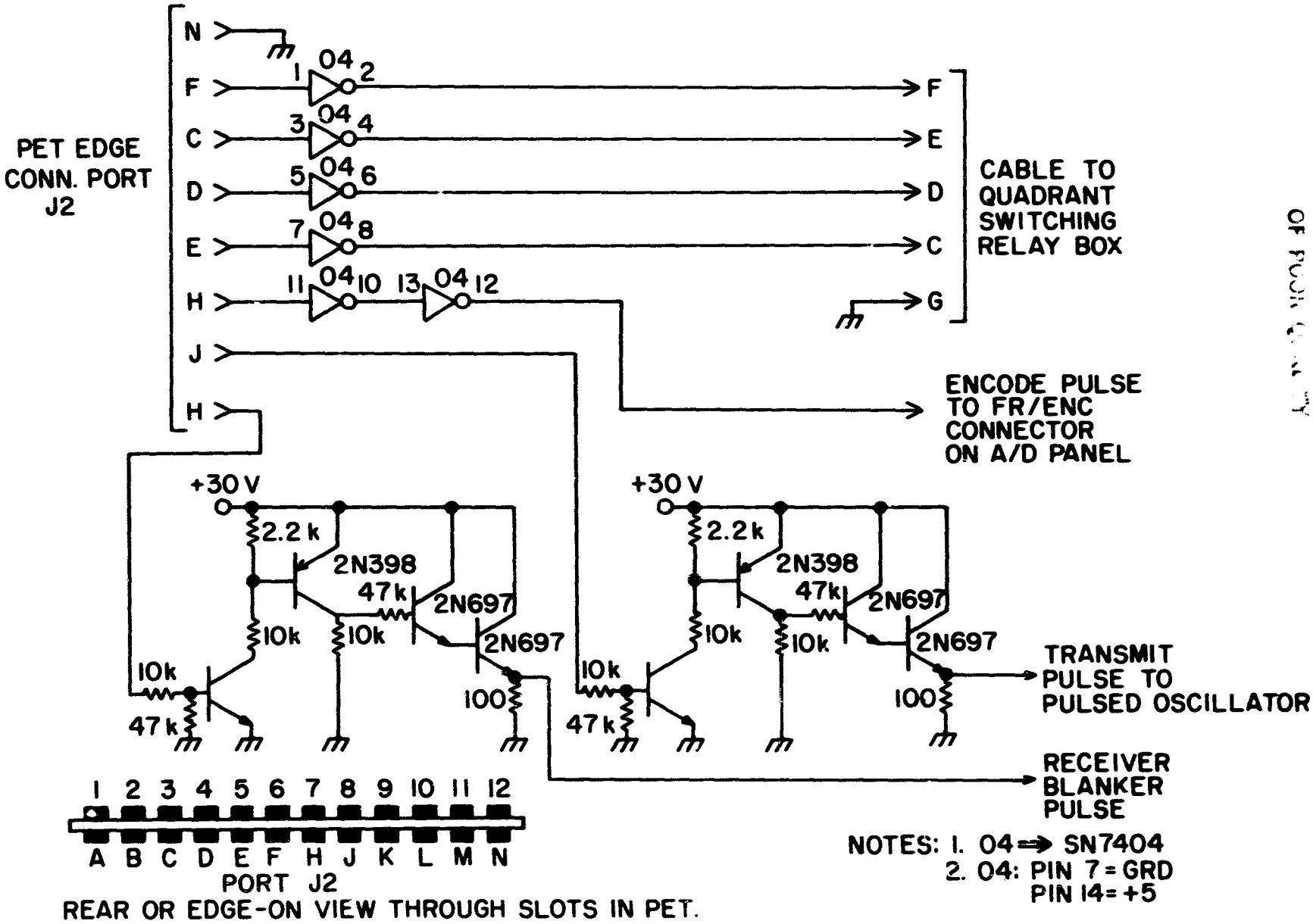

Figure 3.9 PET interface circuitry.

presence of no command, so a high level disables that quadrant). The A/D encode command that determines the start of data sampling is buffered by the two remaining gates. The receiver blanker requires a +28 volt pulse whose length is not critical. A monostable inside the blanker is triggered to blank the receiver for 100 μs. The transmitter is gated on in the pulsed oscillator stage. Figure 3.10 shows the pulsed oscillator with the modifications made to allow a variable pulse length to be transmitter. The oscillator is gated in the last stage and originally had a fixed pulse width of 25 μs, set by a monostable before the gating circuit. The second trigger pulse input, labeled PET TX trigger was added with a switch to select the control input, with the necessary added circuitry. The PET interface shifts the transmit pulse command to the +28 volt level to drive the pulsed oscillator input.

The timing program, called TIMOD is stored on a cassette. When the program is run, it first asks for the desired pulse width and interpulse period. The desired mode of operation is selected from the "menu" as shown in Table 3.1. The interpulse periods shown give pulse repetition frequencies of 50, 75, and 150 pulses per second. In order to limit the number of pulses per second, the transmitting signal usually consists of four pulses (one for each quadrant) followed by a waiting period (the hard-wired pulser has a delay of 300 mS between the end of a frame of four pulses and the beginning of the next, with 33 mS between each pulse in a frame of four pulses). The program will now ask for the waiting period between frames of four pulses, in 1/60 second increments (normally 18). After entering the number, the program will type "press any key to run". A key is then pressed to start collection after the data acquisition program has been started on the PDP-15 computer. The program is stopped by pressing the run/stop key on

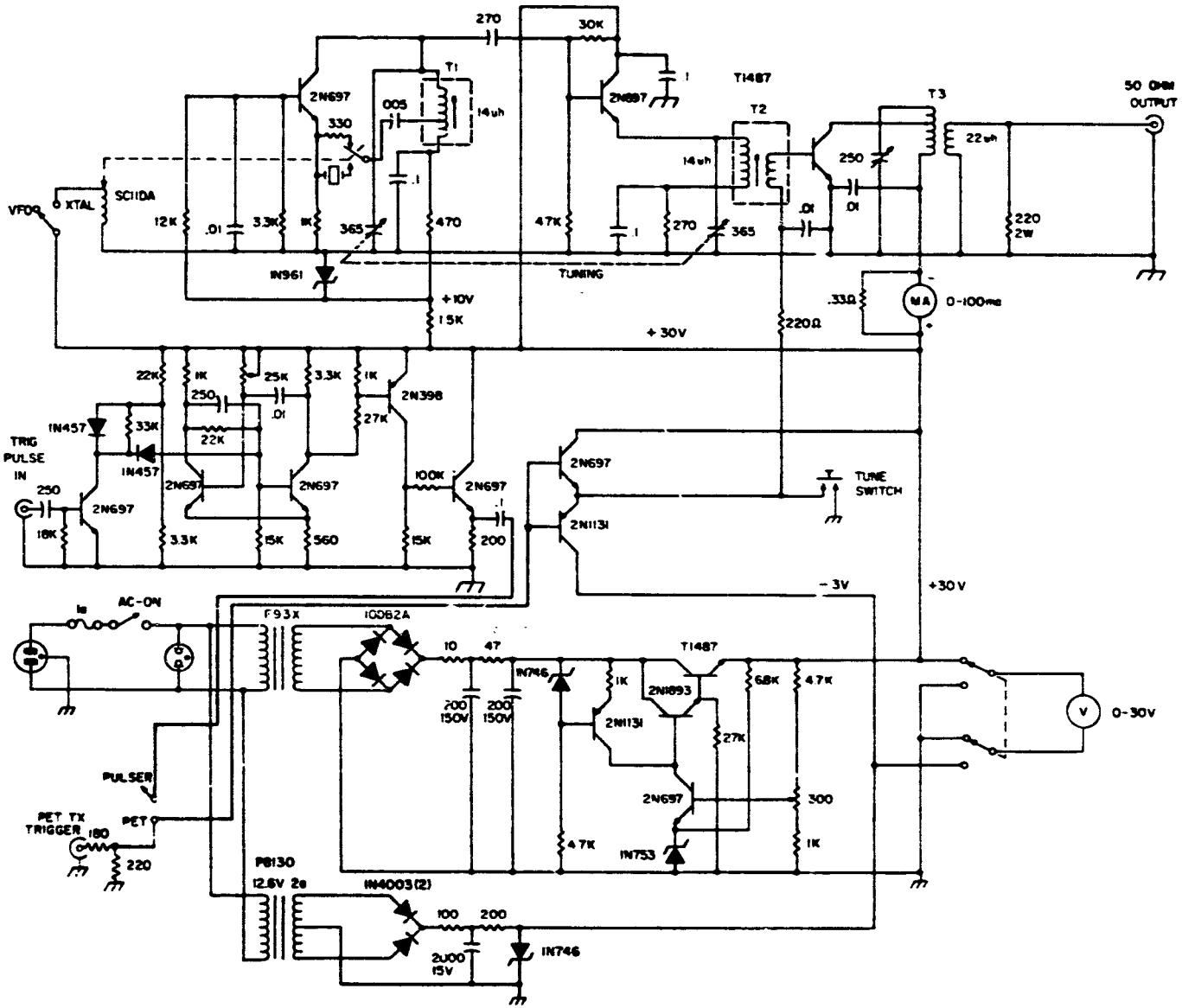

Figure 3.10 The tunable pulsed oscillator.

ORIGINAL PAGE IS OF POOR QUALITY

TABLE 3.1 Menu of pulsewidths and interpulse periods available in the program TIMOD.

PULSEWIDTH (μS)	INTERPULSE PERIOD (mS)		
	6.7	13.3	20
10	A	B	C
15	D	E	F
25	G	H	I
50	J	K	L

the keyboard.

3.3 *Data-Acquisition System*

A Digital Equipment Corporation PDP-15/40 digital computer is used for data acquisition and processing. It has 18-bit words, 32 k of 800 nsec core memory, a real time clock, and an extended arithmatic element for hardware multiply and divide. There are four fixed-head disks for high speed storage, four DECtape drives for bulk data storage, a high speed paper tape punch and reader, a DECwriter terminal which prints at 120 characters per second, and an Infoton cathode-ray terminal. The system software monitor is a background/foreground system and all system programs are resident on disk 0 for fast access. A complete description of the computer system is given by BIRLEY and SECHRIST (1971), and BEAN and BOWHILL (1973). Data are digitized by a Hewlett-Packard model 5610A analog-to-digital converter. Its conversion rate is 100 kHz, corresponding to an apparent height resolution of 1.5 km, and it has direct memory access. The resolution is 10 bits and uses two's-complement coding. Thus, the 0 to 1 volt input range from the receiver corresponds to an A/D output of from 0 to 512 base 10. There is a 16-channel multiplexer ahead of the A/D converter which has been wired to the digital input/output interface, so that the sampled channel can be set by computer control. The bits used to set the multiplexer channel are shown in Table 3.2, and the use of this system is explained next.

The digital input/output interface on the PDP-15 computer allows the computer to control external devices. The subroutine OUT when called in a FORTRAN program transfers the contents of the accumulator into the input/output interface which latches and holds that value until it is changed. The accumulator is loaded prior to the call OUT with the desired value by any arithmetic statement. The interface was earlier used only for control

TABLE 3.2 Pin connections on the PDP-15 computer digital input/output interface, card A14.

PIN NUMBER ON CARD A14	BIT NUMBER	DECIMAL VALUE	PURPOSE
C2	---	---	GROUND
D2	16	65536	A/D CHAN BIT 4
E2	15	32768	A/D CHAN BIT 3
F2	14	16384	A/D CHAN BIT 2
H2	13	8192	A/D CHAN BIT 1
J2	12	4096	QUAD 4 SELECT
K2	11	2048	QUAD 3 SELECT
L2	10	1024	QUAD 2 SELECT
M2	9	512	QUAD 1 SELECT
N2	8	256	UNUSED
P2	7	128	DPDT RELAY
R2	6	64	ANTENNA RELAY
S2	5	32	DIG. ATTN. 32 dB
T2	4	16	DIG. ATTN. 16 dB
U2	3	8	DIG. ATTN. 8 dB
E1	2	4	DIG. ATTN. 4 dB
V2	1	2	DIG. ATTN. 2 dB
B1	0	1	DIG. ATTN. 1 dB

of a digital attenuator which can be commanded to place any value of attenuation ahead of the receiver in 1 dB increments from 0 to 63 dB. This is used in computing a receiver calibration table before collecting differential-absorption data to correct any receiver non-linearities and during data collection to prevent receiver saturation. Additional interface circuitry has been added to enable the input/output interface to control other equipment. Table 3.2 shows the present uses, and their bit number and decimal value. The first seven bits are used to control the digital attenuator stages, where the decimal value loaded is the value of attenuation added. Bit 6 controls a coaxial two-position antenna relay which switches the receiver input between the antenna feed and a low-level 2.66 MHz signal from the transmitter oscillator for use in calibrating the receiver. Bit 7 controls a DPDT relay which is presently used during antenna polarization adjustments with the program POLCHK to switch in attenuators during the ordinary mode pulse return (see WEILAND and BOWHILL (1978), p. 27). Bit 8 is unused. Bits 9 through 12 are used to select the desired antenna quadrant connected to the receiver. The quadrant switching unit is designed so that all antenna quadrants are normally being fe to the receiver, so that when a quadrant is to be selected, the summation of the values of the three unwanted quadrants is loaded. The values to be loaded to select each quadrant are; quadrant 1 = 7168, quadrant 2 = 6656, quadrant 3 = 5632, quadrant 4 = 3584. Bits 13 through 16 are used to command the A/D converter multiplexer to sample a specific channel. The channel signals are fed to the Digital Equipment Corporation custom A/D interface M904 card, slot B23. Two switches were added to the rear A/D connection panel to select normal or PDP-15 control of A/D channel selection.

3.3.1 *Differential-absorption data collection programs.* Since the

fall of 1972, differential-absorption electron concentration data have been collected at the Aeronomy Laboratory field station (geographic coordinates: 40°10'10"N, 88°09'35"W) daily near noon during the winter months. The standard differential-absorption data collection program DLOGD has been used with minor modifications throughout this time period. The transmitted frame consists of two pulses (ordinary and extraordinary modes) separated by 33 mS, repeated every 400 ms as shown in Figure 3.11b. The program has provisions for receiver calibration, noise rejection, real-time processing of data, prevention of receiver saturation, printouts of electron concentration profiles and saturation information every 3.4 minutes, and a final summary of electron concentration and other information at the end of its approximately one hour of data collection. Processing of data to calculate the electron concentrations is done in real time during data collection. The operation of this collection program will be summarized here. A complete discussion has been provided by BEAN and BOWHILL (1973).

The program is loaded and initialized with date and time, and then it switches the calibration signal into the receiver input. The receiver is then automatically calibrated using the digital attenuator to step through its 63 dB range. An output versus input characteristic for the receiver is calculated and stored in a linearization table for correction of all data collected, to eliminate non-linearities in the receiver. After the receiver calibration, data collection is started. The A/D converter samples every 1.5 km in the altitude range of 45 to 90 km. The five data samples taken from 45 to 51 km, where no returns due to electron-concentration gradients are expected, are used as an estimate of the noise that is present on the returns from all altitudes. In this discusion, the array of data obtained at all altitudes from a single pulse will be called a data frame, and 512

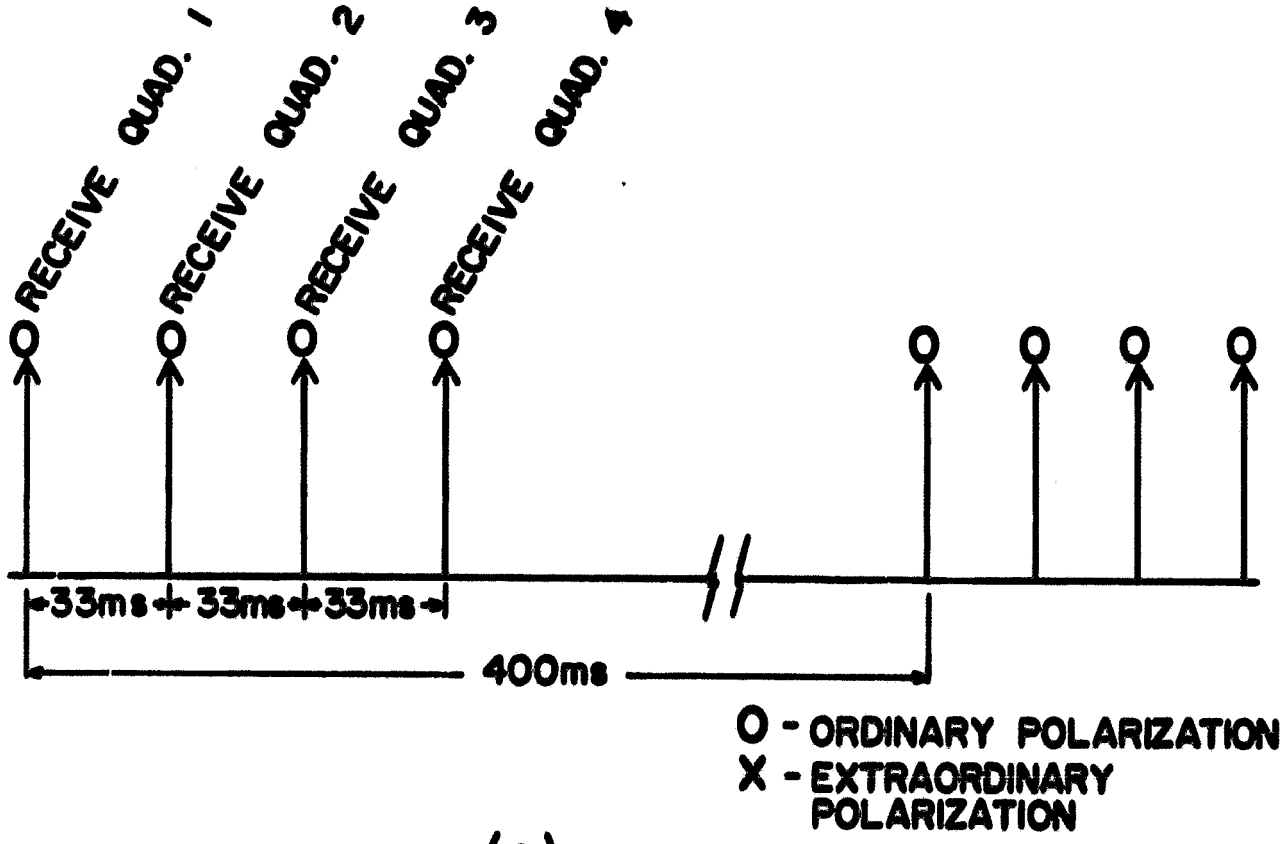

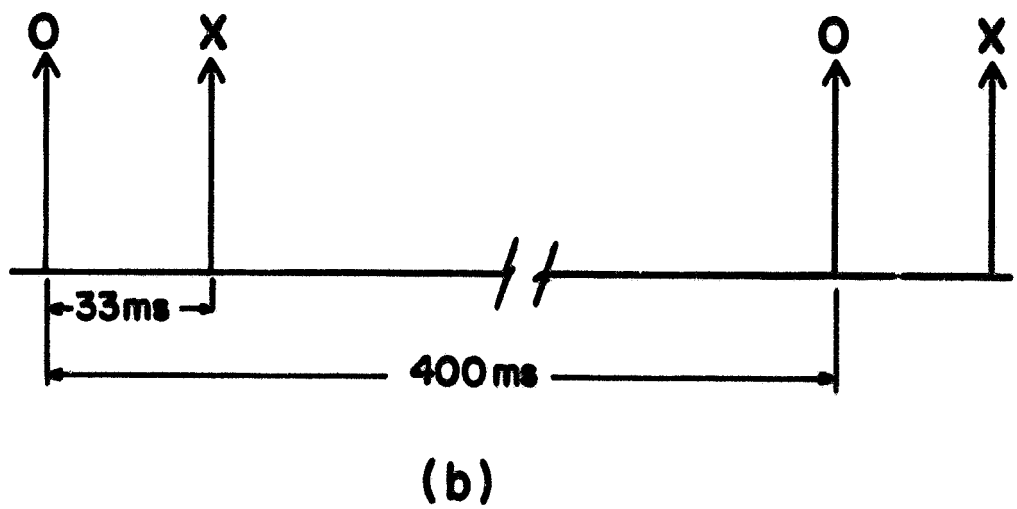

Figure 3.11 (a) Four-pulse data frame used for drifts measurements.
(b) Two-pulse data frame used for differential-absorption measurements.

frames of data, corresponding to 3.4 minutes of data collection, constitute a data file.

To obtain an estimate of the noise, the first nine frames of a file are examined to find the maximum of that frame's noise samples. The nine maxima are compared with each other to find the lowest maximum. The sum of the five noise samples from the frame with the lowest maximum is divided by five to determine the average. This average is multiplied by the square root of a multiplying constant to give a number called the maximum allowable noise. The multiplying constant has been chosen to give useable results. Any frame with an average noise level (determined from the five noise samples) larger than the maximum allowable noise is rejected. The average noise from all frames in a file is later subtracted from the signal returns from each altitude.

To avoid receiver saturation problems, any signal that is above the assumed receiver saturation level of one volt output is rejected. To avoid saturating the receiver, files are alternately collected with 0 dB, 10 dB and 25 dB of attenuation ahead of the receiver. The lowest attenuation file where an excessive number of the data at that altitude are not saturated are retained for further processing. To make this selection, if more than 10 of the 512 samples collected in a file at that attenuation were above the saturation threshold at that altitude, the data from the next higher attenuation file will be used for that altitude. Thus, a file of unsaturated data is obtained from each group of three files collected at different attenuations. Five of these unsaturated files (from a total of 15 files) are collected in just under an hour. The median of the five unsaturated values of electron concentration is then calculated for each altitude. Data are analyzed for the altitude region of 60 to 90 km, and a final profile for the hour of data

collection is printed. The data digitized from 52.5 through 58.5 are not retained for processing by the collection program. Finally, averages are calculated for 3-km-wide slabs centered at 72, 76.5 and 81 km. This is done by averaging the electron-density values for two adjacent altitudes. For example, the 72 km electron density is obtained by averaging the values from 70.5 and 72 km. Since the electron concentration at 70.5 is obtained from

$$\ln(A_x/A_o)\Big|_{72\ \mathrm{km}} - \ln(A_x/A_o)\Big|_{70.5} \tag{3.1}$$

and the electron concentration at 72 km is obtained from

$$\ln(A_x/A_o)\Big|_{73.5\ \mathrm{km}} - \ln(A_x/A_o)\Big|_{72\ \mathrm{km}} \tag{3.2}$$

The average of these two is representative for 72 km. These average values of electron concentration are calculated for 72, 76.5, and 81 km daily, and are plotted along with the A_x/A_o at 81 km (inversely proportional to the total electron content below 81 km) for further study.

3.3.2 *Drifts data collection programs.* Since only one receiver is available, a four-pulse frame must be transmitted during data collection for the drifts experiment, with the receiver input switched to a different antenna quadrant during each pulse. The transmitted pulse frame is shown in Figure 3.11b. The delay between sampling the various quadrants must be taken into account during the processing of data. The data are collected under control of the PDP-15, which is also controlling the antenna quadrant switching unit so that problems in synchronizing the quadrant switching with data storage in the correct array do not arise. Data are collected in groups of 512 frames constituting a file of data that takes about 3.4 minutes to collects. During collection, the fading records from the four quadrants are stored on magnetic disk, or on DECtape for later processing. The collection time of about 3 minutes is used to ensure sufficient statistical

stability of the correlation estimates and to also remain within the limiting period of statistical stationarity of the fading process. The 3.4 minute period was chosen on the basis of data analysis carried out by others (STUBBS, 1973), and because the 512 length fading series would be a convenient length for possible fast-Fourier transform analysis. Other groups (VINCENT et al., 1977) have found that one-minute files were long enough to provide good results, and the additional time resolution was of value in studying rapidly varying winds and wave motions.

The collection programs available are listed in Table 3.3, along with their subroutines and comments on their use. The first collection program, DRIFT1 collected data from 60 to 90 km in 1.5 km intervals. Because of the wide altitude range, it was difficult to keep a good signal-to-noise ratio for the fading records at all altitudes. To prevent receiver saturation at the upper altitudes (which would cause problems when estimating the correlation functions) the system gain would have to be reduced. This degrades the signal-to-noise ratio at the lower altitudes. With a reduced signal level it was difficult to get any usable returns below 72 km. It was decided tha the altitude range of collection should be reduced, and the system sensitivity increased also. The range of altitudes was changed to include only the range of 70.5 to 81 km. The number of altitudes where data were sampled in that range was also reduced to six. This was done to reduce the amount of data storage needed on magnetic tape. The data collected at 20 altitudes for 3.4 minutes required the storage of 40K words of data, or about one third of the capacity of a DECtape. This would have required a good deal of storage for closely spaced data collection. The six altitudes chosen corresponded to the six altitudes where daily differential-absorption data are obtained (i.e., 70.5, 72, 75, 76.5, 79.5, and 81 km). The program DRIFTL

TABLE 3.3 Partial reflection drifts data collection programs

PROGRAM	SUBROUTINES	COMMENTS
DRIFT1		Collects data from 60 to 90 km in 1.5 km intervals (fills one third of a DECtape with one file
	STOP	Checks for collection stopage
	TICK	Counts seconds from computer clock
	OUT	Sets digital attenuator and quadrant
	PPϕ	Checks data switch on console for a 1.
	CTIME2	Calculates the time of day
	INPADF	A/D service routine
	SYNC	Sets a timer to check quadrant collection order
	CLOSE, ENTER	System programs
DRIFTL	Same as above	Collects six altitudes. 10 files fit on one DECtape. Used for collection until March 18, 1979.
DRIFTH	Same as above	Collects six altitudes (75, 78, 81, 84, 87, and 90 km). 10 files fit on one DECtape. Used for all collection after March 18, 1979.

was written to collect data at these six altitudes. Data are collected in files of 512 samples requiring 3.4 minutes to collect, and ten data files can be stored on one DECtape. This program was used for data collection during the winter of 1978-1979, until March 18, 1979 when it was replaced by another data collection program.

The system was at full sensitivity and returns were not saturating the receiver at 81 km, and the returns at 70.5 and at 72 km were seldom usable. It was then decided that the collection altitudes should be moved up and be evenly spread in the altitude range of 75 to 90 km. The program DRIFTH was written to collect data at 75, 78, 81, 84, 87, and 90 km. The system sensitivity must be reduced slightly to prevent receiver saturation at 90 km, but returns at 75 km are still usable. Ten files of data can be stored on a DECtape for processing later. This collection program generally provides the maximum number of usable altitudes of returns using a single system sensitivity at our location, and was used in all drifts data collection after March 18, 1979.

The collection program is stored on DECtape and copied onto disk 3. The fading series are stored on disk 1 during collection, and later transferred to DECtape for later processing. Data should not be written directly onto DECtape during data collection because the access time in writing the data is too long, and the real-time collection process would be delayed during the tape write. The program is loaded with the computer device assignments: A DK3 -4, -5/DK1 2(RETURN). The program is loaded by the system program GLOAD with its subroutines (listed in Table 3.3, and stored in the subroutine library .LIBR5) by typing: ___DRIFTH (ESCAPE). The program will ask for the time, date, the number of samples to be collected, the attenuator, and the name of the file to be written. The number of samples is 540,

and the form of the file name is CHECKXDAT, where X is a number from 1 through 9 or the letter A. The date, time, and attenuation for that file are written in the first block on the data file for later identification. Data collection is started by switching data switch 00 on the computer console to the 1 position. The subroutine INPAD is the A/D converter service routine which stores 31 data samples into core memory. Samples are obtained from 45 to 90 km in 1.5 km intervals, but only six altitude samples are eventually written onto disk storage. To check that the computer and A/D converter are synchronized, a call is made to the subroutine SYNC before the last two antennas are sampled. SYNC sets a timer and upon the expiration of the time checks to see that both sets of samples were collected. If they have not, the computer and A/D converter are not synchronized and the data from the first two antennas are discarded and collection starts over from the first antenna. To check for failure of the A/D interface to transfer data, the subroutine STOP sets a 1.5 second timer. At the end of this time, the flag IRUN is checked. This flag is set to 1 at various parts of the program to signify that collection is continuing. If IRUN is 0, collection has stopped, and STOP forces it to begin again. Data from the six sampling intervals are packed into an array for writing onto the disk after every tenth data frame is collected. Listings of the program DR1FTH and its subroutines are provided in Appendix V.

4. DATA-ANALYSIS TECHNIQUES

4.1 *Analysis of Differential-Absorption Data*

The data collection program normally used (discussed in Chapter 3) provides a printout of electron concentration, ordinary mode return amplitude, extraordinary mode return amplitude, and information on the number of frames of data rejected because of noise or receiver saturation, for the altitude range of 60 to 90 km, every 3.4 minutes. The ordinary mode return strength and rejection due to receiver saturation information is useful in setting the amount of attenuation needed to prevent receiver saturation during the collection of drifts data. The differential-absorption experiment is therefore normally run before collecting drifts data to prevent receiver saturation.

Data collection is normally made during the winter months, for one to two hours per day, for comparison with drifts winds measurements, meteor radar winds measurements, and horizontal winds derived from the coherent scatter radar system at Urbana. Data have also been collected on many days for periods of 8-9 hours per day for the study of the diurnal asymmetry in electron concentrations, and to form time series of electron concentrations to study gravity and planetary waves. Many of these topics will be discussed in later chapters.

Errors in the calculation of electron concentrations may arise from errors in the signal amplitudes due to the finite number of samples taken, systematic errors due to the assumed reflection process, and short-term variations in electron concentrations due to wave motions. The experimental uncertainty in electron concentrations at Urbana was estimated by comparing consecutive electron concentration profiles from two one-hour data collection runs during the time of day at noon when the solar zenith angle is

varying slowly (Wratt, in EDWARDS, 1975). The uncertainty due to scatter in the data was 16 percent at 76.5 and 81 km, and 24 percent at 72 km. This does not include the systematic uncertainties due to incorrect assumptions in modeling the experiment, such as the approximately 10 percent error from assuming a possibly incorrect reflection mechanism (see Chapter 2). AUSTIN (1971) concluded that the experimental uncertainty of data collected at Christchurch, New Zealand was about 20 percent.

4.2 *Analysis of Drifts Data*

The data collection program provides a set of four fading time series at each altitude being sampled. Figure 4.1 is a typical plot of the fading time series shaped at the four antennas. The time between samples is 0.4 seconds, and the total record length is 3.4 minutes. A highly sinusoidal variation in the fading is seen in the early part of the record, with a less regular variation in the remainder of the series. The features shown in the fading series at each antenna do exhibit very consistently similar features. The method of similar fades could be used to estimate the apparent drift velocity directly from this figure. The features shown in the S/E fading series are delayed by about two sampling lags (0.8 seconds) from the features of the S/W fading series. This would indicate an apparent velocity of about 100 m/s towards the east. The N/E fading series shows a similar delay from the N/W fading series, as would be expected. The delay in the fading series from the northern quadrant fading series to the southern quadrant fading series indicates a delay of about two lags for both pairs of series, indicating a southward apparent drift velocity of about 100 m/s.

Although the period of fading is changing throughout the sampled series, the relative time delay between the fading remains fairly constant. The constant delay will give apparent velocities that are correct from this

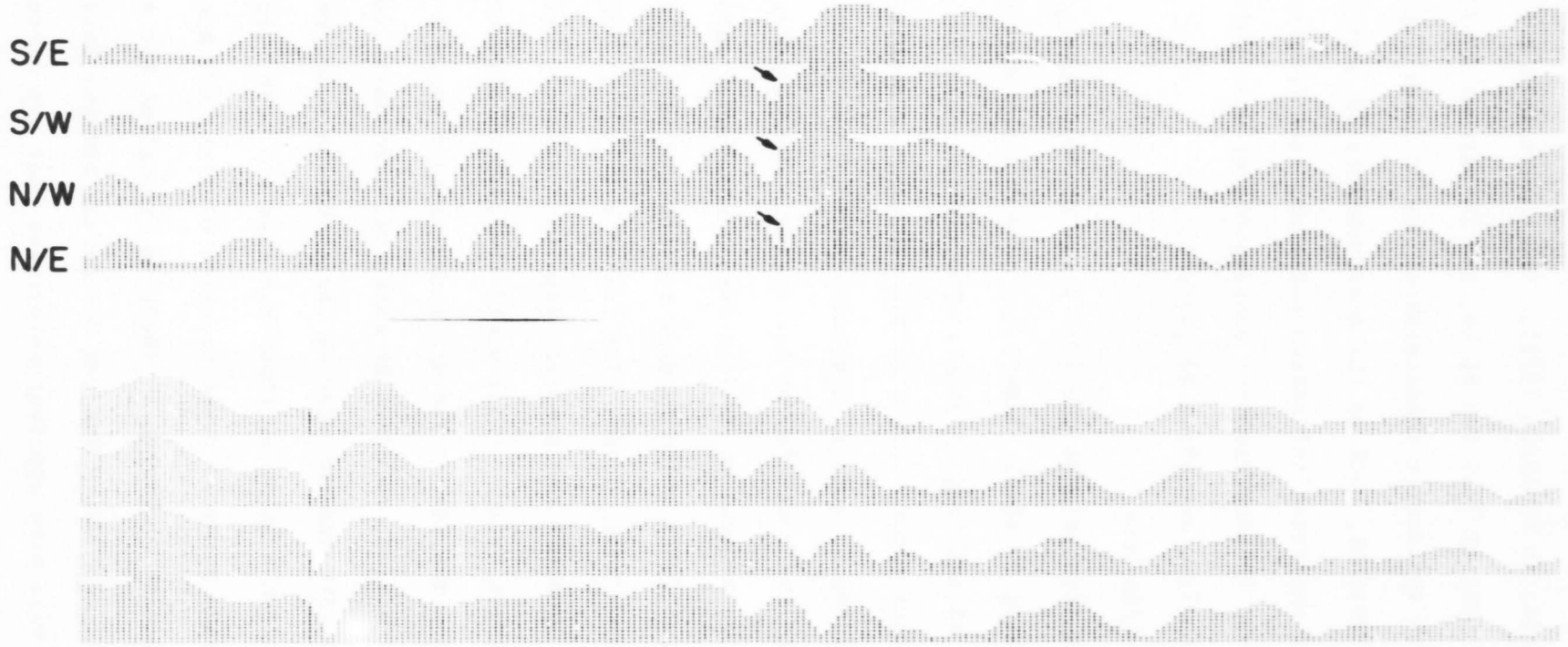

Figure 4.1 Plot of typical fading series measured at the four antennas. The time between samples is 0.4 seconds.

ORIGINAL PAGE IS
OF POOR QUALITY

series, but the varying periodicity in the fading series caused by variations in the size of the ionospheric irregularities will cause errors in the calculated correlation ellipse used in correcting the apparent velocity to obtain the true velocity. This is one of the major sources of error in the drifts winds analysis. This error can be reduced by selecting a shorter segment of the series sampled, where the fading process is stationary. This could only be done after the series is collected. Collecting a shorter time series would on average provide a number of series that are more stationary, but some of the series would be collected with a low degree of stationarity, yielding large errors in the characteristic ellipse used in calculating the true velocity of drifts from that fading series.

Because the four antenna quadrants are not sampled simultaneously, the delay in sampling three of the four quadrants must be taken into account. Since the fading in the D region generally exhibits slow variations (correlation coefficients down to 0.5 after about 5 seconds) compared with the sampling period of 0.4 seconds, and since the delays in sampling for the N/W, S/W, and S/E quadrants are 0.033, 0.066, and 0.099 seconds, respectively, a simple linear interpolation is justified.

4.2.1 *Noise reduction methods.* Noise is not as much of a problem in making drifts measurements as it is in the differential-absorption experiment, because correlations of fading series are being taken. Impulsive noise such as static discharges will cause a higher peak in the autocorrelation at zero lag. Errors in the autocorrelation function can cause errors in the characteristic ellipse, giving errors in the calculated true velocity. If all four quadrants were sampled simultaneously, static discharge noise would appear on all fading series at the same time, and thus would cause a higher cross correlation at zero lag. Because the four quadrants

are not being sampled simultaneously, and static discharge noise is not usually of long enough duration to appear on more than one fading series, no spurious peaks will be formed in the cross-correlation functions.

In order to devise some means of reducing the effects of noise on the correlation functions, the characteristics of the fading series were studied. It was noted that the amplitude of adjacent samples in the time series from the receiver never changed by more than 1/10 volt (about 3 points on Figure 4.1). One exception can be seen in Figure 4.1, at the arrows, where static discharge noise has contaminated the data from three of the four quadrants. Algorithms to eliminate such noise from a normal fading series were then devised. To test the usefulness of noise reduction algorithms, a fading series with static discharge noise and very little signal return was collected at a low altitude when a storm was nearby. Figure 4.2 shows the fading series with no noise reduction algorithm. Spikes in the series are shown at the occurrence of static discharges (the residual signal levels shown after the peaks are due to the linear interpolation used because the quadrants are not sampled simultaneously).

In noise algorithm 1, if the signal level at a sampline time changed by more than 50 (the increment 50 from the A/D converter output corresponds to an increment of 1/10 volt from the receiver output), then the mean of the level at the points before and after it were used in its place.

If: $|IDATA(I) - IDATA(I-1)| > 50$

Then set: $\frac{IDATA(I-1) + IDATA(I+1)}{2} = IDATA(I)$

Figure 4.3 shows the results of processing the noisy data set of Figure 4.2. The algorithm does reduce the level of the spike in half, but produces a long "tail" of residual noise.

ORIGINAL PAGE IS
OF POOR QUALITY

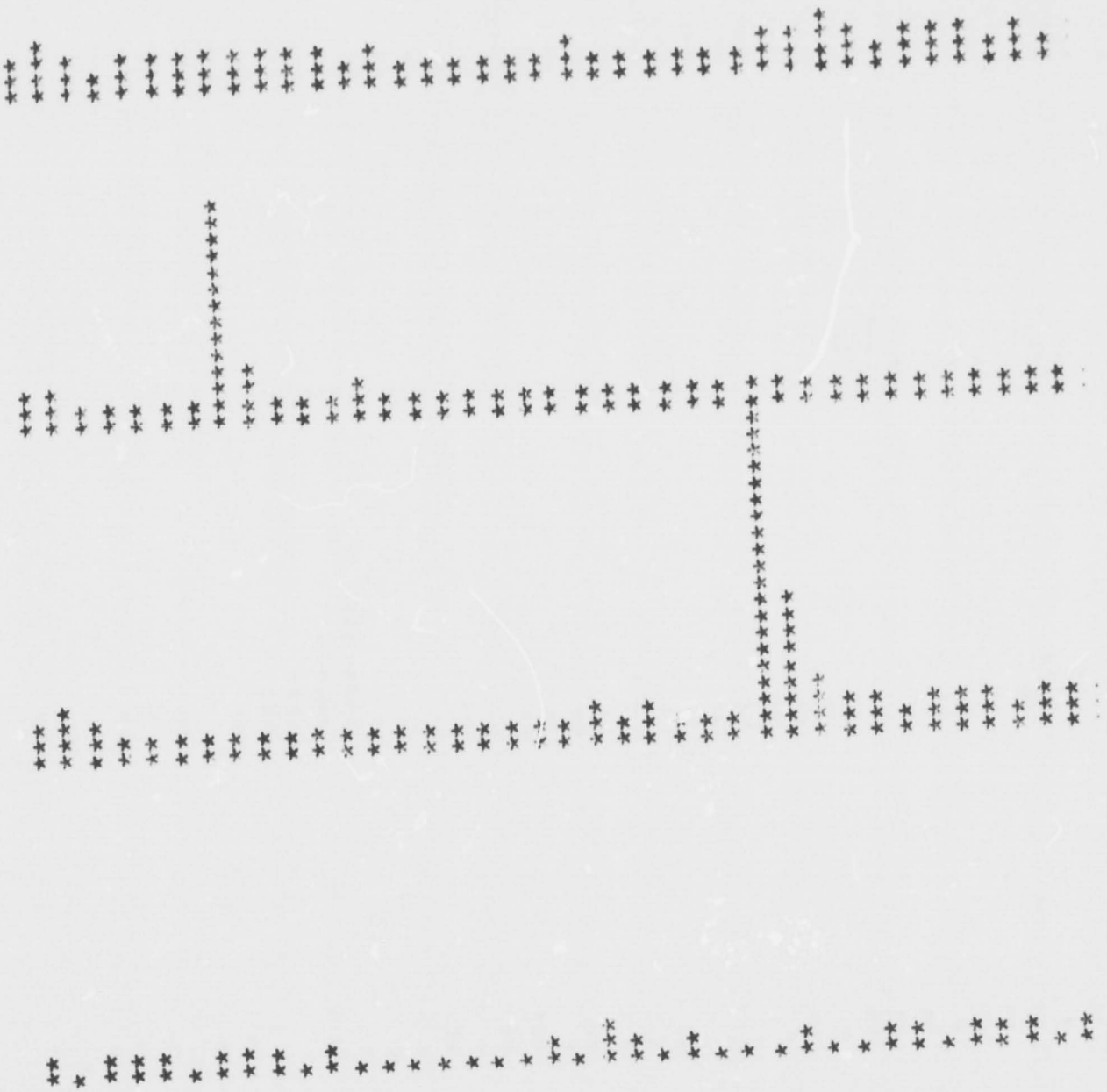

Figure 4.2 Noisy segment of a data file with no noise reduction algorithm.

ORIGINAL PAGE IS
OF POOR QUALITY

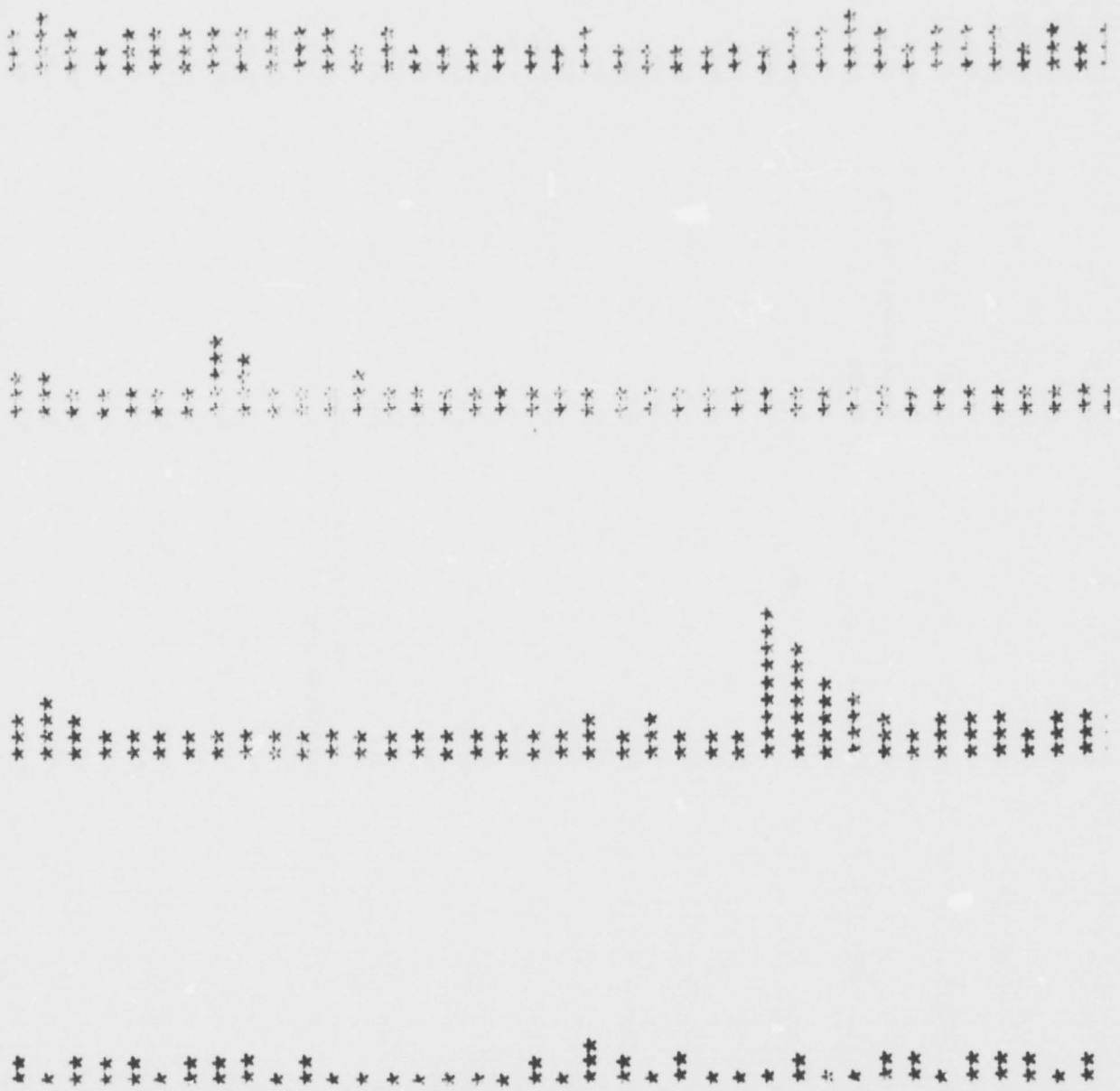

Figure 4.3 Noisy segment of a data file after processing with noise reduction algorithm 1.

To reduce the level of the spike to less than half its initial value, and to eliminate the "tail", algorithm 2 was developed. In this algorithm, if the level at a sampling time changes by more than 50 from the sample before it, then the magnitude of the change is limited to 50.

If: [IDATA(I) - IDATA(I-1)] > 50

Then set: IDATA(I) = IDATA(I-1) + 50

Or if: [IDATA(I) - IDATA(I-1)] < -50

Then set: IDATA(I) = IDATA(I-1) - 50

Figure 4.4 shows the result of putting the noisy data segment through this algorithm. The magnitude of the spike, and hence the possible error in the correlation functions calculated from the series has been reduced considerably. It should be noted that the noisy data used in testing shows the worst-case noise reduction capability of the algorithm, and with the returns at the desired level the average signal level is near one-half volt, so a noise spike saturating the receiver would be only a factor of two larger than the average signal level. Thus, the receiver is limiting the relative magnitude of a noise spike, making it more easily reduced by the noise algorithm.

4.2.2 *Drifts data analysis programs.* The data files collected by the collection programs DIFTHL and DRIFTH consist of 512-sample fading series, from four quadrants, sampled at six altitudes. Ten of these files will fit on a DECtape. The programs that have been written to process these data tapes are shown in Table 4.1. The program DRIFTP was written to read in the data file and process the series from one altitude to calculate the true velocity of the wind. When loaded the program will ask for the name of the file to be processed and then the height in kilometers to be processed. The form of the file names that have been used is CHECKXDAT, where X is a

ORIGINAL PAGE IS
OF POOR QUALITY

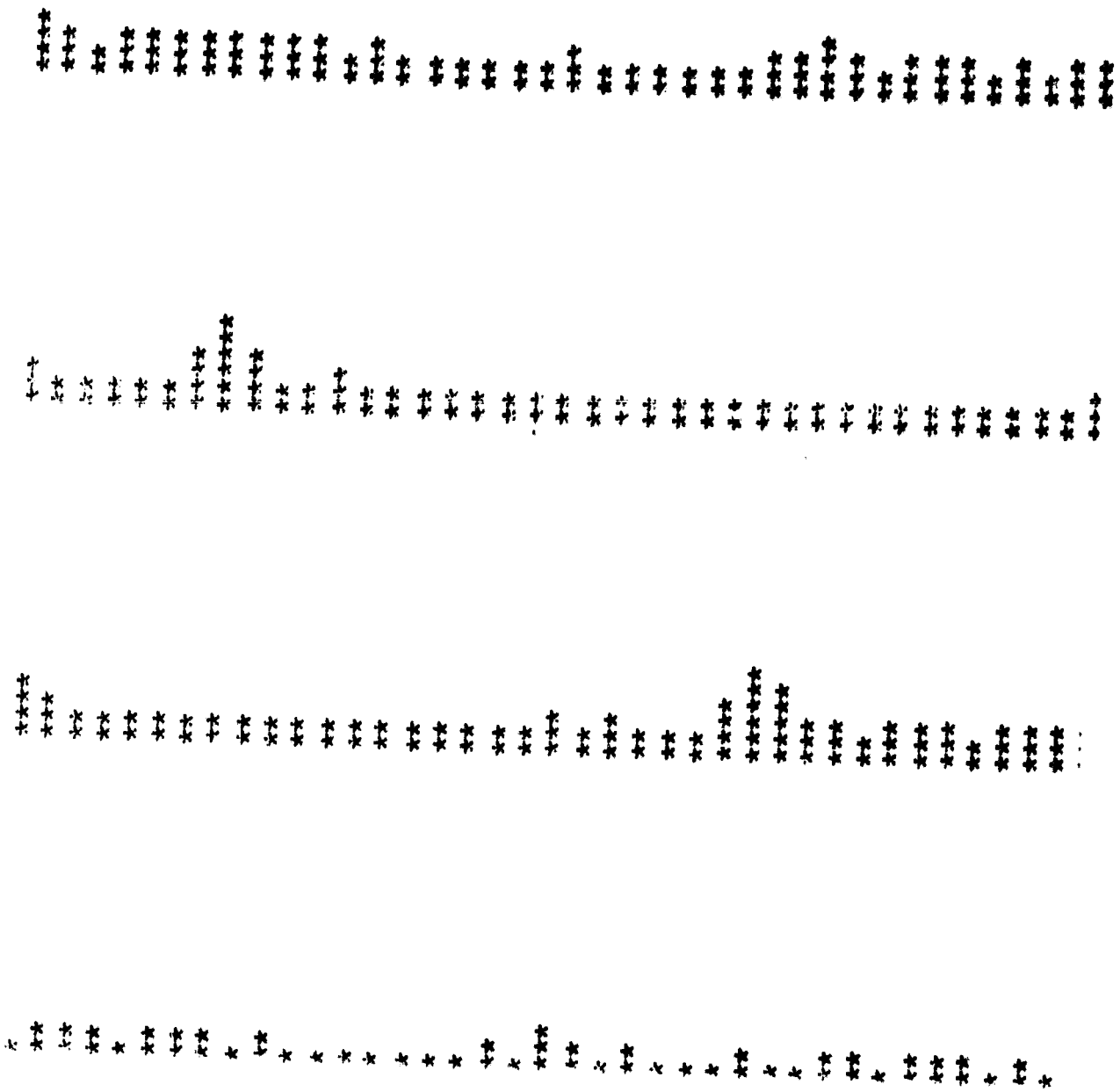

Figure 4.4 Noisy segment of a data file after processing with noise reduction algorithm 2.

TABLE 4.1 Drifts processing programs for data files collected by DRIFTL or DRIFTH data collection programs.

PROGRAM	SUBROUTINES	COMMENTS
DRIFTP		Processes a single altitude in a single file
	BRIGGS	Full correlation analysis
	BRIGS2	Continuation of BRIGGS
	CORLAT	Calculates correlations
	TAUCEF	Finds $\rho = 0.5$ on correlation curves
	MATS	Calculates correlation ellipse
	ARGUS	Calculates apparent drift
	ARCTAN, ANGLRN	Functions
	SEEK, CLOSE	System programs
DRIFTQ	Same as above	Processes a single file at all six altitudes
DRIFTR	Same as above	Processes all six altitudes for ten files on a tape
DRFTPL		Plots fading patterns at four antennas for one altitude
	PLOT	Plotting routine
	SEEK, CLOSE	System programs

number or the letter A. Thus, the ten files on a DECtape are identified by one through A. Processing a single altitude for all four antenna combinations (to be discussed later in this section) requires about ten minutes.

This program was later modified to process all six altitudes for a data file, and named DRIFTQ. When loaded, DRIFTQ will ask for the file name to be processed, and the altitude where processing is to begin. The processing is normally started at 70.5 km, and the program will automatically cycle through the six altitudes in the data file. If the processing needs to be interrupted, it can be restarted at any altitude desired. The time required to process all six altitudes is about one hour.

The program was again modified to automatically process a full DECtape of ten data files at all six altitudes. The time required to process a DECtape is about ten hours, and is usually done overnight, when the computer is not otherwise in use. This program was named DRIFTR. A good deal of effort was required to fit this full-correlation analysis program in the 32K of computer memory, and all but a few memory locations are in use. The operation of the program and the subroutines used to calculate the true velocity will be discussed next.

DRIFTR is first loaded with its subroutines onto disk 3 from the program DECtape labeled "DRIFTS PROCESSING". The binary code of the program on the tape has been named DR, and the required subroutines (listed in Table 4.1) have been renamed the numbers 0 through 8, for ease in loading. The DECtape to be processed is mounted onto tape drive 2. The computer device assignments for program loading are given by: A DK3 -4/NONE -5/DT2 2 (RETURN). The programs are loaded by the system GLOAD by typing in: ___DR, 0, 1, 2, 3, 4, 5, 6, 7, 8 (ESCAPE). The program will then load and execute. The program begins by reading in the data from the first file at

the lowest altitude. The files are assumed to be named CHECK1DAT through CHECKADAT. The data collection date, time, altitude, and receiver attenuation are read from the header on the data file and printed. Data on the file are written in blocks of 240 words. A block formed by the collection program consists of ten frames of data (four quadrants at six altitudes for ten frames gives 240 words). Thus, fifty-two reads are required to read in the full data file. While the file is being read, the data are stored in the array IDATA, which is dimensioned 4 (quadrant number) by 512 (sample number). Next, an interpolation is performed to correct for the fact that the four quadrants are not simultaneously sampled.

Because of the 33 ms spacing between pulses, the second, third, and fourth quadrant sampled are sampled 33, 66, and 99 ms later, respectively, than the first quadrant. The fourth quadrant sampling is a significant fraction (one-fourth) of the 0.4 second period assumed between pulses. The samples are corrected for this error by a linear interpolation. A sample of a relatively slowly varying function taken some amount of time after its assumed sample time contains a fraction of the level that would be sampled at the next assumed sampling time. To correct for this, the difference between the next sample and the current sample is multiplied by the fraction of the sampling interval that the particular quadrant is delayed and subtracted from the current sample.

The data are next processed by noise algorithm 2 to reduce impulsive noise. The average signal level for all four fading series is then summed and stored in the variable AVNOIS, and printed for use in determning the quality of the data. Since the full correlation analysis requires only three fading time series, the extra time series collected results in a four-fold redundancy in the data analysis. The four different groups of three

series can be analyzed separately to obtain four wind estimates (though not entirely independent). The data acceptance yield can be increased because of this redundancy, as the various data selection criteria of the full-correlation analysis are often not met by all four of the three-antenna correlation analyses. In the present data analysis, winds estimates for all of the four three-antenna combinations are made, and wind estimates of those that meet the data selection criteria are averaged to obtain the final true velocity wind estimate for that altitude.

The program DRIFTR cycles through the four three-antenna combinations, and calls the subroutine BRIGGS for each combination to calculate the estimate of true velocity. The subroutine BRIGGS and the other subroutines that it calls (listed in Table 4.1) are described in Appendix IV. The data selection criteria are also described there. Listings of the computer program DRIFTR and its subroutines are provided in Appendix V.

The antenna quadrant numbering convention, and an illustration of the antenna quadrant combinations used in the four separate wind estimates are shown in Figure 4.5. The autocorrelation function obtained at each of the four antennas is shown in Figure 4.6. The variation is due to the fact that each antenna sees a different fading sequence, which can have different characteristics than the others. A return signal diffraction pattern may have a line of little variation traveling across one antenna quadrant, causing a longer correlation time at that antenna. It should be noted that the correlation functions are seldom used beyond the fifth lag and the variation out to that lag is minimal. To remove this statistical variation, the average autocorrelation function from the average of the three autocorrelations is used for velocity calculations in the subroutine BRIGGS. The average autocorrelation function for each of the combinations of three antennas is

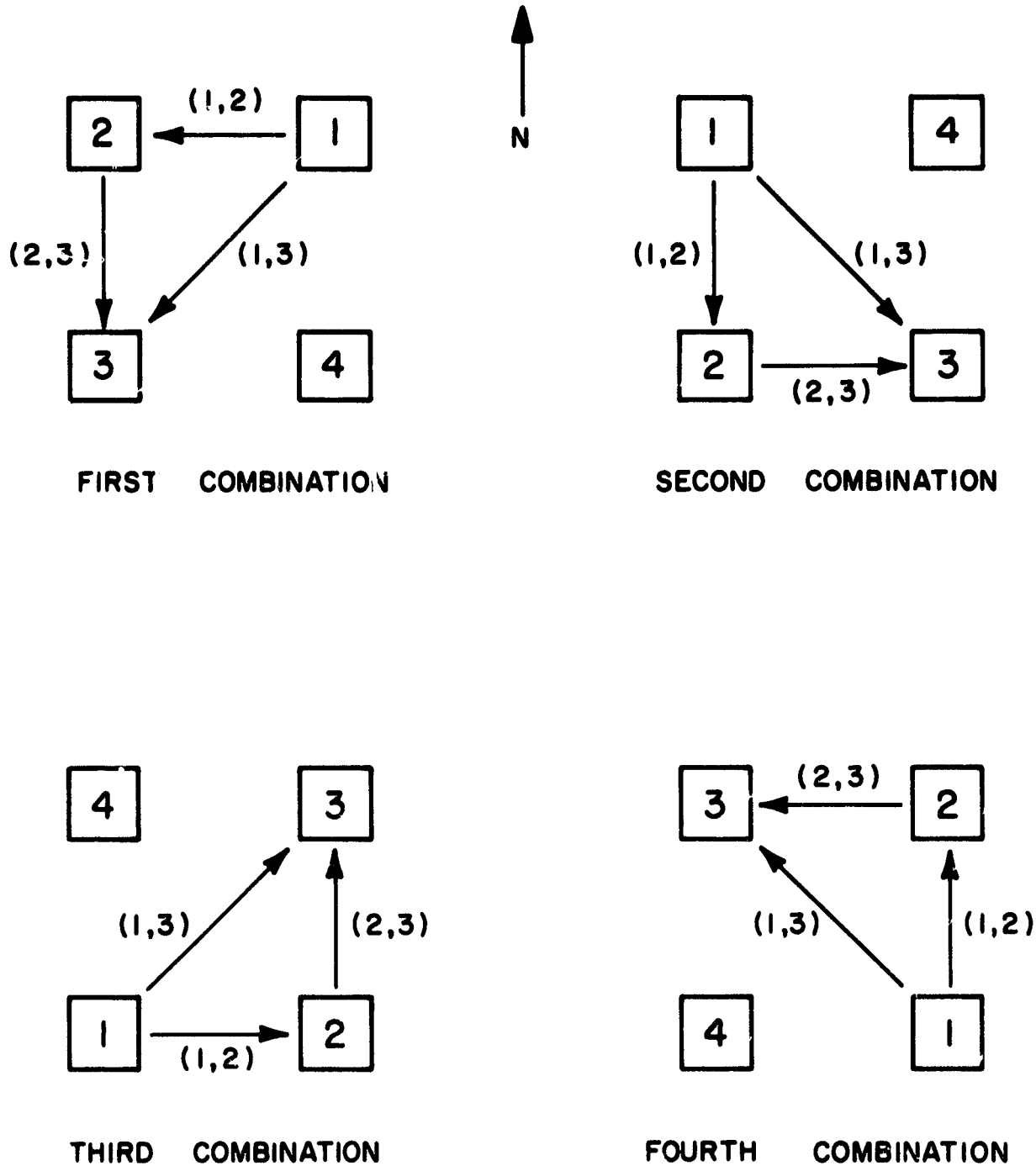

Figure 4.5 Antenna quadrant numbering convention used in the four wind estimates.

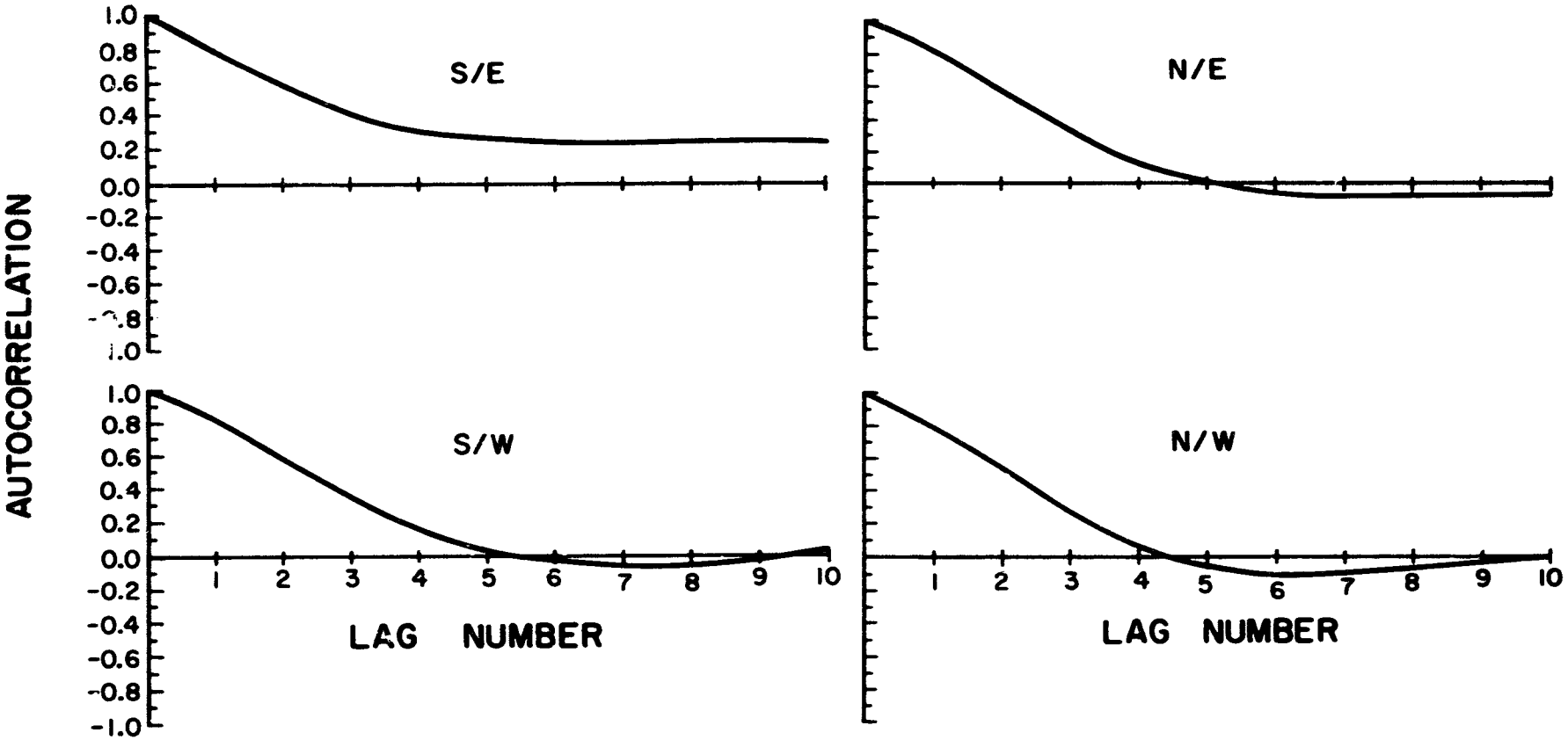

Figure 4.6 Autocorrelation measured from the fading series at each antenna quadrant.

shown in Figure 4.7. The average autocorrelation functions are very consistent out to the fifth lag.

The cross correlation functions for each pair of antenna quadrants are plotted in Figures 4.8 and 4.9. The individual plots are identified by the antenna combination number followed by the antenna pair numbers in parenthesis (see Figure 4.5). The apparent velocity along the line of any of these antenna pairs can be obtained from the lag number of the peak in the cross-correlation function. The antenna spacing is divided by the lag number times the sampling interval (.4 seconds). This velocity is reduced by a factor of one-half to obtain the corresponding ionospheric drift velocity.

The correlation functions obtained at Urbana (40°N) are smooth and symmetric, with a single peak. This leads to a straightforward analysis for the true velocity. MEEK et al. (1979) find that the correlation functions from data obtained at Saskatoon, Saskatchewan (52°N) are often irregular with multiple peaks, while those from Adelaide, Australia (31°S) are symmetrical and single peaked. They attribute the difference to the geographic location of the observing stations. There could be wind shears within the sampling volume, changes in the wind during data collection, or contamination by interference fading between two layers. The effect on a particular fading record may vary, but the cause seems to be a basic difference in the ionospheric conditions at the high-latitude location.

Having four velocity estimates from the fur combinations of three antennas to average will eliminate the errors introduced by using a non-isoceles triangular shaped antenna array (GOLLEY and ROSSITER, 1970; BEYNON and WRIGHT, 1969a,b). The each found a tendency for the correlation ellipse used in the true velocity to be aligned along the direction of the hypotenuse when right-angled triangles are used. This error can be removed when

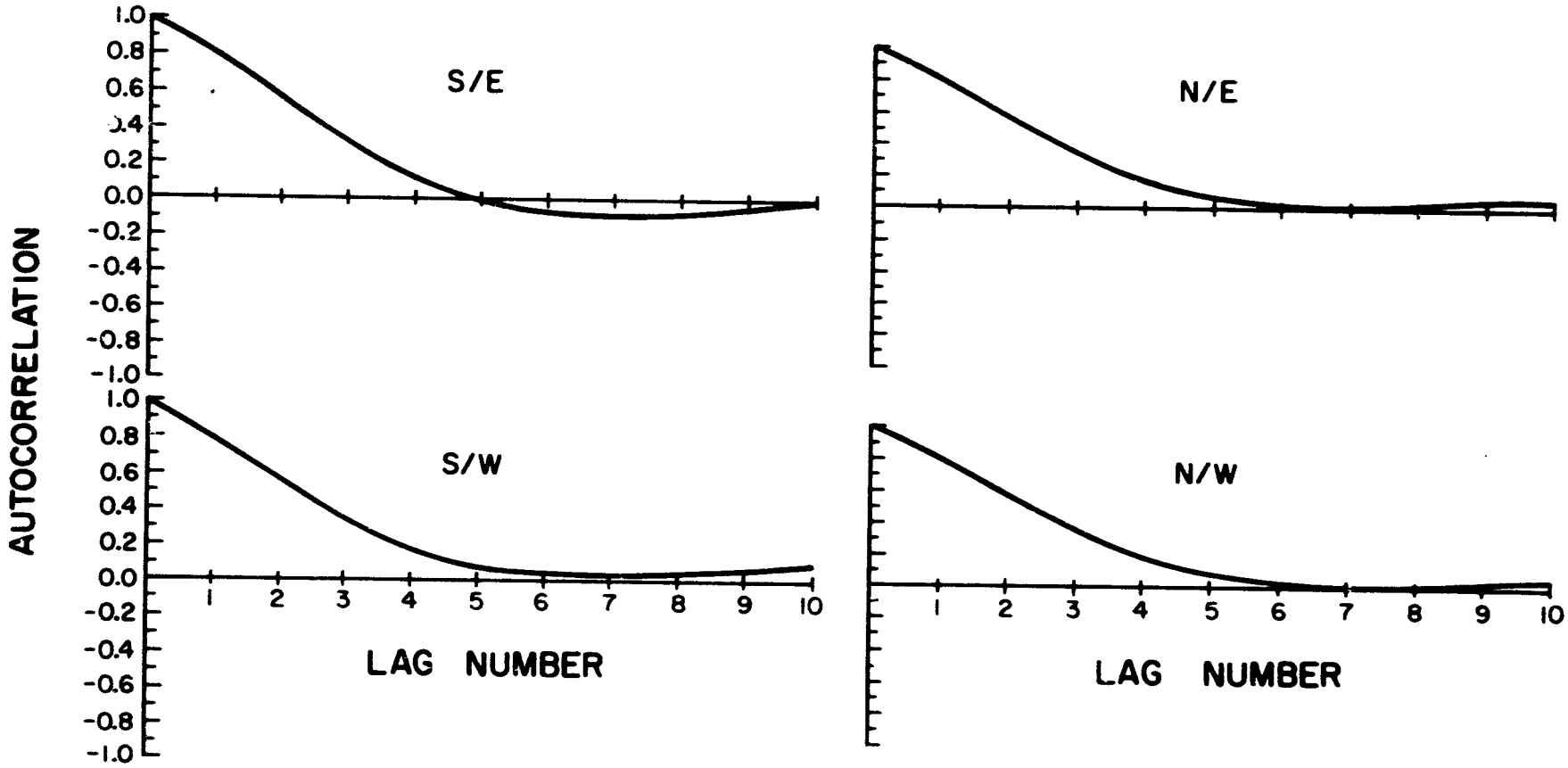

Figure 4.7 Average of the three autocorrelations for each of the four combinations of three antennas.

ORIGINAL PAGE IS
OF POOR QUALITY

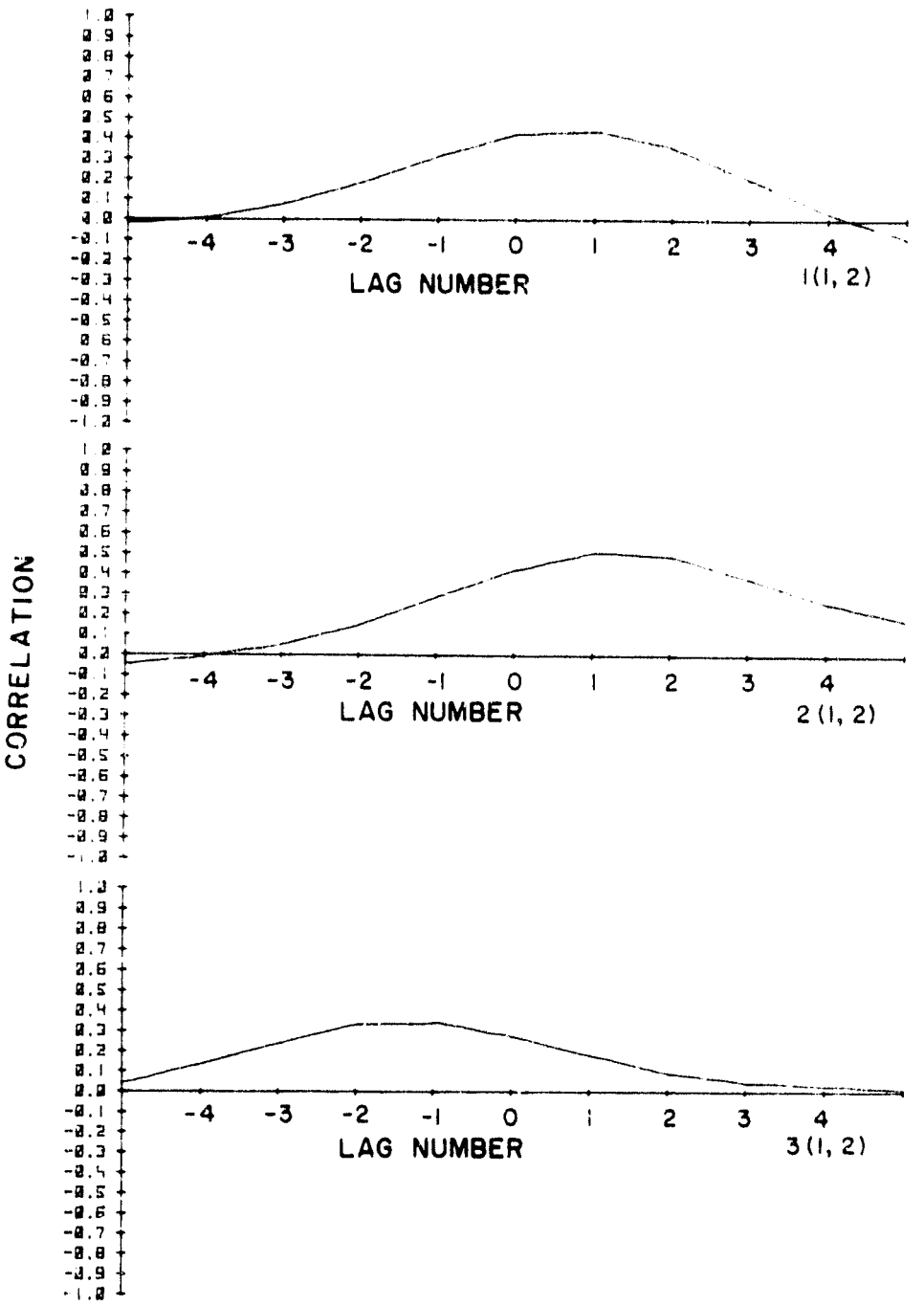

Figure 4.8 Cross-correlation functions for three pairs of antennas. (See text for numbering convention.)

ORIGINAL PAGE IS
OF POOR QUALITY

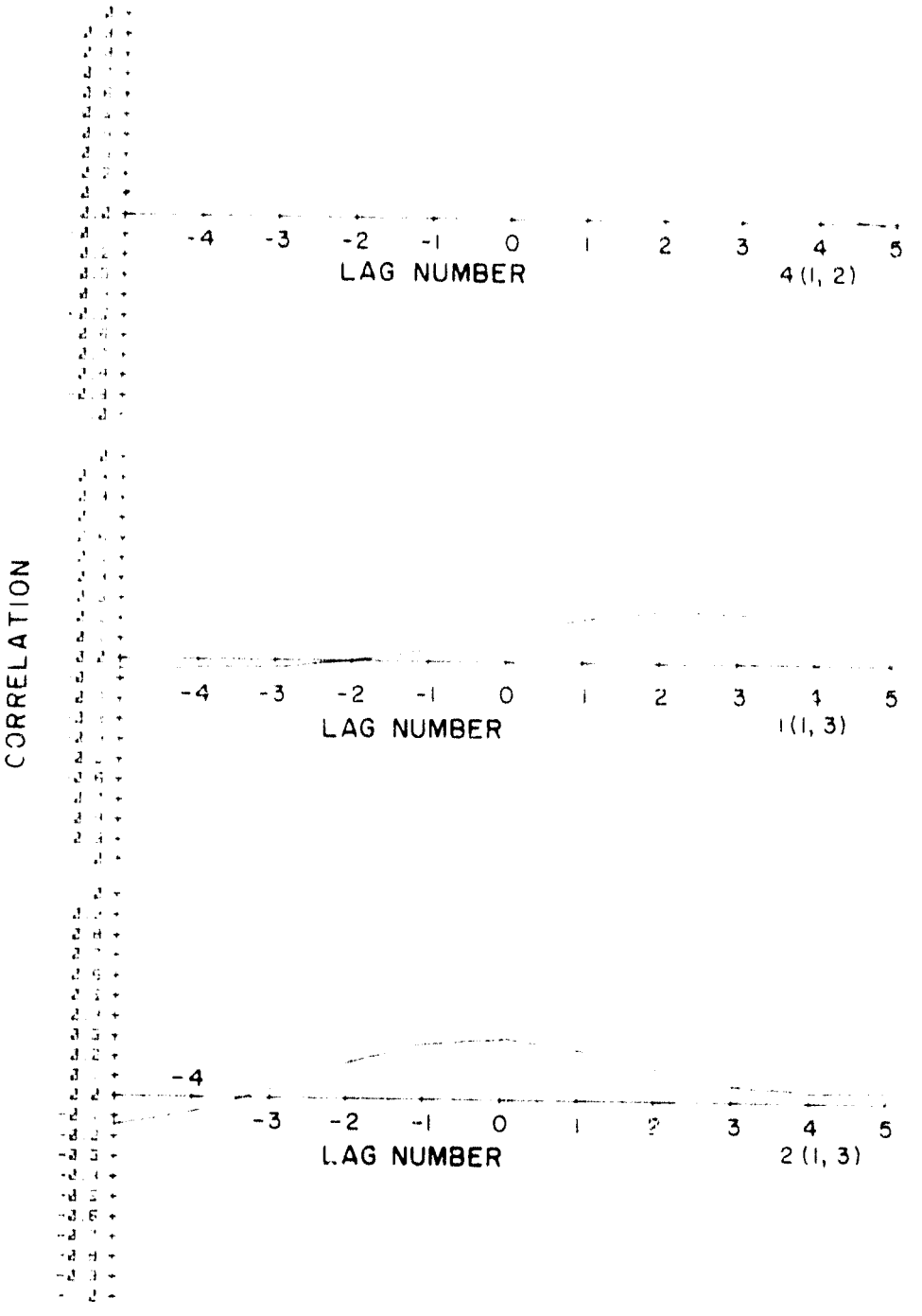

Figure 4.9 Cross-correlation functions for three pairs of antennas. (See text for numbering convention.)

the wind value calculated from a right triangle can be averaged with the wind value calculated from another right triangle, if the hypotenuse of one triangle is perpendicular to the hypotenuse of the other triangle.

The root mean square velocity difference from the four antenna combinations can be calculated to give a measure of the reliability of the wind measurements. To make this calculation, a random set of 85 pairs of true-velocity wind calculations from adjacent antenna triangles was analyzed. For each pair of adjacent triangles the difference in the wind magnitude was calculated and squared. The average of the 85 squared differences was taken to obtain the root mean square velocity difference. The wind directions were treated in the same way. This analysis yielded an uncertainty in wind magnitude of 17 m/s and in wind direciton of 28°.

The computer program DRFTPL was written to read a data file and plot the four antenna fading series, as in Figure 4.1. This is useful for checking the data at all antennas throughout the data file for low signal level, excessive noise, or receiver saturation. The program is loaded with the computer device assignment: A DK3 -4/NONE -5/DT2 2 (RETURN). The programs are loaded by the system program GLOAD by typing: ___ DRFTPL, PLOT (ESCAPE). The program will ask for the file name and then the altitude to be plotted. The subroutine PLOT prints the plot, one data frame of four antenna returns per line, on the DECwriter teletype. Each column on the printout corresponds to a voltage increment from the receiver output of 0.4 volt, and receiver saturation corresponds to the 20 columns alloted to each quadrant on the printout. A listing of the program is provided in Appendix V.

5. CHARACTERISTICS OF ELECTRON CONCENTRATIONS AND WINDS MEASURED AT URBANA

5.1

Electron concentration profiles have been measured daily near local noon at the Aeronomy Laboratory Field Station during the winter months since the fall of 1972. Data are collected for several days per month during the non-winter months. Diurnal data collection runs, starting in the morning and collecting data continuously until dusk are made on a regular basis on Quarterly World Days, and on other occasions to study the diurnal asymmetry in electron concentrations, and for observations of gravity waves.

Urbana is located at the latitude (40°) that is normally considered the low-latitude cutoff for observing the effects of the winter anomaly (ship-board ionospheric absorption measurements by SCHANING (1973) show the cutoff at 37-38°N, and those of SCHWENTEK (1976) show the cutoff at 40°N), but the electron concentration data obtained during the past years have always shown an increased variability during the winter months at Urbana.

Figure 5.1 is a plot of the coefficient of variation (standard deviation/mean) by month of electron concentrations at the three altitudes measured daily, during the months of October 1975 through September 1976. The increase in day-to-day variability shows itself as a clear increase in the coefficient of variation during the winter months of November, December, January, and February.

The A_{∞}/A ratio, whose logarithm represents the total differential absorption occurring below that altitude, gives a good indication of the total electron content below that altitude. At this location, the A_{∞}/A ratio at 81 km can be reliably measured under daylight conditions. Since there is little ionization below 60 km (and certainly relatively far less than will simultaneously be found from 60 to 81 km), the A_{∞}/A ratio at 81 km will be

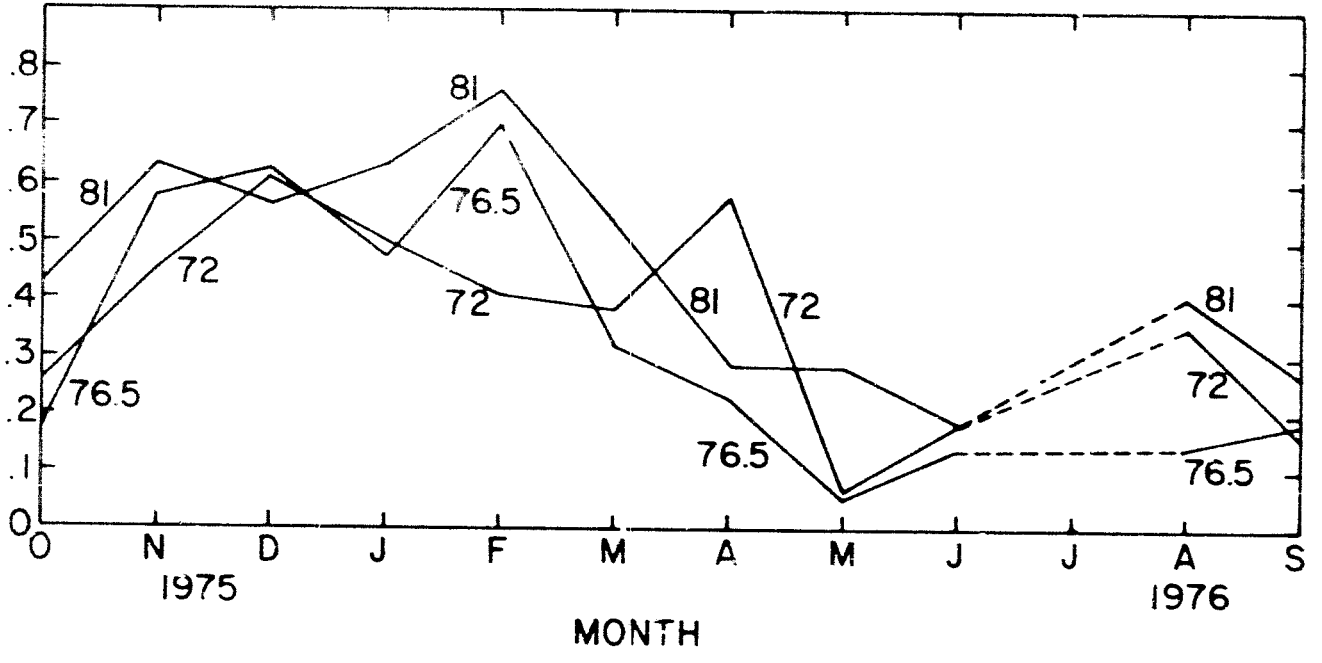

Figure 5.1 Coefficient of variation of electron densities at 72, 76.5, and 81 km, by month, of daily values.

affected mainly by the electron content from 60 to 81 km, and thus will be a good indicator of the D-region electron content below 81 km. The A_x/A_o ratio is inversely proportional to the electron content, so that a low A_x/A_o value indicates a high electron content.

Evidence of increased winter-time variability is demonstrated in Figure 5.2. The figure contains histograms of the A_x/A_o ratio at 81 km for each of the months from November 1979 through March 1980. The distributions in the months of December, January, and February are much more broad than those found in the months of November and March. Data from the other seven winters of data indicates that the increase in variability in general also starts in the latter part of December, and continues through the month of February.

Plots of daily values of electron concentration at 72, 76.5, and 81 km, and the A_x/A_o ratio at 81 km will be shown in Chapter 9, when these data are compared with wind measurements.

5.2 Data Collection Schedules

The main purpose of the data collected at Urbana has been for the study of the winter anomaly. This requires the collection of data over a sufficient length of time to average out short-term fluctuations due to the effects of gravity waves. A collection time of about one hour has become standard. The one-hour data collection yields 15 individual electron concentration profiles, which is not a long enough time series for an analysis of gravity wave activity at that time. This analysis would require a few dozen points in a continuous time series. Many diurnal data collection runs of sufficient length have been made for the study of gravity waves.

The partial-reflection drifts system was completed in the fall of 1978, and winds data have been collected daily following the differential-

ORIGINAL PAGE IS
OF POOR QUALITY

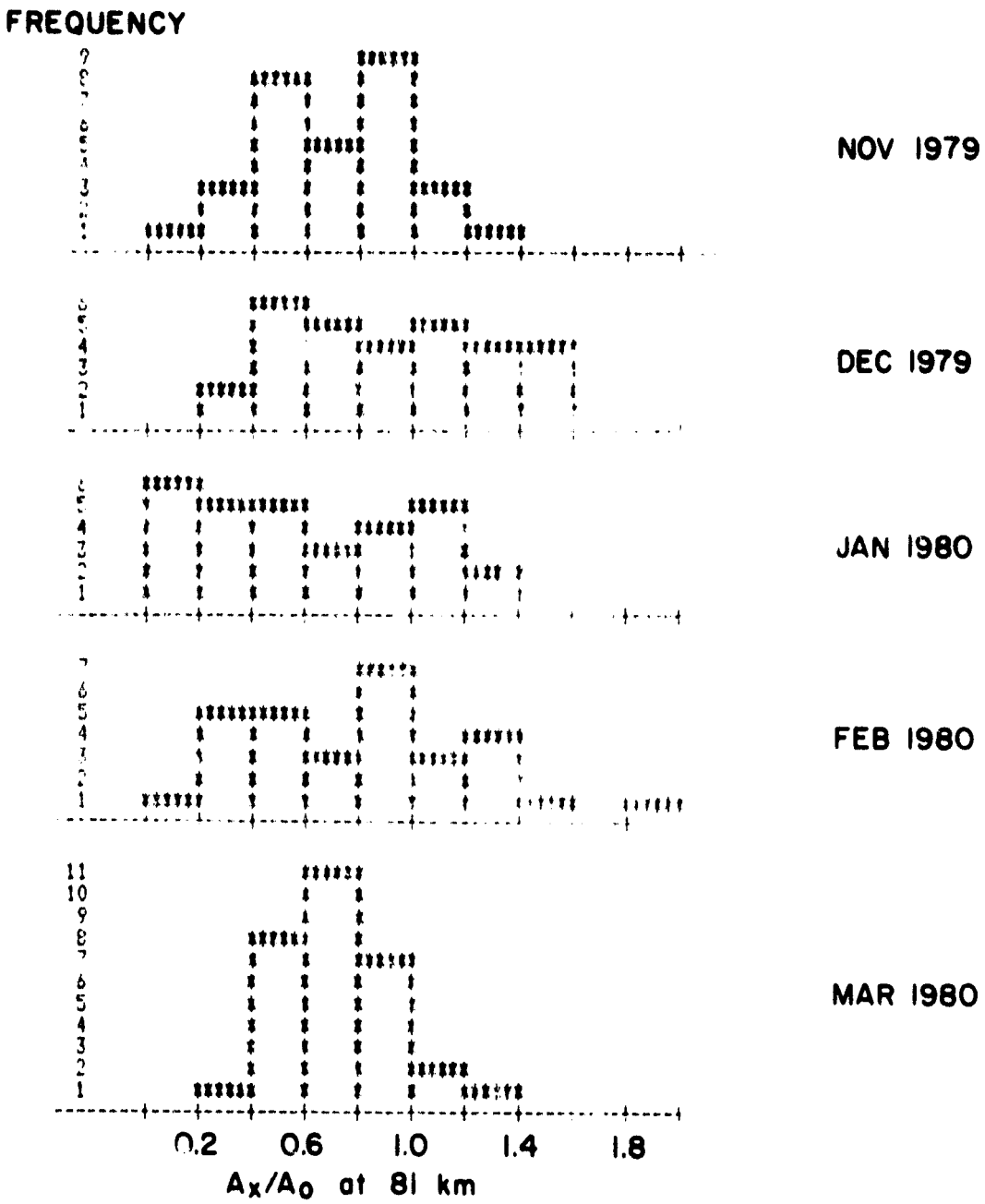

Figure 5.2 Histograms of A_x/A_o at 81 km by month for the year 1979/1980.

absorption data collection near noon for the winter months. During the diurnal data collection runs a wind profile was obtained every hour. The number of winds profiles collected per day was increased to three during the winter of 1980/1981. The Urbana meteor-radar system was operating for many days during the past several years, and winds obtained by that system are available for comparison with data obtained by the partial-reflection system. The meteor radar system runs are continuous runs lasting for several days, and breaks are made in their collection for one hour near local noon to allow the computer to be used for the collection of partial-reflection data. On several occasions during the winter and summer of 1980/1981 data were collected with the Urbana coherent-scatter system on the same day with the partial-reflection system. Because the coherent-scatter antenna pointing direction has a small horizontal component towards the southeast, that system can measure the southeast component of horizontal wind. The results of the comparisons with the coherent-scatter data show a general agreement in wind velocity measurements.

5.3 *Characteristics of Electron Concentration and Wind Measurements Made During the Winter of 1978/1979.*

The drifts experiment equipment was in operation starting on December 26, 1978, and data collection started on that date. Table 5.1 shows the data collection schedule for the winter of 1978/1979. From December 27, 1978 through January 10, 1979 data were collected for nine hours per day, from 0800 through 1700 local standard time. The normal electron concentration data collection program, which runs for about 55 minutes, was run continuously throughout the day with the extra five minutes per hour used for collection of a drifts wind profile. The collection program prints out an electron concentration profile every 3.4 minutes, and the long time series

TABLE 5.1 Data collection schedule for the winter of 1978/1979.

Electron concentration (N) and drifts wind data	
DEC 26, 1978	1 hour N, 1 wind profile
DEC 27-JAN 10, 1979	9 hours N, 9 wind profiles
JAN 11-FEB 22	1 hour N, 1 wind profile
FEB 23-MAR 1	9 hours N, 9 wind profiles
MAR 2-APR 16	1 hour N, 1 wind profile

Meteor radar wind data
JAN 11, 1979-JAN 21, 1979
FEB 19, 1979-FEB 20, 1979

formed from these data are used to study the effects of wave motions, and the diurnal asymmetry in electron concentrations. The nine drifts wind profiles, collected for as much of the day for which returns can be obtained from the D region at this location, are averaged together to provide a single estimate of the prevailing wind.

Following the diurnal data collection runs, the meteor-radar system was operating for the next ten days, providing a good measurement of the 24-hour prevailing wind. Data collected for the remainder of the winter consisted of one hour of electron concentration data followed by a single drifts wind profile, except for the period of February 23 through March 1, where diurnal data collection runs were made. A partial solar eclipse occurred (76% obscuration at Urbana) on February 26, 1979.

5.4 *Characteristics of Electron Concentration and Wind Measurements Made During the Winter of 1979/1980*

Table 5.2 shows the data collection schedule for the winter of 1979/1980. During this winter, one hour of electron concentration data followed by a single drifts profile were collected from November 4, 1979 through April 15, 1980, except for the diurnal data collection runs of February 26 through March 11, 1980. Meteor-radar wind data are available for 22 days during this winter, as listed in Table 5.2.

5.5 *Characteristics of Electron Concentration and Wind Measurements Made During the Winter of 1980/1981*

During this winter there were many days when the meteor-radar system and the coherent-scatter system were operated, providing opportunities for comparison of data obtained by these systems. Table 5.3 shows the data collection schedule for each of these experiments. Data from the partial-reflection experiment were, in general, collected from December 1, 1980

TABLE 5.2 Data collection schedule for the winter of 1979/1980.

Electron concentration (N) and drifts wind data

NOV 4, 1979-FEB 25, 1980 1 hour N, 1 wind profile

FEB 26, 1980-MAR 11, 1980 6 hours N, 5 wind profiles

MAR 12, 1980-APR 15, 1980 1 hour N, 1 wind profile

Meteor radar wind data

JAN 10, 1980-JAN 24, 1980

FEB 16, 1980-FEB 22, 1980

MAR 13, 1980-MAR 25, 1980

TABLE 5.3 Data collection schedule for Fall 1980 through Summer 1981.

Electron concentration (N) and drifts wind data

DEC 1, 1980-DEC 5, 1980	1/2 hour N, 1 wind profile
DEC 6, 1980-DEC 15, 1980	2 hours N, 3 wind profiles
DEC 16, 1980-DEC 19, 1980	1/2 hour N, 1 wind profile
DEC 20, 1980-JAN 19, 1981	2 hours N, 3 wind profiles
JAN 20, 1981-JAN 23, 1981	1/2 hour N, 1 wind profile
JAN 24, 1981-FEB 2, 1981	2 hours N, 3 wind profiles
FEB 3, 1981-FEB 8, 1981	1/2 hour N, 1 wind profile
FEB 17, 1981-FEB 19, 1981	1/2 hour N, 1 wind profile
AUG 3, 1981-AUG 4, 1981	3 N and 3 wind profiles

Meteor radar wind data

DEC 2, 1980 - DEC 5, 1980

DEC 16, 1980-DEC 19, 1980

JAN 20, 1981-JAN 23, 1981

FEB 3, 1981 - FEB 8, 1981

FEB 17, 1981-FEB 20, 1981

Coherent scatter data

NOV 11, 1980

DEC 10, 11, 22, 23, 1980

JAN 14, 15, 16, 26, 27, 28, 29, 1981

AUG 3, 4, 1981

through February 19, 1981. During this winter, the daily data collection time was doubled. A drifts wind profile was first made, followed by an hour of electron-concentration data collection, a winds measurement, a second hour of electron-concentration data, and ending with a third winds measurement. By averaging the three wind profiles for each day, the effects of many of the short-term fluctuations can be removed, providing a better estimate of the 24-hour prevailing wind. This collection procedure was modified to fill about one hour during the 20 days that the meteor-radar system was operating.

6. COMPARISONS OF ELECTRON CONCENTRATIONS AND PARTIAL-REFLECTION DRIFTS WINDS

6.1 *Introduction*

In this chapter, the correlation of electron concentrations at Urbana and drifts winds at Urbana will be discussed. A positive correlation between southward meridional winds and increasing electron concentration would be consistent with the theory that the transport of ionizable minor constituents contributes to the increased variability in electron concentration in the D region.

A previous study of the relationship between meridional winds and electron concentrations measured at the same location was made by MEEK and MANSON (1978), at Saskatoon, Saskatchewan. Their comparison was made using data from 1-3 hour sets of data taken near noon from 11 days in January and February, 1976. Winds were calculated using the full-correlation analysis of the drifts data, and a differential-absorption system was used to determine the electron concentration profiles. They did not find that the peaks in electron concentration were obviously connected with the wind direction. Cross correlations between northward wind components and electron concentrations at the same altitude were computed. The largest correlations were shown at 73 km, with a correlation of -0.46 (60% significance level of -0.44 (58% significance level). They were not able to determine if the variation in ionization was due to a quasi-continuous auroral activity leading to a latitudinal gradient in NO over Saskatoon, or that strong auroral events produced isolated accumulations of NO at higher latitudes which could be sported to Saskatoon. The first theory would predict little time delay between changes in the meridional wind and changes in electron concentration. The second theory would predict a time delay

corresponding to the time required to transport NO from the region of auroral activity to Saskatoon.

FRASER et al. (1981) made a study of the relationship between the meridional winds and electron concentrations measured at the same location in the southern hemisphere (at Christchurch, New Zealand, 44°S). They measured winds using a partial-reflection drifts system operating 24 hours per day, and electron concentrations were measured near noon by the differential absorption technique. During the winter of 1978 they obtained 22 days of data and calculated the correlation between the daily winds and electron concentrations. The highest correlation was found between the electron concentration at 65-75 km and the meridional wind at 80 km, with the significance at the 1% level. The other correlation observed that was significant was between the electron concentration at 60-65 km and the 85 km winds (significant at the 10% level). They found that there was no time delay between the winds shifting more towards the north and the electron concentration increasing. This would indicate a gradient with latitude of NO concentration. The fact that the greatest correlation was found for winds data measured higher in altitude than the electron concentration indicates that a downward vertical transport is present as well.

In the next three sections, data obtained by the Urbana partial-reflection system will be analyzed to determine the relationship between variability in electron concentration and the winds in the D region.

6.2 *Observations From the Winter of 1978/1979*

During the winter of 1978/1979, data were collected from 0800 through 1700 local standard time, for fifteen consecutive days. In this analysis the winds obtained every hour throughout the day were averaged together. The winds at the six altitudes measured (in 3-km intervals, from 70.5 to 81

km) were averaged together to provide a measure of the average prevailing wind for the day in the D region. The electron concentrations used in the comparison represent one-hour averages taken around noon. This represents data from fifteen individual electron-concentration profiles.

Figure 6.1 is a plot of the daily values of electron concentration at 72, 76.5, and 81 km, the A_x/A_o ratio at 81 km, and the meridional wind component, for the fifteen-day period. The theory that southward transport of NO enhances electron concentrations would predict a peak in electron concentration at points where the meridional wind was southward (a minimum on the figure). When comparing the winds with the electron concentration at 72 km, in two-thirds of the cases a stronger southward wind results in a higher electron concentration. At 76.5 km there is little relation evident between the electron concentration and the winds. At 81 km the magnitude of the electron concentration is not directly related to the magnitude of the wind, but an increase in southward wind from one day to the next will usually result in a higher electron concentration on the second day. The best correlation is evident when comparing the winds with the A_x/A_o ratio at 81 km. The A_x/A_o ratio at 81 km is inversely related to the electron concentration, so that a high northward wind should result in a high A_x/A_o ratio. A high degree of correlation can be seen in the figure, with increases in northward wind almost always correlated with increases in the A_x/A_o ratio.

To investigate the relationship between the electron concentration the horizontal wind in two dimensions, the vector winds and A_x/A_o ratio are shown in Figure 6.2. The N/S wind component is shown along the vertical axis (up is northward) and the E/W wind component is shown along the horizontal axis (to the right is eastward). The vector winds show that the E/W component is eastward for all but one of the fifteen days, as would be

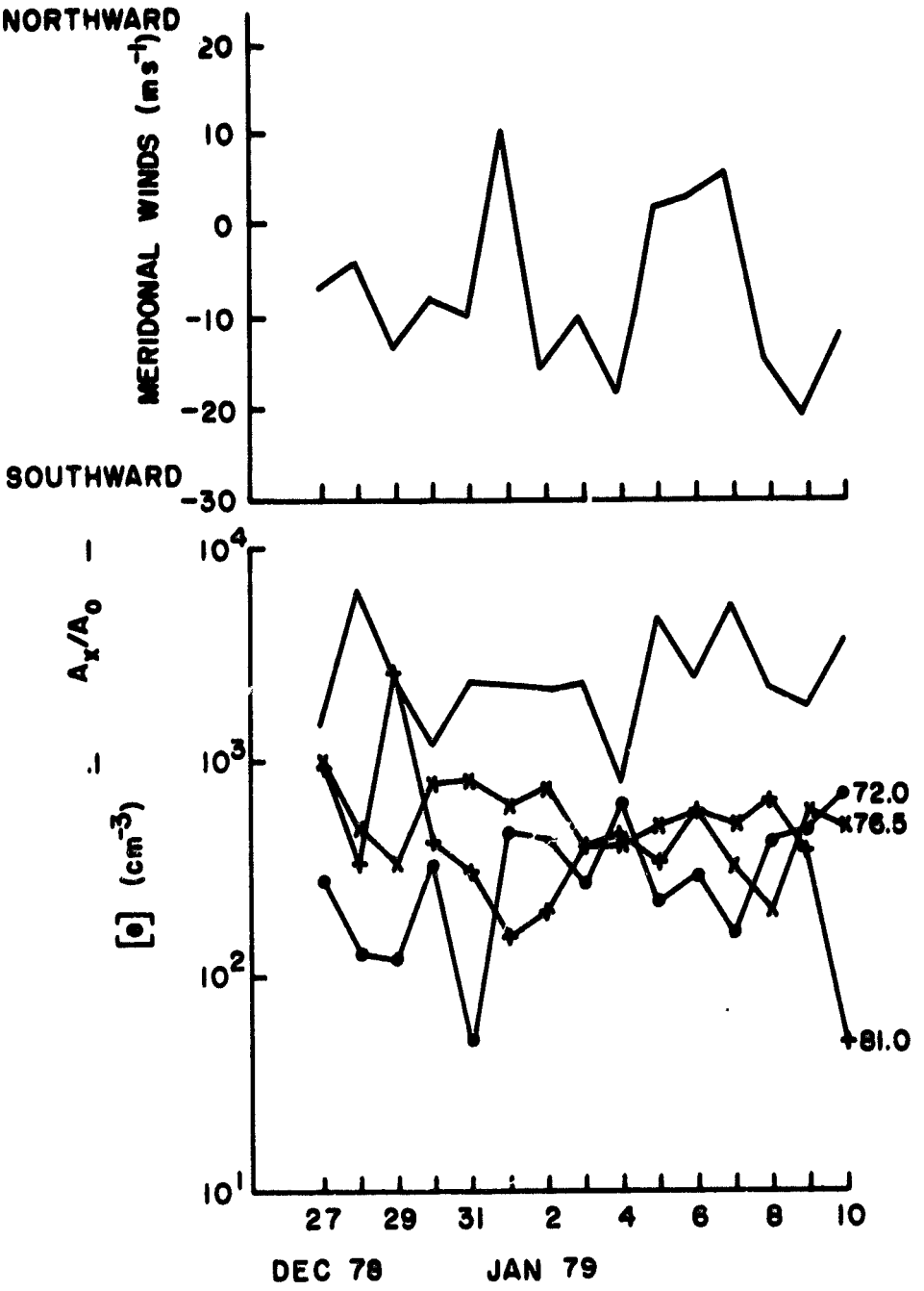

Figure 6.1 Daily plot of noon electron density at 72, 76.5, and 81 km, A_x/A_o at 81 km, and 70.5 to 81 km meridional winds for December 27, 1978 through January 10, 1979.

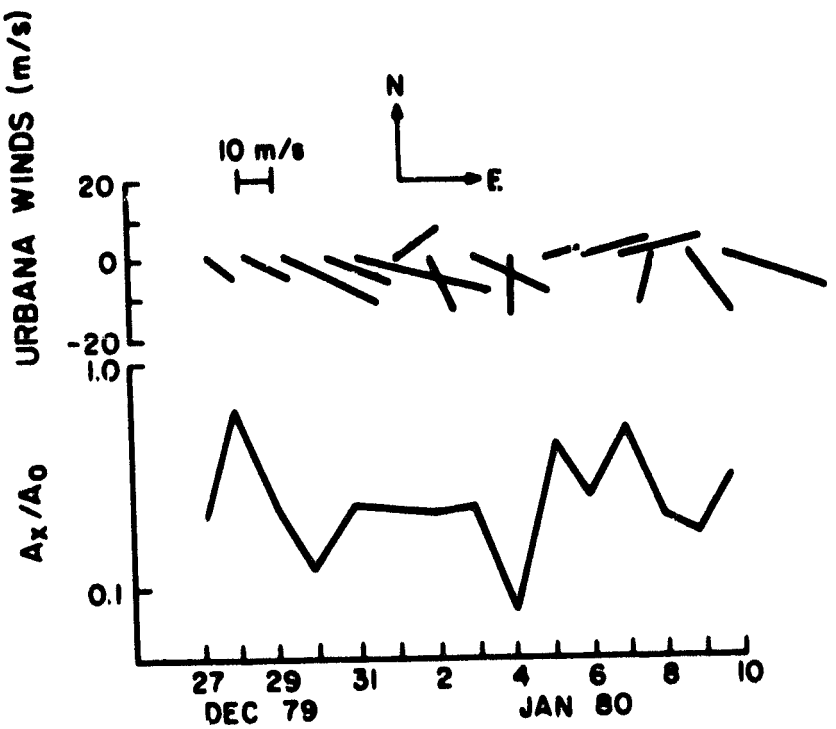

Figure 6.2 Vector D-region winds and A_x/A_o ratio at 81 km, by day.

expected for winter-time circulation. There does not appear to be any relationship between the zonal winds and the A_x/A_o ratio.

Figure 6.3 shows scatter plots of the electron concentration at the altitudes of 72, 76.5, and 81 km versus the N/S wind component. The correlation coefficient and significance level are shown for each altitude on the figure. The correlation between the winds (northward positive) and electron concentrations would be negative to support the transport theory. The only altitude that shows a reasonable correlation is 72 km, with a correlation that is significant at the 20% level. The lack of correlation could be due to the fact that the electron concentration at a single altitude is determined by many factors (wave activity, vertical transport), and that this analysis should be done over a large interval of altitude (as in using the A_x/A_o ratio for comparison), or that the scatter in the electron concentration data is added due to errors in calculating the concentrations from the A_x/A_o profile.

Figure 6.4 shows scatter plots of the electron concentration at 72, 76.5, and 81 km versus the E/W wind. Again, the only significant correlation is shown at 72 km with a level of significance of 15%. The electron concentrations are shown to be correlated with a decrease in the normal eastward zonal wind. FRASER et al. (1981) noted a similar correspondence, with enhanced northward wind and decreased eastward wind (in the southern hemisphere).

Scatter plots of the A_x/A_o ratio at 81 km and the D-region N/S and E/W wind components are shown in Figure 6.5. The correlation between the A_x/A_o ratio at 81 km and the N/S winds is significant at the 7% level. This result supports the theory that horizontal transport is a major cause of the winter anomaly. The correlation between the A_x/A_o ratio at 81 km and the

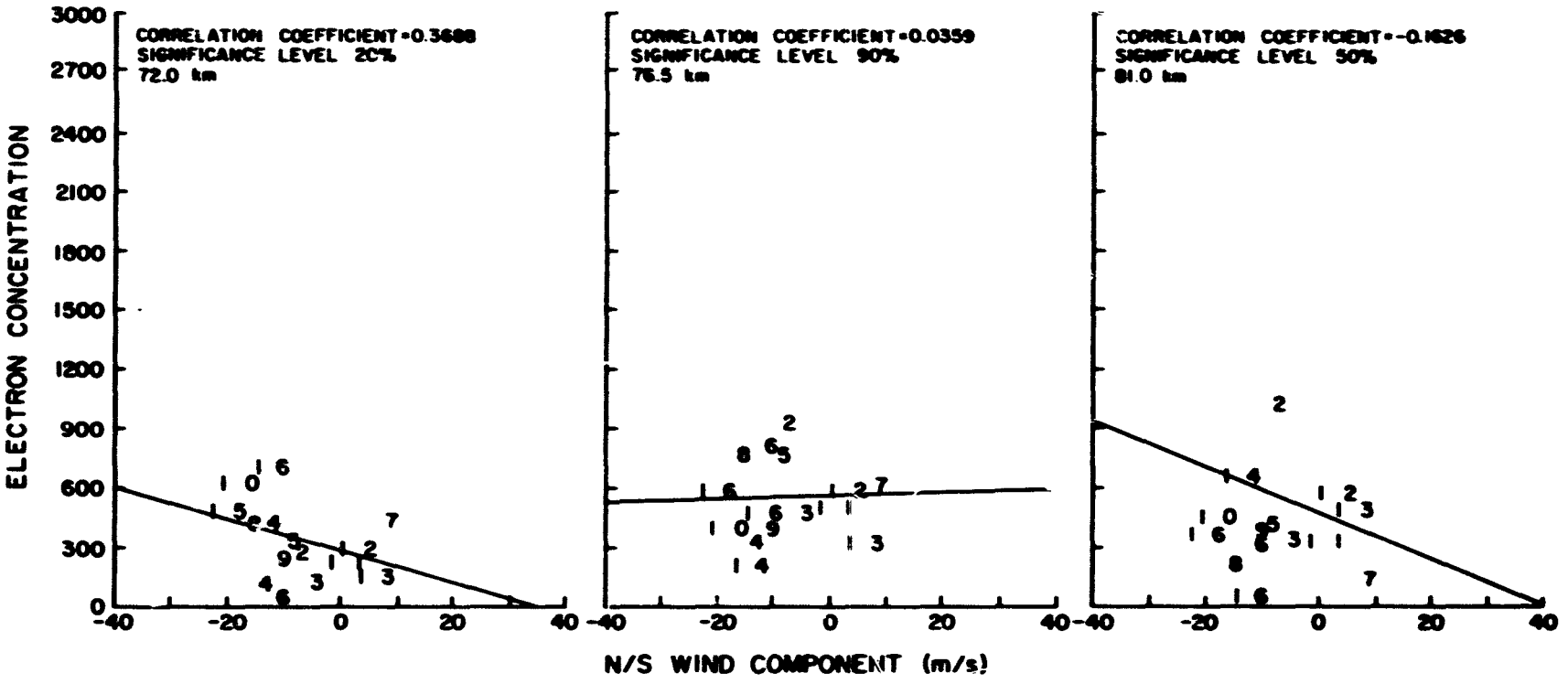

Figure 6.3 Scatter plots of the electron concentration at 72, 76.5, and 81 km versus the north/south wind.

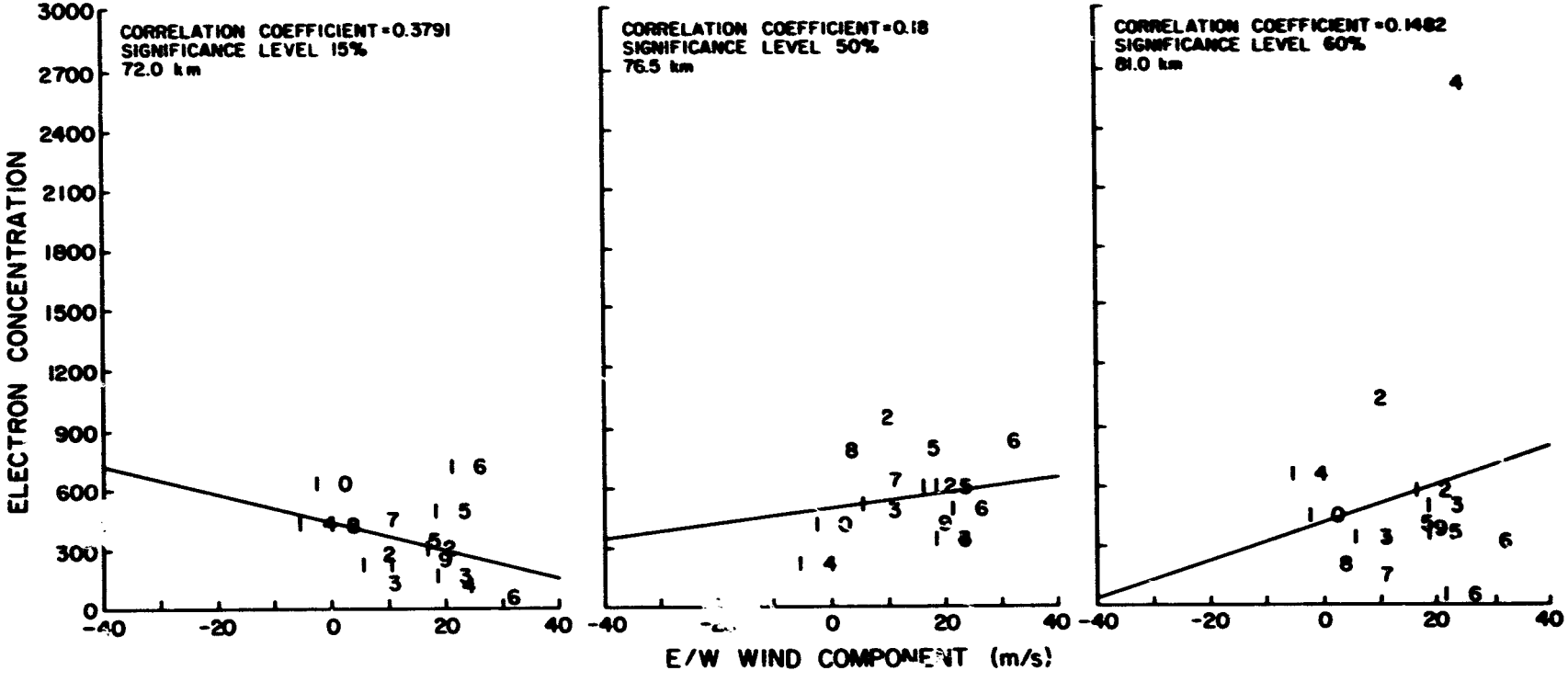

Figure 6.4 Scatter plots of the electron concentration at 72, 76.5, and 81 km versus the east/west wind.

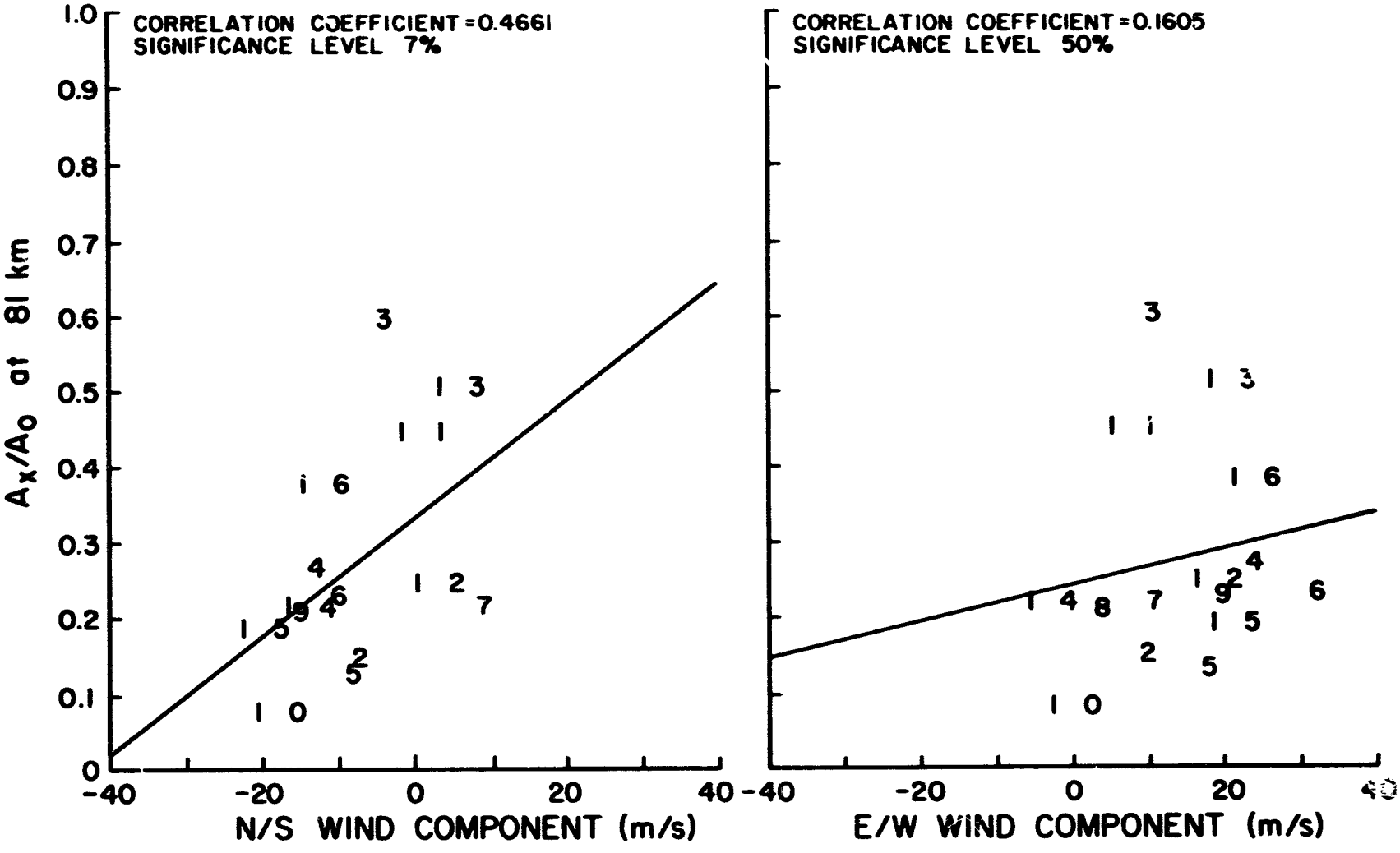

Figure 6.5 Scatter plots of the A_x/A_o ratio at 81 km and the N/S and E/W wind components.

E/W component of wind is not significant.

To identify a possible time delay between a change in meridional wind and a corresponding change in electron concentration, the A_x/A_o data series was shifted in time in the range of -2 days to +4 days, in one-day increments, and correlations were calculated. Figure 6.6 shows scatter plots of the A_x/A_o ratio at 81 km and the N/S wind component, with the A_x/A_o data shifted by the number of days indicated on each plot. For example, in the plot labeled A_x/A_o (-2 days), the A_x/A_o data series starting on December 26 is correlated with the N/S wind data series starting on December 28. The correlation coefficient and significance level are printed on the plot for each shift. The only correlation that is nearly significant is shown for A_x/A_o (+2 days), with a negative correlation coefficient. This result indicates that there is little time delay between a change in the meridional wind and a change in the electron concentration, suggesting a latitudinal gradient in nitric oxide such that the concentration north of Urbana is greater than that at Urbana. Thus, a shift in the wind at Urbana results in a shift in the electron concentration with a delay that is less than one day.

Following the diurnal data collection period, the daily collection time was reduced to about one hour per day, with 15 electron concentration profiles, and one wind profile being collected. Figure 6.7 shows the daily value of the meridional wind component and the electron concentration at 72, 76.5, and 81 km, and the A_x/A_o ratio at 81, for the period of January 10 through January 31, 1979. A 5-day running mean of the wind values was computed and plotted on Figure 6.7 also, to help remove the effects of irregular wind measurements due to wave motions, etc. No obvious correlation can be seen between the winds and the electron concentrations or the A_x/A_o

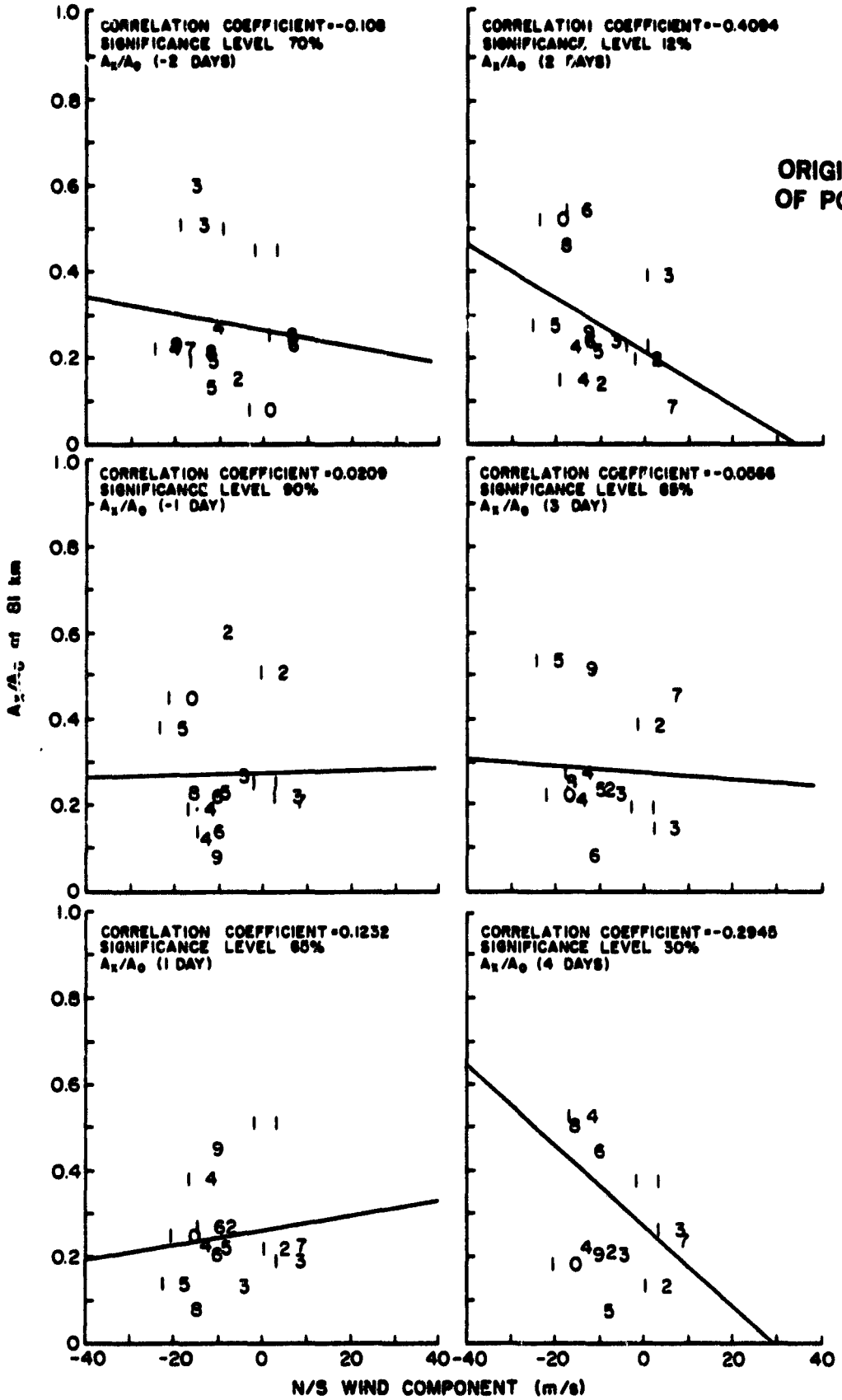

ORIGINAL PAGE IS
OF POOR QUALITY

Figure 6.6 Scatter plots of the A_x/A_o ratio at 81 km and the N/S wind component, with the A_x/A_o. Data shifted by the number of days indicated on each plot.

ORIGINAL PAGE IS
OF POOR QUALITY

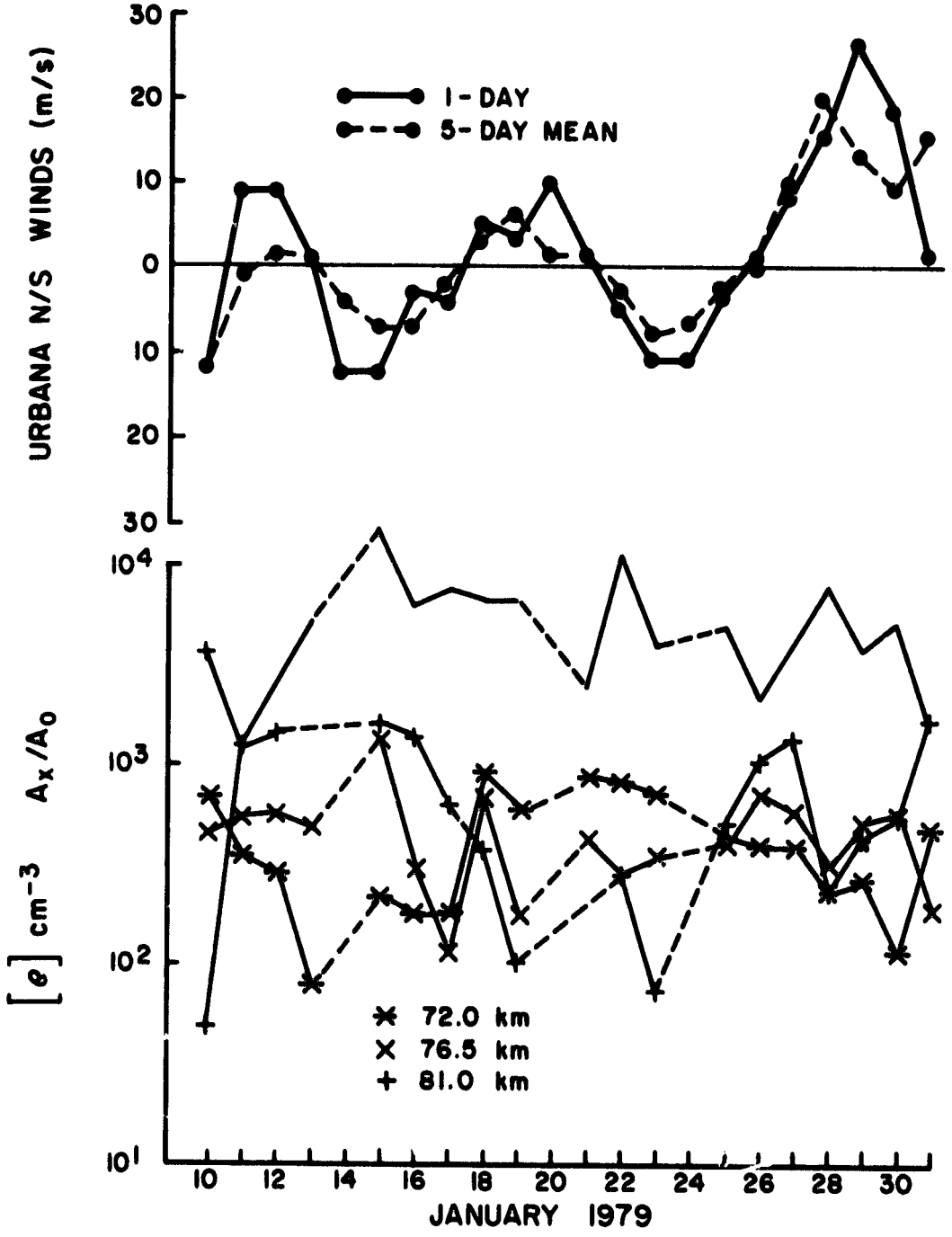

Figure 6.7 Daily meridional wind values and the electron concentration at 72, 76.5, and 81 km, and the A_x/A_o ratio at 81 km, for the period of January 10 through January 31, 1979.

ratio. This indicates that a single wind profile is not in general a good indicator of the 24-hour prevailing wind. MANSON et al. (1978) compared noon winds consisting of the median of up to 12 soundings with daily mean winds, and found that below 100 km the 24-hour wind was well predicted by the noon winds, Figure 6.8 shows data obtained similarly in the month of February, 1979, at Urbana. Again, there is little correlation between the 5-day mean of single noon winds and the A_x/A_o ratio.

Another series of diurnal data collection runs was made for seven days from February 23 through March 1, 1979. The winds plotted on Figure 6.8 (heavy line section) for that period represent an 8-hour average taken during the daylight hours. When comparing the N/S winds with the A_x/A_o ratio at 81 km there is no systematic correlation. To demonstrate this, the scatter diagram of Figure 6.9 was plotted. There is no correlation evident between the N/S winds and the A_x/A_o ratio at 81 km, this is not necessarily in contradiction with the theory that the winter anomaly is a result of the transport of nitric oxide from the auroral zone for two reasons. First, the observed wind variability may be only a local variation. In order for transport of an atmospheric constituent to take place over the 2000 km path from the auroral zone to Urbana, the winds would have to be consistently southward over the long distance. This effect may occur only during the passage of a large-scale disturbance such as a planetary wave, which can propagate upwards to the mesosphere only during winter. Second, the lifetime of nitric oxide is longer during the winter months, which allows it to be transported over the long distance only during the winter. The main loss mechanism of nitric oxide in the upper D region and lower E region is the photodissociation process, so the lifetime of nitric oxide is significantly longer during the winter months because of the lower solar zenith angle and

ORIGINAL PAGE IS
OF POOR QUALITY

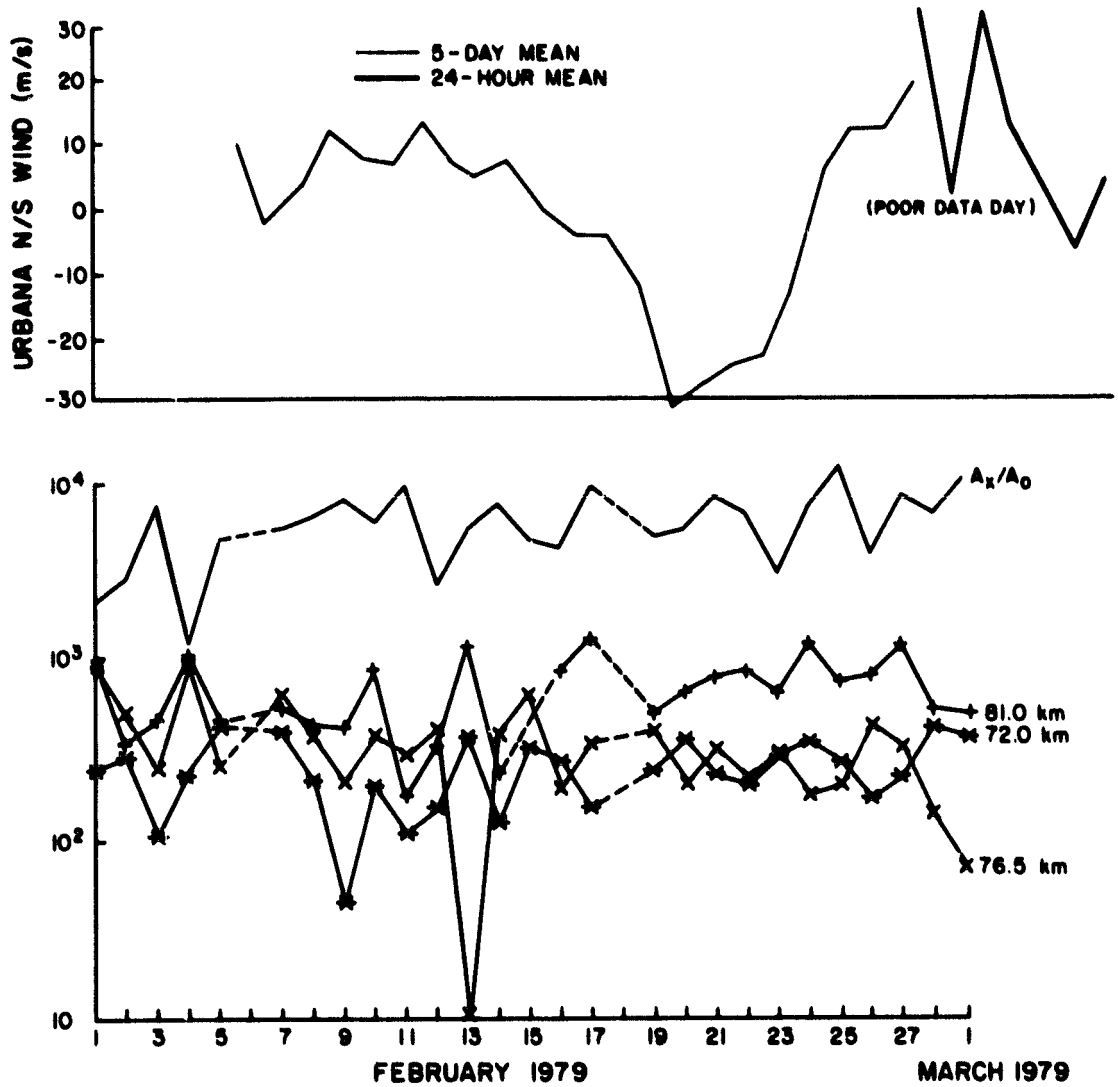

Figure 6.8 N/S winds and electron concentration at 72, 76.5, and 81 km, and the A_x/A_O ratio at 81 km for February 1979.

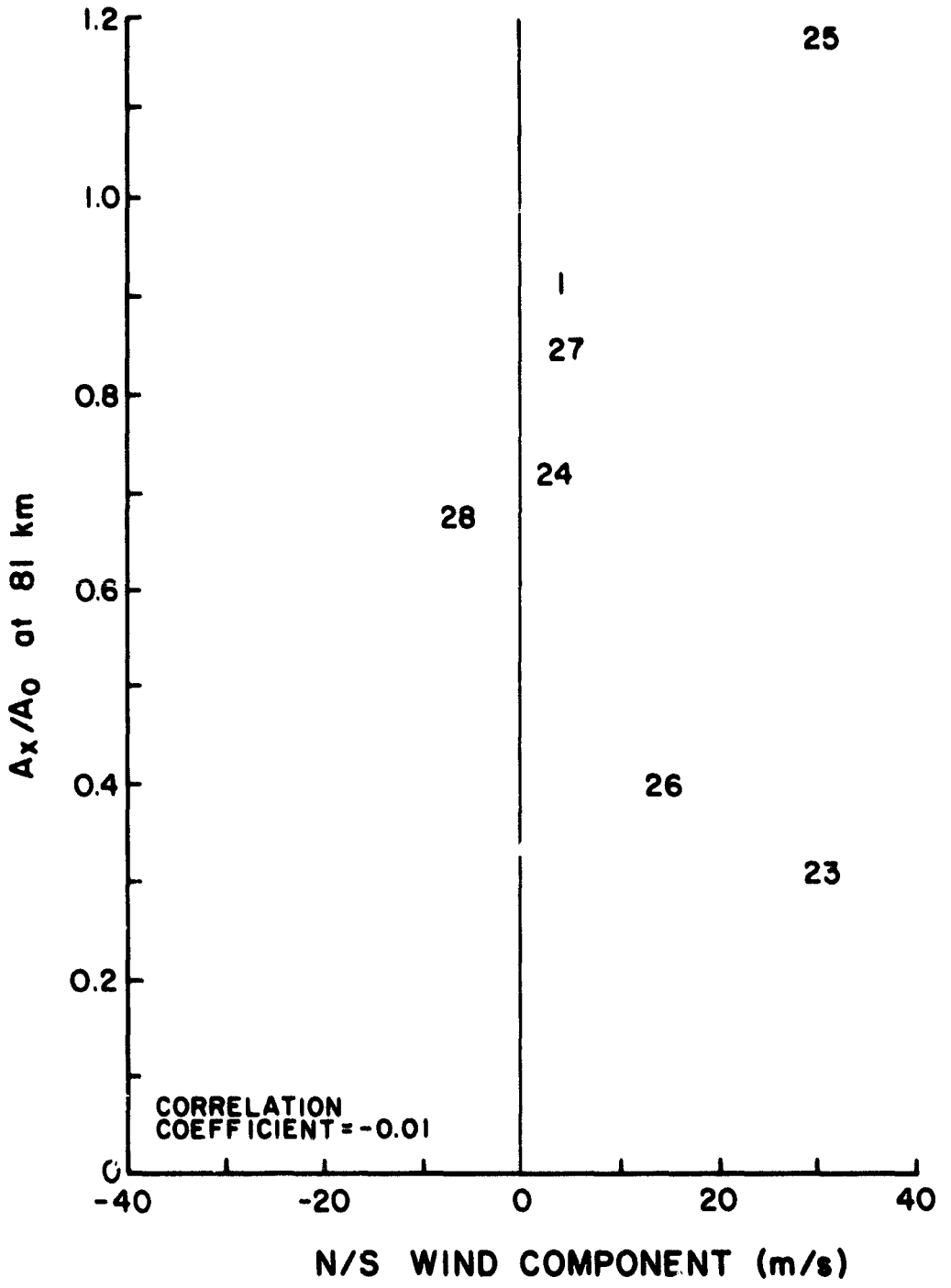

Figure 6.9 Scatter plot of meridional wind and A_x/A_o ratio at 81 km for the period of February 23 through March 1, 1979.

shorter days (see Chapter 1). Planetary wave propagation will be discussed in Chapter 8, and comparisons of winds observed at two distant stations will be shown in Chapter 9.

6.3 *Observations From the Winter of 1979/1980*

During the winter of 1979/1980, data collection took place for one hour, with one winds profile, during most of the winter season, except for the period of February 26 through March 11, 1980, where diurnal data were obtained. Figure 6.10 shows the N/S winds and the A_x/A_o ratio at 81 km for the diurnal data collection period. Again, these data were taken during a non-winter period, and no correlation can be seen between the winds and the A_x/A_o ratio.

6.4 *Observations From the Winter of 1980/1981*

During this winter data were taken for two hours daily, with the wind value for each day being the average of three wind measurements spaced through the two-hour collection period (the winds are averaged over the sampling window of 75 to 90 km). This should provide a wind estimate that more closely approximates the 24-hour prevailing wind, and a value for the A_x/A_o ratio at 81 km that is less affected by variations due to wave motions such as gravity waves.

Figure 6.11 is a plot of the daily N/S and E/W wind components and the A_x/A_o ratio at 81 km for December 1980. There is no apparent correlation between the N/S winds and the A_x/A_o ratio at 81 km, during any part of the month, even if one of the plots is shifted in time by a day or two. There is a strong negative correlation evident between the eastward wind component and the A_x/A_o ratio at 81 km during the period of December 6 through December 21. The daily values of N/S and E/W wind components and the A_x/A_o ratio at 81 km for January 1981 are shown in Figure 6.12. Again, there is

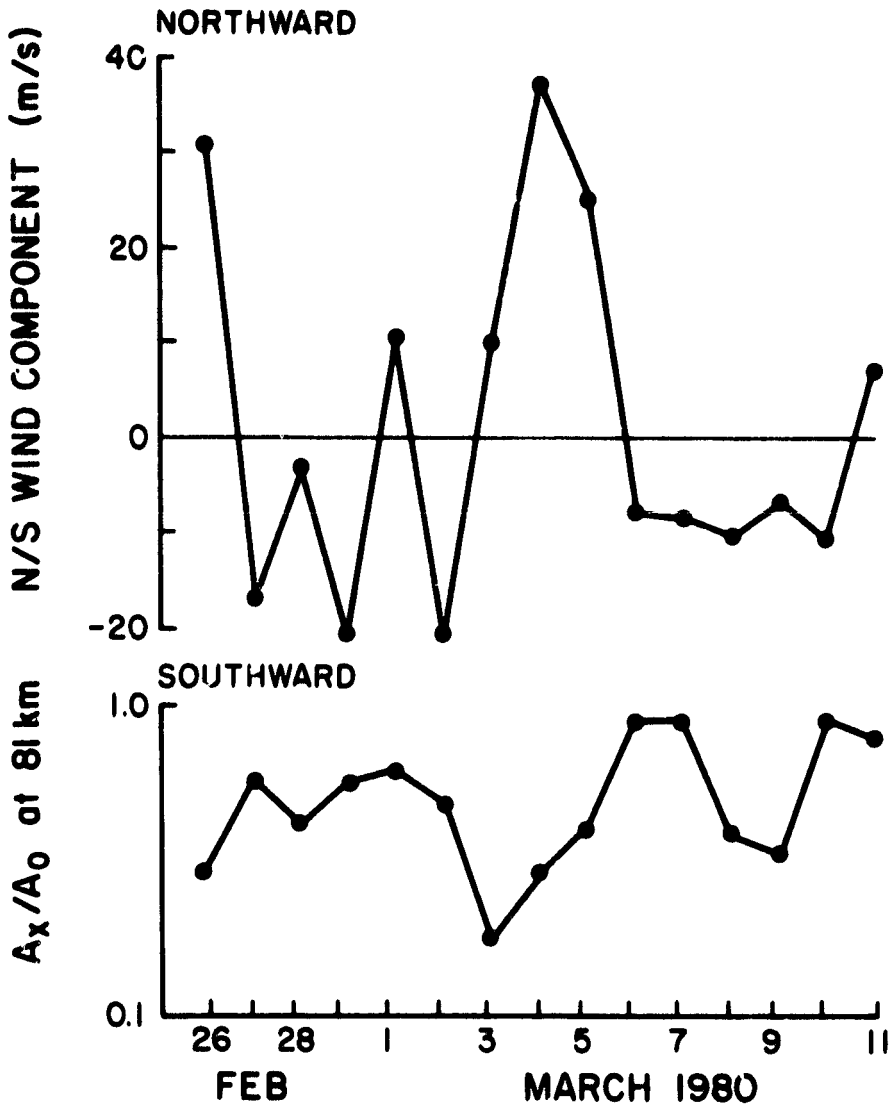

Figure 6.10 N/S winds and the A_x/A_o ratio at 81 km for the period of February 26 through March 11, 1980.

ORIGINAL PAGE IS
OF POOR QUALITY

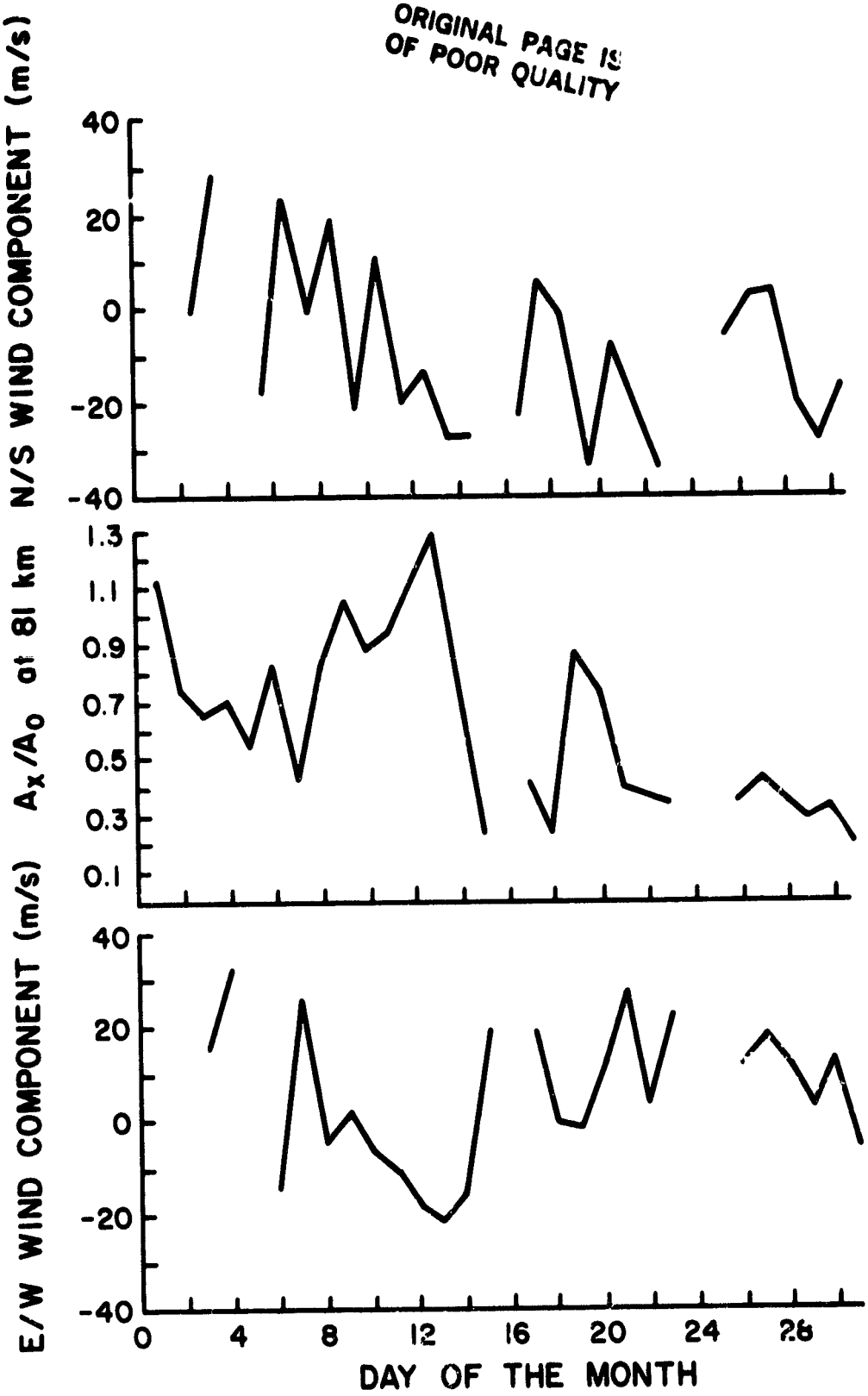

Figure 6.11 Daily N/S and E/W wind components and A_x/A_o ratio at 81 km for December 1980.

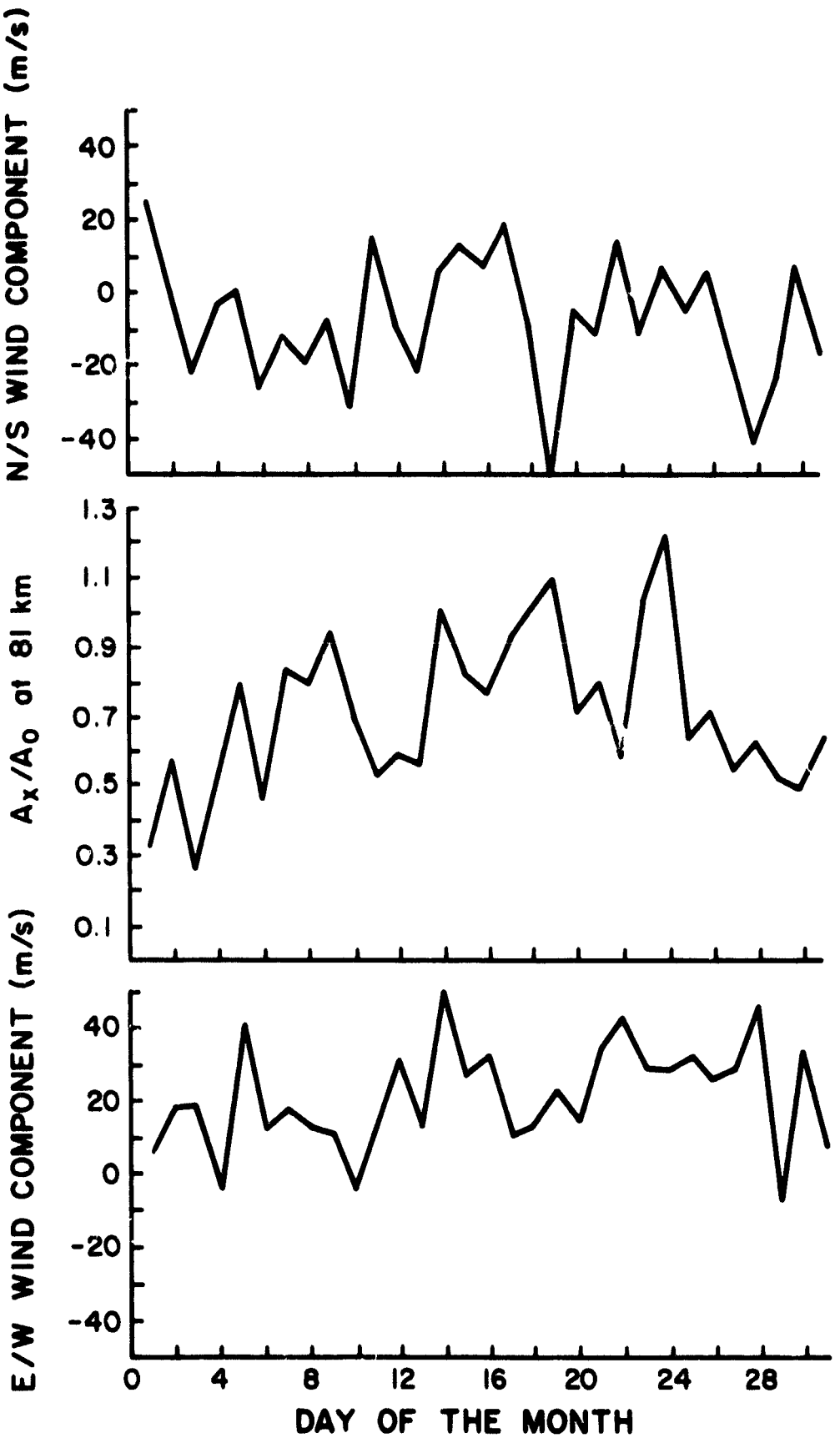

Figure 6.12 Daily N/S and E/W wind components and A_x/A_o ratio at 81 km for January 1981.

no apparent correlation between the N/S wind component and the A_x/A_o ratio, even when shifting one of the plots in time by a day or two. There is no longer any obvious correlation between the E/W wind component and the A_x/A_o ratio at 81 km. To more closely investigate the observed correlations, scatter diagrams of the wind components versus the A_x/A_o ratio at 81 km were plotted, and correlations were calculated. Figure 6.13 is a scatter diagram of the daily N/S wind component and the A_x/A_o ratio at 81 km for the months of December 1980 and January 1981. As expected there is no significant correlation shown in the figure.

The scatter diagrams of the E/W wind component and the A_x/A_o ratio at 81 km for the months of December 1980 and January 1981 are shown in Figure 6.14. The correlation shown between the E/W wind component and the A_x/A_o ratio at 81 km for December 1980 is shown in the scatter diagram, with the significance of the correlation at the 2% level. REES et al. (1979) found a significant correlation between high ionospheric absorption and the eastward zonal winds at about 90 km, during the western European Winter Anomaly Campaign of the winter 1975/1976, at mid-latitudes in the northern hemisphere.

The lack of correlation between the N/S wind component and the A_x/A_o ratio at 81 km is probably due to the fact that the 24-hour prevailing meridional wind component is not accurately predicted by the three wind profiles taken near noon. The results of correlations using the average of three wind profiles are not much improved over the results obtained when using one wind profile per day, when looking at the N/S component. The E/W wind component, being much larger in amplitude seems to be less susceptible to the "noise" caused by waves and irregular winds.

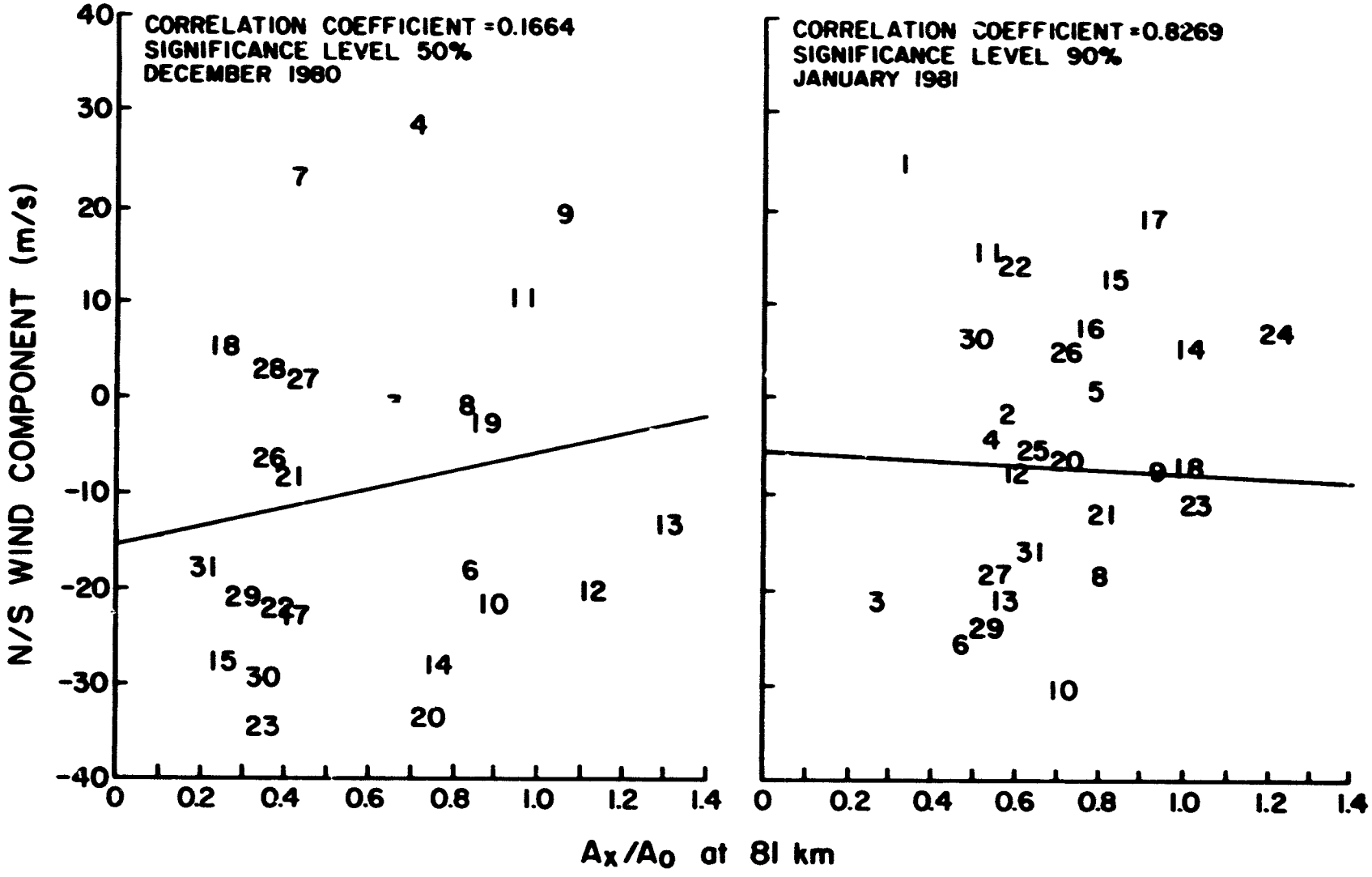

Figure 6.13 Scatter plots of daily N/S wind component and the A_x/A_o ratio at 81 km for the months of December 1980 and January 1981.

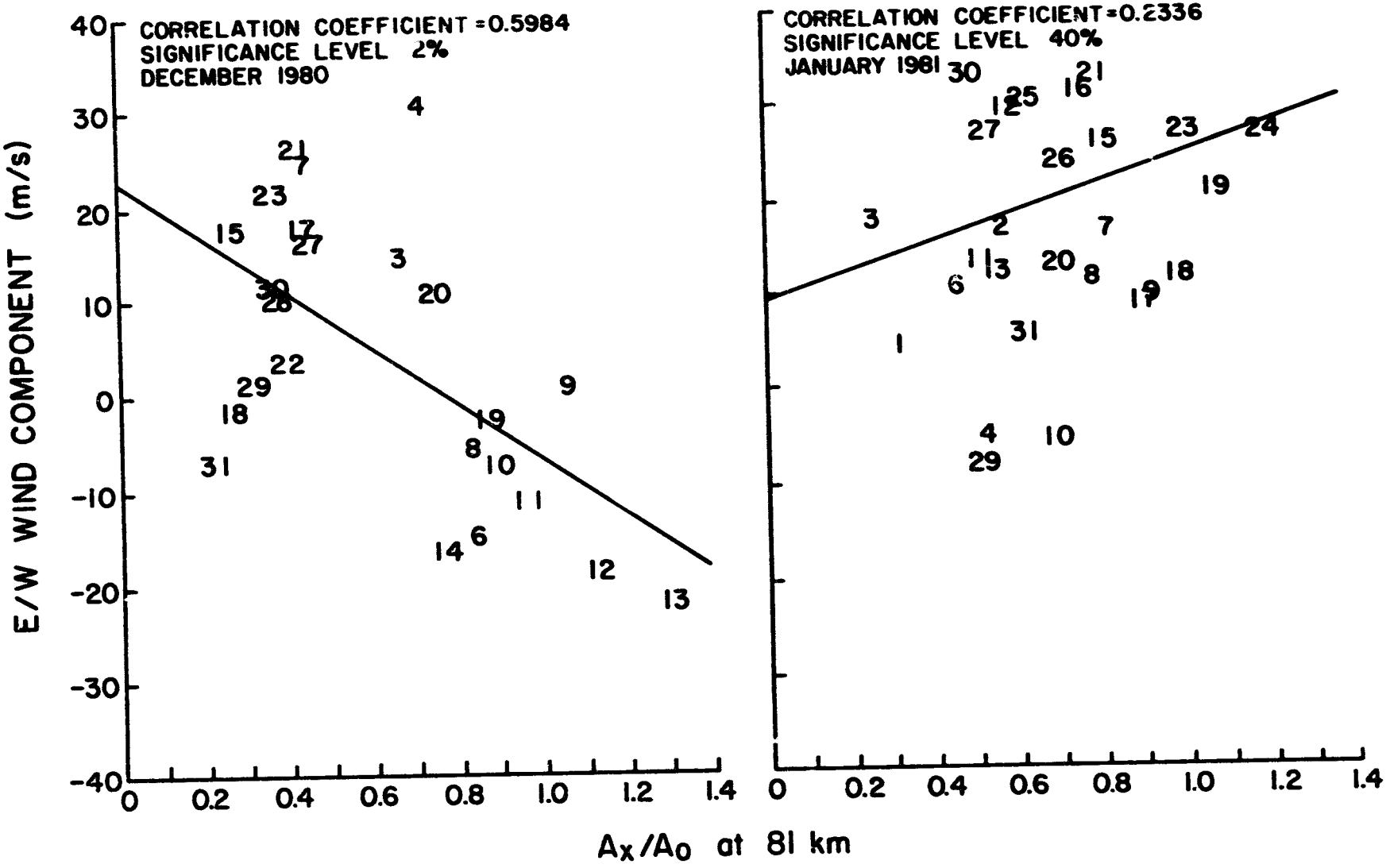

Figure 6.14 Scatter plots of daily E/W wind component and the A_x/A_o ratio at 81 km for the months of December 1980 and January 1981.

6.5 *Summary*

In this chapter the winds and electron concentrations measured at a single station have been compared. The data that are of good quality indicate that there is a significant link between the winds and electron concentration in the mesosphere during the winter. In order to establish if the transport is occuring from isolated patches of nitric oxide created in the auroral zone and transported southward, or if there is a constant gradient of nitric oxide with latitude, observations from more than one station are needed. Comparisons of winds from two observing stations with electron concentrations at Urbana will be shown in Chapter 9.

7. COMPARISONS OF ELECTRON CONCENTRATIONS AND METEOR-RADAR WINDS AT URBANA

7.1 *Introduction*

The Urbana meteor radar system is capable of measuring the meridional wind component in the mesosphere. The meteor-radar system has the advantage over the partial reflection drifts system of being able to make wind measurements 24 hours per day, and not just during the daylight hours. This provides a measurement of the 24-hour prevailing wind.

A previous study of the relationship was made at Urbana from a limited data set of four non-consecutive days by GELLER et al. (1976), from the winter of 1974/1975. Meteor-radar data were collected from about noon on one day until about noon the next day. Partial-reflection data were collected before and after the meteor-radar data collection period for about an hour. Their results showed consistently that high A_x/A_o ratios (corresponding to low electron concentrations) occurred with northward meridional winds, and that low A_x/A_o ratios occurred with southward velocities.

HESS and GELLER (1978) did some further analysis on the four days of data from the winter of 1974/1975 and on thirteen additional days of data obtained during 1975 and 1976. Of the thirteen additional days of data, four of the days were in winter months. Correlations were calculated between the winds, A_x/A_o ratios, and electron concentrations, all at various altitudes. They found a strong correlation between the N/S winds at any altitude in the range of 84.5 to 92.5 km and the electron concentration at 76.5 km (significant at about the 3% level). The correlation that they found between the A_x/A_o ratio at 81 km and the N/S winds at 92.5 km was significant at the 20% level. They found no significant correlation between N/S winds and electron concentrations for non-winter data.

During the past two winters a considerable amount of additional data have been obtained on days when both experiments have been operating. Much of these data have been collected in groups of several consecutive days, so that time delays, trends, and the time scales of observed variability in the two sets of data may be compared.

7.2 *Meteor Radar Technique*

The meteor-radar experiment measures the velocity of the neutral air by measuring the Doppler shift of radio-frequency signals scattered off of the ionized trails left by meteors in the upper atmosphere. As a meteor enters the atmosphere, the friction causes intense heat and ionization of a trail behind it. The vaporization of meteors begins at about 120 km and continues for the small grain-sized meteors usually observed until about 80 km. Thus, the meteor-radar technique can be used to measure wind velocities in the altitude range of 80 to 120 km. Radial wind velocities are determined from the Doppler shift of the reflected signal.

The meteor-radar system at Urbana is a pulse phase-coherent single station system. A pulse system allows the range to be easily determined. The transmitter, which is of unusually high power for this type of system (ensuring a large number of usable echoes per hour) has a peak power output capability of five megawatts, operating on a frequency of 40.92 MHz. The transmitting and receiving antennas are directed northward, so that the N/S wind component is being accurately measured in the radial velocity determined from the Doppler shift of the return signal. The angle of arrival is determined by an interferometer arrangement of three Yagi antennas. The relative phases of the return signals obtained by the three antennas are used to determine the azimuth and elevation of the return. The PDP 15/40 computer is used for real-time processing of winds data. Because the timing

of meteors, and the altitude where ionized trails occur is not under control of the experimenter, various algorithms must be used to interpolate the available wind velocity measurements in time and altitude (HESS and GELLER, 1976; GELLER et al., 1977). A high echo rate is essential in reducing the amount of interpolation necessary. The technique does provide a very good estimate of the 24-hour N/S wind component for comparison with electron concentrations measured by the partial-reflection system.

7.3 *Results*

The winds data used in this chapter are formed by an average of the wind measurements for 24 hours, measured from noon to noon. Figure 7.1 is a plot of the A_x/A_o ratio at 81 km and the meteor radar winds at 86 km for January, February, and March of 1980. The A_x/A_o ratio is inversely proportional to the electron concentration below 81 km, so the theory that transport of nitric oxide is a major cause of the winter anomaly would predict a dip in the A_x/A_o ratio occurring for southward wind velocities. There is a strong correlation evident between the A_x/A_o ratio and winds in the month of January, with the features in the A_x/A_o ratio curve following those of the winds curve, with a delay of one day in the first half of the month. In the month of February there again appears to be a delay of one day between wind shifts and a change in the A_x/A_o ratio. March also shows similar features in the two sets of data with a one-day delay in the first half of the month, but in the later half of the month there is no longer any correlation shown. Figure 7.2 shows the A_x/A_o ratio at 82 km, and the 86 km meteor radar winds for December 1980, January 1981, and February 1981. A good correlation can be seen in the two sets of data during December, January, and the first half of February, with a delay of one day between winds and the A_x/A_o ratio. There is no correlation seen in the later part of the month of February.

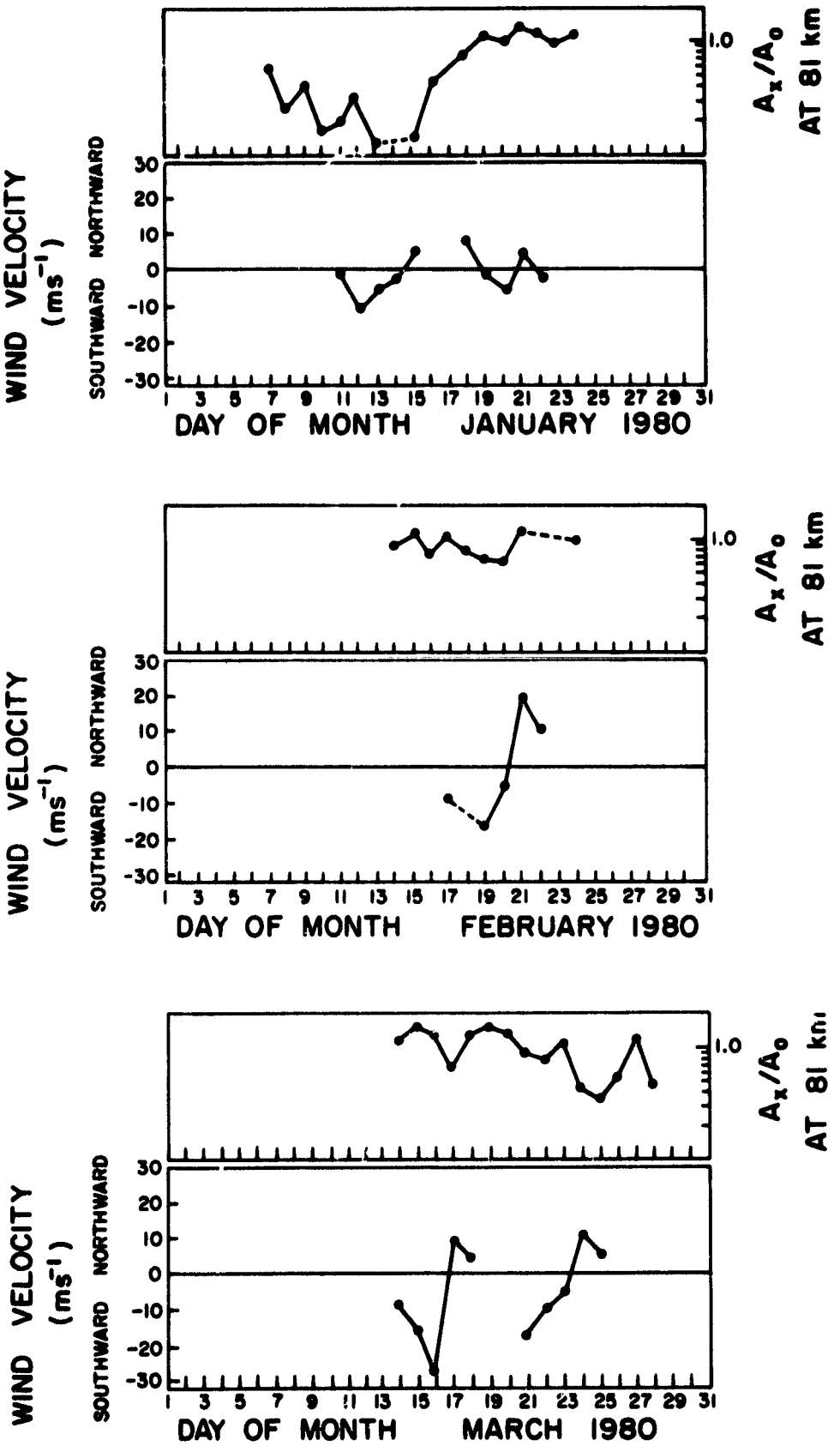

Figure 7.1 A_x/A_o ratio at 81 km, and 86 km meteor radar N/S winds for January, February, and March of 1980.

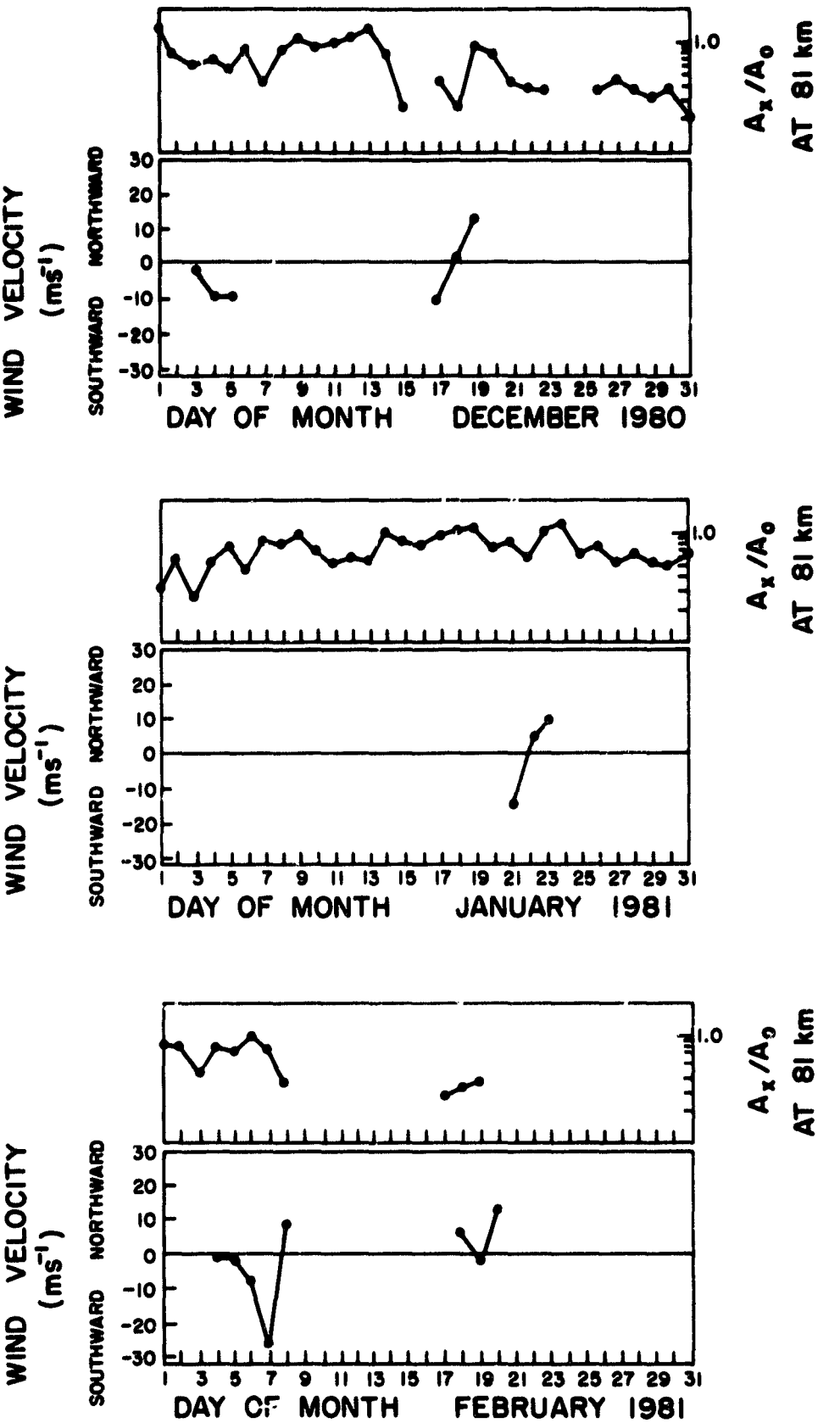

Figure 7.2 A_x/A_o ratio at 81 km, and the 86 km meteor radar winds for December 1980, January 1981, and February 1981.

To quantify the correlations evident in these two figures, correlations were calculated between the N/S winds and the A_x/A_o ratio at 81 km. Because the relationship seen varies by season and year, correlations were calculated for all of the data, and various groups of data by season and year. Winds from three different altitudes were calculated, and correlations were calculated with the A_x/A_o data delayed by a day or two days. The assumption in the analysis is that the prevailing 24-hour wind is representative of the N/S wind over a significant part of the path from the auroral zone, so that a constituent being transported along that path may travel at that velocity for a day or more. Therefore, an enhancement at Urbana may not result immediately after a shift in the meridional winds towards the south.

Table 7.1 is the correlation coefficient matrix of meteor radar N/S winds and the A_x/A_o ratio at 81 km. The winds used in the calculations are from 82, 86, and 90 km. The winds at 82 km are not as reliable as those at the other two altitudes because of the lower number of meteor-trail returns that occur at that altitude. The number of days of data used in each correlation are shown. The significance levels (t-test) are shown in parentheses after each value of correlation coefficient.

The correlation for all days of data (the dates of collection used in this analysis are all of those on Figures 7.2 and 7.3) is not significant at either altitude, even with the time delay in the A_x/A_o data. The data taken during winter only (winter is defined here as December through mid-February) show a strong correlation (2% significance level at 86 km) with a delay of one day. The lack of correlation shown for all data must be due to the lack of correlation of non-winter data. The correlation with higher altitude winds is not as good as that with the lower altitude winds, and is not significant. Because the correlation evident in Figures 7.1 and 7.2 is greater

TABLE 7.1 Correlation coefficient matrix of meteor radar N/S winds (northward positive) and the A_x/A_o ratio at 81 km. The significant levels are shown in parentheses, and the length of shift refers to the number of days that the A_x/A_o data are delayed.

ALL DAYS	NUMBER OF DAYS	86 km Winds	90 km winds
No shift	39	-.21 (20%)	.05 (80%)
1-day shift	28	.12 (50%)	.01 (95%)
2-day shift	20	-.34 (20%)	-.06 (80%)
ALL WINTER DAYS			
No shift	22	.04 (85%)	.19 (40%)
1-day shift	16	.59 (2%)	.2 (30%)
2-day shift	11	-.16 (70%)	.05 (90%)
WINTER 1979/1980			
No shift	9	.11 (80%)	.62 (5%)
1-day shift	6	.54 (20%)	.55 (20%)
2-day shift	5	-.05 (95%)	.46 (40%)
WINTER 1980/1981			
No shift	13	.12 (90%)	.14 (60%)
1-day shift	10	.74 (2%)	.25 (50%)
2-day shift	6	-.28 (60%)	.57 (20%)
WINTER 1980/1981 82 km Winds			
No shift	13	.52 (5%)	
1-day shift	10	.14 (70%)	

for the winter of 1980/1981, the data were grouped by year and correlations calculated. As expected, the correlation during the winter of 1980/1981 is greater (significant at the 2% level) than the correlation during the winter of 1979/1980. The winds at 90 km are not, in general correlated with the A_x/A_O ratio at 81 km. This result is expected because any ionizable constituent would have to be well below 90 km to be transported vertically downwards during the one-day time delay observed. To investigate the correlation between the winds measured at nearly the same altitude as the A_x/A_O ratio, the 82 km winds were correlated with the A_x/A_O ratio for the winter of 1980/1981. The correlation is significant at the 5% level for winds and A_x/A_O ratios measured on the same day. This result suggests a vertical transport time on the order of one day from 86 km down to 82 km, that is present throughout the winter.

In conclusion, a strong significant correlation is shown between the N/S wind component at 86 and 82 km, and the A_x/A_O ratio at 81 km, during the winter months. This result supports the theory that the horizontal transport of constituents is a major cause of the winter anomaly. The results of this comparison are in agreement with those of the partial reflection drifts winds and electron concentrations comparison of Chapter 6. The correlations shown using meteor-radar winds are better due to the quality of the 24-hour wind available from that experiment. Since the zonal component is not available from the meteor-radar experiment, care must be taken to establish that the transport is indeed from the auroral zone, and more than one station is required. The winds measured at two stations will be compared with electron concentrations in Chapter 9.

8. INVESTIGATION OF PLANETARY WAVE ACTIVITY

8.1 *Review of Planetary Wave Theory*

When hemispheric maps of atmospheric field variables are spatially Fourier decomposed, the first few zonal wave components are called planetary waves. Wave number zero represents a symmetric axial flow about the pole. The first few planetary waves account for nearly all of the deviation from zonal mean values of geopotential height and temperature. VAN LOON et al. (1973) have found that planetary wave numbers 1 and 2 account for 99.9 percent of the variance from the mean values at the 10 mb level at 65°N, in January. (This is the latitude of maximum planetary wave intensity at this stratospheric altitude).

These planetary waves are strongest in the middle atmosphere in winter. This is because in general, the planetary waves are forced from the troposphere and propagate upwards if height and temperature structure will permit it. Observations of planetary waves above 30 km are limited, but evidence from Meteorological Rocket Network, radiometer, and ground-based ionospheric observations indicates that these waves do extend upward to the mesosphere and even higher during winter (BROWN and WILLIAMS, 1971; CAVALIERI et al., 1974).

Planetary waves are classified as stationary or traveling by their period. Waves of period less than 30 days are classified as traveling, and those of period greater than 30 days are classified as stationary. Traveling planetary waves are seen as steady progressive patterns on daily maps. Stationary planetary waves are believed to be caused by zonally asymmetric heating (of land versus ocean) and by the flow of zonal winds over topography. Although no clear source of traveling planetary waves has been identified, they are believed to be caused by fluctuations in the forcing.

MADDEN and JULIAN (1972, 1973) studied traveling extratropical planetary waves with periods near five days. While most of the observations of this wave have been in the troposphere, RODGERS (1976) has observed the five-day wave in the upper stratosphere from satellite data. FRASER (1977) observed the five-day wave in the mesosphere from ionospheric absorption data. Traveling planetary waves were observed in the E-region by CAVALIERI (1976) in data from a network of ionosonde stations in the northern hemisphere at mid-latitudes. He observed the presence of planetary-scale fluctuations in the period range of 10-15 days.

CHARNEY and DRAZIN (1961) were the first to theoretically investigate the possibility of the propagation of stationary planetary waves from the troposphere to the stratosphere. Using a β-plane geometry, they found that planetary waves could only propagate upwards when the mean wind was eastward and of moderate magnitude. They predicted that vertical propagation would occur during the equinoxes only, when the winds in the stratosphere are eastward and weak. DICKINSON (1968), using spherical geometry showed that this cutoff velocity was higher than that predicted by CHARNEY and DRAZIN. He also showed that the cutoff velocity would be increased for planetary waves propagating near the equator, and decreased for those propaging near the pole. His work demonstrated that planetary waves could propagate to high altitudes during winter.

Rossby waves are a special case of planetary waves. Rossby waves are the two-dimensional idealization of planetary waves on a plane tangent to the earth. The waves owe their existence to the variation of the Coriolis force with latitude, and this variation must be included on the plane. The Coriolis parameter $f = 2\Omega \sin\theta$, where Ω is the angular velocity of the earth and θ is the latitude, is regarded as a linear function on the plane. The

value of f anywhere on the plane can be written as $f = f_o + \beta y$ where $\beta = \frac{\partial f}{\partial y}$. The plane where the Coriolis parameter follows this variation is called the beta plane. The x axis will be the direction of the wave's propagation directed eastward, and the y axis is directed northward. The x and y components of the momentum equation and the continuity equation can be written as (HOLTON, 1972)

$$(\frac{\partial}{\partial t} + u\frac{\partial}{\partial x} + v\frac{\partial}{\partial y})\ u - fv = -\frac{\partial \Phi}{\partial x} \tag{8.1}$$

$$(\frac{\partial}{\partial t} + u\frac{\partial}{\partial x} + v\frac{\partial}{\partial y})\ v + fu = -\frac{\partial \Phi}{\partial y} \tag{8.2}$$

$$\frac{\partial u}{\partial x} + \frac{\partial v}{\partial y} = 0 \tag{8.3}$$

where

u = Eastward velocity

v = Northward velocity

Φ = Geopotential

Forming the vorticity equation from equations (8.1) and (8.2), and noting that from equation (8.3) the divergence term is zero, we obtain

$$(\frac{\partial}{\partial t} + u\frac{\partial}{\partial x} + v\frac{\partial}{\partial y})\ \zeta + v\frac{\partial f}{\partial y} = 0 \tag{8.4}$$

where ζ is the vorticity. This equation states that the absolute vorticity is conserved following horizontal movement. If we assume that the motion consists of a basic state zonal velocity with a small perturbation u'

$u = u'$

$v = v'$

$\zeta = \zeta'$

A perturbation stream function Ψ can be defined as

$$u' = -\frac{\partial \Psi}{\partial y}$$

$$v' = \frac{\partial \psi}{\partial x}$$

with $\zeta' = \Delta^2 \psi$. The perturbation form of equation (8.4) is given by

$$\left(\frac{\partial}{\partial t} + \bar{u}\frac{\partial}{\partial x}\right) \nabla^2 \psi + \beta \frac{\partial \psi}{\partial x} = 0 \tag{8.5}$$

We now assume that β is a constant on the plane, neglect terms involving products of perturbation quantities, and assume a solution of the form

$$\psi = A\{\exp[ik_x(x - ct)]\} \cos k_y y \tag{8.6}$$

k_x is the zonal wave number, C is the zonal phase speed, and k_y is the latitudinal wave number. The wave number is given by $2\pi/(\text{wavelength})$. Substituting equation (8.6) into equation (8.5) gives

$$(-ik_x c + ik_x \bar{u})\ (-k_x^2 - k_y^2) + ik_x \beta = 0 \tag{8.7}$$

In order that the solution satisfy equation (8.6), the phase speed must be

$$c = \bar{u} - \frac{\beta}{(k_x^2 + k_y^2)} \tag{8.8}$$

where $\beta = \frac{\partial f}{\partial y} = \frac{2\Omega \cos\theta}{a}$, and a is the radius of the earth. Equation (8.8) shows that the Rossby wave propagates westward relative to the main flow, and that the wave speed depends on the zonal and meridional wave numbers.

For a stationary Rossby wave the wave speed is zero, so we are left with

$$\bar{u} = \frac{\beta}{k_x^2 + k_y^2} \tag{8.9}$$

This quantity will always be positive, demonstrating that the zonal wind must always be eastward to set up a standing Rossby wave.

The local period for a Rossby wave with no mean wind is given by (MADDEN, 1979)

$$\tau = n(n + 1)/2m \tag{8.10}$$

where m is the zonal wave number (number of wave cycles in one earth circumference), and $n-m$ is the number of latitudes between the poles at which the stream function of the wave vanishes. This indicates that with a constant longitudinal scale (m constant), decreasing the latitudinal scale (increasing $n-m$) results in a slower westward propagation. Table 8.1 contains estimates of periods of Rossby waves of various modes (after SALBY and ROPER, 1980). These wave periods were calculated as solutions to Laplace's tidal equation with an equivalent depth of about 10 km, and a realistic temperature structure.

8.2 *Previous Observations of Rossby Waves in the Mesosphere*

Observations of Rossby waves in the mesosphere are not as numerous as those taken in the troposphere and stratosphere because of the difficulty in obtaining data from the mesosphere. Rossby waves have been observed in the E region by BROWN and WILLIAMS (1971), DELAND and CAVALIERI (1973), and CAVALIERI (1976), from ionosonde data. Few observations have been made below the E region because it is the lowest altitude where data are readily obtainable with modest equipment.

Time series of wind measurements can be obtained by the meteor radar experiment and analyzed to identify Rossby wave activity. CLARK (1975) observed a 2-day wave consistently in meteor radar data obtained in summer and late fall measurements at Durham, New Hampshire (43°N, 71°W). The 2-day wave was also observed by KINGSLEY et al. at Sheffield, England (53°N, 2°W) in summer and winter, in meteor radar winds time series. They found that the 2-day wave was strongest in summer and gave way to waves of longer period (on the order of ten days) in the winter season. Data from meteor-radar experiments in Garchy, France and Obninsk, USSR were also analyzed by KINGSLEY et al., and 2-, 6-, and 10-day waves were present. SALBY and ROPER

TABLE 8.1 Rossby periods for equivalent depths of 9.9 and 6.3 km and several horizontal modes (m,n) (after SALBY and ROPER, 1980).

		Period (days)	
	n	h = 9.9 km	h = 6.3 km
	1	1.2	1.3
	2	5.1	6.1
m = 1	3	8.3	9.6
	4	12.5	14.7
	5	17.2	19.2
	2	1.6	1.9
	3	3.7	4.5
m = 2	4	5.9	7.0
	5	8.5	10.0
	6	11.6	13.2
	3	2.1	2.2
	4	3.6	4.2
m = 3	5	5.6	5.8
	6	7.6	8.2
	7	10.0	10.4

(1980) analyzed meteor radar winds data obtained at Atlanta, Georgia (34°N, 84°W) over a three-year interval. The power spectra and cross spectra of the zonal and meridional velocities between 80 and 100 km were calculated. Local maxima in the spectra were found at periods of 1.6, 2.2, 5, and 17 days.

Analysis of mesospheric fields are also practical with the recent advent of satellite data. Satellite experiments such as the pressure modulated radiometer measure the outgoing infrared radiation of the atmosphere from different layers, and this can be used to calculate mean temperatures up to the mesosphere.

OFFERMAN et al. (1979) analyzed radiant fluxes from channel 3000 of the pressure modulated radiometer on Nimbus 6, which effectively measures the mean temperature on a layer about 20 km thick, centered at about 80 km during the Western European winter anomaly campaign of the winter of 1975/76. The magnitude of the variation is small since the average temperature of the region is nearly constant, because the temperature changes in the upper and lower boundaries are often of opposite sign. Therefore, the data indicates the trend of the temperature in the region. They observed dominant spectral components with periods of about 7 and 10-13 days in the temperature data. The observed variations were also found to be significantly correlated over a horizontal distance of 2000 km, indicating the extent of the wave structures.

Time series of winds measured by the partial reflection drifts experiment at Adelaide, Australia (35°S, 139°E) were analyzed by VINCENT and STUBBS (1977). Data obtained in a seven day period in June 1973 showed a strong variability with a 2-3 day period, in the zonal and meridional wind components. (It should be noted that the forcing of planetary waves in the

troposphere in the Southern Hemisphere will differ from that in the Northern Hemisphere because of the different topography, which will result in the forcing of waves of different periods.)

GREGORY and MANSON (1967a) analyzed a series of noon partial reflection electron concentration data obtained at Christchurch, New Zealand (44°S, 173°E) made during 1963-1967. Variability was found to be much increased during the winter months as compared with the summer months. The variability whose periodicity is on the order of days is suggested to be due to the effect of planetary waves which propagate to mesospheric altitudes during the winter months.

Rossby waves were observed in winds data obtained by the partial reflection drifts experiment at Saskatoon by MANSON et al. (1978). They observed waves with periods of 2-3, 4-5, and greater than 20 days. Later data obtained at Saskatoon using a system capable of operating 24 hours per day were analyzed by season to establish the seasonal variation of Rossby waves (MANSON et al., 1981). They observed waves throughout the year with periods of 2.2, 4.4, and 6 days. There were few cases of clearly cominant wave periods. In the summer data thegre were fewer peaks in the coherences between winds measured at different altitudes, and they were of lower significance. This would be explained by the lower wave energy found in the summer months The Saskatoon data shows a close agreement with those of SALBY and ROPER (1980), with both stations observing the 2.2 and 5 day waves with their amplitude increasing during the winter months.

8.3 *Observations of Rossby Wave Activity from Electron Concentration Variability*

The effects of planetary waves in the mesosphere are shown in the increased variability in the day-to-day values of electron concentrations,

shown in Chapter 5. In order to identify the wave periods present in the electron concentration series obtained during the past eight winters, a Fourier analysis was performed. Data are available at three altitudes (72, 76.5, and 81 km) daily for about 150 days per winter and wave periods displaying peaks in the power spectra in the daily data at all three altitudes were identified. Table 8.2 shows the periods of waves observed in the power spectra. The wave periods observed vary from year to year, but several of the wave periods appear during most of the years. The dominant wave periods seen are 2.7, 3.1, 4, 5.3, and 6 days. These wave periods are similar to those found by the other investigators mentioned earlier. The exact wave periods are difficult to compare because of the different frequency resolution being used in each analysis.

To investigate the effect of Rossby wave activity, a segment of Urbana data obtained during the winter of 1978/1979 will be examined more closely. The data were obtained from December 27, 1978 through January 10, 1979, with data collected continuously from about 0800 through 1700 local standard time. Electron concentration profiles were obtained every 3.4 minutes. To form a single time series for the entire 15-day collection period, the approximately 160 electron concentration values obtained from 0800 through 1700 local time each day were placed in the appropriate place in the long time series with zeros placed in the long time series during the night when data were not obtained. The resulting long time series was analyzed by an 8192-point Fourier transform to identify dominant periods in the electron-concentration variability. Figure 8.1 shows the spectrum of electron-concentration fluctuations at 72 km during the 15-day collection period. A clearly defined dominant mode, with a period of 2.77 days is seen in the spectrum. This wave period is in the range of wave periods found in Rossby

TABLE 8.2 Periods of waves observed in the power spectra of electron concentrations measured at three altitudes.

WINTER	WAVE PERIODS (DAYS)
1972/1973	2.7, 4, 6
1973/1974	None significant
1974/1975	2.7, 3.1, 3.5, 6
1975/1976	2.8, 4, 6, 9
1976/1977	2.4, 3.1, 4, 7, 16
1977/1978	2.6, 3.1, 3.6, 5.3, 9
1978/1979	2.7, 3.1, 3.3, 5.3
1979/1980	2.4, 2.7, 3.6, 4, 8, 12

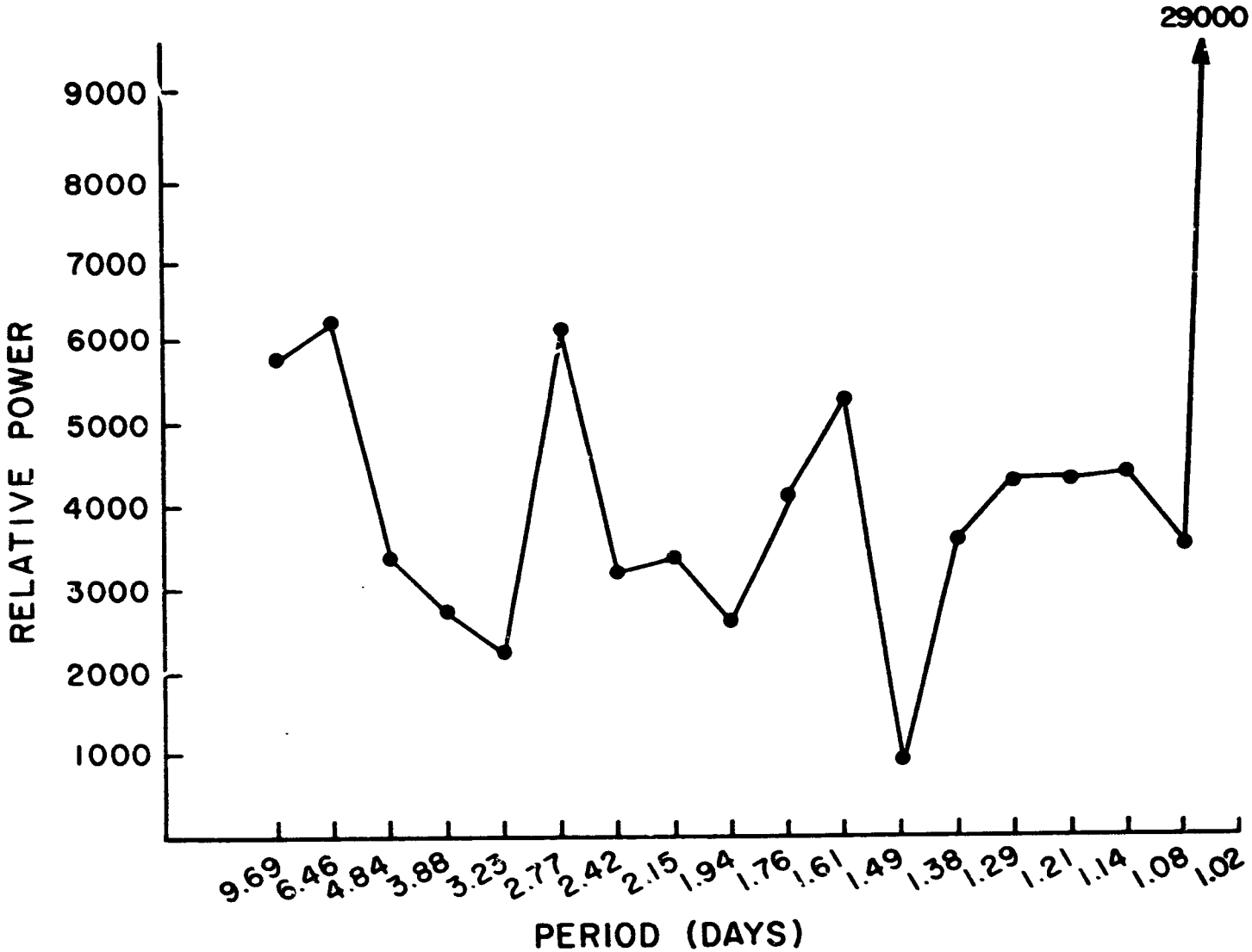

Figure 8.1 Spectrum of electron concentration fluctuations at 72 km during the winter of 1978/1979.

waves. It is believed that the fluctuations in the electron concentration result from the effect of Rossby waves. Figure 8.2 is a plot of the electron concentration measured at 72 km and the 2.77-day period component obtained from the Fourier transform. (The diurnal plots of electron concentration for each day have been individually smoothed by Fourier processing to remove fluctuations of periods less than four hours.) The visual correlation between the 2.77-day period component and the daily electron concention plot shown in the figure is fairly good from December 27 through January 5, with disagreement after that date, a result of longer period waves shown in the spectrum. This figure demonstrates that a well defined frequency component is seen in the day-to-day electron concentration that is present for several cycles.

Rossby waves should propagate upwards to mesospheric altitudes only during winter, and so the fluctuations in electron concentration should be strongest during winter. In order to study how the amplitude of the 2.8-day fluctuation changes during the winter and spring seasons, shorter length Fourier transforms were calculated from the daily noon electron concentration time series at regular intervals throughout the collection season. A sixteen-point Fourier transform was calculated from groups of sixteen points, spaced every five days, throughout the winter. By plotting the relative power of a particular component in the spectra calculated every five days, the change in amplitude for that component during the season can be shown. Figure 8.3 shows this running FFT of the 2.8-day period component in the electron concentration at 81 km for the winter of 1978/1979. The first sixteen-point Fourier transform is centered on about January 1, 1979, and the first shift corresponds to the sixteen-point Fourier transform centered on January 6, 1979. The figure shows that the relative power in that

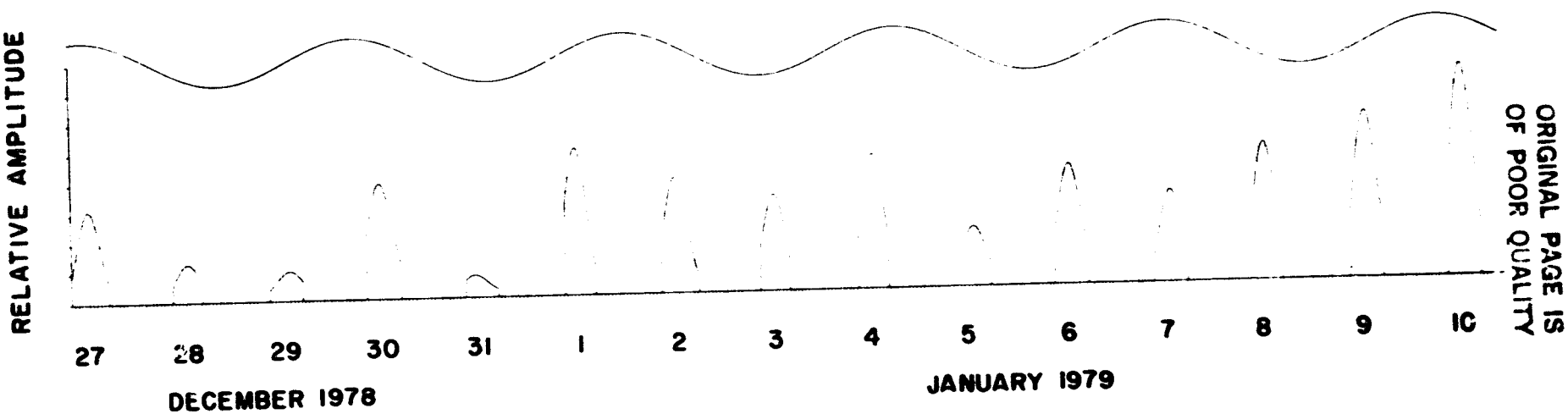

Figure 8.2 Electron concentration at 72 km for December 27, 1978 through January 10, 1979, and the 2.77 day period component of the FFT of the electron concentration data.

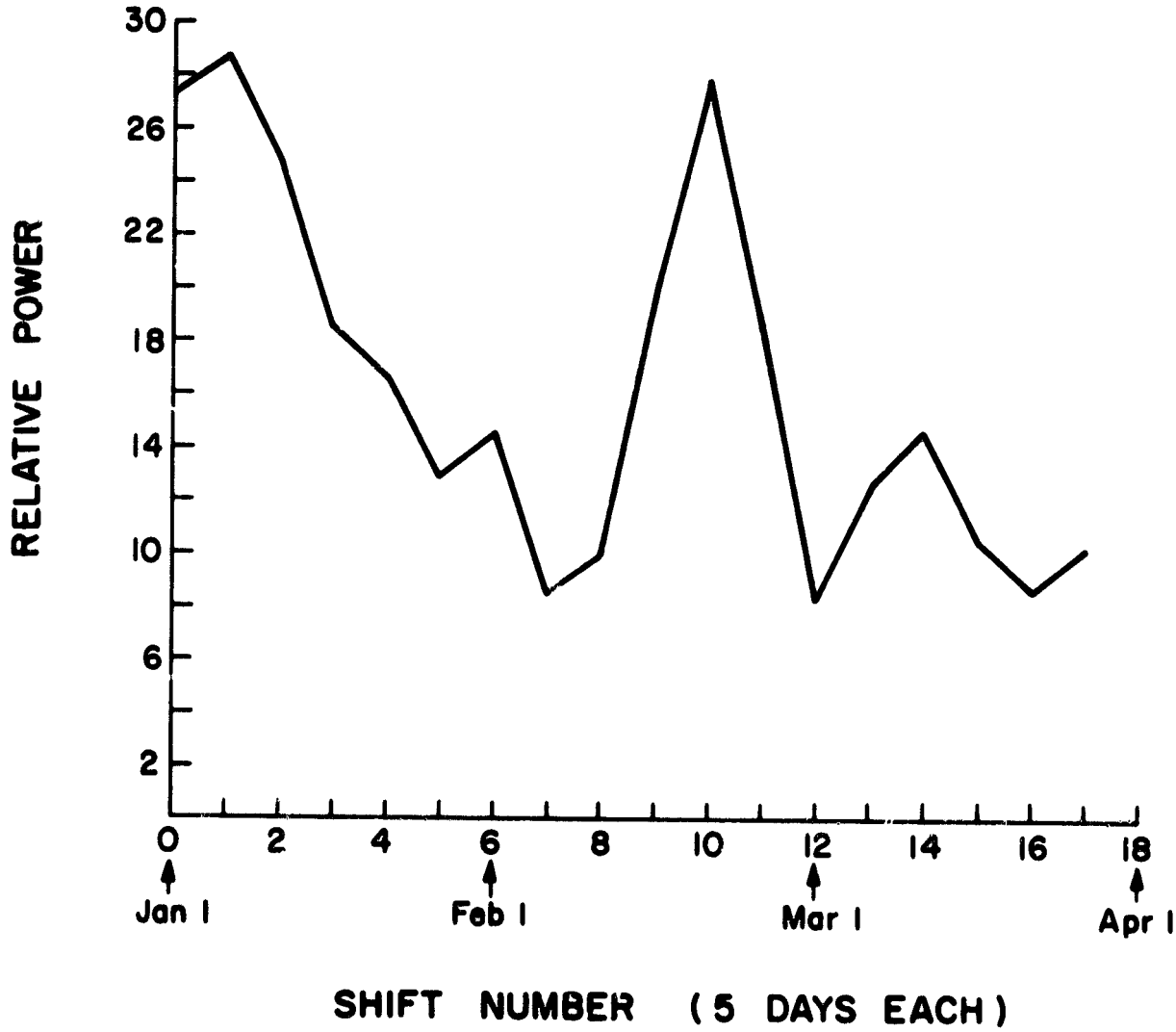

Figure 8.3 Relative power of the 2.8 day period component in the electron concentration at 81 km for the winter of 1978/1979.

component peaks at around January 5, decays through February 6, peaks again on February 21, drops quickly through March 1, and remains at a low level during the spring.

The data collection schedule during this season did not include the month of December, so the build-up of the 2.8-day component is not shown. The data collection made during the winter of 1974/1975 includes the entire month of December. Figure 8.4 is the running FFT showing the relative power of the 3.1-day period component in the electron concentration data at 76.5 km for the winter of 1974/1975 (the 3.1-day component is dominant during the winter of 1974/1975). The first sixteen-point FFT is centered on about December 1, with each shift giving the FFT centered 5 days later. This figure shows the build-up of variability occuring during most of the month of January, peaking on about January 21, and dropping within two weeks to a low value where it remains until spring. This peaking of the 3.1-day component in winter is consistent with the theoretical work of DICKINSON (1968) who showed that planetary waves could propagate to high altitudes during winter. The increase in variability in the months of January and the first half of February are consistently observed in the electron concentrations measured at Urbana during every winter season. The horizontal scale of Rossby waves will be shown in Chapter 9, with correlations between two distant observing stations.

8.4 *Investigation of Stratospheric-Mesospheric Coupling using Satellite Data*

8.4.1 *Introduction.* Planetary scale waves of periods similar to those observed in the mesosphere are present in air pressure data taken at ground level. The similarity in wave period and horizontal scale of the wave fluctuations observed at both altitudes suggests that a coupling may exist

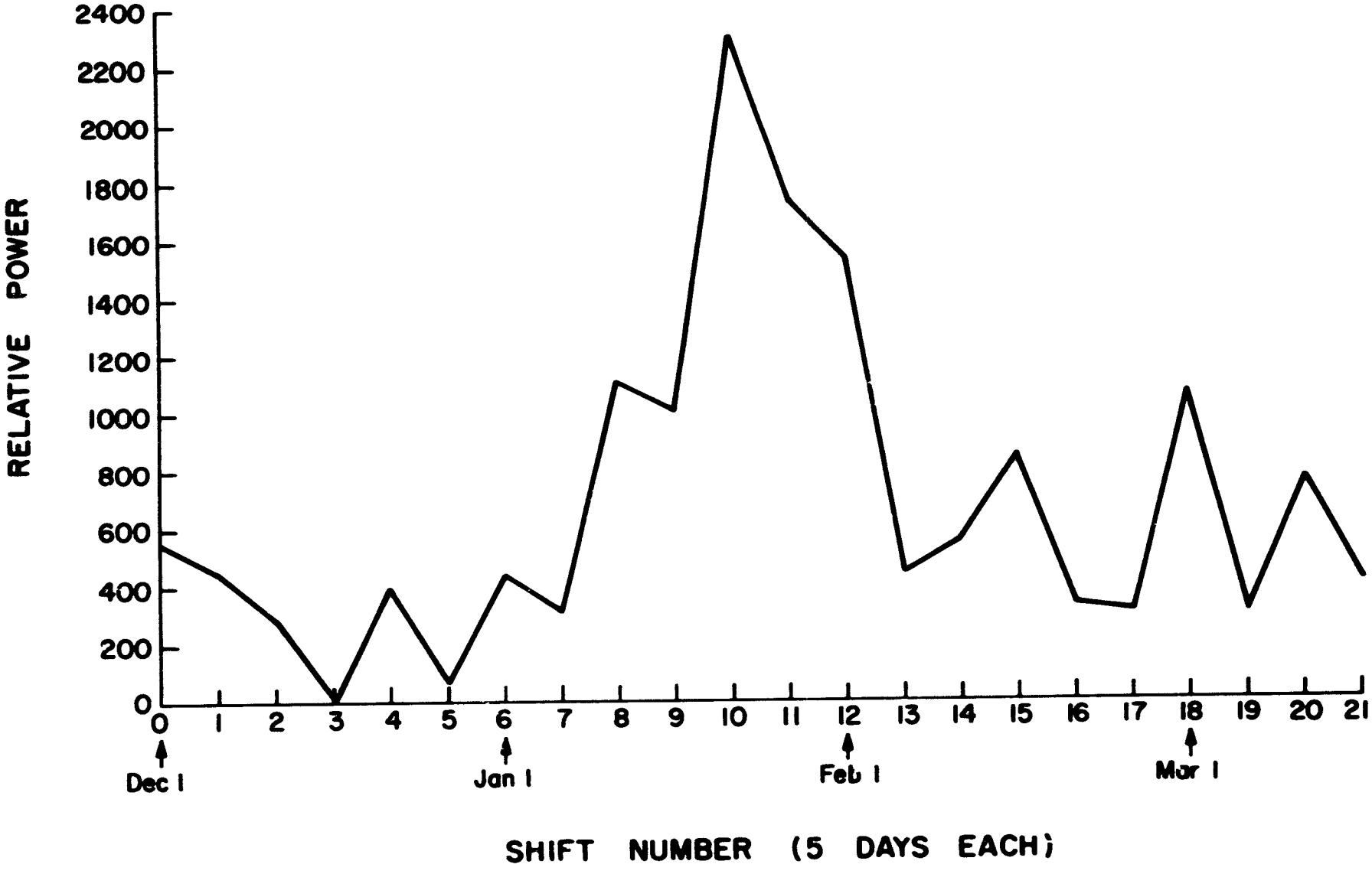

Figure 8.4 Relative power of the 3.1 day period component in the electron concentration at 76.5 km for the winter of 1974/1975.

between the lower atmosphere and the ionosphere. BROWN and WILLIAMS (1971) examined the day-to-day variability of isopleths of electron density in the E region and 10 mb (about 30 km) geopotential, and found a good correlation between them in winter months. They found that the variations in the height of the electron density isopleths followed closely the height variations of the lower altitude geopotential height. CAVALIERI et al. (1974) have shown a correlation between the height of E-region electron concentration isopleths, D-region f-min, VLF phase data, and 10 mb geopotential height, during winter. An analysis of E-region minimum virtual height data obtained from a network of ionosonde stations in the Northern Hemisphere (at an average latitude of 51°) was conducted by CAVALIERI (1976), using data from the winter of 1970/1971. He observed travelling planetary waves with a period of 10-15 days. When correlating the E-region data with 30 mb satellite data he found a positive correlation for the stations above about 50°N, and a generally negative correlation for stations south of about 50°N. This would suggest a latitudinal cut-off of coupling effects at 50°N.

ROSE and WIDDEL (1977) compared short wave radio absorption data with ground air pressure, and found no permanent correlation when comparing the data sets for an entire year. They did find larger amplitudes in the fluctuations in both sets of data during the winter months, suggesting the same wave excitation mechanism at both levels.

In the Southern Hemisphere, FRASER and THORPE (1976) did a cross-spectral analysis of 30 mb temperatures and ionosonde f-min data from near Christchurch, New Zealand for the years 1964/1967. They found a significant coherence at a period of about six days. In a companion paper, FRASER and WRATT (1976) compared plots of mesospheric electron concentrations, mesospheric winds, 40 km temperatures, and lower stratospheric temperatures,

during the winter of 1972. They found no evidence of stratospheric/mesospheric coupling, except for a few days during July, when electron concentration enhancements occurred simultaneously with temperature increases in the stratosphere. MANSON (1976) did a superposed epoch analysis using winter f-min and 30 mb temperatures, from the years of 1969 through 1974, at Christchurch. He found a significant correlation in most of the data, with large variations in the degree of stratosphere/ionosphere coupling from year to year.

In order to investigate the possible coupling between the stratosphere and the mesosphere at this location, various parameters measured by the partial-reflection system were compared with 0.4 mbar geopotentials obtained by the TIROS N series of satellites. Using the TIROS operational vertical sounding data, the National Meteorological Center has produced daily analyses of geopotential height at the 5-, 2-, 1-, and 0.4-mbar levels since 1978. The data set used in this analysis runs from December 26, 1978 through March 15, 1979.

The effects of possible Rossby wave propagation upwards to mesospheric heights have been shown in the electron-concentration data. If the observed variability is a result of Rossby waves propagating upwards from the troposphere, the degree of coupling should be investigated. The data available for comparison with the 0.4 mbar geopotential include electron concentrations and winds at Urbana, and winds at Saskatoon, Saskatchewan (these data were provided by A. H. Manson, see Chapter 9).

8.4.2 *Results.* The daily values of 0.4 mbar geopotential height at Urbana, 0.4 mbar geopotential at Saskatoon, N/S winds as Saskatoon, A_x/A_o ratio at 81 km at Urbana, 72 km electron concentration at Urbana, and N/S winds at Urbana (during the diurnal collection dates only) are plotted in

Figure 8.5, for 80 days, starting on December 26, 1978. When comparing the geopotentials with the mesospheric data, there appears to be no consistent similarity in the plots, for any of the mesospheric data. The data shown here and the E/W winds data from both stations when all plotted on an expanded scale show no obvious correlation between the stratospheric data and the mesospheric data. The only significant correlation can be seen on two days in the data set when large jumps in the geopotential result in increases in the electron concentration at 72 km. On January 19 (day number 25) the geopotential jumps significantly (at Saskatoon) and a large jump also occurs in the 72 km electron concentration at Urbana. On February 8 (day number 45) the geopotential jumps significantly at both Urbana and Saskatoon, and a small increase is seen in the Urbana electron concentration at 72 km.

In general, there is no clear correlation between stratospheric and mesospheric data. Obviously there is no simple direct coupling from the stratosphere to the mesosphere, and the variability seen in one altitude range can be localized only. It may be that only waves of large enough extent, such as Rossby waves, propagate upwards to mesospheric heights, and then only during winter when the prevailing winds are blowing towards the east.

In order to identify waves that are propagating from the stratosphere to the mesosphere, Fourier and cross-spectral analysis methods will be used. The power spectra of the daily A_x/A_o ratio at 81 km for the years of 1978/1979 and 1979/1980 are shown in Figure 8.6. Peaks in the spectra from both years are seen at periods of 2.9 and about 3.8 days. The spectra do not show very dominant peaks, indicating a low wave amplitude or waves that occur only during a small portion of the data series (the data series length

ORIGINAL PAGE IS
OF POOR QUALITY

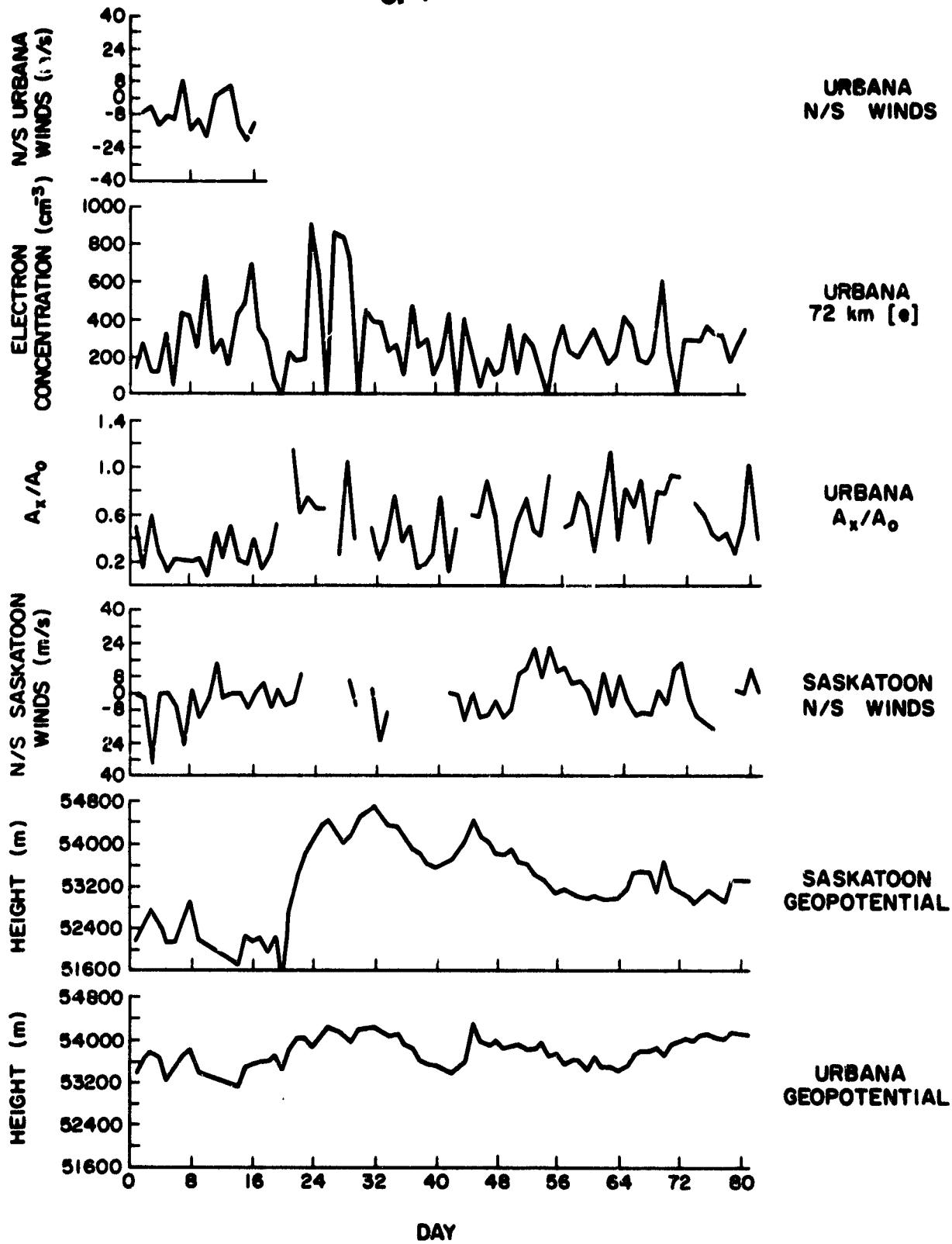

Figure 8.5 Comparison of Urbana 0.4 mbar geopotential, Saskatoon 0.4 mbar geopotential, Saskatoon winds, Urbana A_x/A_O, Urbana 72-km electron concentration, and Urbana winds, for 80 days, starting on December 26, 1978.

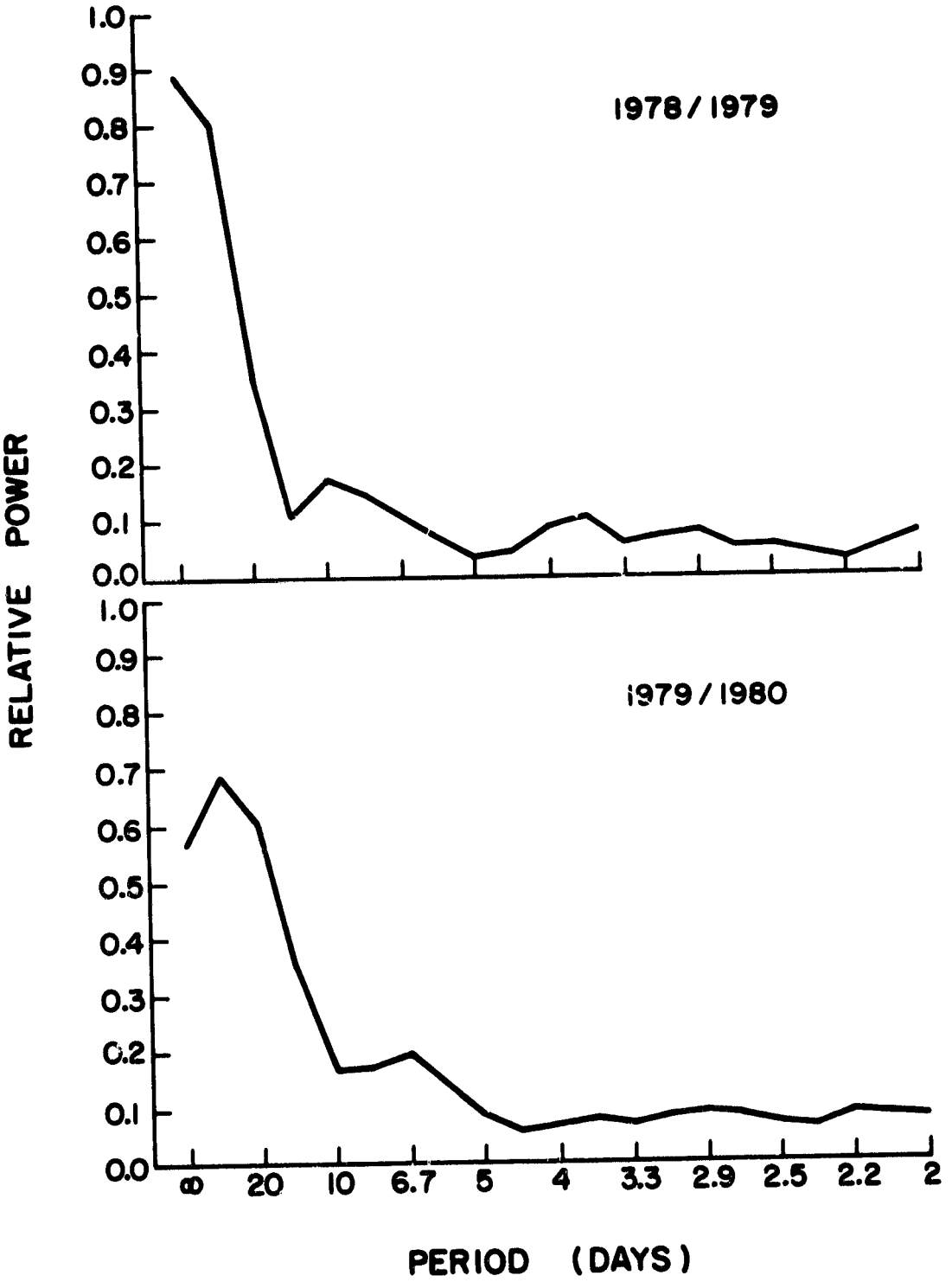

Figure 8.6 FFT of the A_x/A_o ratio at 81 km for 1978/1979 and for 1979/1980.

is about 150 days). Figure 8.7 shows a running FFT of the A_x/A_o at 81 km for the winter of 1978/1979. Each figure is the power spectrum of 32 points of the A_x/A_o data time series from that winter, starting at the date marked on each figure. It can be seen that the variability at a given period indeed does not last for the entire season. A 2.6-day wave is shown for a 32-day length series starting on December 26, and its power is down considerably in the 32-day length series starting on January 5. The January 25 series shows a 3.6-day variability, which remains strong through the February 14 series.

The power spectrum of the 0.4 mbar geopotential over Urbana for the winter of 1978/1979 is shown in Figure 8.8. The spectrum shows a peak at a period of 4 days, which was also present in the spectrum of A_x/A_o data for that winter.

To identify if there is a definite relationship between the variability observed in the stratosphere and the mesosphere, coherences were calculated. Because the observed wave periods vary during the observation season, the coherences must be calculated over only portions of the season. Figure 8.9 is a plot of the running coherence squared between the 0.4 mbar geopotential and the 81 km A_x/A_o ratio over Urbana. This analysis is done with groups of 32 days, with the starting date shown on each individual plot. The horizontal line on each plot shows the 10% significance level, for *a posteriori* selected data. The significance level was estimated by dividing the 10% probability by the number of data groups shown (six), giving a required probability of 1.67% for an equivalent of an *a priori* significance level for an individual 32-day set of data of 10% (see Appendix VI). No values of coherence squared shown on the plots are significant at the 10% level. The lack of significant coherence may be due to the fact that the A_x/A_o data

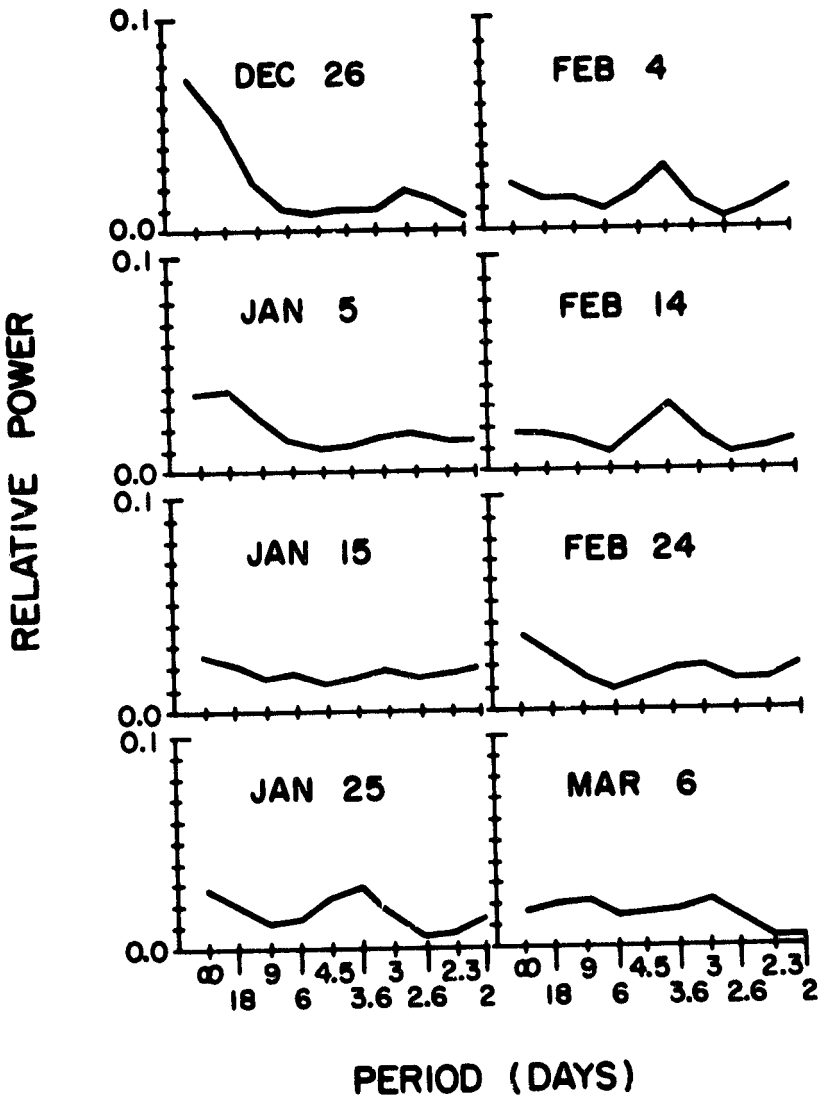

Figure 8.7 Running FFT of the A_x/A_o ratio at 81 km for the winter of 1978/1979. The starting date for each is shown on the figure.

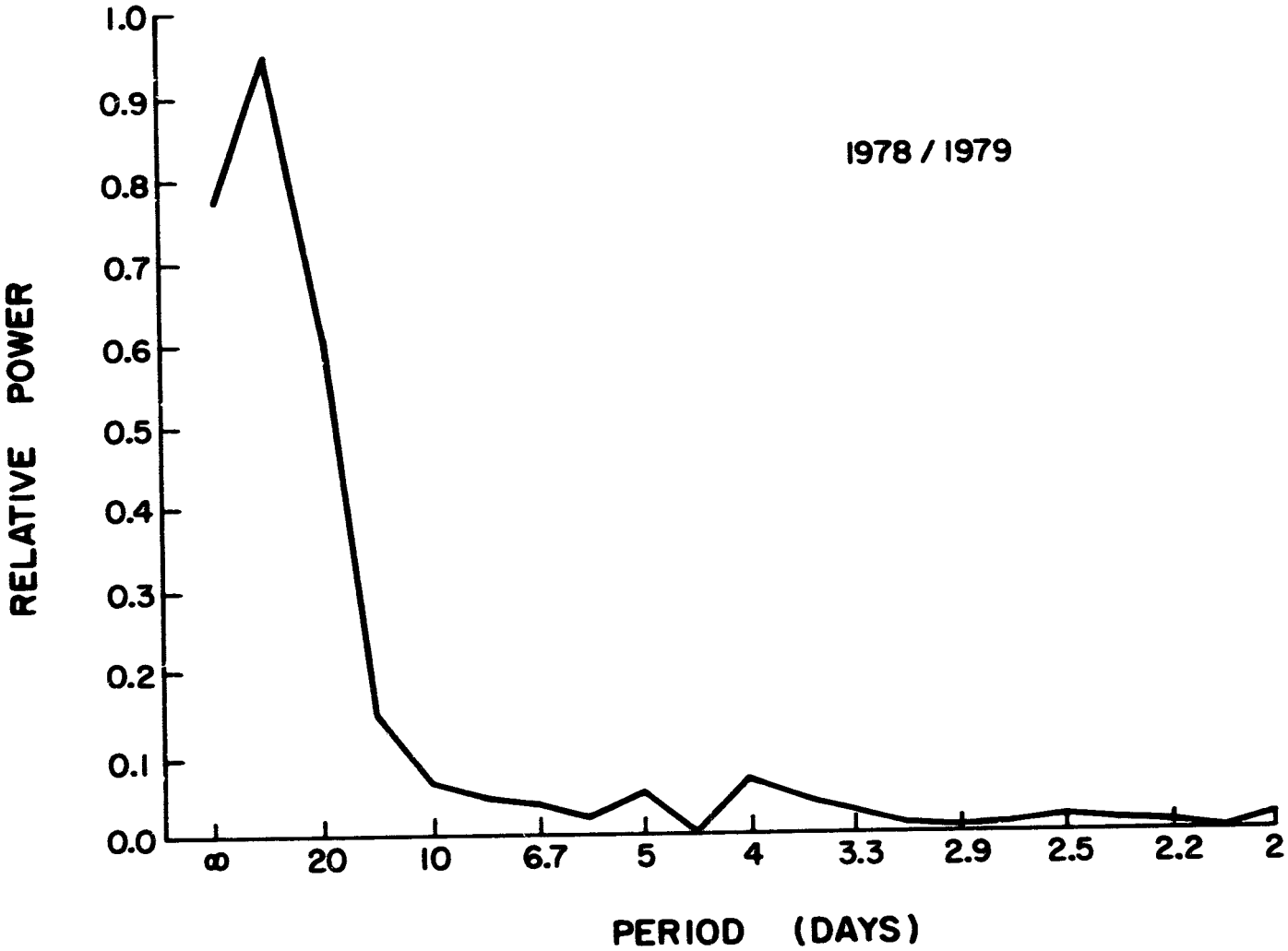

Figure 8.8 FFT of the 0.4 mbar geopotential over Urbana for the winter of 1978/1979.

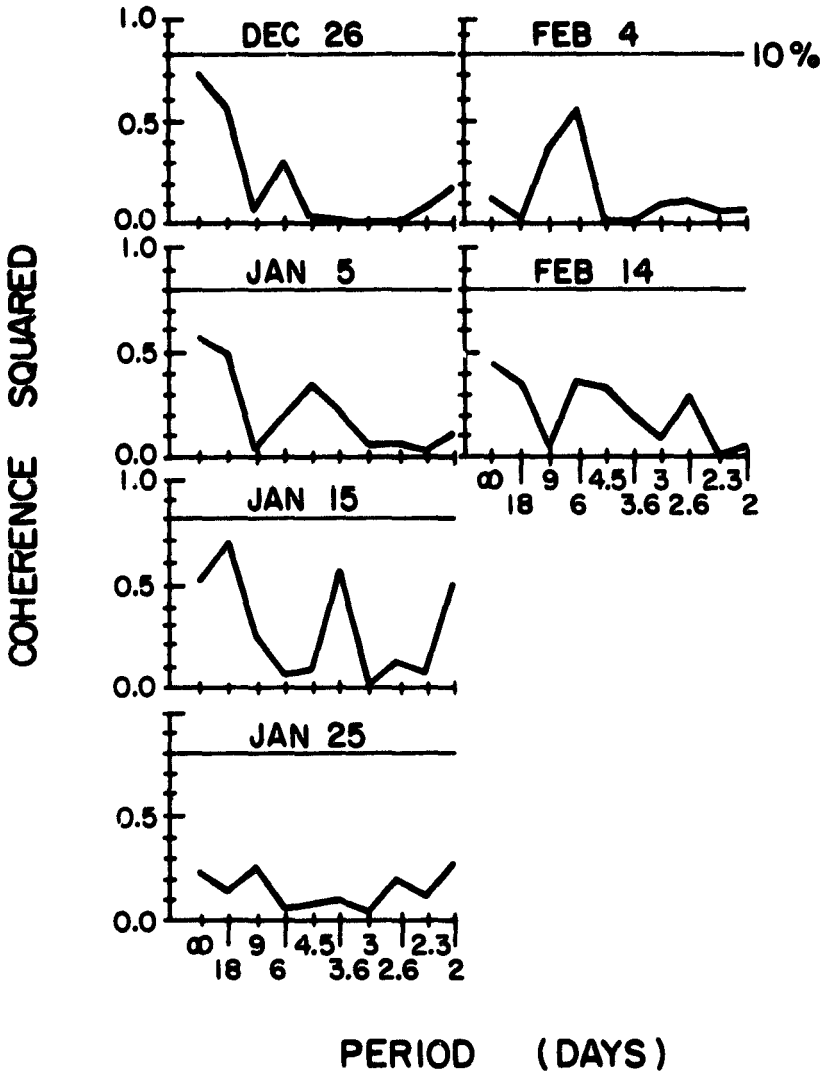

Figure 8.9 Running coherence squared between the 0.4 mbar geopotential over Urbana and the 81-km A_x/A_o ratio at Urbana. The starting date for each is shown on the figure.

representing the electron concentration over many kilometers may not be as sensitive as the electron concentration at a single altitude in showing the effects of a Rossby wave.

Figure 8.10 is a plot of the running coherence squared between the 0.4 mbar geopotential and the 72 km electron concentration over Urbana. The horizontal line on each plot shows the 10% significance level for *a posteriori* data selection. Again, no coherence is seen at the 10% level for any of the data groups. The highest coherence seen is in the 32-day data group starting on January 25. The peak at a period of 3 days is significant at about the 20% level. A peak in the coherence at the same period is seen in the 32-day group starting on February 4, which is significant at about the 25% level. These two groups together indicate a coherence significant at about the 15% level during February. This indicates that there may be a weak couping between the stratosphere and the mesosphere during this time, but it is difficult to establish because of the weakness of the coupling, or its short duration.

To establish the scale of the observed variability to determine if the variability may be due to Rossby waves, the 0.4 mbar geopotential data for the Northern Hemisphere were Fourier transformed in two dimensions (space and time) at 60°N latitude for the 30 day period starting on December 25, 1978. Figure 8.11 shows the amplitude of westward propagating m = 1 waves of various periods. Peaks in the spectrum are shown at the two periods where significant coherences were observed between the 0.4 mbar geopotential and the 72 km electron concentration during that winter (at periods of 4.5 and 2.6 days).

This result indicates that there may be a coupling between the stratosphere and the mesosphere that occurs with the propagation of Rossby waves.

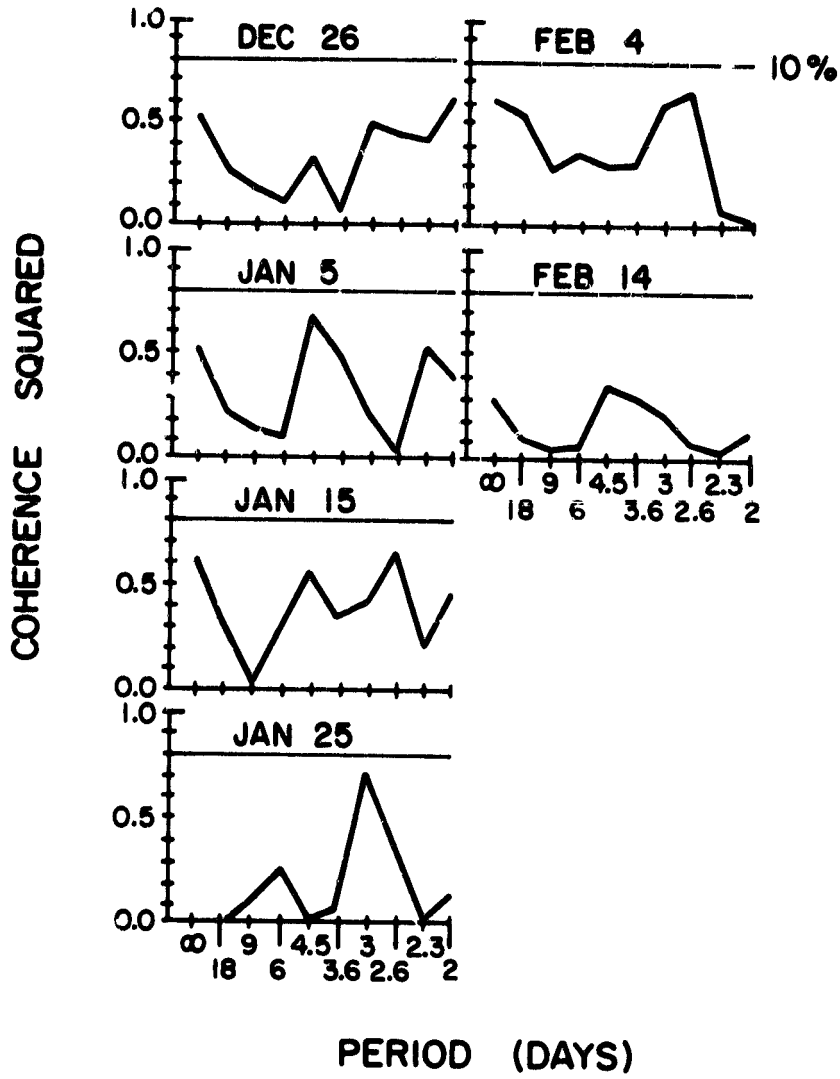

Figure 8.10 Running coherence squared between the 0.4 mbar geopotential over Urbana and the 72-km electron concentration at Urbana. The starting date for each is shown on the figure.

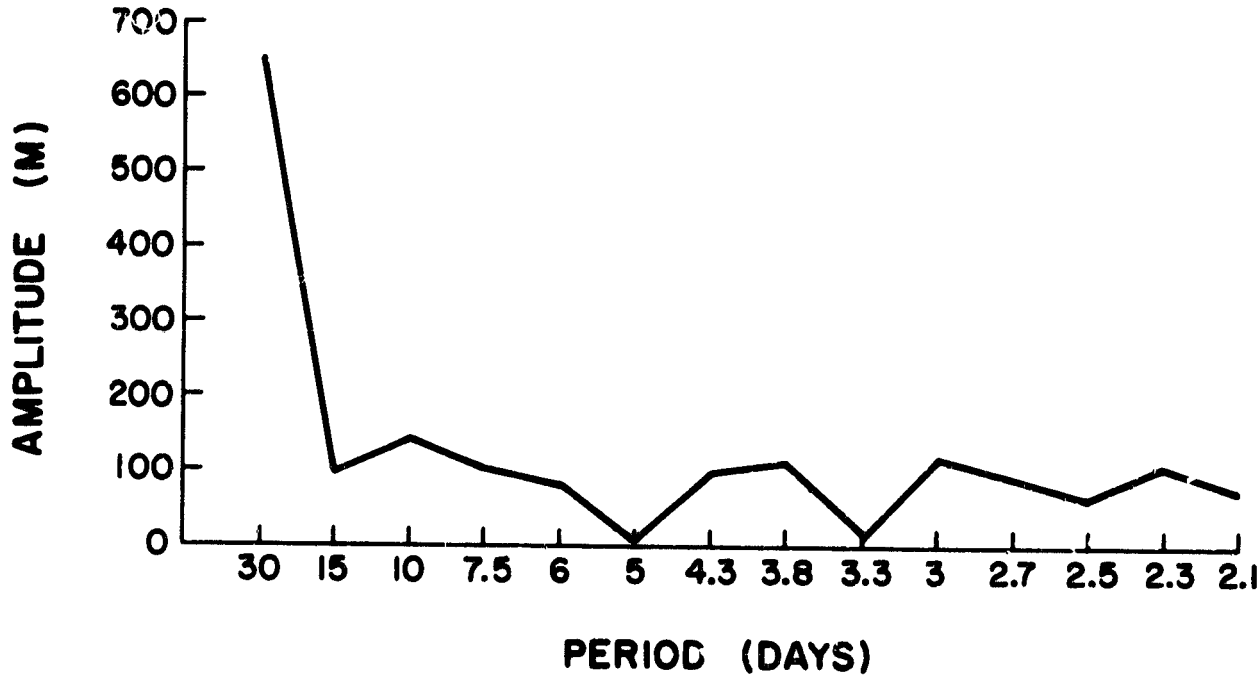

Figure 8.11. Amplitude of westward propagating m = 1 waves of various periods.

9. COMPARISONS OF MEASUREMENTS MADE AT SASKATOON AND URBANA

9.1 *Introduction*

A significant correlation has been shown between the electron concentrations measured at Urbana and the winds measured at Urbana by two techniques. This shows a link between the atmospheric circulation and the electron concentration in the D region. Because of the correlation seen between the E/W component of the winds measured at Urbana and the winds, it is important to determine that the wind structure from the auroral zone to Urbana is such that transport can occur from the auroral zone.

LABITZKE et al. (1978) have analyzed the circulation over the northern hemisphere during the Western European Winter Anomaly Campaign of the winter of 1975/1976, using radiosonde, meteor wind, rocket, and satellite data. Their preliminary results indicate that measuring the wind direction at a single location where the absorption is also measured may not be as important an determining the circulation in the entire region through which the gases are transported.

Mesospheric wind data are available for comparison with the Urbana data from the partial reflection drifts experiment at Saskatoon, Saskatchewan. Daily values of the winds at 80 and 97 km for the years of 1978 and 1979, provided to me by A. H. Manson, will be used for comparison with the winds and electron concentrations measured at Urbana. Saskatoon is located at 52 N, 107 W, and is just south of the southern boundary of the auroral zone. Urbana is located at 40 W, 88 N, so that Urbana is about 1200 km east, and about 1200 km south of Saskatoon.

9.2 *Characteristics of Saskatoon Winds Data*

Winds data have been collected continuously at Saskatoon since September 1978. Winds are calculated using a real-time full-correlation

analysis (MEEK, 1981). Daily winds are measured at 3 km intervals for most of the D region. The winds data used in this analysis are tidally corrected values for 6 km wide slabs centered at 80 and 97 km.

9.3 *Comparison of Data*

The winds data from both stations are available in N/S and E/W components, so the data will be shown as vectors. Because the Urbana winds data are considered reliable for indicating the 24-hour prevailing wind only during the dates when data were averaged over an 8-hour period, only those data will be shown for comparison. A correlation between the Saskatoon N/S winds and the Urbana electron concentrations would be a good indication of transport between the auroral zone and Urbana, because Saskatoon is near the southern boundary of the auroral zone. A delay in time between wind changes at Saskatoon and electron concentration changes at Urbana is likely because of the distance between the observing stations.

The daily values of electron density at 72, 76.5, and 81 km, and A_x/A_o at 81 km, Saskatoon vector winds at 80 km, and Urbana vector winds for the winter months of 1978/1979 are plotted in Figures 9.1 through 9.3. The wind vector for each day is drawn in the direction of the wind, with northward being up and eastward to the right. The A_x/A_o data are a more reliable indicator of the D-region electron content and will be discussed in comparison with the winds data.

When comparing the vectors winds at the two stations in December 1978 and January 1979, the direction of the winds is in the same compass quadrant for all but four of the fifteen days of available data. This indicates that the circulation is of large horizontal extent during this period. When comparing the winds from the two stations during late February 1979, the vector winds are in the same compass quadrant during only half of the days where

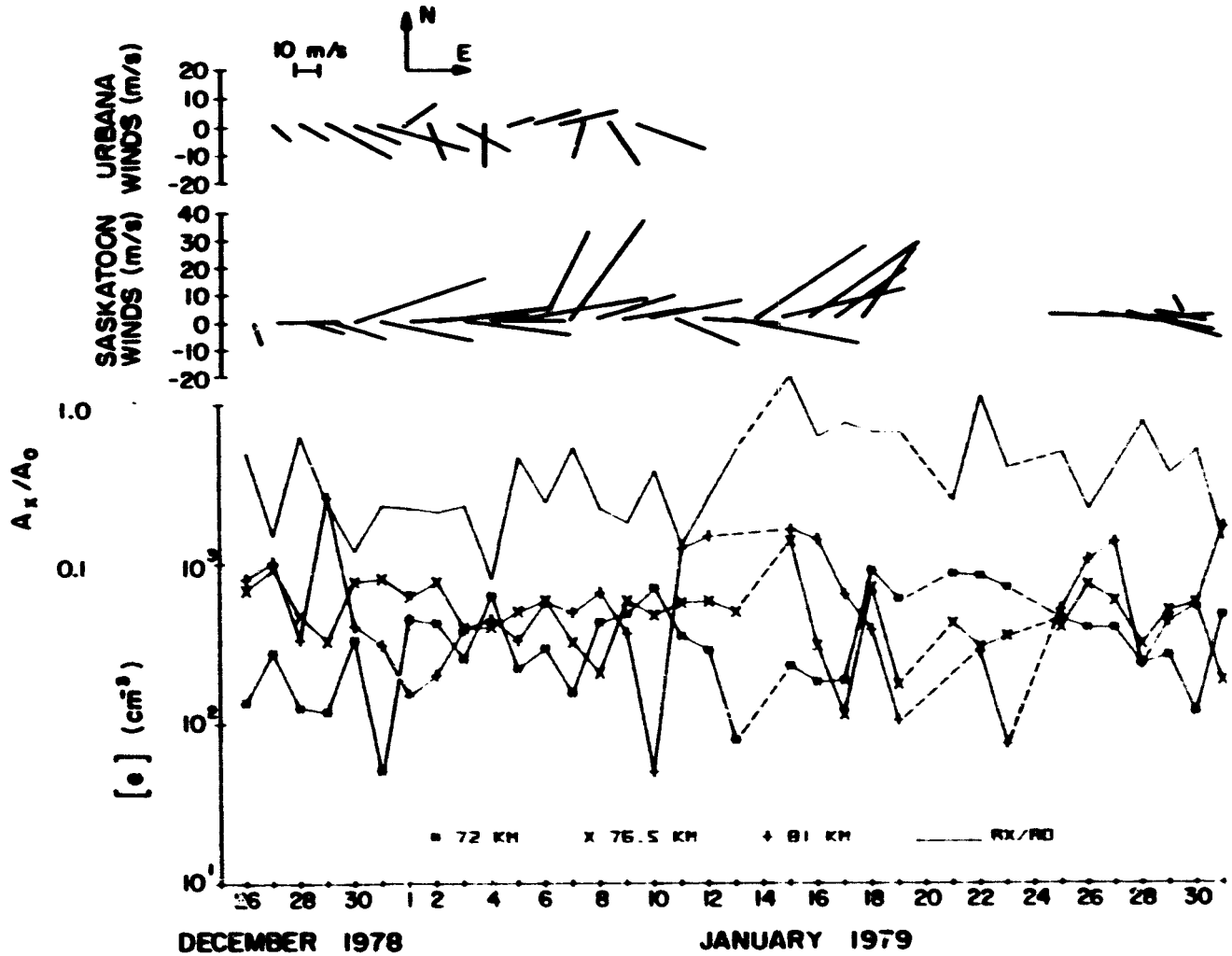

Figure 9.1 Daily plot of electron density at 72, 76.5, and 81 km, A_x/A_o at 81 km, Saskatoon vector winds at 80 km, and Urbana vector winds, for December 1978 and January 1979.

ORIGINAL PAGE IS
OF POOR QUALITY

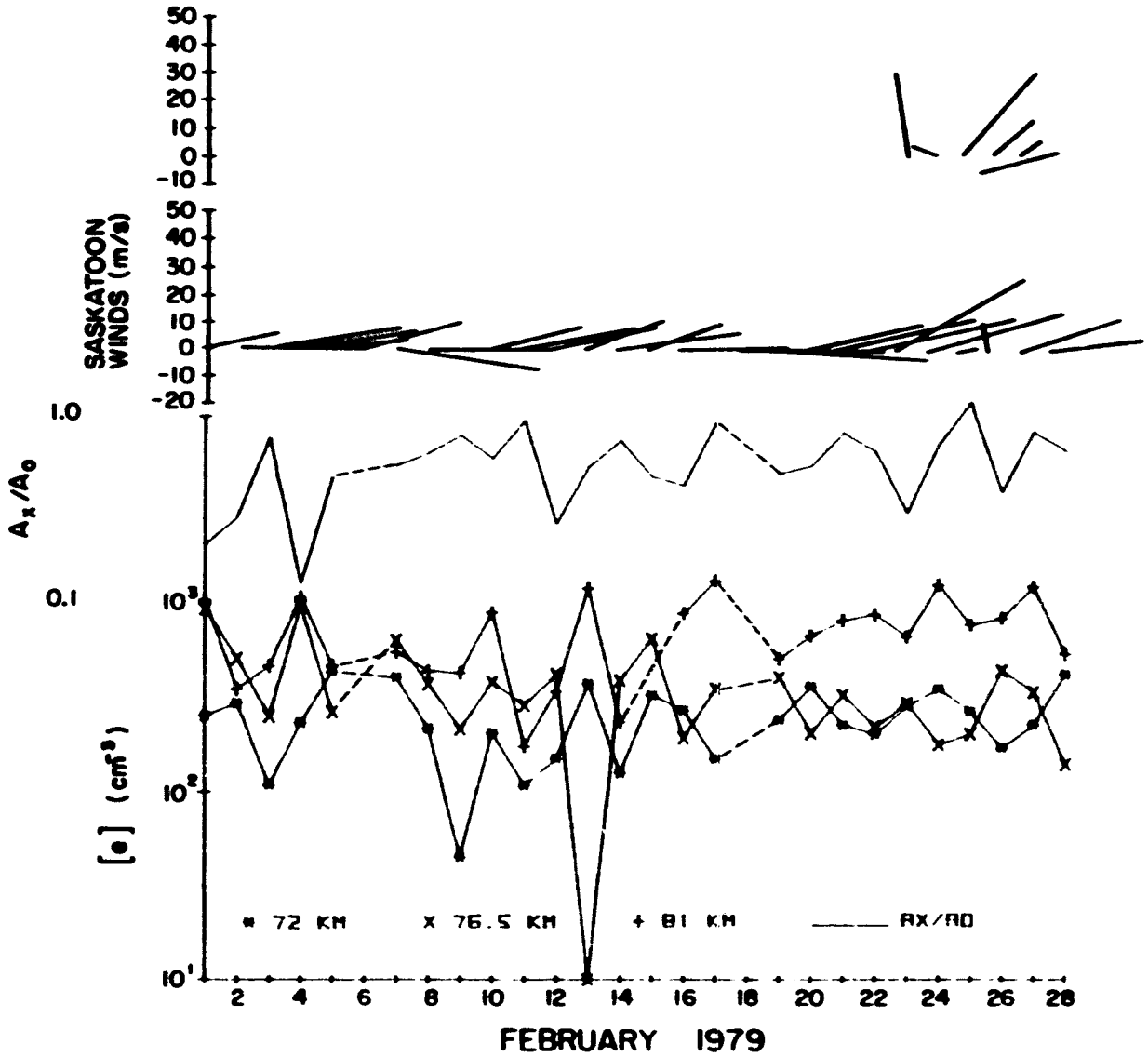

Figure 9.2 Daily plot of electron density at 72, 76.5, and 81 km, A_x/A_o at 81 km, Saskatoon vector winds, and Urbana vector winds for February 1979.

ORIGINAL PAGE IS
OF POOR QUALITY

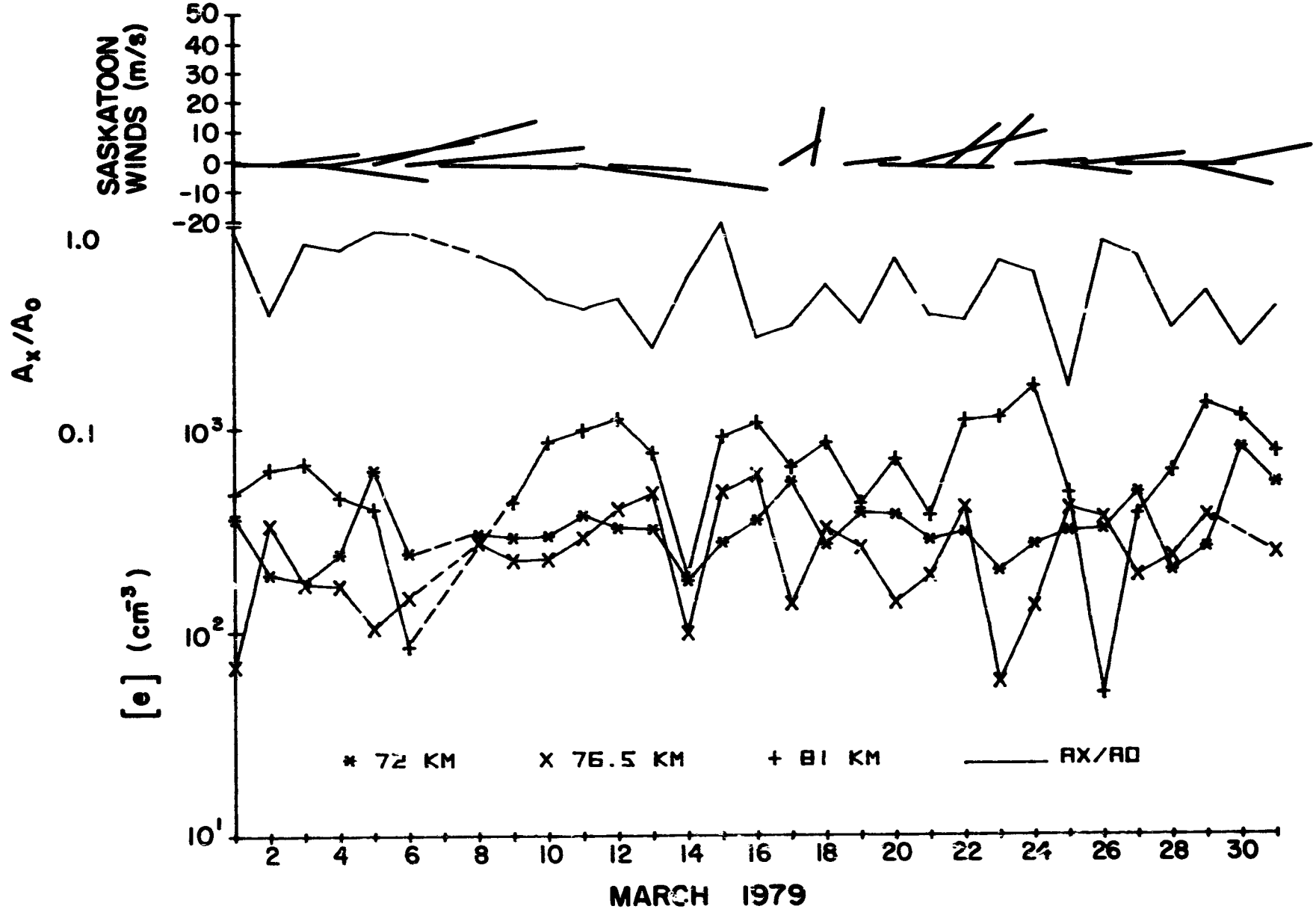

Figure 9.3 Daily plot of electron density at 72, 76.5, and 81 km, A_x/A_O at 81 km, and Saskatoon vector winds for March 1979.

ORIGINAL PAGE
OF POOR QUALITY

data are available. The circulation seems to be of a smaller horizontal extent during this non-winter period. This would imply that the transport of gases from the auroral zone would occur only during the period near January in the winter of 1978/1979. The correlations between winds and electron concentrations measured at Urbana shown earlier were significant only during January and early February of the winter of 1978/1979.

When comparing the Saskatoon winds with the Urbana electron concentrations, the E/W component shows no apparent correlation with the A_x/A_O ratio during any of the months. There is little obvious correlation between the N/S component of the Saskatoon winds and Urbana A_x/A_O ratio, except during the month of January. There is no fixed relationship between the Saskatoon winds and the A_x/A_O ratio in January, but the major increases in the A_x/A_O ratio (decreasing electron concentration) occur during times when the Saskatoon winds are northward. The dates of January 6, 7, and 14 through 18 show increased A_x/A_O ratio data with northward winds.

Figures 9.4 through 9.8 are plots of the data collected at Saskatoon and Urbana for the months of November 1979 through March 1980. The length of the Urbana data is much longer during this winter so the increase in correlation should be seen from November to late December. The variability in the A_x/A_O data is obviously greater during the month of January 1980, than it is during the month of November 1979. The variability in the N/S component of the Saskatoon winds is also greater in January 1980 than it is in November 1979.

There is little relationship between the N/S Saskatoon wind component and the A_x/A_O ratio at Urbana during November or the first half of December. A relationship between the winds and the A_x/A_O data is shown starting in mid-December. Southward winds from December 15 through December 19 result

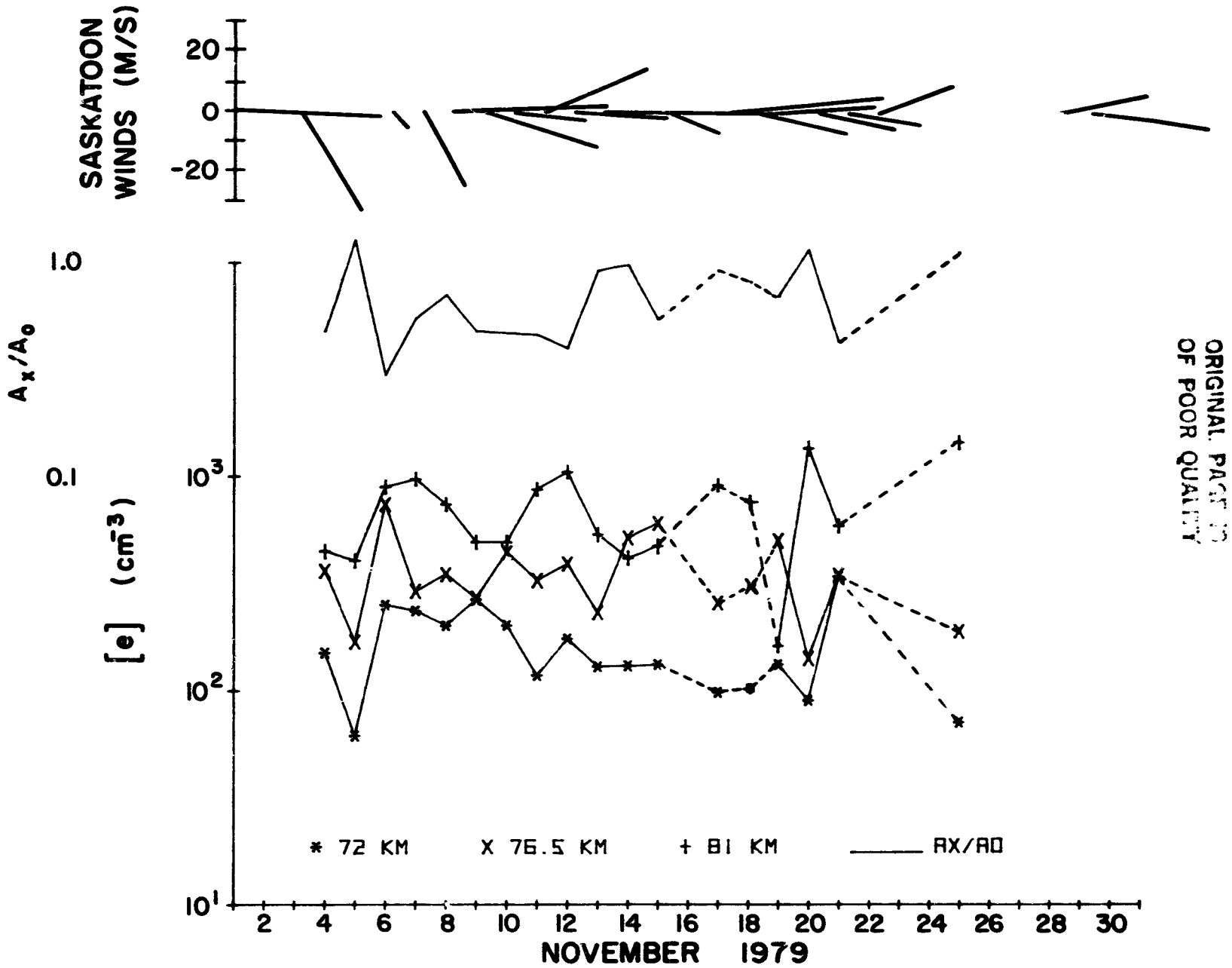

ORIGINAL PAGE IS
OF POOR QUALITY

Figure 9.4 Daily plot of electron density at 72, 76.5, and 81 km, A_x/A_O at 81 km.

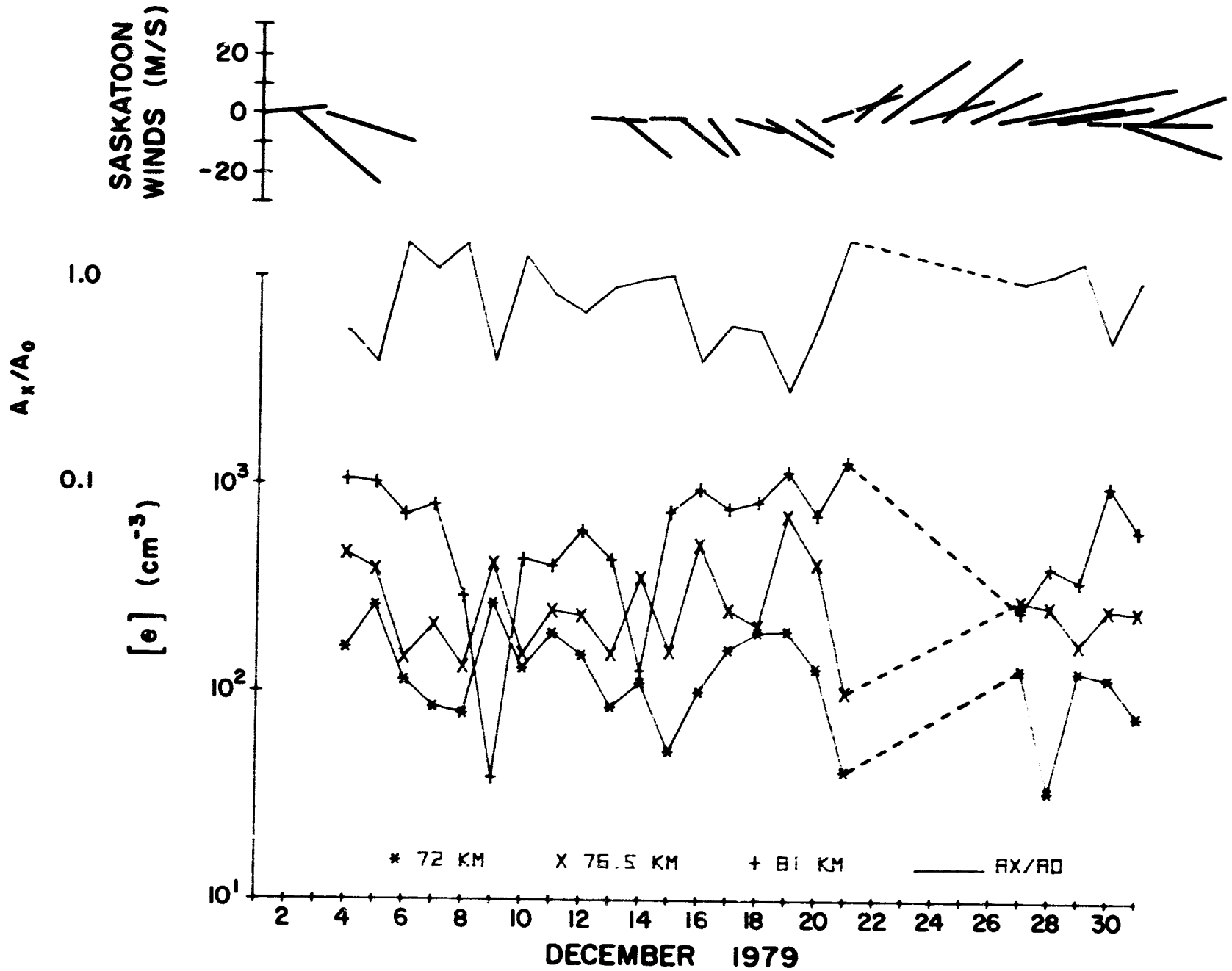

Figure 9.5 Daily plot of electron density at 72, 76.5, and 81 km, A_x/A_o at 81 km.

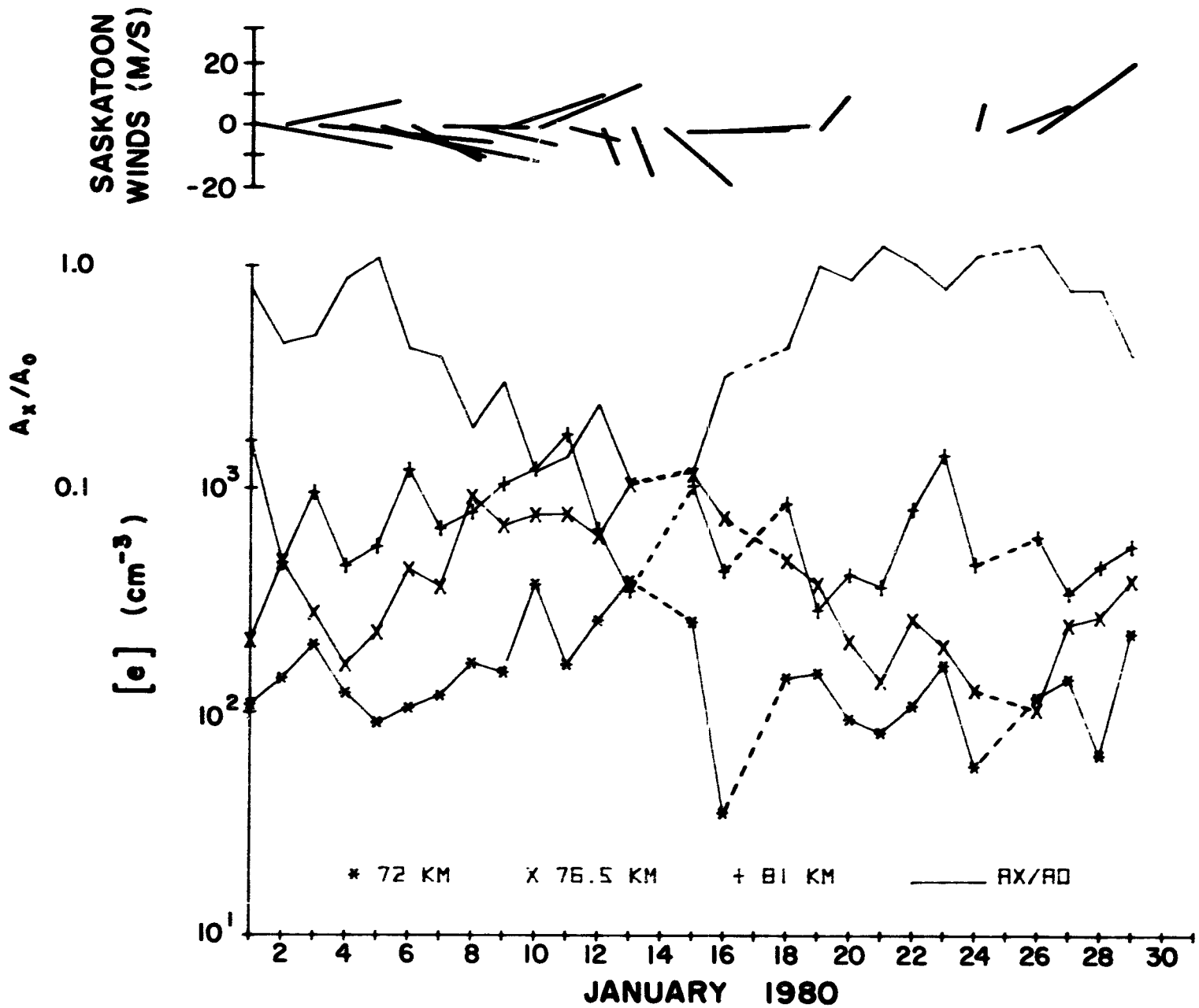

Figure 9.6 Daily plot of electron density at 72, 76.5, and 81 km, A_x/A_o at 81 km.

ORIGINAL PAGE IS
OF POOR QUALITY

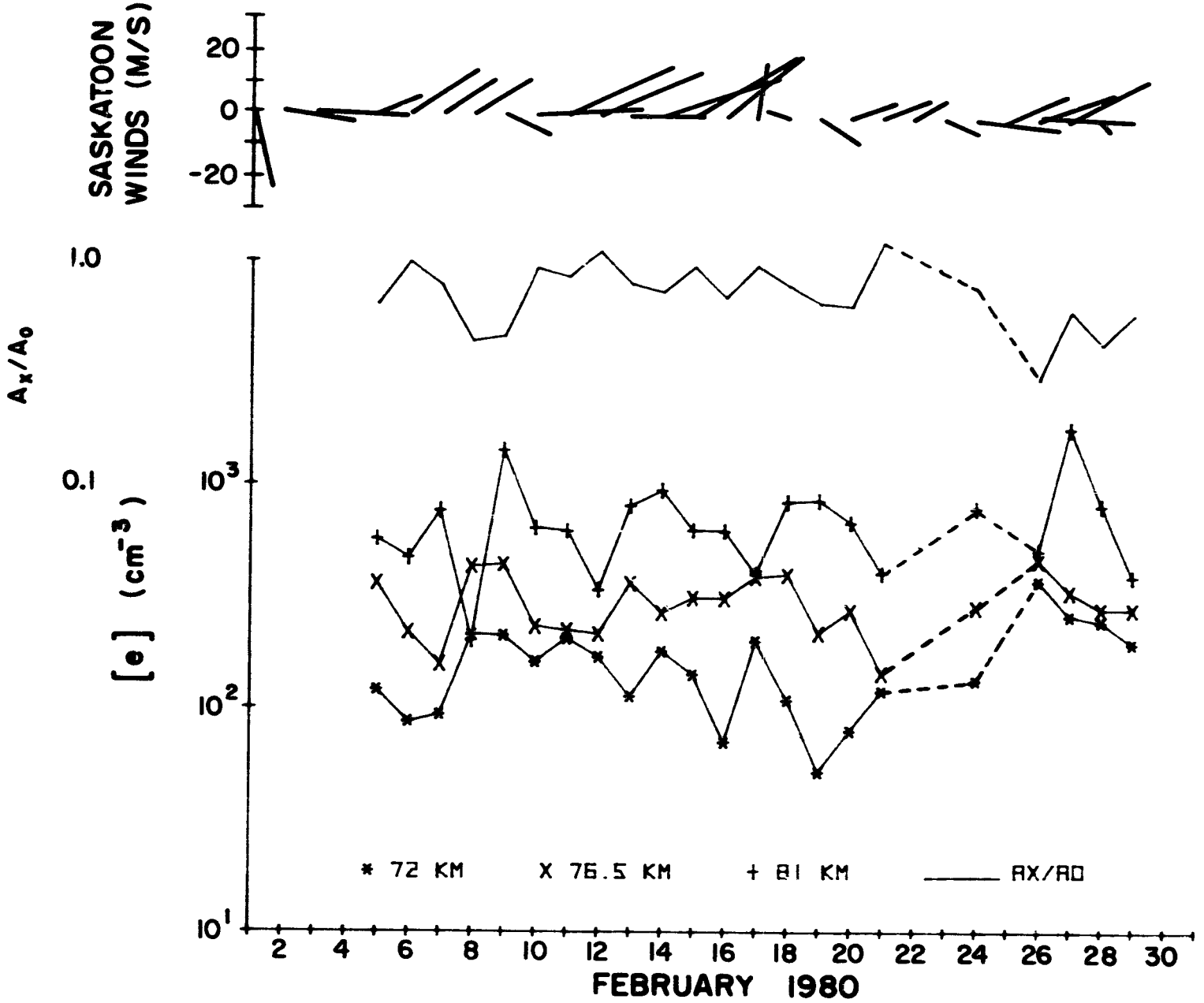

Figure 9.7 Daily plot of electron density at 72, 76.5, and 81 km, A_x/A_o at 81 km.

ORIGINAL PAGE IS
OF POOR QUALITY

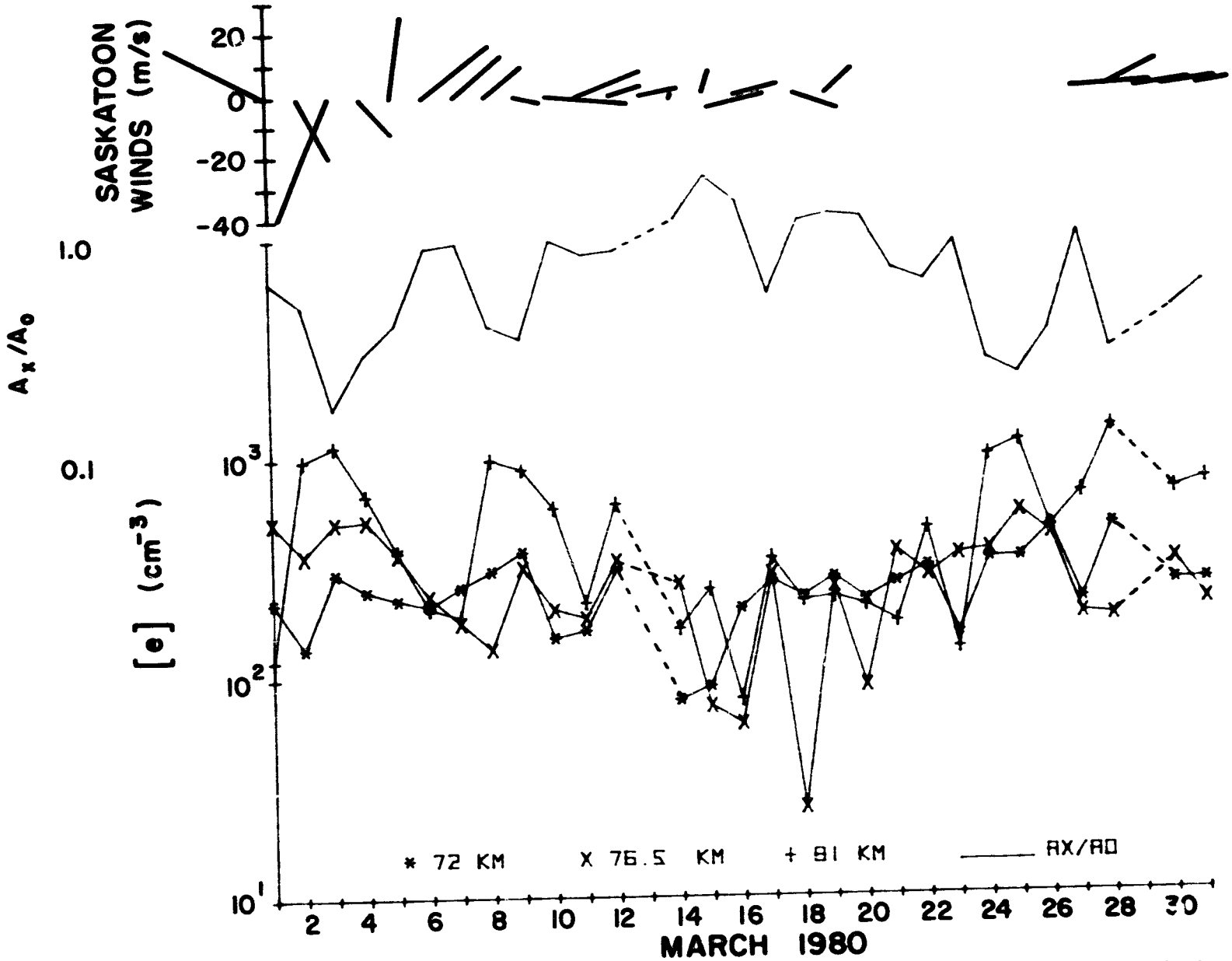

Figure 9.8 Daily plot of electron density at 72, 76.5, and 81 km, A_x/A_C at 81 km.

ORIGINAL PAGE IS OF POOR QUALITY

in a lowering of the A_x/A_o ratio (increasing electron concentration), and northward winds from December 20 through January 2 are accompanied by an increased A_x/A_o ratio during that period. When the wind becomes more southward on January 5, the A_x/A_o ratio drops until the winds become more northward on January 15. During the month of February 1980, the N/S component of the Saskatoon winds is towards the north and the A_x/A_o ratio is consistently high during most of the month. From late February 1980 through March 1980 there is no obvious correlation between the winds and the A_x/A_o data.

There is, in general, a correlation shown between the N/S component of the winds measured at Saskatoon and the A_x/A_o ratio measured at Urbana. To more closely investigate this relationship and how it varies during the year, correlations were calculated.

Figure 9.9 shows scatter plots of the N/S wind component (northward positive) and the A_x/A_o ratio at Urbana for 90 days, starting on December 1, 1979. The number of days that the winds data are shifted relative to the A_x/A_o data is indicated on each plot. (For example, in the -2 days plot, winds data starting on November 29 are compared with A_x/A_o data starting on December 1.) The value of the correlation coefficient between the data is shown on each plot. The maximum correlation shown (which was not very good) occurred with no delay between the Saskatoon and Urbana data, with a correlation coefficient of 0.2864. The scatter plots indicate a weak correlation for the data taken from the 90-day period. The correlations shown between winds and electron concentrations measured at the same location were also weak over large portions of the winter, and significant for part of the winter only. The Saskatoon winds and Urbana electron concentrations are probably also correlated during only a part of the winter.

To investigate the degree of correlation between the winds at Saskatoon

ORIGINAL PAGE IS
OF POOR QUALITY

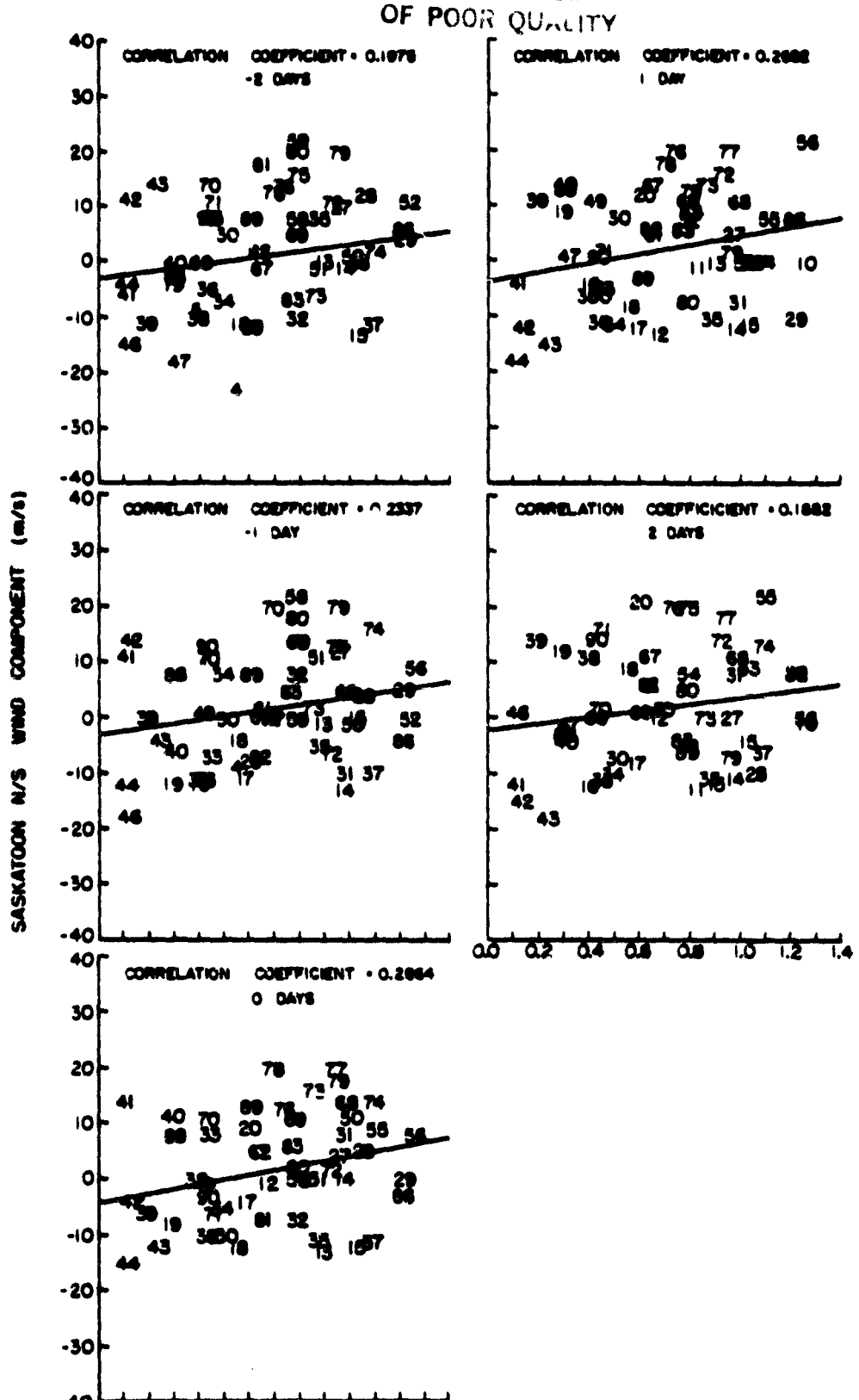

Figure 9.9 Scatter plots of the N/S wind component (northward positive) and the A_x/A_o ratio at Urbana for 90 days, starting on December 1, 1979. The number of days that the winds data are shifted relative to the A_x/A_o data is indicated on each plot.

and the A_x/A_O ratio at Urbana, correlations were calculated for groups of 30 days, spaced every five days throughout tne winter. The winds data were shifted by up to plus and minus five days, in one-day increments, relative to the Urbana A_x/A_O data. The delay indicated in the shift in time for maximum correlation will estimtae the transport time from the auroral zone to Urbana that would be present.

Figure 9.10 shows the running shifted correlations between the Saskatoon 80 km N/S winds and Urbana A_x/A_O ratio data for the winter of 1978/1979. The starting date for each 30-day correlation group is shown on each plot. A negative shift indicates that a change in Saskatoon winds occurs before a change in Urbana A_x/A_O ratio. The horizontal line on each plot shows the ten-percent level of significance for *a posteriori* selected data sets (see Appendix VI). The correlation peaks, with no shift between the sets of data, for the 30-day groups starting on December 31 through January 20. This correlation is significant at the 40% level in the 30-day groups starting on December 31, January 5, and January 20. A strong correlation (significant at the 4% level) is shown for a shift of -4 days in the 30-day groups starting on January 25 and January 30. The four-day delay between Saskatoon winds and Urbana A_x/A_O ratio changes would indicate an average southward velocity component of 3.5 M/S along the path from the auroral zone

In the 30-day groups starting on February 9 and February 14 the correlation peaks with the changes in A_x/A_O occurring one day before the shifts in the N/S wind. This result could occur because of the 1200 km east-west distance between the stations, if the A_x/A_O shifts are caused by perturbations in the flow due to Rossby waves, which propagate westwards.

Figure 9.11 shows the running shifted correlations between the 80-km N/S winds at Saskatoon and the 81-km A_x/A_O data for the winter of 1979/1980.

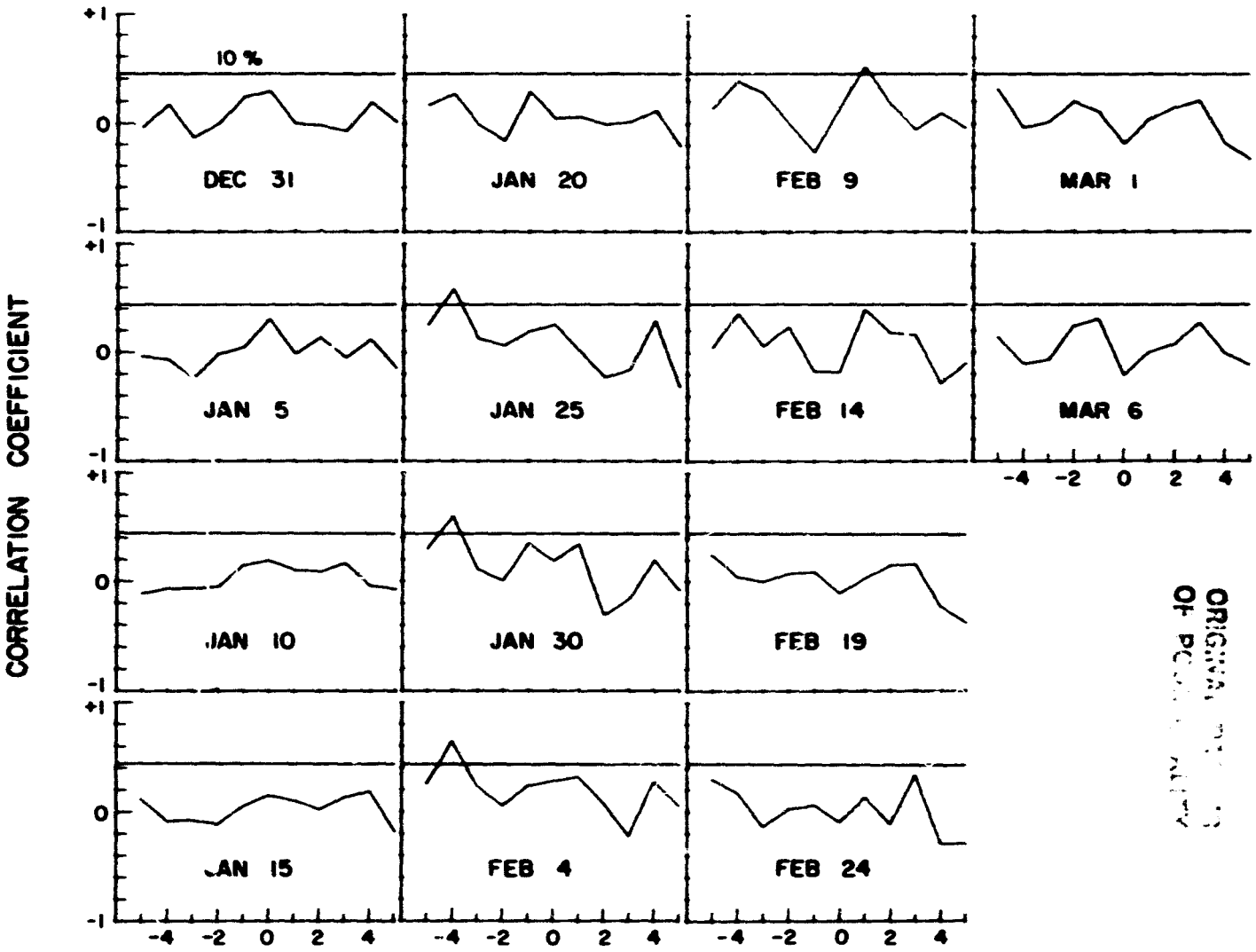

Figure 9.10 Running shifted correlations between Saskatoon 80-km N/S winds and Urbana 81-km A_x/A_O ratio data for 1978/1979. The starting date for each 30-day correlation group is shown on each plot, a negative shift indicates that a change in winds occurs before a change in A_x/A_O.

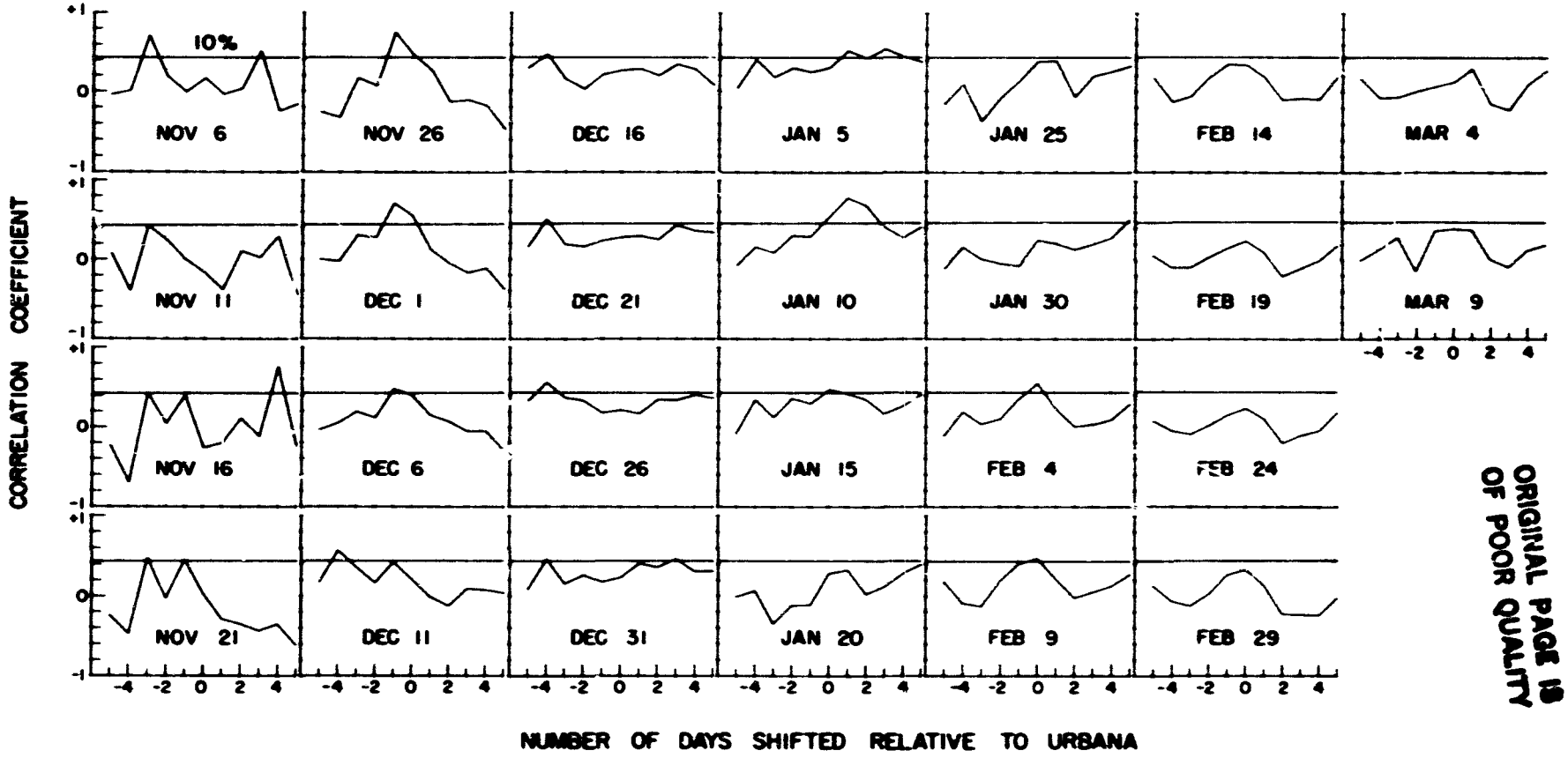

ORIGINAL PAGE IS
OF POOR QUALITY

Figure 9.11 Running shifted correlations between Saskatoon 80-km N/S winds and Urbana 81-km A_x/A_o ratio data for 1979/1980. The starting date for each 30-day correlation group is shown on each plot. A negative shift indicates that a change in winds occurs before a change in A_x/A_o.

The horizontal line on each plot is the 10% level of significance. The data set for this year is much longer, so the changes during the winter can be seen. The correlations in the 30-day groups starting in the month of November have two significant peaks. This could be a result of the propagation of a Rossby wave of a 3-day period through the region. The 30-day groups starting on November 26 through December 11 have a significant peak at -1 day shift. This would indicate an average southward horizontal velocity component of 14 M/S. The 30-day groups starting on December 16 through January 5 do not show a dominant peak in the correlations. Starting on January 15, the correlations show a dominant, often significant peak at no shift, and this continues through the March data.

The correlation plots indicate that there is no simple constant relationship between the winds measured at Saskatoon and the electron measured at Urbana. The data observed at the two stations at times are related with no time delay between wind changes and A_x/A_O ratio changes. This would support the idea that there is a latitudinal gradient of nitric oxide present, so that with a large-scale circulation shift, the wind shift measured at Saskatoon would also occur at Urbana with a corresponding shift in the concentration of ionizable nitric oxide at Urbana. A correlation with a time delay would indicate that transport of a "cloud" of ionizable nitric oxide from the auroral zone to Urbana occurred under favorable circulation conditions. It appears that both of these conditions occur at different times during the winter.

The analysis is further complicated by the fact that the observation stations are at different longitudes (with a spacing along the east-west direction about equal to their spacing along the north-south direction). An observed delay may be in fact due to a perturbation in the circulation that

is propagating along the east-west direction. In particular, the propagation of a Rossby wave towards the west may result in a shift in the A_x/A_o ratio at Urbana that occurs before a shift in the winds at Saskatoon. The correlation analysis does indicate that there is no single constant relationship shown, and the coupling mechanism between the two locations changes during the winter.

9.4 *Investigation of Coupling between the Two Stations due to Rossby Waves*

The observed correlation between the data at the two stations may be a result of perturbations in the flow due to the propagation of Rossby waves in the mesosphere. To investigate this type of coupling, and to determine during what part of the winter season it occurs, Fourier and cross-spectral analyses have been performed on the data from the two stations. To determine the frequency range of variability of the N/S component of the winds at Saskatoon, the power spectra at two altitudes were calculated. Figure 9.12 shows the power spectra of the N/S winds at 80 and 97 km for the winter of 1978/1979. Peaks in the spectra occur at both altitudes in the period range of 4.5 to 5 days, and near 2.5 days. Figure 9.13 is the running power spectra of the 97-km Saskatoon N/S wind component. Each power spectrum plot is calculated from 32 days of data starting on the date shown on each individual plot. A 4.5-day period fluctuation occurs during the first two 32-day groups of the data in the figure. The 2.3-day component in the spectra is lower in power, and occurs later in the season, remaining for about a month.

To establish that the variability in the data observed at discrete frequencies at both stations is related, coherence squared spectra were calculated. Figure 9.14 shows the coherence squared between the 81-km A_x/A_o ratio at Urbana and the N/S component of the 97-km wind at Saskatoon. The

ORIGINAL PAGE IS
OF POOR QUALITY

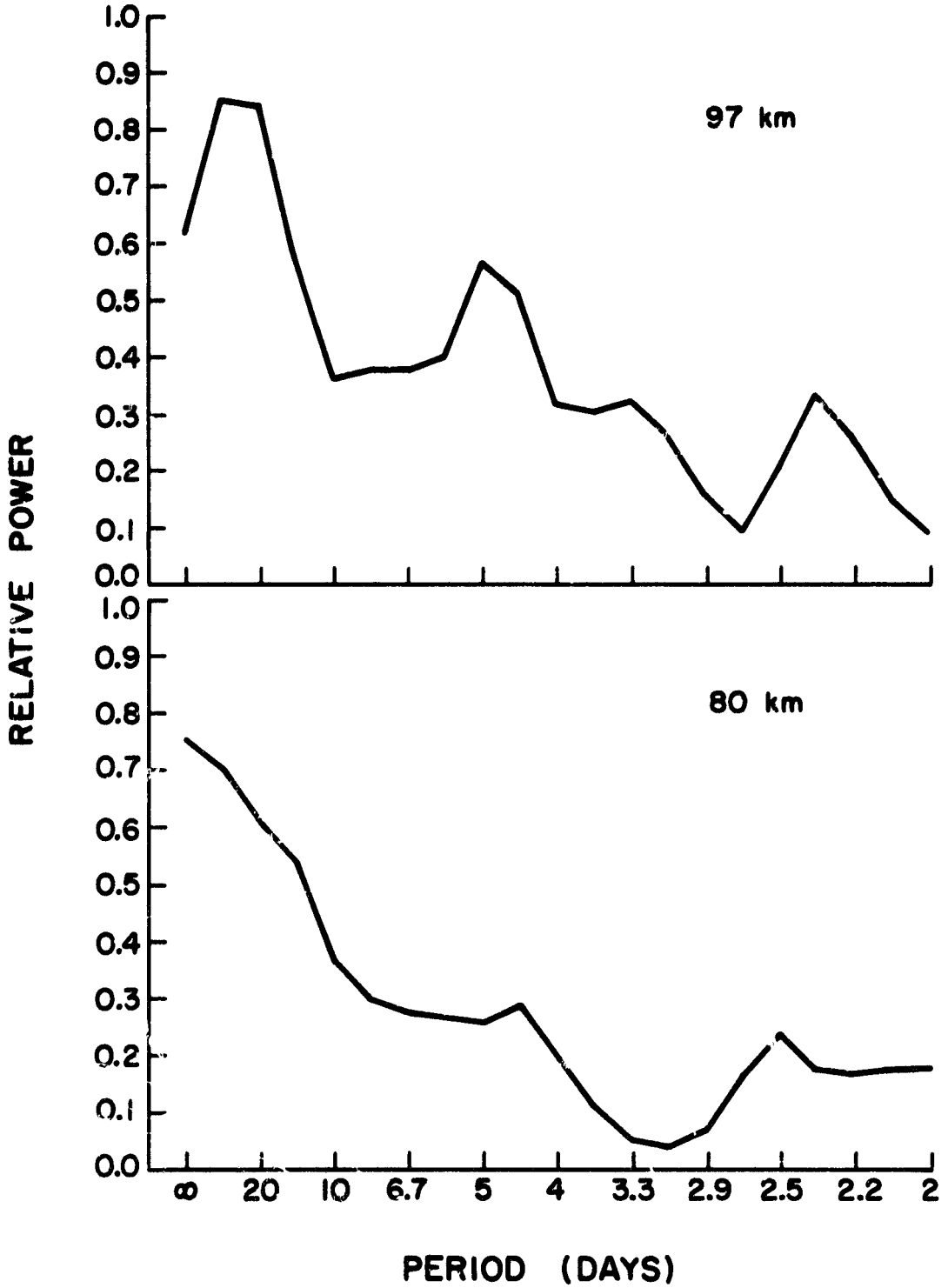

Figure 9.12 Power spectra of Saskatoon N/S winds at 80 and 97 km during the winter of 1978/1979.

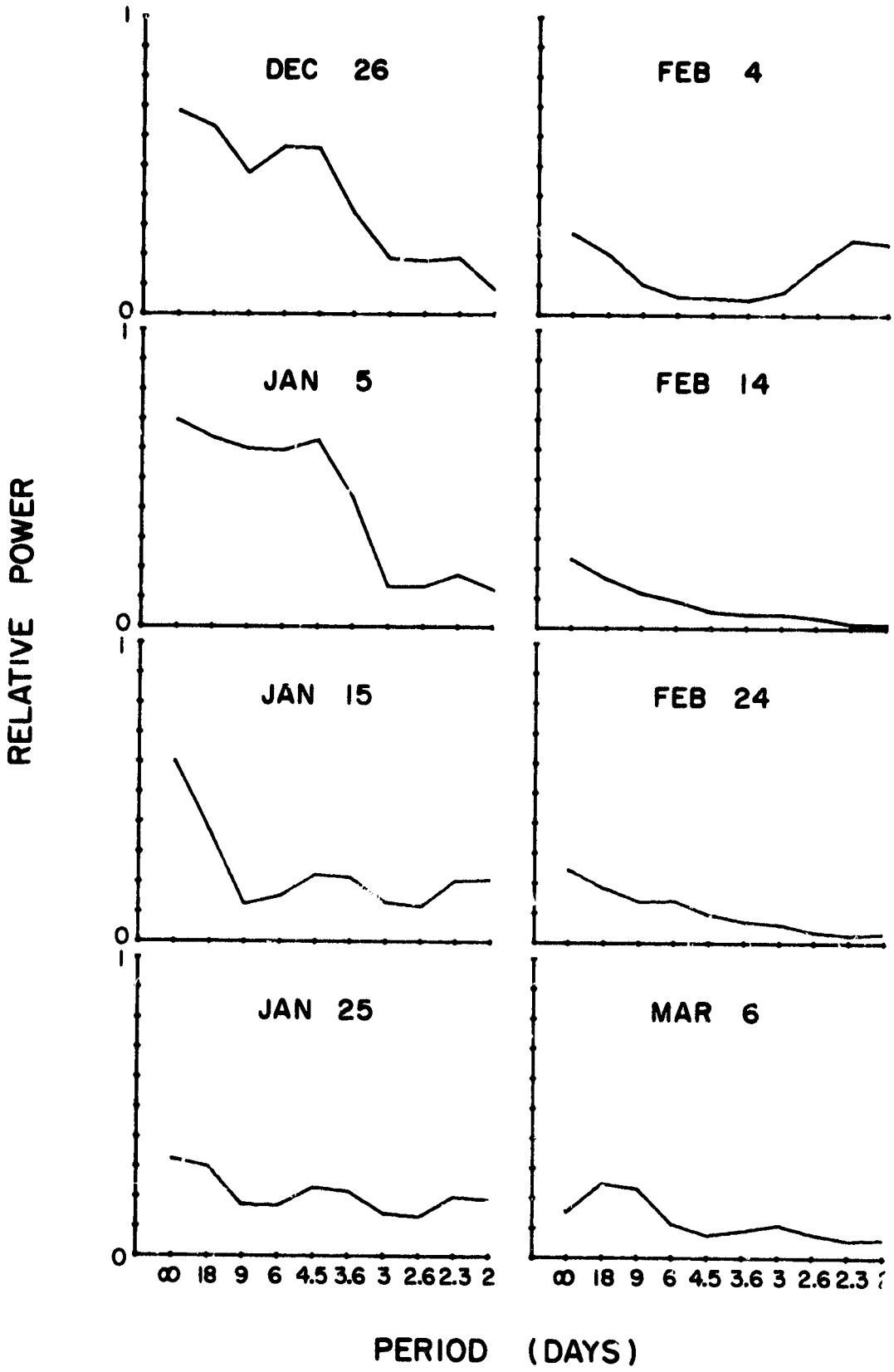

Figure 9.13 Running power spectra of the Saskatoon N/S 97-km wind component for the winter of 1978/1979. The starting date for the 32-day group is shown on each plot.

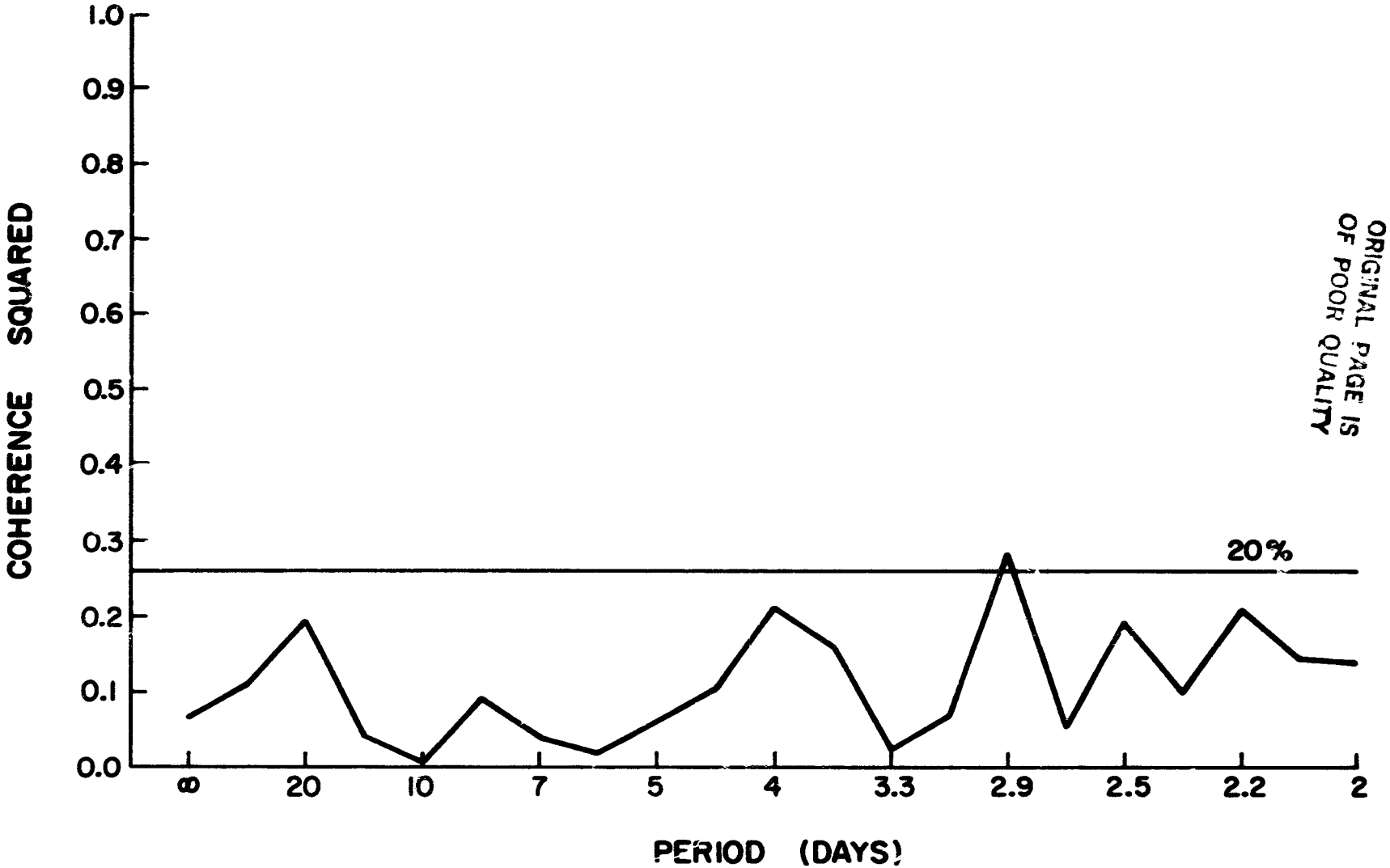

ORIGINAL PAGE IS
OF POOR QUALITY

Figure 9.14 Coherence squared between the 81-km A_x/A_o ratio at Urbana and the N/S component of the 97-km wind at Saskatoon. The horizontal line indicates the 20% level of significance.

horizontal line indicates the 20% level of significance. The only period where there is significance at the 20% level for the data taken for the entire winter is at 2.9 days. Variability at this period is shown in the power spectrum (see Figure 9.13) only in the 32-day group starting on March 6. The coherences at the periods of 4.5 to 5.0 and near 2.5 days are not significant at the 20% level when the data from the entire winter are considered. Because the coupling process is changing throughout the winter, shorter segments of data taken through the winter will be considered.

Figure 9.15 is the running coherence squared between the 81-km A_x/A_o ratio at Urbana and the N/S component of the 97-km wind at Saskatoon. The horizontal line on each plot indicates the 10% level of significance. For *a posteriori* data selection see Appendix VI. A peak in the coherence squared at 2.6 days occurs in the data, starting in the 32-day group starting on February 4, but it is significant only in the February 24 data set. A coherence squared between the 0.4 mbar geopotential and 72-km electron concentration at Urbana that is significant at the 20% level occurred in the 32-day group of data starting on January 25 (see Figure 8.10), indicating that a Rossby wave of that period may have been present at that time. In Figure 9.10, the shifted correlation coefficient data calculated for the 32-day groups starting on February 9, 14, and 24 indicate that changes in electron concentration at Urbana occur before corresponding changes in wind at Saskatoon. A possible explanation for this is that the perturbations in the flow due to the propagation of Rossby waves would occur at Urbana before Saskatoon because the waves are propagating towards the west. The coherence data shown in Figure 9.15 indicate that a Rossby wave was present, with a period of 2.6 days, during this time period (see February 24 data set) which could cause the observed correlation. A peak in the coherence squared at

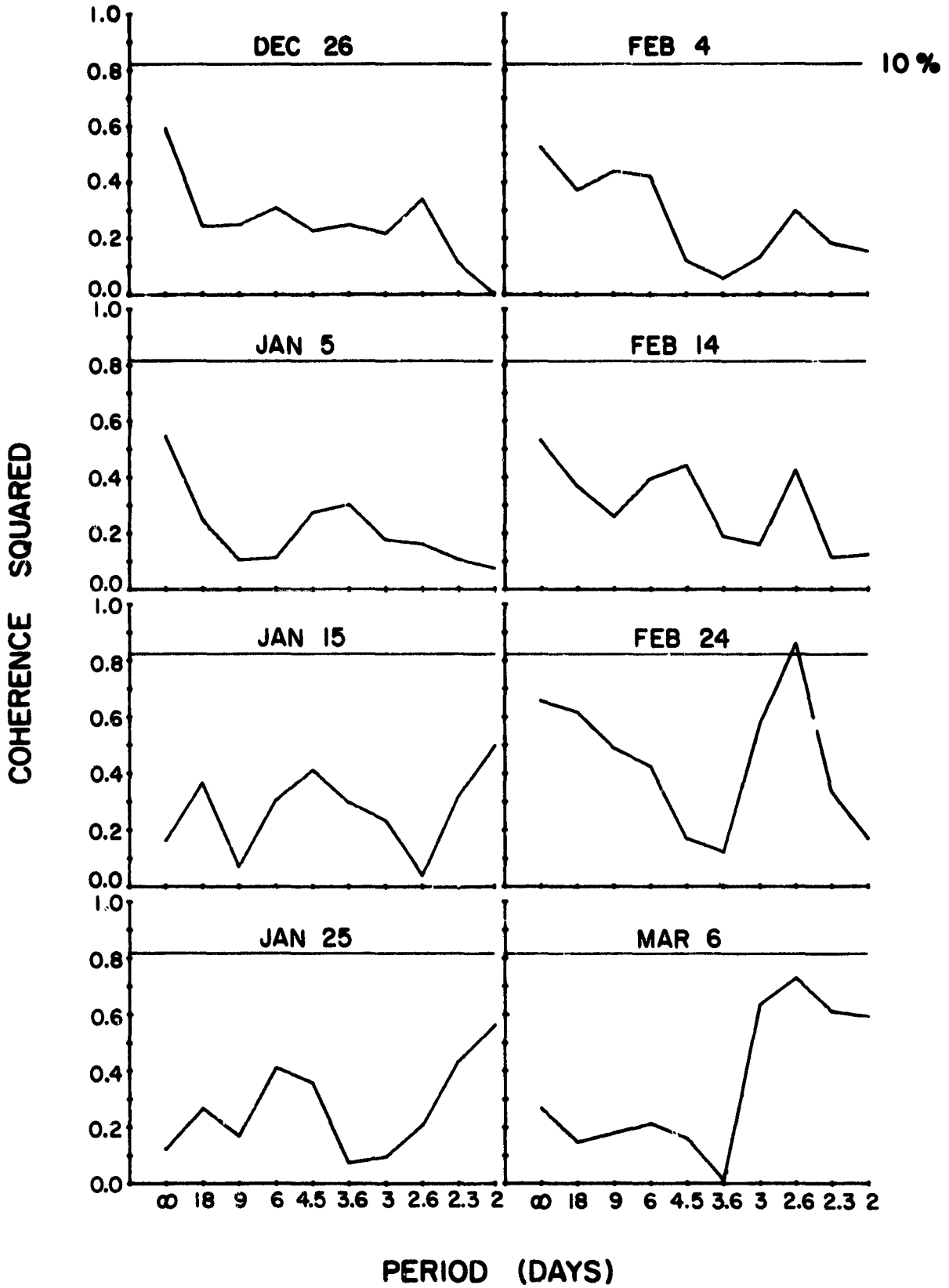

Figure 9.15 Running coherence squared between the 81-km A_x/A_O ratio at Urbana and the N/S component of the 97-km wind at Saskatoon for winter 1978/1979. The starting date for each 32-day group is shown on each plot. The horizontal line on each plot indicates the 10% level of significance.

the 4.5-day period is shown in several of the 32-day groups during the winter, but is not significant at the 10% level in any of the groups.

The power spectra of the Saskatoon N/S wind component at 80 and 97 km, during the winter of 1979/1980 are shown in Figure 9.16. The spectrum at 80 km shows peaks at periods of 2.24 and 4.4 days, and the spectrum at 97 km shows a peak at a period of 6.7 days. The power spectrum of the A_x/A_o data measured during the winter of 1979/1980 shows a peak at a period of 6.7 days also (see Figure 8.6).

To determine if the fluctuations observed at the two stations during the winter of 1979/1980 are related, coherences were calculated. Figure 9.17 shows the coherence squared between the 81-km A_x/A_o ratio at Urbana and the N/S component of the 97-km wind at Saskatoon during the winter of 1979/1980. The peaks in the coherence squared that are significant at the 20% level occur at periods of 3.3 and 2.2 (significant at the 10% level) days. The 6.7 day period fluctuation does not have a significant coherence. The length of the data set for this winter is longer than that of the year before, and the fluctuations may not occur or remain coherent throughout the winter. To investigate these changes, coherences were calculated for shorter data segments throughout the winter.

Figure 9.18 is the running coherence squared between the 81-km A_x/A_o ratio at Urbana and the N/S component of the 97-km wind at Saskatoon. The starting date for each 32-day group is shown on the plot. The horizontal line on each plot indicates the 10% level of significance for data selection. There are no peaks that are significant at the 10% level in the plots through the group starting on January 15. The possible 3-day variability shown in the correlation coefficient plots (Figure 9.11) for the groups starting on November 6, 11, and 16 is apparent in the coherence plots

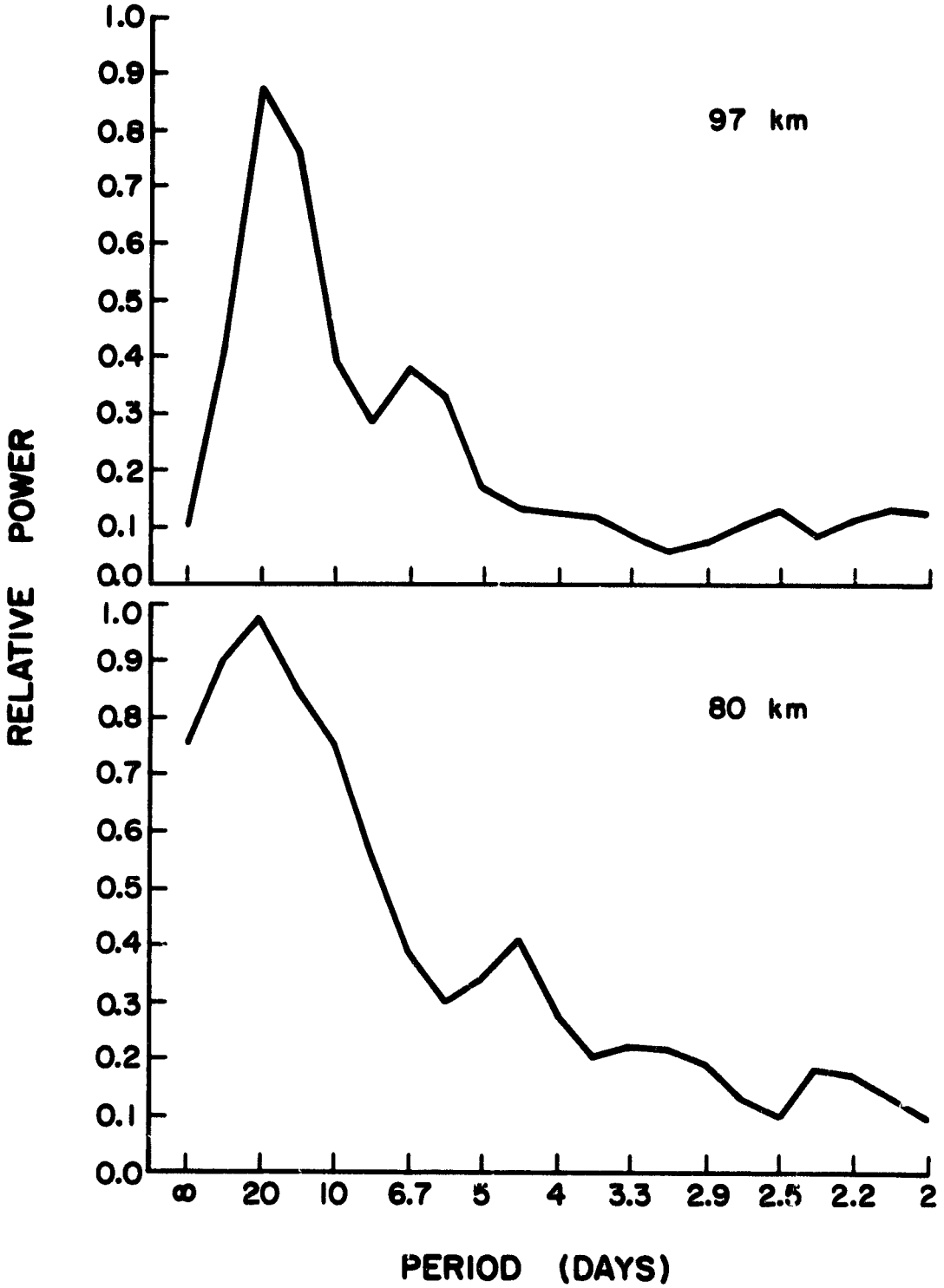

Figure 9.16 Power spectra of the Saskatoon N/S wind component at 80 and 97 km during the winter of 1979/1980.

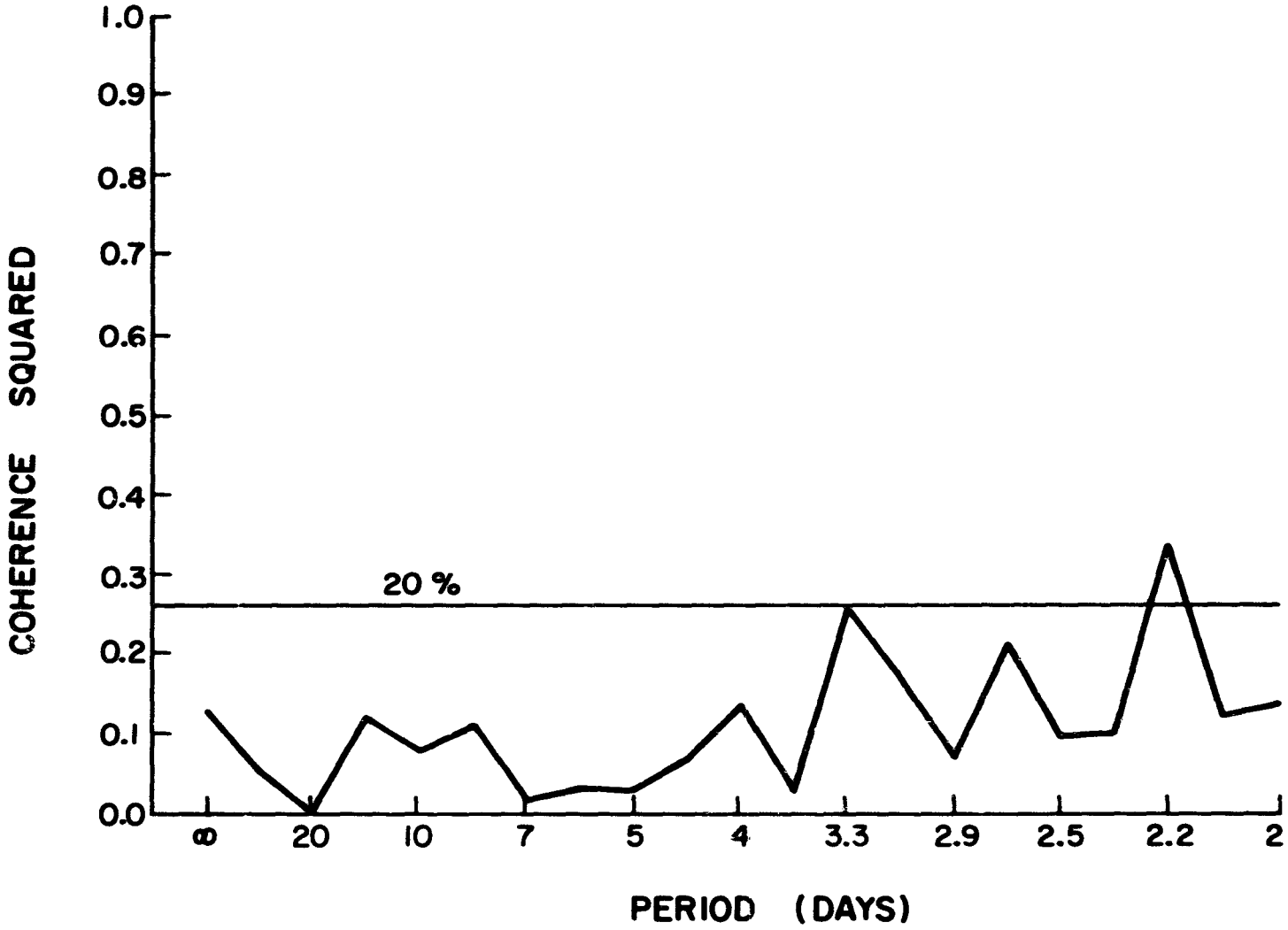

Figure 9.17 Coherence squared between the 81-km A_x/A_c ratio at Urbana and the N/S component of the 97-km wind at Saskatoon during the winter of 1979/1980. The horizontal line indicates the 20% level of significance.

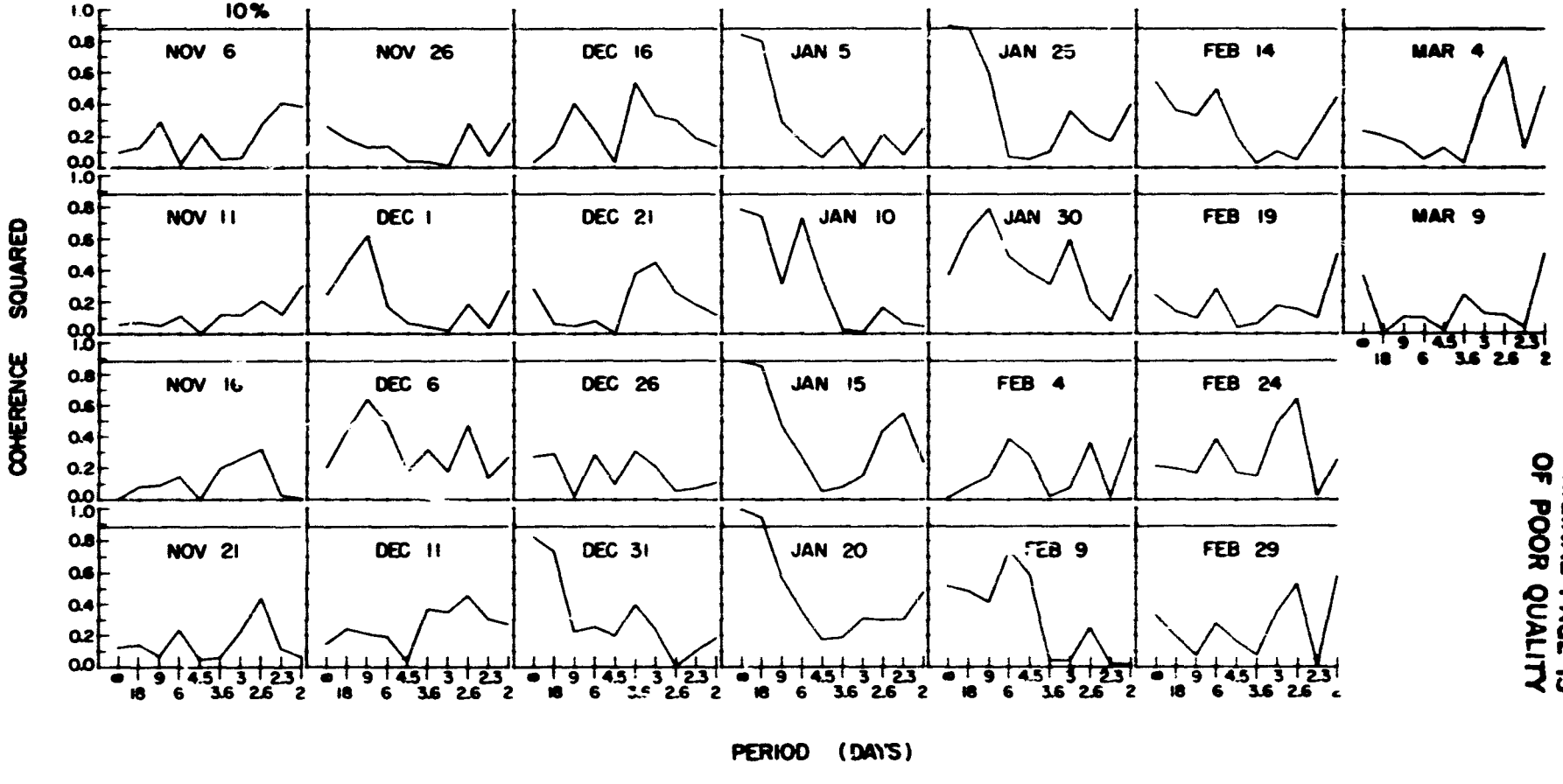

ORIGINAL PAGE IS
OF POOR QUALITY

Figure 9.18 Running coherence squared between the 81-km A_x/A_O ratio at Urbana and the N/S component of the 97-km wind at Saskatoon. The starting date for each 32-day group is shown on the plot. The horizontal line on each plot indicates the 10% level of significance.

in November, with a peak in the coherence at a period of about 3 days. The level of the coherence generally increases starting on December 6, and remains at a higher level through the group starting on March 4. This is consistent with the theory that the observed variability is due to the propagation of Rossby waves during the winter, and due to more localized motions during the rest of the year.

Peaks in the coherence squared significant at the 10% level appear at a period of 18 days in the groups starting on January 20 and 25. The 6.7-day fluctuation that was shown in the power spectrum of Saskatoon winds accompanies a peak in coherence at about the 25% level of significance in the group starting on January 10 and February 9. A peak in the coherence remains in the next four groups of data at that period, but it is not significant.

The results shown in this section indicate that there is at times a significant coupling in the data observed at Saskatoon and Urbana at discrete frequencies, possibly due to the propagation of Rossby waves. There is a significant coherence between the two stations at the same frequency where a significant coherence was found between data measured in the stratosphere and mesosphere, during the winter of 1978/1979. The possibility that a change in A_x/A_o at Urbana occurs before a change in winds at Saskatoon because of the westward propagation of a Rossby wave was confirmed by a high coherence at a period of 2.6 days during that time. The observed coherences increase in level during the month of December when compared with the month of November, which is in agreement with the theory that Rossby waves may propagate upwards to mesospheric altitudes only during winter.

10. SUMMARY OF CONCLUSIONS AND SUGGESTIONS FOR FUTURE WORK

10.1 *Summary*

The principal observations and conclusions of this study are presented below.

(1) Increased winter-time variability in the electron concentrations is consistently observed at Urbana (40°N), particularly in the period starting in late December and lasting through mid-February.

(2) When comparing the partial-reflection drifts winds and the electron concentrations measured at the same location during the period of January through mid-February, the A_x/A_o ratio at 81 km is significantly correlated with the southward upper D-region wind, with no time delay. This would support the theory that transport is a major cause of the winter anomaly in the mesosphere at midlatitudes. There is also a significant correlation seen between the E/W wind component and the 72-km electron concentration measured at the same location, with enhancements in the electron concentration with decreasing eastward wind.

No correlation is seen between the winds and electron concentrations measured at the same location outside the winter period (no correlations after mid-February).

(3) An extended set of data was used in comparing meteor radar winds and partial-reflection electron concentrations at the same location. A correlation significant at the 2% level, for data taken in the period of December through mid-February, is seen between 86-km winds and the 81-km A_x/A_o ratio, with a delay of one day between wind changes and electron concentration changes.

(4) The power spectra of electron concentrations in the mesosphere for a nine-year set of data indicate that dominant discrete-frequency

fluctuations in the range of Rossby wave periods are observed throughout the mesosphere during all but one of the winters. The amplitude of these fluctuations is shown to peak in late January or mid-February.

(5) Only a weak and questionable coupling was observed between the 0.4 mbar geopotential and Urbana electron concentrations. No significant coherence was found, and the periods where coherencies peak change in a time scale of about three weeks.

The spatial/temporal Fourier transform of the geopotential at a latitude of 60°N around the globe indicates that westward propagating m = 1 Rossby waves were present at that time, at the same periods where peaks in the coherences were observed.

(6) No correlation was observed between the E/W component of the winds at Saskatoon and the Urbana electron concentrations. There is no direct connection between Saskatoon N/S winds and Urbana electron concentrations that remains constant throughout the winter. Correlations calculated for short segments of the winter indicate that the relationship between the data observed at the two stations varies considerably during the winter. At times, a significant correlation is seen with no time delay between the data sets; this would support the idea that there is a latitudinal gradient of NO present. At other times, there is a delay between the shifts in wind and the changes in the A_x/A_o ratio at Urbana, indicating that a "cloud" of NO was being transported to Urbana. Both of these conditions occur at different times. The analysis is complicated by the large separation in the east-west direction between the stations. A significant coherence was observed between the Urbana and Saskatoon data at discrete frequencies. A coherence of lower significance level also was found between the stratosphere and the mesosphere with the same period, at that same time, when data from the three

experiments (0.4 mbar satellite geopotential, Urbana electron concentration, and Saskatoon winds) were available.

10.2 *Suggestions for Future Work*

In order to obtain a good estimte of the 24-hour prevailing winds at Urbana, data need to be collected over as much of the day as possible, and the present data collection software is not practical for the collection of data over a long period of time. The computer is also needed by the other experiments at the Aeronomy Laboratory Field Station and would not be available for the exclusive use with the drifts experiment for much of the winter. A great improvement in the quantity of data that can be collected, and the ease of performing comparisons with the other experiments at Urbana (meteor radar and coherent scatter) would be increased if a separate microcomputer data-collection system similar to that used at Saskatoon (MEEK, 1981) were operating. Many interesting comparisons of data obtained by the several experiments operating at Urbana would be possible if the data were obtained simultaneously.

APPENDIX I

Sen-Wyller Formula for Refractive Index

The following assumptions are made in the derivation:

(1) The medium is a slightly ionized gas.

(2) The mass of neutral particles is much greater than the mass of electrons.

(3) The influence of electron-electron collisions is negligible when compared with the influence of electron-neutral.

(4) The collision frequency of electrons is proportional to the square of the electron velocity.

(5) The electric field energy is negligible compared with the thermal energy so that neutrals and electrons have Maxwell-Boltzmann velocity distributions.

A generalized permittivity tensor is formed in terms of the elements ε_I, ε_{II}, and ε_{III}, which are the permittivities associated with the principal axes defined by the directions of the wave normal and the earth's magnetic field. The permittivity elements are given by:

$$\varepsilon_I = (1 - a) - jb$$

$$\varepsilon_{II} = \frac{1}{2}(f - d) + \left(\frac{j}{2}\right)(c - e)$$

$$\varepsilon_{III} = \left[a - \frac{1}{2}(c + e)\right] + j\left[b - \frac{1}{2}(f + d)\right]$$

where:

$$a = \frac{\omega_o^2}{\nu_m^2} \int_{3/2} \left(\frac{\omega}{\nu_m}\right)$$

$$b = \frac{5\,\omega_o^2}{2\,\omega\nu_m} \subset_{5/2} \left(\frac{\omega}{\nu_m}\right)$$

$$c = \frac{\omega_o^2\,(\omega - \omega_H)}{\omega\nu_m} \subset_{3/2} \left(\frac{\omega - \omega_H}{\nu_m}\right)$$

$$d = \frac{5\,\omega_o^2}{2\,\omega\nu_m} \subset_{5/2} \left(\frac{\omega - \omega_H}{\nu_m}\right)$$

$$e = \frac{\omega_o^2\,(\omega + \omega_H)}{\omega\nu_m} \subset_{3/2} \left(\frac{\omega + \omega_H}{\nu_m}\right)$$

$$f = \frac{5\,\omega_o^2}{2\,\omega\nu_m} \subset_{5/2} \left(\frac{\omega + \omega_H}{\nu_m}\right)$$

and:

ω = operating frequency

ω_o^2 = plasma frequency $\equiv \frac{Ne}{m\varepsilon_o}$

ω_H = angular gyrofrequency $\equiv \frac{eB}{m}$

ν_m = electron-neutral collision frequency associated with the most probable electron energy

N = electron concentration (M^{-3})

e = electron charge = 1.6×10^{-19} C

m = electron mass = 9.1×19^{-31} kg

ε_o = permittivity of free space = 8.55×10^{-12} F/M

B = earth's magnetic field (Webers/M^2)

The semiconductor integrals are approximated to within 1% error by the polynomials given by BURKE and HARA (1963) listed in Appendix II.

The generalized refractive index $\eta_{o,x}$ is defined as $\eta_{o,x} = (u - jk)$ and is given in terms of the permittivity elements as:

$$\eta_{o,x} = \left[\frac{A + B \sin^2\theta \pm (B^2 \sin^4\theta - C^2 \cos\theta)^{\frac{1}{2}}}{D + E \sin^2\theta} \right]^{\frac{1}{2}}$$

where:

$A = 2\epsilon_I (\epsilon_I + \epsilon_{III})$

$B = \epsilon_{III} (\epsilon_I + \epsilon_{III}) + \epsilon_{II}^2$

$C = 2\epsilon_I \epsilon_{II}$

$D = 2\epsilon_I$

$E = 2\epsilon_{III}$

θ = angle between the wave normal and the direction of the earth's magnetic field

APPENDIX II

SEMICONDUCTOR INTEGRAL APPROXIMATIONS

The following semiconductor integral approximations are from BURKE and HARA (1963)

$$\mathcal{F}_{3/2}(x) \simeq \frac{x^4 + a_3x^3 + a_2x^2 + a_1x + a_0}{x^6 + b_5x^5 + b_4x^4 + b_3x^3 + b_2x^2 + b_1x + b_0}$$

where:

$a_3 = 2.4653115 \times 10^1$

$a_2 = 1.1394160 \times 10^2$

$a_1 = 1.1287513 \times 10^1$

$a_0 = 2.3983474 \times 10^{-2}$

$b_5 = 2.4656819 \times 10^1$

$b_4 = 1.2049512 \times 10^2$

$b_3 = 2.8958085 \times 10^2$

$b_2 = 1.4921254 \times 10^2$

$b_1 = 9.3877372$

$b_0 = 1.8064128 \times 10^{-2}$

$$\mathcal{F}_{5/2}(x) \simeq \frac{x^3 + c_2x^2 + c_1x + c_0}{x^5 + d_4x^4 + d_3x^3 + d_2x^2 + d_1x + d_0}$$

where:

$c_2 = 6.6945939$

$c_1 = 1.6901002 \times 10^1$

$c_0 = 1.1630641$

$d_4 = 6.6314497$

$d_3 = 3.5355257 \times 10^1$

$d_2 = 6.8920505 \times 10^1$

$d_1 = 6.4093464 \times 10^1$

$d_0 = 4.3605732$

APPENDIX III

ASSUMED COLLISION-FREQUENCY PROFILE

The assumed collision-frequency profile is related to the atmospheric pressure by the following relation (GREGORY and MANSON, 1969):

$$\nu = 6.4 \times 10^{7} p$$

where p is the atmospheric pressure in millibars, and ν is given in units of s^{-1}. The atmospheric pressure for the latitude of Urbana is taken from the atmospheric model by KANTOR and COLE (1965) up to 80 km, and from the atmospheric model by CHAMPION (1967) above 80 km. Seasonal variations in these models are taken into account by forming a separate pressure profile for winter, summer, and equinox periods. December, January, and February are considered winter months, and June, July, and August are considered summer months. All other months are considered to be in the equinox period. The pressure data are stored in function CN, listed in Appendix V.

APPENDIX IV

DESCRIPTION OF DRIFTS WIND PROCESSING SUBROUTINE BRIGGS

The full correlation analysis computer program employed on the PDP-15 computer is an adapted version of the program written and used by The University of Adelaide (Australia) research group under the direction of Prof. B. H. Briggs, and was derived from the theory of BRIGGS et al. (1950), and also the later work due to FOOKS (1965).

Input data

(1) The position vectors of the three antennas in r,θ coordinates, where the axial system used is left-handed with the x axis to the north and the y axis to the east. There is no restriction on the shape or orientation of the antenna array used, e.g., employing N/E, N/W, and S/W as the first, second, and third quadrant antennas. The r,θ coordinates will be stored respectively in the array locations CR(I), CTHETA (I), I = 1,3. These are then converted to x,y coordinates (CX(I), CY(I), I = 1,3), from which the difference vectors for the antenna pairs (N/W, N/E), (S/W, N/E), and (S/W, N/W) are computed and stored as x and y components in DX(I) and DY(I), I = 1,3, respectively. This order for the pairs is preserved in the subscripting of all arrays containing data relating to these difference vectors. These are then converted to r,θ coordinates DR(I) and DTHETA(I), and several parameters related to these are stored for later use: DRSQ(I) = DR(I)^2, SIN2DT(IO = sin(DTHETA(I) x 2, and COS2DT(I) = cos(DTHETA(I) x 2).

(2) The three "simultaneous" input time series are stored in IDATA(I), I = 1,3, with the order of antenna quadrants corresponding to that of the coordinates in 1.

(3) The sampling intervals between successive measurements of the amplitude fading time series must remain constant, and is stored in DELTAT

in units of seconds (0.4 seconds in our system).

(4) The number of data points in each time series (512 in our system) is stored in NDATA(I), I = 1,3.

(5) The control parameters NSHIFA and NSHIFC are, respectively, the number of shifts to be made in calculating the auto- and cross correlation functions.

Autocorrelation

Computation of $\rho_{11}(I)$, $\rho_{22}(I)$, and $\rho_{33}(I)$ for I = 1, NSHIFA with the autocorrelation functions stored in IRHO (I,J), J = 1, 2, 3.

Mean Autocorrelation

(1) Calculate the average value for the I^{th} shift and store in DUM2 and in AMNACF(I).

(2) Test DUM2 against the value for the $(I-1)^{th}$ shift which is stored in DUM1. If the function is decreasing, continue calculating the mean, and if it is increasing, terminate the calculation.

If $I \leq 4$ at termination, an error is indicated.

If I < NSHIFA, set MAXTAU = I-1.

If I = NSHIFA, set MAXTAU = I-2.

Thus, AMNACF (MAXTAU) is the maximum value taken by the mean (AMINRH) in general.

(3) Determine the value of the time shift when the correlation coefficient ρ has the value 1/2. Due to the fact that the data are scaled by 10^6, this is done by calling subroutine TAUACF at the point of 5×10^5. The output from this subroutine is stored in TMHALF.

Cross Correlation

Subroutine CORLAT is called for data sets I and J, and the results are stored in IRHO (K,2), i.e., call CORLAT (I,J,2,NSHIFC). Then call for J,I

and store in IRHO (K,3), i.e., call CORLAT (J,I,3,NSHIFC). Thus IRHO (K,2) contains ρ_{IJ} and IRHO (K,3) contains ρ_{JI}. The array IRSTOR(I) is equivalenced to IRHO, and the total correlation function is now stored in this array by reversing IRHO (K,3) into IRSTOR and storing IRHO (K,2) after this. The first element of IRSTOR is IRHO (NSHIFC, 3) (the last element of this array). The first elements of IRHO (K,3) and IRHO (K,2) are zero shift elements and are identical, so the reversing is terminated at IRHO (2,3). Then the NSHIFC elements of IRHO (K,2) are stored, giving a total size of 2 x NSHIFC - 1 to the array IRSTOR.

A simple successive comparison is used to determine the maximum value of this array MAX-IRSTOR(I)$_{MAX}$ with K the corresponding index of IRSTOR. The calculation is terminated if K is within three of NSHIFC near the ends of the function. The function is then fitted by a quartic in order to estimate the actual maximum value, and the corresponding number of shifts.

Having found the position of zero slope, the maximum value of the fourth order polynomial is calculated as follows:

$$RHOMAX = PX^4 + QX^3 + RX^2 + \delta X + MAX$$

(for X = 0, the cross correlation function must have the value previously decided upon as the approximate maximum, i.e., MAX). The corresponding time delay is TD(KVECT) = ((K - NSHIFC) + XX) * DELTAT, with K the index in IRSTOR, and XX the correction applied to K by the fitting of the maximum value. The origin is referred now to zero-shift by subtracting NSHIFC. DELTAT converts the units to time in seconds.

Calculation of τ, τ_m a.

These quantities are estimated by computing the number of shifts in the autocorrelation function for which AMNACF(J) = RHOMAX. This is achieved by CALL TAUACF (RHOMAX, TM(KVECT), NOKAY), returning the value τ_m in TM(KVECT)

by polynomial fit. Also calculated are TCDSQ(KVECT) = TD^2(KVECT) + TM^2(KVECT), where KVECT = 1,2,3 corresponding to the subscripts of ρ_{12}, ρ_{13}, and ρ_{23}. In the theory of FOOKS (1965), τ_{ij}^2 = TCDSQ, τ_m = TM, and TD = τ'.

Estimation of the Correlation Ellipse

The characteristic ellipse is assumed to pass through the endpoints of the three vectors

$$(V_c')_k = \left(\frac{d_k}{\tau_k}\ ,\ \theta_k\right)$$

with its center at the origin. The parameters of the ellipse are calculated using a method similar to that in Appendix I of Fook's paper. Here an expression of the form

$$CX(1) + CX(2)\cos 2\theta_k + CX(3)\sin 2\theta_k = \frac{1}{r_k^2}$$

is solved for CX(I), I = 1,2,3 for the three sets of r_k, θ_k using the subroutine MATS. The ellipse axis parameters AAXIS and BAXIS are obtained from the expressions

$$AAXIS = (CX(1) + DUM1)^{-1/2}$$

$$BAXIS = (CX(1) - DUM1)^{-1/2}$$

where

$$DUM1 = (CX^2(2) + CX^2(3))^{-1/2}$$

By selecting the positive square root for DUM1 we assume that AAXIS > BAXIS, and thus AAXIS is the semi-major axis of the ellipse. Computer also is AXRATI = AAXIS/BAXIS.

Estimation of the Drift Velocities

The three vectors $V_{ij}' = d_{ij}/\tau_{ij}'$ are calculated from the difference vectors for the antenna positions with the values of the time shift for maximum cross-correlation TD(I), and stored as x, y, and r coordinates in CX(I), CY(I), and CR(I). The approximate values of the apparent drift speed

and direction are then computed using the method described by FOOKS (1965) (Appendix II) and stored in VD = V_a and PHI = ϕ_a.

Corrected values of V_a and ϕ_a are then computed following the methods of Fooks. Using an iterative procedure, the values of V_a and ϕ_a are readjusted by removing the respective error estimates ΔV_a and $\Delta\phi_a$ (propagated error functions of the previous V_a and ϕ_a estimates). The process is repeated until ΔV_a and $\Delta\phi_a$ are small, or until 100 iterations have been made.

Estimation of the True Velocity, V:

The true velocity is found by drawing a tangent to the characteristic ellipse parallel to the V'_{12}, V'_{13}, V'_{23} line just calculated. If the line perpendicular to this tangent has slope m relative to the major axis, the true velocity is estimated by

$$V = \frac{\text{AAXIS}^2}{V_a}\left(\frac{1 + m^2/\text{AXRATI}^4}{1 + m^2}\right)^{1/2}$$

The characteristic velocity, V_c is estimated by

$$V_c = V\left(\frac{1 + m^2}{1 + m^2/\text{AXRATI}^2}\right)\cdot\left(\frac{\text{AAXIS}^2}{V_a{}^2}\right)^{1/2}$$

ORIGINAL PAGE IS
OF POOR QUALITY

APPENDIX V

COMPUTER PROGRAMS

```
C       DRIFTH
        DIMENSION FNAM(2),DATE(2),LO1(31),LO2(31),LX1(31),LX2(31)
        1,KS(240)
        COMMON /A/ ITIM(4),ISEC
        IEND=130050
C BEGIN R-T SUBROUTINE TO CHECK FOR COLLECTION STOPAGE
        CALL STOP(JK,KWA,IRUN)
C HOLD UP ACTION OF STOP
        KWA=1
        WRITE(6,5)
5       FORMAT(5H TIME)
        READ(4,10) ITIM
10      FORMAT(4I1)
C START CLOCK
        CALL TICK(ISEC)
        WRITE(6,15)
15      FORMAT(5H DATE)
        READ(4,20) DATE
20      FORMAT(2A5)
25      FORMAT(18H NUMBER OF SAMPLES)
30      FORMAT(I5)
        WRITE(6,35)
35      FORMAT(35H SET SWITCH 00 TO 1 TO COLLECT DATA)
C BEGIN COLLECTION
40      CONTINUE
        NCO=1
        WRITE(6,25)
        READ(4,30) NSAM
        WRITE(6,45)
45      FORMAT(11H DB SETTING)
        READ(4,50)IDB
50      FORMAT(I2)
        IDB=IDB+64
C SET ATTENUATOR TO DESIRED ATTENUATION
        CALL OUT
C ZERO FRAME NUMBER
        ID=0
        WRITE(6,55)
55      FORMAT(10H FILE NAME)
        READ(4,20) FNAM
        CALL ENTER(2,FNAM)
C WAIT IF DESIRED
        CALL PPO
C WRITE HEADER BLOCK
        CALL CTIME2
        WRITE(2) DATE,ITIM,IDB
C STARTS STOP
70      CONTINUE
        KWA=0
        NCO=NCO+24
        GO TO 151
150     CONTINUE
        NCO=1
        KWA=0
151     CONTINUE
        JK=0
        NNNN=IDB+7168
C GET TWO SETS OF ORDINARY SAMPLES
        CALL OUT
        CALL INPAD(LO1,31,ICOM)
75      IF(JK.EQ.1.OR.ICOM.EQ.-513) GO TO 70
        IF(ICOM.NE.1) GO TO 75
C LET STOP KNOW THAT COLLECTION IS PROCEEDING
        IRUN=1
C  WAIT 1 MS TO MAKE SURE THAT NO SAMPLES ABOVE 90 KM ARE COLLECTED
C  BY THE NEXT CALL TO INPAD
```

ORIGINAL PAGE IS
OF POOR QUALITY


```
      DO 77 J=1,100
77    CONTINUE
      NNNN=IDB+6656
      CALL OUT
      CALL INPAD(LO2,31,ICOM)
76    IF(JK.EQ.1.OR.ICOM.EQ.-513) GO TO 70
      IF(ICOM.NE.1) GO TO 76
      IRUN=1
      DO 78 J=1,100
78    CONTINUE
C CHECK FOR SYNCHRONIZATION BY STARTING A TIMER
      CALL SYNC(ISYN)
      NNNN=IDB+5632
      CALL OUT
      CALL INPAD(LX1,31,ICOM)
80    IF(JK.EQ.1.OR.ICOM.EQ.-513.OR.ISYN.EQ.1) GO TO 70
      IF(ICOM.NE.1) GO TO 80
      IRUN=1
      DO 82 J=1,100
82    CONTINUE
      NNNN=IDB+3584
      CALL OUT
      CALL INPAD(LX2,31,ICOM)
81    IF(JK.EQ.1.OR.ICOM.EQ.-513.OR.ISYN.EQ.1) GO TO 70
      IF(ICOM.NE.1) GO TO 81
      IRUN=1
      IDM=ID
      ID=ID+1
      KWA=1
      J1=NCO
      KS(J1)=LO1(21)
      KS(J1+1)=LO1(23)
      KS(J1+2)=LO1(25)
      KS(J1+3)=LO1(27)
      KS(J1+4)=LO1(29)
      KS(J1+5)=LO1(31)
      KS(J1+6)=LO2(21)
      KS(J1+7)=LO2(23)
      KS(J1+8)=LO2(25)
      KS(J1+9)=LO2(27)
      KS(J1+10)=LO2(29)
      KS(J1+11)=LO2(31)
      KS(J1+12)=LX1(21)
      KS(J1+13)=LX1(23)
      KS(J1+14)=LX1(25)
      KS(J1+15)=LX1(27)
      KS(J1+16)=LX1(29)
      KS(J1+17)=LX1(31)
      KS(J1+18)=LX2(21)
      KS(J1+19)=LX2(23)
      KS(J1+20)=LX2(25)
      KS(J1+21)=LX2(27)
      KS(J1+22)=LX2(29)
      KS(J1+23)=LX2(31)
      IF(NCO.GE.217) GO TO 100
      IF(ID.GT.NSAM) GO TO 90
      GO TO 70
100   CONTINUE
C WRITE SAMPLES
      WRITE(2) IDM,KS
      GO TO 150
C SET ID=130050 TO SIGNIFY THE END OF FILE
90    CONTINUE
      WRITE(2) IEND,KS
      KWA=1
      CALL CLOSE(2)
      GO TO 40
      END
```

ORIGINAL PAGE IS
OF POOR QUALITY


```
      SUBROUTINE CTIME2
      COMMON /A/ITIM(4),ISEC
C
C  LOAD CURRENT ELAPSED TIME SINCE LAST CALL TO CTIME2
C
      ITSEC=ITSEC+ISEC
      ISEC=0
C
C  KEEPS TRACE OF SECONDS AND INCREMENTS MINUTES
C
5     CONTINUE
      IF(ITSEC.GE.60) ITIM(4)=ITIM(4)+1
      IF(ITSEC.GE.60) ITSEC=ITSEC-60
      IF(ITSEC.GE.60) GO TO 5
C
C  INCREMENT TENS OF MINUTES
C
10    IF(ITIM(4).GT.9) ITIM(3)=ITIM(3)+1
      IF(ITIM(4).GT.9) ITIM(4)=ITIM(4)-10
      IF(ITIM(4).GT.9) GO TO 10
C
C  INCREMENT HOURS
C
20    IF(ITIM(3).GT.5) ITIM(2)=ITIM(2)+1
      IF(ITIM(3).GT.5) ITIM(3)=ITIM(3)-6
      IF(ITIM(3).GT.5) GO TO 20
C
C  INCREMENT TENS OF HOURS
C
      IF(ITIM(2).GT.9) ITIM(1)=ITIM(1)+1
      IF(ITIM(2).GT.9) ITIM(2)=ITIM(2)-10
      IF(ITIM(1).GT.2) ITIM(1)=0
      RETURN
      END


      .GLOBL TICK,.DA
/ TICK COUNTS SECONDS
/ FORTRAN IV CALL: CALL TICK(ISEC)
TICK  0
      JMS*  .DA
      JMP   .+2
ISEC  0
      DZM*  ISEC            /ZERO SECONDS
      .TIMER 60,S1,5        /START CLOCK
      JMP*  TICK            /RETURN
S1    0                     /SERVICE ROUTINE FOR INTERRUPT
      DAC   TEMP            /STORE ACCUMULATOR
      ISZ*  ISEC            /INCREMENT BY ONE SECOND
      .TIMER 60,S1,5        /DO AGAIN
      LAC   TEMP            /RESTORE ACCUMULATOR
      .RLXIT S1             /RETURN
TEMP  0
      .END


/ROUTINE PPO CHECKS DATA SWITCH 00 FOR A 1 OR 0
/
      .GLOBL PPO
PPO   0
PR    LAS                   /GET THE CONSOLE DATA SWITCH
      AND   (400000         /NUMBER 00
      SNA                   /IS IT A 1 ?
      JMP   PR              /NO, CHECK AGAIN
      JMP*  PPO             /RETURN TO SINTST
      .END



      .TITLE OUT
      .GLOBL OUT
OUT   0
      705704
      JMP*  OUT
      .END
```

ORIGINAL PAGE IS
OF POOR QUALITY


```
        INPADF
        .TITLE  A/D CONVERTER SERVICE ROUTINES FOR DG.-FB.
/       DFKM1B V3A SERVICE ROUTINES FOR THE HP 5610A A TO D
/  CONVERTER.  THESE ROUTINES PERMIT INPUT OF ANY SPECIFIED
/  NUMBER OF SAMPLES INTO A CORE BUFFER.  INPUT MAY BE OVER-
/  LAPPED WITH PROGRAM EXCUTION, AND CONTROL MAY BE RELINQUISHED
/  TO LOWER PRIORITY PROGRAMS WHILE DATA TRANSFER TAKES PLACE.
/    MACRO-15 CALLING SEQUENCE:
/       JMS     INPAD
/       NUMBER OF SAMPLES REQUIRED
/       BUFFER ADDRESS
/       COMPLETION FLAG ADDRESS
/       REAL-TIME SUBROUTINE ADDRESS, PRIORITY LEVEL IN BITS 0-2
/  (EXAMPLE: 500000+RTSUBA)
/  (RETURNS HERE IMMEDIATELY)
/       IF THE 4TH WORD AFTER THE JMS IS 0, NO REAL-TIME SUBROUTINE
/  WILL BE ACTIVATED.  NOTE:  THE PRIORITY CODE FOR MAINSTREAM IS 1
/       THE COMPLETION FLAG IS CLEARED BY THE CALL TO INPAD,
/  AND SET TO +1 FOR NORMAL COMPLETION OR -1001 IF A DATA
/  TIMING ERROR OCCURS.
/
/
ADWCR=26                        /A-D WORD COUNT
ADCAR=ADWCR+1                   /AND CURRENT ADDRESS REGISTERS
.SCOM=100                       /MONITOR'S COMMUNICATION AREA
ADWI=703724                     /A-D CONVERTER WRITE INITIALIZE
ADSO=703701                     /SKIP ON WORD COUNT OVERFLOW
ADST=703721                     /SKIP ON DATA TIMING ERROR
ADCO=703704                     /CLEAR OVERFLOW FLAG
ADCT=703744                     /CLEAR TIMING FLAG
/
/  ENTRY POINT FOR A-D INTERFACE INITIALIZATION
/
        .GLOBL  INPAD,.DA
INPAD   0
        JMS*    .DA
        JMP     .+4
INAR    0
INWC    0
INFLAG  0
INR     JMP     INSET           /REPLACED BY 'LAC*      INWC'
        TCA
        DAC*    (ADWCR)         /SET WORD COUNT
        LAW     -1
        TAD*    INAR            /BUFFER ADDRESS -1
        DAC*    (ADCAR)         /   TO CURRENT ADDRESS REG.
        DZM*    INFLAG          /CLEAR FLAG
        DZM     INSUB0          /CLEAR REAL-TIME SUBROUTINE
        ADWI                    /INITIALIZE INTERFACE
        JMP*    INPAD           /RETURN
/
/   THE FOLLOWING CODE IS EXECUTED ONLY ONCE
INSET   LAC*    (.SCOM+55)      /GET ENTRY POINT ADDERSS OF .SETUP
ADSVA   DAC     .
        JMS*    .-1             /CALL .SETUP TO CONNECT ADINT TO API
        ADSO
        ADINT
        DZM*    (204
        LAC     (LAC*   INWC
        DAC     INR             /MODIFY INSTRUCTION
        JMP     INR             / AND JUMP TO IT
/
/
/INTERRUPT SERVICE ROUTINE.  EXECUTED IMMEDIATELY AFTER COMPLETION
/  OF DATA TRANSFER.  DETERMINES STATUS OF A-D INTERFACE, SETS
/  COMPLETION FLAG AND ACTIVATES REAL-TIME SUBROUTINE.
/  RUNS AT API LEVEL 0.
/
/
ADINT   0
        DBA                     /PAGE ADDRESSING MODE
        DAC     ADSVA           /SAVE AC
        ADST                    /TIMING ERROR?
        SKP!CLA!IAC             /NO,+1 TO AC
        LAW     -1001           /YES, ERROR CODE
        DAC*    INFLAG          /SET FLAG
```

```
        ADCO                    /CLEAR
        ADCT                    /   INTERFACE FLAGS
ADXIT   LAC     ADSVA           /RESTORE AC
        DBR                     /SET TO LEAVE HARDWARE API LEVEL
        JMP*    ADINT           /RETURN TO INTERRUPTED PROGRAM
        .END
```

```
        .GLOBL STOP,.DA
/STOP CHECKS FOR COLLECTION STOPAGE
/FORTRAN IV CALL: CALL STOP(NT,OR,RUN)
/
STOP    0
        JMS*    .DA
        JMP     .+4
NT      0                       /FLAG TO INDICATE STOPAGE
OR      0                       /IS PROGRAM TRYING TO COLLECT
RUN     0                       /COLLECTION PROCEEDING
        DZM*    NT              /SET FLAG TO ZERO
        .TIMER  200,AGE,6       /START TIMER
        JMP*    STOP            /RETURN
AGE     0                       /SERVICE ROUTINE
        DAC     WHEN            /SAVE AC
        DZM*    NT              /SET FLAG TO ZERO
        LAC*    OR              /GET PROGRAM STATUS
        SZA                     /IS IT COLLECTING?
        JMP     TI              /NO, DON'T CHECK FOR STOPAGE
        LAC*    RUN             /YES, CHECK
        SZA
        JMP     TI              /YES
        ISZ*    NT              /NO, SET FLAG
TI      .TIMER  200,AGE,6       /DO AGAIN
        LAC     WHEN            /RESTORE AC
        .RLXIT  AGE             /RETURN
WHEN    0
        .END
```

```
        .GLOBL SYNC,.DA
/SYNC CHECKS FOR A/D SYNCHRONIZATION
/FORTRAN IV CALL: CALL SYNC(SYP)
/
SYNC    0
        JMS*    .DA
        JMP     .+2
SYP     0
        DZM*    SYP             /SET FLAG TO ZERO
        .TIMER  10,ERO,6        /START TIMER
        JMP*    SYNC            /RETURN
ERO     0                       /SERVICE ROUTINE
        DAC     NERP            /STORE AC
        ISZ*    SYP             /SET FLAG TO ONE

        LAC     NERP            /RESTORE AC
        .RLXIT  ERO             /RETURN
NERP    0
        .END
```

```
      FUNCTION CN(NT,MONTH)
      DIMENSION H(9),P(9,3)
      DATA H(1),H(2),H(3),H(4),H(5),H(6),H(7),H(8),H(9)/55.0,60.0,
     1 65.0,70.0,75.0,80.0,85.0,90.0,100.0/
      DATA P(1,1),P(2,1),P(3,1),P(4,1),P(5,1),P(6,1),P(7,1),P(8,1),
     1 P(9,1)/.4409,.2395,.1194,.05588,.02423,1.18E-2,4.449E-3,1.650E-3,
     2 2.699E-4/
      DATA P(1,2),P(2,2),P(3,2),P(4,2),P(5,2),P(6,2),P(7,2),P(8,2),
     1 P(9,2)/.4060,.2087,.1034,.04888,.02187,.0109,4.495E-3,1.857E-3,
     2 3.549E-4/
      DATA P(1,3),P(2,3),P(3,3),P(4,3),P(5,3),P(6,3),P(7,3),P(8,3),
     1 P(9,3)/.3669,.1863,.09157,.04395,.02012,.0104,4.533E-3,1.950E-3,
     2 4.100E-4/
      MONTH=MONTH+6
      IF(MONTH.GT.12) MONTH=MONTH-12
      IF(MONTH.EQ.12.OR.MONTH.LE.2) J=1
```

```
C     SUMMER: JUNE, JULY, AUGUST
      IF((MONTH.GE.3.AND.MONTH.LE.5).OR.(MONTH.GE.9.AND.MONTH.LE.11))J=2
C     EQUINOX: MARCH, APRIL, MAY, SEPT, OCT, NOV
      IF(MONTH.GE.6.AND.MONTH.LE.8) J=3
C     WINTER: DEC, JAN, FEB
      IF(HT.LT.55.) GO TO 111
      DO 110 I=1,9
      IF(HT-H(I))  1,2,3
    3 GO TO 110
    2 APHT=P(I,J)
      GO TO 120
    1 A=HT-H(I-1)
      B=H(I)-H(I-1)
      P1=ALOG10(P(I-1,J))
      P2=ALOG10(P(I,J))
      PHT=(A/B)*(P2-P1)+P1
      APHT=10.0**PHT
C     APHT IS PRESSURE AT HT
      GO TO 120
  110 CONTINUE
      GO TO 120
  111 APHT=P(I,J)*(2.7183**(-(HT-55.)/7.2))
C     P=P(0)*EXP((HT-HT(0)9/H
C     H IS PRESSURE SCALE HEIGHT AVERAGE BETWEEN 30 AND 55 KM
C     U.S.STANDARD ATMOSPHERE 1962, FROM MURGATROYD, 'REP.PROG.PHYS'
C     VOL 33,P819
  120 CN=6.4E7*APHT
C     GREGORY AND MANSON
      CONTINUE
      RETURN
      END
```

```
      DRIFTR
      REAL IDATA,NCLNSH,KERROR
      LOGICAL ONE
      DIMENSION FNAM(2),DATE(2),ITIM(4),ORIENT(4),E(2),ANT(4)
      DIMENSION DP1(31),DP2(31),DP3(31),DP4(31),DKS(240),KS(240)
      COMMON /AA/ NDATA(4),IDATA(4,512),RAD(3),CTHETA(3),NAUTO,NC,ONE
      COMMON /BB/ NIRHO(4),IRHO(20,4),AMNACF(21),AMINRH,MAXTAU,DELTAT
      COMMON /DD/ ID(3),T,IH,NBLK,IP,CON(3),DTHETA(3)
      DATA ANT(1)/5HN-E  /,ANT(2)/5HN-W  /,ANT(3)/5HS-W  /
      DATA ANT(4)/5HS-E  /
      DATA E(1)/5HCHECK/,F1/4H1DAT/,F2/4H2DAT/,F3/4H3DAT/,F4/4H4DAT/
      DATA F5/4H5DAT/,F6/4H6DAT/,F7/4H7DAT/,F8/4H8DAT/,F9/4H9DAT/
      DATA F10/1HADAT/
      DATA F/4H1DAT/
      ORIENT(1)=45.
      ORIENT(2)=315.
      ORIENT(3)=225.
      ORIENT(4)=135.
      NDATA(1)=512
      NDATA(2)=512
      NDATA(3)=512
      NDATA(4)=512
      RAD(1)=119.5
      RAD(2)=119.5
      RAD(3)=119.5
      NAUTO=3
      DT=.033/.4
      LNAM=0
      WRITE(6,33)
33    FORMAT(4HXX  )
4     CONTINUE
      LNAM=LNAM+1
      IF(LNAM.EQ.1) E(2)=F1
      IF(LNAM.EQ.2) E(2)=F2
      IF(LNAM.EQ.3) E(2)=F3
      IF(LNAM.EQ.4) E(2)=F4
      IF(LNAM.EQ.5) E(2)=F5
      IF(LNAM.EQ.6) E(2)=F6
      IF(LNAM.EQ.7) E(2)=F7
      IF(LNAM.EQ.8) E(2)=F8
      IF(LNAM.EQ.9) E(2)=F9
      IF(LNAM.EQ.10) E(2)=F10
      IF(LNAM.GE.11) PAUSE
      KK9=0
```

ORIGINAL PAGE IS
OF POOR QUALITY

ORIGINAL PAGE IS
OF POOR QUALITY


```
6       CONTINUE
        ALT=70.5
        GO TO 21
20      CONTINUE
        KK9=0
        IF(ALT.EQ.81.0) GO TO 4
        IF(ALT.EQ.79.5)ALT=81.0
        IF(ALT.EQ.76.5)ALT=79.5
        IF(ALT.EQ.75.0)ALT=76.5
        IF(ALT.EQ.72.0)ALT=75.0
        IF(ALT.EQ.70.5)ALT=72.0
21      CONTINUE
        JALT=IFIX(ALT/1.5-29.)
23      FORMAT(F4.1)
        CALL SEEK(2,E)
        READ(2) DATE,ITIM,IDB
        IDB=IDB-64
        WRITE(6,5)
5       FORMAT(1H1,80X/40X)
        WRITE(6,35) DATE,ITIM,IDB,ALT
35      FORMAT(10X,2A5,10X,4I1,10X,I2,3H DB,10X,F6.1,3H KM)
        WRITE(6,36)
36      FORMAT(//12X)
40      CONTINUE
        READ(2) ID,KS
        IF(ID.EQ.130050) GO TO 60
        KK=1
        DO 45 N=1,240
        DKS(N)=FLOAT(KS(N))
45      CONTINUE
44      CONTINUE
        KK9=KK9+1
        IF(KK9.GE.513) GO TO 60
        DP1(18)=DKS(KK)
        DP1(19)=DKS(KK+1)
        DP1(21)=DKS(KK+2)
        DP1(22)=DKS(KK+3)
        DP1(24)=DKS(KK+4)
        DP1(25)=DKS(KK+5)
        DP2(18)=DKS(KK+6)
        DP2(19)=DKS(KK+7)
        DP2(21)=DKS(KK+8)
        DP2(22)=DKS(KK+9)
        DP2(24)=DKS(KK+10)
        DP2(25)=DKS(KK+11)
        DP3(18)=DKS(KK+12)
        DP3(19)=DKS(KK+13)
        DP3(21)=DKS(KK+14)
        DP3(22)=DKS(KK+15)
        DP3(24)=DKS(KK+16)
        DP3(25)=DKS(KK+17)
        DP4(18)=DKS(KK+18)
        DP4(19)=DKS(KK+19)
        DP4(21)=DKS(KK+20)
        DP4(22)=DKS(KK+21)
        DP4(24)=DKS(KK+22)
        DP4(25)=DKS(KK+23)
        KK=KK+24
        IDATA(1,KK9)=DP1(JALT)
        IDATA(2,KK9)=DP2(JALT)
        IDATA(3,KK9)=DP3(JALT)
        IDATA(4,KK9)=DP4(JALT)
        IF(KK.GE.240) GO TO 40
        GO TO 44
60      CONTINUE
        CALL CLOSE(2)
        D=DT
        DO 62 K=2,4
        B1=IDATA(K,1)
        DO 61 I=2,512
        B2=IDATA(K,I)
        IDATA(K,I)=B2+DS(B1-B2)
61      B1=B2
62      D=D+DT
        AVNOIS=0.
```

ORIGINAL PAGE IS
OF POOR QUALITY


```
      DO 75 IK=1,4
      DO 70 JK=2,512
      AVNOIS=AVNOIS+IDATA(IK,JK)
      CHECK=(IDATA(IK,JK)-IDATA(IK,JK-1))
      ACHECK=ABS(CHECK)
      IF(ACHECK.LE.50.) GO TO 74
      IF(CHECK)71,72,73
71    IDATA(IK,JK)=IDATA(IK,JK-1)-50.
      GO TO 74
72    GO TO 74
73    IDATA(IK,JK)=IDATA(IK,JK-1)+50.
74    CONTINUE
70    CONTINUE
75    CONTINUE
      AVNOIS=AVNOIS/2044.
      WRITE(6,80) AVNOIS
80    FORMAT(5X,22HAVERAGE SIGNAL LEVEL=,F7.0)
      DO 65 NC=1,4
      K=NC
      DO 63 J=1,3
      CTHETA(J)=ORIENT(K)
      CON(J)=ANT(K)
      IF(K.EQ.4) K=0
63    K=K+1
      CALL BRIGGS
      DO 64 I=1,512
      D=IDATA(1,I)
      IDATA(1,I)=IDATA(2,I)
      IDATA(2,I)=IDATA(3,I)
      IDATA(3,I)=IDATA(4,I)
64    IDATA(4,I)=D
65    CONTINUE
      GO TO 20
      STOP
      END


      SUBROUTINE BRIGGS
      REAL IDATA,NCLNSH,KERROR
      LOGICAL ONE
      DIMENSION IRSTOR(42),CXS(3),CYS(3),CY(3),ERR(3),VIM(3),VID(3)
      DIMENSION TN(3),TCDSQ(3),DRSQ(3),SN2DTH(3),CS2DTH(3)
      DIMENSION O5(4),O6(3,2),O7(7),O8(7),POL(2)
      COMMON /AA/ NDATA(4),IDATA(4,512),RAD(3),CTHETA(3),NAUTO,NC,ONE
      COMMON /BB/ NIRHO(4),IRHO(20,4),AMNACF(21),AMINRH,MAXTAU,DELTAT
      COMMON /CC/ PI,PID2,PIM2,PID2M3,RDTDG,DGTRD,FRADEG,KERROR
      COMMON /DD/ ID(3),T,IH,NBLK,IP,CON(3),DTHETA(3)
      COMMON /EE/ CX(3),MISS,TMHALF,TD(3),DX(3),DY(3),DR(3),CR(3)
      COMMON /FF/ O1(20,4),O2(20),O3(3,42),O4(3,4),SM(3,4),NTOP
      EQUIVALENCE (IRSTOR,IRHO)
      DATA POL(1)/5HX-MOD/,POL(2)/5HO-MOD/
      DATA ER1/4H    /,ER2/4HACF2/,ER3/4HTHLF/,ER4/4HXHF1/
      DATA ER5/4HDIF1/,ER6/4HDIF2/,ER7/4HTRHO/,ER8/4HMISS/,ER9/4HHYPE/
      DATA ER10/4HVC=-/
      PI=3.141592653
      PID2=1.5707963
      PIM2=6.2831853
      PID2M3=4.7123889
      RDTDG=57.2957795
      DGTRD=1.74532925E-02
      NSHIFA=19
      NSHIFC=19
      DELTAT=.4
      NDATA(1)=512
      NDATA(2)=512
      NDATA(3)=512
      NDATA(4)=512
C
C
C
      KERROR=ER1
      DO 4 I=1,3
      DUM1=CTHETA(I)*DGTRD
      CX(I)=RAD(I)*COS(DUM1)
      CXS(I)=CX(I)
      CY(I)=RAD(I)*SIN(DUM1)
4     CYS(I)=CY(I)
```

```
      IF(CX(1).EQ.0..AND.CX(2).EQ.0..AND.CX(3).EQ.0.) GO TO .
C     COMPUTE DIFFERENCE VECTORS
      KVECT=0
      DO 5 I=1,2
      JDUM=I+1
      DO 5 J=JDUM,3
      KVECT=KVECT+1
      DUM1=CX(J)-CX(I)
      DUM2=CY(J)-CY(I)
      DX(KVECT)=DUM1
      DY(KVECT)=DUM2
      DRSQ(KVECT)=DUM1*DUM1+DUM2*DUM2
      DR(KVECT)=SQRT(DRSQ(KVECT))
      DUM9=ARCTAN(DUM1,DUM2)
      DTHETA(KVECT)=ANGLRN(DUM9,0.,PIM2)
      TNDTH=DUM2/DUM1
      TNSQDT=TNDTH*TNDTH
      DUM1=1.+TNSQDT
      SN2DTH(KVECT)=2.*TNDTH/DUM1
      CS2DTH(KVECT)=(1.-TNSQDT)/DUM1
5     CONTINUE
      DO 9 I=1,NAUTO
      CALL CORLAT(I,I,I,NSHIFA)
      DO 8 KM=1,NSHIFA
8     O1(KM,I)=1.E-5*FLOAT(IRHO(KM,I))
9     CONTINUE
      WRITE(6,46)
46    FORMAT(40H0 0 0 0 0 0 0 0 0 0 0 0 0 0 0 0 0 0 0 0 )
      DUM1=1.E6
      AMNACF(1)=DUM1
      DUM3=1./FLOAT(NAUTO)
      O2(1)=1.
      DO 11 I=2,NSHIFA
      S=0.
      DO 10 J=1,NAUTO
10    S=S+10.*FLOAT(IRHO(I,J))
      DUM2=S*DUM3
      O2(I)=1.E-6*DUM2
      AMNACF(I)=DUM2
C     IF(DUM1.LE.DUM2) GO TO 12
      DUM1=DUM2
11    CONTINUE
      I=NSHIFA
12    IF(I.GE.4) GO TO 13
      KERROR=ER2
      WRITE(6,84) KERROR
      GO TO 1
13    IF(I.GE.NSHIFA) GO TO 14
      MAXTAU=I-1
      GO TO 15
14    MAXTAU=I-2
15    AMINRH=AMNACF(MAXTAU)
      CALL TAUACF(5.E5,TMHALF,NOKAY)
      IF(NOKAY.EQ.1) GO TO 16
      KERROR=ER3
      WRITE(6,84) KERROR
      GO TO 1
16    CONTINUE
C     COMPUTE CROSS FNS. AND TIME PARAMETERS
      KVECT=0
      NZERL1=NSHIFC-1
      NZERP1=NSHIFC+1
      NTOP=NZERL1+NSHIFC
      NCOUNT=0
      DO 43 I=1,2
      JDUM=I+1
      DO 42 J=JDUM,3
C     FOOKS RHO12 EQUALS CORLAT(2,1)
      KVECT=KVECT+1
      CALL CORLAT(J,I,2,NSHIFC)
      CALL CORLAT(I,J,3,NSHIFC)
C     REVERSE IRHO(3) INTO IRSTOR
      DO 18 K=1,NZERL1
      L=NZERP1-K
18    IRSTOR(K)=IRHO(L,3)
      DO 19 K=NSHIFC,NTOP
      L=K-NZERL1
19    IRSTOR(K)=IRHO(L,2)
```

ORIGINAL PAGE IS
OF POOR QUALITY

ORIGINAL PAGE IS
OF POOR QUALITY


```
      MCOUNT=MCOUNT+1
      IF(MCOUNT-2) 20,21,22
20    MCO=1
      GO TO 23
21    MCO=3
      GO TO 23
22    MCO=2
23    CONTINUE
C     IRSTOR NOW CONTAINS FOOKS, IRHO(I,J), POS, AND NEG
      DO 25 KM=1,NTOP
25    O3(MCOUNT,KM)=1.E-5*FLOAT(IRSTOR(KM))
C     FIND POSITION OF MAXIMUM
      MAX=IRSTOR(1)
      K=1
      DO 26 L=2,NTOP
      IF(MAX.GE.IRSTOR(L)) GO TO 26
      MAX=IRSTOR(L)
      K=L
26    CONTINUE
      IF(IABS(K-NSHIFC).LE.NSHIFC-3) GO TO 27
      KERROR=ER4
      GO TO 59
27    CONTINUE
C     FIT QUARTIC TO FIVE POINTS AND SOLVE FOR ZERO DERIVATIVE
      CF=FLOAT(IRSTOR(K+2))-2.*FLOAT(IRSTOR(K))+FLOAT(IRSTOR(K-2))
      CG=FLOAT(IRSTOR(K+2))-FLOAT(IRSTOR(K-2))
      CH=FLOAT(IRSTOR(K+1))-FLOAT(IRSTOR(K-1))
      CK=FLOAT(IRSTOR(K+1)-2*IRSTOR(K)+IRSTOR(K-1))
      P=(CF-4.*CK)/2.4
      Q=(CG-2.*CH)/1.2
      R=-(CF-16.*CK)/2.4
      S=-(CG-8.*CH)/1.2
C     FOLLOWING FINDS ZERO OF DERIVATIVE OF QUADRIC
C     WHICH LIES BETWEEN X=-1 AND X=+1
      XA=-1.
      XB=1.
      FA=((4.*P*XA+3.*Q)*XA+R+R)*XA+S
      FB=((4.*P*XB+3.*Q)*XB+R+R)*XB+S
      IF(FA*FB) 32,29,28
28    XERROR=ER5
      GO TO 59
29    IF(FA.EQ.0.) GO TO 30
      XX=XB
      GO TO 36
30    IF(FB.EQ.0.) GO TO 31
      XX=XA
      GO TO 36
31    KERROR=ER6
      GO TO 59
32    X=(XA*FB-XB*FA)/(FB-FA)
      FC=(4.*P*X+3.*Q)*X+R+R)*X+S
      IF(FC.EQ.0.) GO TO 35
      IF(FA*FC.LT.0.) GO TO 33
      FB=(FA*FB)/(FA+FC)
      GO TO 34
33    FB=FA
      XB=XA
34    FA=FC
      XA=X
      IF(ABS(XA-XB).GT.1.E-4) GO TO 32
35    XX=X
C     USE THIS VALUE XX TO ESTABLISH MAX OF RHO
36    RHOMAX=(((P*XX+Q)*XX+R)*XX+S)*XX+FLOAT(MAX)*10.
      TD(KVECT)=(FLOAT(K-NSHIFC)+XX)*DELTAT
C     FIND WHERE THIS VALUE OF RHO OCCURS ON AMNACF
      CALL TAUACF(RHOMAX,TM(KVECT),NOKAY)
      GO TO (38,37),NOKAY
37    KERROR=ER7
      GO TO 59
      GO TO 59
38    TCDSQ(KVECT)=TD(KVECT)*TD(KVECT)+TM(KVECT)*TM(KVECT)
      O4(MCOUNT,1)=1.E-6*RHOMAX
      O4(MCOUNT,2)=TD(KVECT)
      O4(MCOUNT,3)=TM(KVECT)
      O4(MCOUNT,4)=TCDSQ(KVECT)
42    CONTINUE
43    CONTINUE
```

ORIGINAL PAGE IS
OF POOR QUALITY


```
      DO 44 KVECT=1,3
      SM(KVECT,1)=1.
      SM(KVECT,2)=CS2DTH(KVECT)
      SM(KVECT,3)=SN2DTH(KVECT)
      SM(KVECT,4)=TCDSQ(KVECT)/DRSQ(KVECT)
44    CONTINUE
      CALL BRIGS2
84    FORMAT(1H ,A4)
59    WRITE(6,84) KERROR
1     CONTINUE
      RETURN
      END



      SUBROUTINE BRIGS2
C     SUBROUTINE BRIGS2 ESTIMATES CORRELATION ELLIPSES
      REAL IDATA,NCLNSH,KERROR
      LOGICAL ONE
      DIMENSION O8(11),POL(2),O5(4),CY(3),ERR(3),VIM(3),VID(3),O6(3,2)
      DIMENSION O7(7)
      COMMON /AA/ NDATA(4),IDATA(4,512),RAD(3),CTHETA(3),NAUTO,NC,ONE
      COMMON /BB/ NIRHO(4),IRHO(20,4),AMNACF(21),AMINRH,MAXTAU,DELTAT
      COMMON /CC/ PI,PID2,PIM2,PID2M3,RDTDG,DGTRD,FRADEG,KERROR
      COMMON /DD/ ID(3),T,IM,NBLK,IP,CON(3),DTHETA(3)
      COMMON /EE/ CX(3),MISS,TMHALF,TD(3),DX(3),DY(3),DR(3),CR(3)
      COMMON /FF/ O1(20,4),O2(20),O3(3,42),O4(3,4),SM(3,4),NTOP
      DATA POL(1)/5HX-MOD/,POL(2)/5HO-MOD/
      DATA ER1/4H    /,ER2/4HACF2/,ER3/4HTHLF/,ER4/4HXHF1/
      DATA ER5/4HDIF1/,ER6/4HDIF2/,ER7/4HTRHO/,ER8/4HMISS/,ER9/4HMYPE/
      DATA ER10/4HVC=-/
      CALL MATS(SM,CX,3,MISS)
      NSHIFA=19
      IF(MISS.LE.0) GO TO 45
      KERROR=ER8
      WRITE(6,84) KERROR
      GO TO 1
45    CONTINUE
      A=CX(1)
      B=CX(2)
      C=CX(3)
      DUM1=SQRT(C*C+B*B)
      IF(A.GT.DUM1) GO TO 46
      KERROR=ER9
      VS=1.E2
      PHS=0.
      GO TO 47
46    AAXIS=1./SQRT(A-DUM1)
      BAXIS=1./SQRT(A+DUM1)
      AXRATI=AAXIS/BAXIS
      THETA=ANGLRN(ARCTAN(-B,-C)$.5,0.,PI)
      A=TMHALF$AAXIS
      P=THETA$RDTDG
      B=TMHALF$BAXIS
      AXISMA=A
      NCLNSH=P
      O5(1)=P
      O5(2)=A
      O5(3)=B
      O5(4)=AXRATI
47    DO 48 I=1,3
C     SOLVE FOR DRIFT
      DUM1=1./TD(I)
      CX(I)=DX(I)$DUM1
      CY(I)=DY(I)$DUM1
      CR(I)=DR(I)$DUM1
48    ERR(I)=CR(I)$DUM1
      DO 51 IJ5=1,3
      VIM(IJ5)=SQRT(CX(IJ5)$CX(IJ5)+CY(IJ5)$CY(IJ5))
      VID(IJ5)=RDTDG$ARCTAN(CX(IJ5),CY(IJ5))
      O6(IJ5,1)=VIM(IJ5)
      O6(IJ5,2)=VID(IJ5)
51    CONTINUE
C     SOLVE FOR MEAN PERPENDICULAR TO CX, CY JOINS
      DUM1=0.
      DUM2=0.
```

ORIGINAL PAGE IS
OF POOR QUALITY


```
      DO 52 I=1,2
      JDUM=I+1
      DO 52 J=JDUM,3
      A=CX(J)*CY(I)-CX(I)*CY(J)
      B=CX(J)-CX(I)
      C=CY(J)-CY(I)
      A=A/(B*B+C*C)
      DUM1=DUM1-A*C
52    DUM2=DUM2+A*B
      VD=SQRT(DUM1*DUM1+DUM2*DUM2)/3.
      PHI=ARCTAN(DUM1,DUM2)
      P=PHI*RDTDG
      PHS=PHI
      VS=VD
      DO 58 IJKL=1,2
      PPP=PHI*RDTDG
      IF(IJKL.EQ.1) GO TO 53
      CALL ARGUS(DTHETA,VD,PHI,CR,ERR,LL,B1,B2,E1,E2)
      VD=B1
      VS=B1
      PHS=B2
      PHI=B2
      E2=E2*RDTDG
      P=PHI*RDTDG
      A=FLOAT(K)
      B2=B2*RDTDG
      IF(KERROR.EQ.ER9) GO TO 59
C     SOLVE FOR TRUE VELOCITY
53    CONTINUE
      P=PHI-THETA
      C=COS(P)
      S=SIN(P)
      IF(ABS(C).GE.1.E-8) GO TO 54
      V=BAXIS*BAXIS/VD
      GO TO 56
54    A=S/C
      R=AXRATI*AXRATI
      IF(R.LT.1.E-3) R=2.E2
      P=ANGLRN(ATAN(A/R)-P,-PID2,PID2)
      PHI=PHI+P
      A=A*A
      B=A/R
      C=B+1.
      S=B/R+1.
      A=A+1.
      R=S/A
      B=AAXIS*AAXIS
      S=B*C/(VD*VD)
      IF(R.LE.0.) GO TO 55
      V=B*SQRT(R)/VD
      RR=R*(A-S)/C
      IF(RR.LE.0.) GO TO 55
      VC=AAXIS*SQRT(RR)
      GO TO 56
55    KERROR=ER10
      WRITE(6,84) KERROR
56    CONTINUE
      PHI=PHI*RDTDG
      FIFI=PHI
      PHI=PHI*DGTRD
      GGRD=VS*SIN(PHI)
      BART=VS*COS(PHI)
      IF(IJKL.EQ.2) GO TO 57
      VS=VS/2.
      V=V/2.
      GGRD=GGRD/2.
      BART=BART/2.
      PPPP=PI/2.-(PPP*PI/180.)
      VSNORT=VS*SIN(PPPP)
      VSEAST=VS*COS(PPPP)
      O7(1)=VC
      O7(2)=VS
      O7(3)=V
      O7(4)=GGRD
      O7(5)=PPP
      O7(6)=FIFI
      O7(7)=BART
      GO TO 58
```

ORIGINAL PAGE IS
OF POOR QUALITY


```
57      CONTINUE
        B1=B1/2.
        V=V/2.
        GORD=GORD/2.
        DART=DART/2.
        B22=PI/2.-(B2*PI/180.)
        B1NORT=B1*SIN(B22)
        B1EAST=B1*COS(B22)
        OB(1)=VC
        OB(2)=B1
        OB(3)=E1
        OB(4)=B1EAST
        OB(5)=V
        OB(6)=GORD
        OB(7)=B2
        OB(8)=E2
        OB(9)=B1NORT
        OB(10)=FIFI
        OB(11)=DART
58      CONTINUE
        WRITE(6,76)
        WRITE(6,74) (O2(LI),LI=1,NSHIFA)
        WRITE(6,82) (O7(LI),LI=1,7)
        WRITE(6,83) (OB(LI),LI=1,11),LL
        GO TO 1
59      WRITE(6,84) KERROR
60      GO TO 1
74      FORMAT(1H ,10F7.3)
76      FORMAT(10X/20X,29HMEAN AUTOCORRELATION FUNCTION)
82      FORMAT(10X/11X,55HDRIFT RESULTS USING FIRST ESTIMATE OF APPARENT
        1 VELOCITY/1X,23HESTIMATED APP. VELOCITY,21X,22HTRUE VELOCITY
        2       VC=,F7.2/1X,4HVEL=,F7.2,33X,4HVEL=,F7.2,4X,4HE-W=,F7.2/1X
        3,4HPHI=,F7.2,33X,4HPHI=,F7.2,4X,4HN-S=,F7.2)
83      FORMAT(10X/11X,47HDRIFT RESULTS USING CORRECTED APPARENT
        1 VELOCITY/1X,23HCORRECTED APP. VELOCITY,7X,7HCOMPTS.,7X,
        222HTRUE VELOCITY       VC=,F7.2/1X,4HVEL=,F7.2,2X,6HERROR=,F6.2
        3,3X,4HE-W=,F7.2,5X,4HVEL=,F7.2,4X,4HE-W=,F7.2/1X,4HPHI=,F7.2,
        42X,6HERROR=,F6.2,3X,4HN-S=,F7.2,5X,4HPHI=,F7.2,4X,4HN-S=,F7.2,
        51X/1X,15HNO. ITERATIONS=,I2)
84      FORMAT(1H ,A4)
1       CONTINUE
        RETURN
        END



        FUNCTION ARCTAN(X,Y)
        COMMON /CC/ PI,PID2,PIM2,PID2M3,RDTDG,DRTRD,FRADEQ
        IF(X) 5,1,6
1       IF(Y) 3,2,4
2       WRITE(6,8)
        ARCTAN=0.
        GO TO 7
3       ARCTAN=PID2M3
        GO TO 7
4       ARCTAN=PID2
        GO TO 7
5       ARCTAN=PI+ATAN(Y/X)
        GO TO 7
6       ARCTAN=ATAN(Y/X)
7       IF(ARCTAN.LT.0.) ARCTAN=ARCTAN+PIM2
        RETURN
8       FORMAT(1X,22HARCTAN 0/0, SET=0 RADS)
        END



        FUNCTION ANGLRN(ANGLE,END1,END2)
        IF(END2-END1) 2,9,1
1       ENDHI=END2
        ENDLO=END1
        GO TO 3
2       ENDHI=END1
        ENDLO=END2
3       RANGE=ENDHI-ENDLO
        ANGLRN=ANGLE
4       IF(ANGLRN-ENDHI) 6,5,5
```

ORIGINAL PAGE IS
OF POOR QUALITY

```
5       ANGLRN=ANGLRN-RANGE
        GO TO 4
6       IF(ANGLRN-ENDLO) 7,8,8
7       ANGLRN=ANGLRN+RANGE
        GO TO 6
8       IF(ANGLRN.GT.ENDHI) GO TO 10
        RETURN
9       WRITE(6,12)
        GO TO 11
10      WRITE(6,13)
11      WRITE(6,14) ANGLE,END1,END2
        STOP
12      FORMAT(1X,18H ERR FUNC ANGLRN  ,3X,11H RANGE ZERO,3X,5H STOP)
13      FORMAT(1X,18H ERR FUNC ANGLRN  ,3X,11H CYCLE OPEN,3X,5H STOP)
14      FORMAT(1X,6H PARAM,3E20.10)
        END


        SUBROUTINE ARGUS(Z,B1,B2,FM,ERR,LL,C1,C2,E1,E2)
        DIMENSION Z(3),B(2),FM(3),ERR(3),FC(3),R(2,1),A(3,2),DF(3),G(2,2)
        B(1)=B1
        B(2)=B2
        ERQ=1.E-6
        QO=1.E10
        LL=0
1       DO 2 I=1,3
        ARG=B(2)-Z(I)
        S=1./COS(ARG)
        FC(I)=S*B(1)
        A(I,1)=S
2       A(I,2)=B(1)*SIN(ARG)*S*S
        DO 3 J=1,3
3       DF(J)=FM(J)-FC(J)
        DO 4 L=1,2
        R(L,1)=0.
        DO 4 J=1,3
4       R(L,1)=R(L,1)+A(J,L)*DF(J)/(ERR(J)*ERR(J))
        DO 5 L=1,2
        DO 5 K=1,2
        G(L,K)=0.
        DO 5 J=1,3
5       G(L,K)=G(L,K)+A(J,L)*A(J,K)/(ERR(J)*ERR(J))
        DET=G(1,1)*G(2,2)-G(2,1)*G(1,2)
        Y1=(G(2,2)*R(1,1)-G(1,2)*R(2,1))/DET
        Y2=(R(1,1)-G(1,1)*Y1)/G(1,2)
        R(1,1)=Y1
        R(2,1)=Y2
        Q1=0.
        DO 6 J=1,3
6       Q1=Q1+DF(J)*DF(J)/(ERR(J)*ERR(J))
        Q=ABS(QO-Q1)
        LL=LL+1
        QO=Q1
        IF(Q.LE.ERQ) GO TO 8
        IF(LL.GE.8) GO TO 8
        DO 7 J=1,2
7       B(J)=B(J)+R(J,1)
        GO TO 1
8       E1=SQRT(G(2,2)/DET*Q1)
        E2=SQRT(G(1,1)/DET*Q1)
        C1=B(1)
        C2=B(2)
        RETURN
        END


        SUBROUTINE MATS(S,A,NSPEC,NISS)
        DIMENSION S(3,4),A(3)
        NISS=-1
        NM=NSPEC+1
        N=NSPEC
        DO 7 I=2,N
        II=I-1
        DO 7 J=1,II
        IF(S(I,J)) 1,7,1
```

ORIGINAL PAGE IS
OF POOR QUALITY


```
1       IF(ABS(S(J,J))-ABS(S(I,J))) 3,2,2
2       R=S(I,J)/S(J,J)
        GO TO 5
3       R=S(J,J)/S(I,J)
        DO 4 K=1,MM
        B=S(J,K)
        S(J,K)=S(I,K)
4       S(I,K)=B
5       JJ=J+1
        DO 6 K=JJ,MM
6       S(I,K)=S(I,K)-R*S(J,K)
7       CONTINUE
        IF(ABS(S(N,N))-1.E-10) 8,8,9
8       MISS=1
        GO TO 12
9       A(N)=S(N,MM)/S(N,N)
        DO 11 I=2,N
        JJ=N-I+1
        B=0.
        I1=N-I+2
        DO 10 K=I1,N
10      B=B+S(JJ,K)*A(K)
        IF(ABS(S(JJ,JJ))-1.E-10) 8,8,11
11      A(JJ)=(S(JJ,MM)-B)/S(JJ,JJ)
12      CONTINUE
        RETURN
        END


        SUBROUTINE TAUACF(RHOMAX,TAU,NOKAY)
        COMMON /BB/ NIRHO(4),IRHO(20,4),AMNACF(21),AMINRH,MAXTAU,DELTAT
        NOKAY=1
        IF(RHOMAX.GE.AMINRH) GO TO 1
        NOKAY=2
        GO TO 5
1       AMINDI=ABS(1.-RHOMAX)
        K=1
        DO 2 L=2,MAXTAU
        IF(AMINDI.LE.ABS(RHOMAX-AMNACF(L))) GO TO 2
        AMINDI=ABS(RHOMAX-AMNACF(L))
        K=L
2       CONTINUE
        IF(K.NE.1) GO TO 3
        TAU=SQRT(AMINDI/(1.-AMNACF(2)))
        GO TO 5
3       A=.5*(AMNACF(K-1)-2.*AMNACF(K)+AMNACF(K+1))
        B=.25*(AMNACF(K+1)-AMNACF(K-1))
        C=AMNACF(K)
        IF(ABS(A).GE.1.E-04) GO TO 4
        TAU=(FLOAT(K)-1.+(RHOMAX-C)/(2.*B))*DELTAT
        GO TO 5
4       TAU=(FLOAT(K)-1.-(B+SQRT(B**2-A*(C-RHOMAX)))/A)*DELTAT
5       CONTINUE
        RETURN
        END


        SUBROUTINE CORLAT(J1,J2,J3,NSHIFT)
        REAL IDATA
        DIMENSION X(550),Y(550)
        COMMON /AA/ NDATA(4),IDATA(4,512),RAD(3),CTHETA(3),NAUTO,NC,ONE
        COMMON /BB/ NIRHO(4),IRHO(20,4),AMNACF(21),AMINRH,MAXTAU,DELTAT
        NDAT=NDATA(J1)
        DO 1 JXY=1,NDAT
        X(JXY)=IDATA(J2,JXY)
1       Y(JXY)=IDATA(J1,JXY)
        SX=0.
        SY=0.
        SSX=0.
        SSY=0.
        DO 2 JXY=1,NDAT
        SSX=SSX+X(JXY)*X(JXY)
2       SX=SX+X(JXY)
        IF(J1.EQ.J2) GO TO 4
        DO 3 JXY=1,NDAT
        SSY=SSY+Y(JXY)*Y(JXY)
```

ORIGINAL PAGE IS
OF POOR QUALITY

```
3       SY=SY+Y(JXY)
        GO TO 5
4       SY=SX
        SSY=SSX
5       DO 7 JD=1,NSHIFT
        NS=JD-1
        NP=NDAT-NS
        S=0.
        DO 6 J=1,NP
        III=J+NS
6       S=S+X(J)*Y(III)
        G=1./FLOAT(NP)
        IRHO(JD,J3)=(S-SX*SY*G)/SQRT((SSX-SX*SX*G)*(SSY-SY*SY*G))*1E6+.5
        IJI=NDAT-NS
        XX=X(IJI)
        YY=Y(JD)
        SX=SX-XX
        SY=SY-YY
        SSX=SSX-XX*XX
7       SSY=SSY-YY*YY
8       NIRHO(J3)=NSHIFT
        RETURN
        END

C DRFTPL                                                                C
C DAT SLOT 2 IS ASSIGNED TO DATA TAPE
        REAL IDATA,NCLNSH,KERROR
        LOGICAL ONE
        DIMENSION FNAM(2),DATE(2),ITIM(4),ORIENT(4),ANT(4)
        DIMENSION DP1(31),DP2(31),DP3(31),DP4(31),DKS(240),KS(240)
        COMMON /AA/ NDATA(4),IDATA(4,512),RAD(3),CTHETA(3),NAUTO,NC,ONE
        COMMON /BB/ NIRHO(4),IRHO(20,4),AMNACF(21),AMINRH,MAXTAU,DELTAT
        COMMON /DD/ ID(3),T,IH,NBLK,IP,CON(3),DTHETA(3)
        DATA ANT(1)/5HN-E  /,ANT(2)/5HN-W  /,ANT(3)/5HS-W  /
        DATA ANT(4)/5HS-E  /
        ORIENT(1)=45.
        ORIENT(2)=315.
        ORIENT(3)=225.
        ORIENT(4)=135.
        NDATA(1)=512
        NDATA(2)=512
        NDATA(3)=512
        NDATA(4)=512
        RAD(1)=119.5
        RAD(2)=119.5
        RAD(3)=119.5
        NAUTO=3
        DT=.033/.4
4       CONTINUE
        KK9=0
6       CONTINUE
        WRITE(6,11)
11      FORMAT(16H WHICH DATA FILE)
        READ(4,15) FNAM
15      FORMAT(2A5)
C GET HEIGHT BOUNDARIES
        WRITE(6,22)
        READ(4,23) ALT
22      FORMAT(6HHEIGHT)
        JALT=IFIX(ALT/1.5-29.)
23      FORMAT(F4.1)
C OPEN FILE
        CALL SEEK(2,FNAM)
        READ(2) DATE,ITIM,IDB
        IDB=IDB-64
        WRITE(6,5)
5       FORMAT(1H1,80X/40X)
C WRITE HEADER
        WRITE(6,35) DATE,ITIM,IDB,ALT
35      FORMAT(10X,2A5,10X,4I1,10X,I2,3H DB,10X,F6.1,3H KM)
        WRITE(6,36)
36      FORMAT(//12X)
40      CONTINUE
C READ TWO DATA FRAMES
        READ(2) ID,KS
C CHECK FOR END OF FILE
        IF(ID.EQ.130050) GO TO 60
```

ORIGINAL PAGE IS
OF POOR QUALITY


```
      KK=1
      DO 45 N=1,240
      DKB(N)=FLOAT(KB(N))
45    CONTINUE
44    CONTINUE
      KK9=KK9+1
      IF(KK9.GE.513) GO TO 40
      DP1(18)=DKB(KK)
      DP1(19)=DKB(KK+1)
      DP1(21)=DKB(KK+2)
      DP1(22)=DKB(KK+3)
      DP1(24)=DKB(KK+4)
      DP1(25)=DKB(KK+5)
      DP2(18)=DKB(KK+6)
      DP2(19)=DKB(KK+7)
      DP2(21)=DKB(KK+8)
      DP2(22)=DKB(KK+9)
      DP2(24)=DKB(KK+10)
      DP2(25)=DKB(KK+11)
      DP3(18)=DKB(KK+12)
      DP3(19)=DKB(KK+13)
      DP3(21)=DKB(KK+14)
      DP3(22)=DKB(KK+15)
      DP3(24)=DKB(KK+16)
      DP3(25)=DKB(KK+17)
      DP4(18)=DKB(KK+18)
      DP4(19)=DKB(KK+19)
      DP4(21)=DKB(KK+20)
      DP4(22)=DKB(KK+21)
      DP4(24)=DKB(KK+22)
      DP4(25)=DKB(KK+23)
      KK=KK+24
      IDATA(1,KK9)=DP1(JALT)
      IDATA(2,KK9)=DP2(JALT)
      IDATA(3,KK9)=DP3(JALT)
      IDATA(4,KK9)=DP4(JALT)
      IF(KK.GE.240) GO TO 40
      GO TO 44
40    CONTINUE
C CLOSE FILE
      CALL CLOSE(2)
      D=DT
      DO 62 K=2,4
      B1=IDATA(K,I)
      DO 61 I=2,512
      B2=IDATA(K,I)
      IDATA(K,I)=B2+DB(B1-B2)
61    B1=B2
62    D=D+DT
      DO 75 IK=1,4
      DO 70 JK=2,512
      CHECK=(IDATA(IK,JK)-IDATA(IK,JK-1))
      ACHECK=ABS(CHECK)
      IF(ACHECK.LE.50.) GO TO 74
      IF(CHECK)71,72,73
71    IDATA(IK,JK)=IDATA(IK,JK-1)-50.
      GO TO 74
72    GO TO 74
73    IDATA(IK,JK)=IDATA(IK,JK-1)+50.
74    CONTINUE
70    CONTINUE
75    CONTINUE
      CALL PLOT
      GO TO 4
      STOP
      END
```

ORIGINAL PAGE IS
OF POOR QUALITY


```
10 REM THIS PROGRAM IS DESIGNED TO
20 REM OUTPUT SPECIFIC USER-CONTROLLED
30 REM TIMING PULSES THROUGH USER PORT
40 REM A ON THE PET 2001. AVAILABLE TI
50 REM PULSE WIDTHS ARE  10  1[illegible]  2[illegible] AND
60 REM [illegible]0 MICROSECONDS. AVAILABLE INTER-
70 REM PULSE PERIODS ARE  [illegible].7  13.3  AND
80 REM 20 MILLISECONDS. THE MACHINE
90 REM LANGUAGE PROGRAM STARTS IN THE
100 REM FIRST CASSETTE BUFFER AND MAY
110 REM RUN INTO THE SECOND CASSETTE BUF-
120 REM FER. VARIABLE LOCATIONS ARE THE
130 REM LAST 7 ADDRESSES IN THE SECOND
140 REM CASSETTE BUFFER. THE MACHINE
150 REM LANGUAGE PROGRAM RUNS CONTIN-
160 REM UOUSLY UNLESS INTERRUPTED BY THE
170 REM USER BY PRESSING THE SPACE BAR.
180 REM LINES PA0-PA6 ARE USED ON THE
190 REM USER PORT FOR OUTPUT.
200 REM
250 REM START USER QUERY
260 PRINT"[illegible]           INTERPULSE PERIOD(MSEC)"
270 PRINT
280 PRINT"[illegible]          [illegible].7       13.3       20"
290 PRINT
300 PRINT"[illegible]PULSE  10  A          B          C"
310 PRINT"[illegible]IDTH   1[illegible]  D          E          F"
320 PRINT"[illegible]MICRO  2[illegible]  G          H          I"
330 PRINT"[illegible] SEC   50  J          K          L"
340 PRINT
350 PRINT"[illegible]IEW MODE"
360 INPUT A[illegible]  IF A[illegible]"" THEN 360
370 M=ASC(A[illegible])-64
380 REM
390 REM *LOAD INITIALIZATION*
400 RESTORE
410 N1=664
420 N2=661
430 S=0
440 GOSUB 2740
450 REM
460 REM *LOAD HACKS 1-2*
470 N1=662
480 N2=695
490 S=0
500 GOSUB 2740
510 REM
520 REM *LOAD TH PULSE  HACKS 3-4*
530 ON M GOTO 550 550 550 670 670 670 830,830,830,990,990,990
540 REM *TH PULSE 10 USEC*
550 N1=696
560 N2=718
570 S=0
580 GOSUB 2740
590 REM SKIP DATA STATEMENTS
600 N1=696
610 N2=777
620 S=1
630 GOSUB 2740
640 GOTO 1100
650 REM *TH PULSE 15 USEC*
660 REM SKIP DATA STATEMEN[illegible]
670 N1=696
680 N2=718
690 S=1
700 GOSUB 2740
710 N1=696
720 N2=719
730 S=0
740 GOSUB 2740
750 REM SKIP DATA STATEMENTS
760 N1=696
770 N2=753
780 S=1
790 GOSUB 2740
800 GOTO 1160
810 REM *TH PULSE 25 USEC*
820 REM SKIP DATA STATEMENTS
830 N1=696
840 N2=742
850 S=1
```

```
860 GOSUB 2740
870 N1=696
880 N2=724
890 S=0
900 GOSUB 2740
910 REM SKIP DATA STATEMENTS
920 N1=696
930 N2=724
940 S=1
950 GOSUB 2740
960 GOTO 1220
970 REM #TX PULSE 50 USEC#
980 REM SKIP DATA STEMENTS
990 N1=696
1000 N2=771
1010 S=1
1020 GOSUB 2740
1030 N1=696
1040 N2=724
1050 S=0
1060 GOSUB 2740
1070 GOTO 1220
1080 REM #LOAD HACKS 5-7#
1090 REM #TX PULSE 10 USEC#
1100 N1=719
1110 N2=794
1120 S=0
1130 GOSUB 2740
1140 GOTO 1270
1150 REM #TX PULSE 15 USEC#
1160 N1=720
1170 N2=795
1180 S=0
1190 GOSUB 2740
1200 GOTO 1270
1210 REM #TX PULSES 25-50#
1220 N1=725
1230 N2=800
1240 S=0
1250 GOSUB 2740
1260 REM #LOAD INTERPULSE PERIOD#
1270 ON M GOTO 1290,1630,2110,1400,1790,2270,1510,1950,2430,1510,1950,2430
1280 REM #IPP 6.7 MSEC (TX 10)#
1290 N1=795
1300 N2=819
1310 S=0
1320 GOSUB 2740
1330 REM SET HACK1 AND END
1340 POKE 1014,150
1350 POKE 1015,2
1360 POKE 1016,50
1370 POKE 1017,3
1380 GOTO 2570
1390 REM #IPP 6.7 MSEC (TX 15)#
1400 N1=796
1410 N2=820
1420 S=0
1430 GOSUB 2740
1440 REM SET HACK1 AND END
1450 POKE 1014,150
1460 POKE 1015,2
1470 POKE 1016,51
1480 POKE 1017,3
1490 GOTO 2570
1500 REM #IPP 6.7 MSEC (TX 25-50)#
1510 N1=801
1520 N2=825
1530 S=0
1540 GOSUB 2740
1550 REM SET HACK1 AND END
1560 POKE 1014,150
1570 POKE 1015,2
1580 POKE 1016,56
1590 POKE 1017,3
1600 GOTO 2570
1610 REM #IPP 13.3 MSEC (TX 10)#
1620 REM SKIP TO IPP 13.3
1630 N1=691
1640 N2=715
1650 S=1
1660 GOSUB 2740
```

```
1670 N1=795
1680 N2=826
1690 S=0
1700 GOSUB 2740
1710 REM SET HACK1 AND END
1720 POKE 1014,150
1730 POKE 1015,2
1740 POKE 1016,57
1750 POKE 1017,3
1760 GOTO 2570
1770 REM *IPP 13.3 MSEC (TX 15)*
1780 REM SKIP TO IPP 13.3
1790 N1=691
1800 N2=715
1810 S=1
1820 GOSUB 2740
1830 N1=796
1840 N2=827
1850 S=0
1860 GOSUB 2740
1870 REM SET HACK1 AND END
1880 POKE 1014,150
1890 POKE 1015,2
1900 POKE 1016,58
1910 POKE 1017,3
1920 GOTO 2570
1930 REM *IPP 13.3 MSEC (TX 25-50)*
1940 REM SKIP TO IPP 13.3
1950 N1=691
1960 N2=715
1970 S=1
1980 GOSUB 2740
1990 N1=801
2000 N2=832
2010 S=0
2020 GOSUB 2740
2030 REM SET HACK1 AND END
2040 POKE 1014,150
2050 POKE 1015,2
2060 POKE 1016,63
2070 POKE 1017,3
2080 GOTO 2570
2090 REM *IPP 13.3 MSEC (TX 10)*
2100 REM SKIP TO IPP 13.3
2110 N1=691
2120 N2=747
2130 S=1
2140 GOSUB 2740
2150 N1=795
2160 N2=834
2170 S=0
2180 GOSUB 2740
2190 REM SET HACK1 AND END
2200 POKE 1014,150
2210 POKE 1015,2
2220 POKE 1016,66
2230 POKE 1017,3
2240 GOTO 2570
2250 REM *IPP 13.3 MSEC (TX 15)*
2260 REM SKIP TO IPP 13.3
2270 N1=691
2280 N2=747
2290 S=1
2300 GOSUB 2740
2310 N1=796
2320 N2=835
2330 S=0
2340 GOSUB 2740
2350 REM SET HACK1 AND END
2360 POKE 1014,150
2370 POKE 1015,2
2380 POKE 1016,67
2390 POKE 1017,3
2400 GOTO 2570
2410 REM *IPP 13.3 MSEC (TX 25-50)*
2420 REM SKIP TO IPP 13.3
2430 N1=691
2440 N2=747
2450 S=1
2460 GOSUB 2740
2470 N1=801
2480 N2=840
```

ORIGINAL PAGE IS
OF POOR QUALITY


```
2490 S=0
2500 GOSUB 2740
2510 REM SET HACK.1 AND END
2520 POKE 1014,150
2530 POKE 1015,2
2540 POKE 1016,72
2550 POKE 1017,3
2560 REM SET WAITING PERIOD
2570 PRINT"SET WAITING PERIOD IN 1/60 SEC INTERVALS"
2580 INPUT B
2590 REM READY TO RUN
2600 PRINT"READY. PRESS ANY KEY TO RUN."
2610 GET A$  IF A$="" THEN 2610
2620 SYS(634)
2630 IF PEEK(59418)=251 THEN 2590
2640 T=TI
2650 D=TI-T
2660 IF D<B THEN GOTO 2650
2670 GOTO 2620
2680 REM REDO USER QUERY
2690 GOTO 260
2700 END
2710 REM
2720 REM
2730 REM DATA READ SUBROUTINE
2740 FOR I=N1 TO N2
2750 READ D
2760 IF S=1 GOTO 2780
2770 POKE I,D
2780 NEXT I
2790 RETURN
2800 REM
2810 REM
2820 REM *INITIALIZATION*
2830 DATA 120,160,255,140,67,232
2840 DATA 160,4,140,247,3,160,6,140,242,3
2850 DATA 160,17,140,244,3,160,251
2860 DATA 169,0,141,79,232
2870 REM *TIME HACK 1*
2880 DATA 204,26,232,208,3,109,248,3
2890 DATA 73,191,73,255,234,234
2900 DATA 234,234,234,141,79,232
2910 REM *TIME HACK 2*
2920 DATA 73,223,73,255,234
2930 DATA 234,234,234,234,8
2940 DATA 40,141,79,232
2950 REM *TIME HACKS 3-4 (10 USEC)*
2960 DATA 73,223,73,255,234
2970 DATA 141,79,232
2980 DATA 73,191,73,255,162,10
2990 DATA 202,208,253,234,234,234
3000 DATA 141,79,232
3010 REM *TIME HACKS 3-4 (15 USEC)*
3020 DATA 73,223,73,255,8,40
3030 DATA 141,79,232
3040 DATA 73,191,73,255,162,9
3050 DATA 202,208,253,234,234,234
3060 DATA 141,79,232
3070 REM *TIME HACKS 3-4 (25 USEC)*
3080 DATA 73,223,73,255,234,234
3090 DATA 234,234,234,8,40
3100 DATA 141,79,232
3110 DATA 73,191,73,255,162,7
3120 DATA 202,208,253,234,234,234
3130 DATA 141,79,232
3140 REM *TIME HACKS 3-4 (50 USEC)*
3150 DATA 73,223,73,255,162,7,202
3160 DATA 208,253,234,234,234
3170 DATA 141,79,232
3180 DATA 73,191,73,255,234,234
3190 DATA 234,234,234,8,40
3200 DATA 141,79,232
3210 REM *TIME HACK 5*
3220 DATA 73,209,73,255,162,32
3230 DATA 202,208,253,234,234,234
3240 DATA 141,79,232
3250 REM *TIME HACK 6*
3260 DATA 41,240,141,243,3
3270 DATA 173,245,3,72,40,169,0
3280 DATA 109,244,3,104,141,244,3
3290 DATA 41,15,170,173,244,3
3300 DATA 10,141,244,3,8,104
```

ORIGINAL PAGE IS
OF POOR QUALITY

```
3310 DATA 141,245,3,138,13,243,3
3320 DATA 162,17,202,208,253
3330 DATA 141,24,232
3340 REM *TIME HACK 7*
3350 DATA 73,255,73,255,162,47
3360 DATA 202,208,253,234,234,234
3370 DATA 141,24,232
3380 REM *IPP FILLER   6.7 MSEC*
3390 DATA 162,230,202,8,40,8,40
3400 DATA 8,40,208,247,206,242,3
3410 DATA 174,242,3,234,240,3
3420 DATA 108,246,3,88,96
3430 REM *IPP FILLER - 13.3 MSEC*
3440 DATA 140,243,3,160,5,162,251
3450 DATA 202,56,176,0,208,250
3460 DATA 136,208,247,172,243,3
3470 DATA 206,242,3,174,242,3,240,3
3480 DATA 108,246,3,88,96
3190 REM *IPP FILLER - 19.3 MSEC*
3500 DATA 140,243,3,160,4,162,253
3510 DATA 202,8,40,8,40,208,249
3520 DATA 136,208,246,8,40,8,40
3530 DATA 234,234,234,172,243,3,206
3540 DATA 242,3,174,242,3,240,3
3550 DATA 108,246,3,88,96
3560 REM
3570 REM THE END'
3580 REM
READY.
```

```
      SUBROUTINE PLOT
      REAL IDATA
      DIMENSION POINT(82)
      COMMON /AA/ NDATA(4),IDATA(4,512),RAD(3),CTHETA(3),NAUTO,NC,ONE
      DATA STAR/1H*/,BLANK/1H /,DOT/1H./
      DO 4 I=1,512
      DO 1 J=1,80
1     POINT(J)=BLANK
      POINT(1)=DOT
      POINT(21)=DOT
      POINT(41)=DOT
      POINT(61)=DOT
      DO 2 K=1,4
      J=20*(K-1)
      L=FLOAT(J)+.03906*IDATA(K,I)+1.
      DO 3 N=J,L
3     POINT(N)=STAR
2     CONTINUE
      WRITE(6,100) (POINT(J),J=1,80)
100   FORMAT(1H ,80A1)
4     CONTINUE
      RETURN
      END
```

APPENDIX VI

CALCULATION OF SIGNIFICANCE LEVELS

A priori significance levels for the correlations are calculated by the "t test".

A posteriori significance levels for the correlations are calculated by increasing the percentage value of the significance level required by a factor equal to the number of degrees of freedom divided by the total data series length (JULIAN, 1971, 1975). For example, in Figure 9.10, the *a priori* significance level of 2.5% results in an *a posteriori* significance level of 10%.

The significance levels for coherence squared estimates were discussed by BLACKMAN and TUKEY (1958). The number of degrees of freedom of each estimate is approximately (PANOFSKY and BRIER, 1958)

$$df = \frac{2N - (M/2)}{M}$$

where

M = number of lags

N = number of samples

The *a priori* significance levels of the coherence are given by PANOFSKY and BRIER (1958). The level of coherence squared β exceeded with a probability p is given by

$$\beta = 1 - p^{1/[(df/2) - 1]}$$

For the *a posteriori* significance level, the probability p in the above expression should be replaced by the probability p', where $p' = p(df/n_s)$, and n_s is the total number of data samples in the entire series (JULIAN, 1975).

REFERENCES

AUSTIN, G. L. (1971), A direct measuring differential phase experiment, J. Atmos. Terr. Phys., 33, 1667-1674.

AUSTIN, G. L. and A. H. MANSON (1969), On the nature of the irregularities that produce partial reflections of radio waves from the lower ionosphere (70 - 100 km), Radio Sci., 4, 35-40.

BEAN, T. A. and S. A. BOWHILL (1973), Analysis of partial-reflection data from the solar eclipse of July 10, 1972, Aeron. Rep. No. 55, Aeron. Lab., Dep. Elec. Eng., Univ. Ill., Urbana-Champaign.

BELROSE, J. S. (1970), Radio wave probing of the ionosphere by the partial reflection of radio waves (from heights below 100 km), J. Atmos. Terr. Phys., 32, 567-596.

BELROSE, J. S. and M. J. BURKE (1964), Study of the lower ionosphere using partial reflection, J. Geophys. Res., 69, 2799-2818.

BEYNON, W. J. G. and J. C. WRIGHT (1969a), Ionospheric drift measurements on adjacent aerial arrays, J. Atmos. Terr. Phys., 31, 119-133.

BEYNON, W. J. G. and J. C. WRIGHT (1969b), The analysis of ionospheric drift data in the closely spaced receiver method, J. Atmos. Terr. Phys., 31, 593-596.

BIRLEY, M. H. and C. F. SECHRIST, JR (1971), Partial-reflection data collection and processing using a small computer, Aeron. Rep. No. 42, Aeron. Lab., Dep. Elec. Eng., Univ. Ill., Urbana-Champaign.

BLACKMAN, R. B., and J. W. TUKEY (1958), The Measurement of Power Spectra from the Point of View of Communications Engineering, Dover Publications, Inc., New York.

BRIGGS, B. H., G. J. PHILLIPS and D. H. SHINN (1950), The analysis of observations on spaced receivers of the fading of radio signals, Proc. Phys.

Soc., B, 63, 106-121.

BROWN, G. M. and D. C. WILLIAMS (1971), Pressure variations in the stratosphere and ionosphere, J. Atmos. Terr. Phys., 33, 1321-1328.

BUDDEN, K. G. (1961), Radio Waves in the Ionosphere, Cambridge University Press, London.

BUDDEN, K. G. (1965), Effect of collisions on the formulas on magneto-ionic theory, Radio Sci., 69D, 191-211.

BURKE, M. J. and E. H. HARA (1963), Tables of the semiconductor integrals $C_p(X)$ and their approximations for use with the generalized Appleton-Hartree magneto-ionic formulas, Rep. 1113, Defence Research Telecommunications, Establishment, Ottawa, Canada.

CAVALIERI, D. J. (1976), Traveling planetary-scale waves in the E-region, J. Atmos. Terr. Phys., 38, 965-977.

CAVALIERI, D. J., R. J. DELAND, T. A. POTEMRA and R. F. GAVIN (1974), The correlation of VLF propagation variations with atmospheric planetary-scale waves, J. Atmos. Terr. Phys., 36, 561-574.

CHAMPION, K. S. W. (1967), Variation with season and latitude of density, temperature, and composition in the lower thermosphere, Space Res. VII, North-Holland, Amsterdam, 1101-1118.

CHANDRA, H. and R. A. VINCENT (1977), Radio wave scattering from the southern hemisphere D-region, J. Atmos. Terr. Phys., 39, 1011-1016.

CHARNEY, J. G. and P. G. DRAZIN (1961), Propagation of planetary-scale disturbances from the lower into the upper atmosphere, J. Geophys. Res., 66, 83-109.

CLARK, R. R. (1975), Meteor wind measurements at Durham, New Hampshire (43 N, 71 W), J. Atmos. Sci., 32, 1689-1693.

COHEN, D. J. (1971), Modeling the D-region partial reflection experiment, Penn. State Rep. 378, Ionospheric Res. Lab., Penn State Univ., University Park, Penn.

COHEN, D. J. and A. J. FERRARO (1973), Modeling the D-region partial-reflection experiment, Radio Sci., 8, 459-465.

CRAVENS, T. E. and A. I. STEWART (1978), Global morphology of nitric oxide in the lower E region, J. Geophys. Res., 83, 2446-2452.

DA SILVA, L. C. and S. A. BOWHILL (1974), An evaluation of the partial-reflection technique and results from the winter 1971-1972 D region, Aeron. Rep. No. 63, Aeron. Lab., Dep. Elec. Eng., Univ. Ill., Urbana-Champaign.

DELAND, R. J. and D. J. CAVALIERI (1973), Planetary-scale fluctuations of pressure in the E-layer f-min, and pressure in the stratosphere, J. Atmos. Terr. Phys., 35, 125-132.

DENNY, B. W. and S. A. BOWHILL, (1973), Partial-reflection studies of D-region winter variability, Aeron. Rep. No. 56, Aeron. Lab., Dep. Elec. Eng., Univ. Ill., Urbana-Champaign.

EDWARDS, B. (1973) (Ed.), Research in Aeronomy, October 1, 1971 - March 31, 1973, Prog. Rep. 73-1, Aeron. Lab., Dep. Elec. Eng., Univ. Ill., Urbana-Champaign.

EDWARDS, B. (1975) (Ed.), Research in Aeronomy, October 1, 1974 - March 31, 1975, Prog. Rep. 75-1, Aeron. Lab., Dep. Elec. Eng., Univ. Ill., Urbana-Champaign.

EVANS, J. V. (1969), Theory and practice of ionosphere study by Thomson scatter radar, Proc. IEEE, 57, 596-530.

FEDOR, L. S. (1967), A statistical approach to the determination of three-dimensional ionospheric drifts, J. Geophys. Res., 72, 5401-5415.

FEJER, J. A. (1955), The interaction of pulsed radio waves in the ionosphere, J. Atmos. Terr. Phys., 7, 322-332.

FELGATE, D. G. (1970), On the point source effect in the measurement of ionospheric drifts, J. Atmos. Terr. Phys., 32, 241-245.

FLOOD, W. A. (1968), Revised theory for partial reflection D-region measurements, J. Geophys. Res., 73, 5585-5598.

FLOOD, W. A. (1969), Reply, J. Geophys. Res., 74, 5183-5186.

FOOKS, G. F. (1965), Ionospheric drift measurements using correlaton analysis; methods of computation and interpretation of results, J. Atmos. Terr. Phys., 27, 979-989.

FRASER, G. J. (1977), The 5-day wave and ionospheric absorption, J. Atmos. Terr. Phys., 39, 121-124.

FRASER, G. J., B. B. LIM, G. K. PRISK and M. J. SMITH (1981), An association between mesospheric winds and electron densities, J. Atmos. Terr. Phys., 43, 263-267.

FRASER, G. J. and M. R. THORPE (1976), Experimental investigations of ionospheric/stratospheric coupling in southern mid-latitudes - 1. Spectra and cross-spectra of stratospheric temperatures and the ionospheric f-min parameter, J. Atmos. Terr. Phys., 38, 1003-1011.

FRASER, G. J. and R. A. VINCENT (1970), A study of D-region irregularities, J. Atmos. Terr. Phys., 32, 1591-1607.

FRASER, G. J. and D. S. WRATT (1976), Experimental investigations of ionospheric/stratospheric coupling in southern mid-latitudes - 2. Comparison of mesospheric electron densities and drifts with stratospheric temperatures and winds, J. Atmos. Terr. Phys., 38, 1013-1016.

GARDNER, F. F., and J. L. PAWSEY (1953), Study of the ionospheric D-region using partial reflections, J. Atmos. Terr. Phys., 3, 321-344.

GEISLER, J. E. and R. E. DICKINSON (1968), Vertical motions and nitric oxide in the upper mesosphere, J. Atmos. Terr. Phys., 30, 1505-1521.

GELLER, M. A., S. A. BOWHILL and G. C. HESS (1977), A description of the University of Illinois meteor radar system and some first results, J. Atmos. Terr. Phys., 39, 15-24.

GELLER, M. A., G. C. HESS and D. WRATT (1976), Simultaneous partial reflection and meteor radar wind observations at Urbana, Illinois, during the winter of 1974-1975, J. Atmos. Terr. Phys., 38, 287-290.

GELLER, M. A. and C. F. SECHRIST, JR. (1971), Coordinated rocket measurements on the D-region winter anomaly - II. Some implications, J. Atmos. Phys., 33, 1027-1040.

GOLLEY, M. G. and D. E. ROSSITER (1970), Some tests of methods of analysis of ionospheric drift records using an array of 89 aerials, J. Atmos. Terr. Phys., 32, 1215-1234.

GREGORY, J. B. and A. H. MANSON (1969a), Seasonal variations of electron densities below 100 km at midlatitudes - I., J. Atmos. Terr. Phys., 31, 683-701.

GREGORY, J. B. and A. H. MANSON (1969b), Seasonal variations of electron densities below 100 km at midlatitudes - II., J. Atmos. Terr. Phys., 31, 703-729.

HENRY, G. W., JR. (1966), Instrumentation and preliminary results from shipboard measurements of vertical incidence ionospheric absorption, Aeron. Rep. No. 13, Aeron. Lab., Dep. Elec. Eng., Univ. Ill., Urbana-Champaign.

HESS, G. C. and M. A. GELLER (1976), The Urbana meteor-radar system: Design, development, and first observations, Aeron. Rep. No. 74, Aeron. Lab., Dep. Elec. Eng., Univ. Ill., Urbana-Champaign.

HESS, G. C. and M. A. GELLER (1978), Urbana, meteor-radar observations during GRMWSP/CTOP periods, J. Atmos. Terr. Phys., 40, 895-903.

HINES, C. O. and R. R. RAO (1968), Validity of three-station methods of determining ionospheric motions, J. Atmos. Terr. Phys., 30, 979-993.

HOLT, O. (1969), Discussion of paper by W. A. Flood, 'Revised theory for partial reflection D-region measurements', J. Geophys. Res., 74, 5179-5182.

HOLTON, J. R. (1972), An Introduction to Dynamic Meteorology, Academic Press, New York, 1-319.

JULIAN, P. R. (1971), Some aspects of variance spectra of synoptic scale tropospheric wind components in midlatitudes and in the tropics, Mon. Weather Rev., 99, 954-965.

JULIAN, P. R. (1975), Comments on the determination of significance levels of the coherence statistic, J. Atmos. Sci., 32, 836-837.

KANTOR, A. J. and A. E. COLE (1965), Monthly atmospheric structure surface to 80 km, J. Appl. Meteorol., 4, 228-237.

KINGSLEY, S. P., H. G. MULLER, L. NELSON, and A. SCHOLEFIELD (1978), Meteor winds over Sheffield (53°N, 2°W), J. Atmos. Terr. Phys., 40, 917-922.

KNECHT, T. W. (1966) (Ed.), Research in Aeronomy, October 1, 1965 - March 31, 1966, Prog. Rep. 66-1, Aeron. Lab., Dep. Elec. Eng., Univ. Ill., Urbana-Champaign.

LABITZKE, K., K. PETZOLDT, and H. SCHWENTEK (1979), Planetary waves in the strato- and mesosphere during the Western European Winter Anomaly Champaign 1975/76 and their relation to ionospheric absorption, J. Atmos. Terr. Phys., 41, 1149-1162.

MADDEN, R. A. (1979), Observations of large-scale traveling Rossby waves, Rev. Geophys. Space Phys., 17, 1935-1949.

MADDEN, R. A. and P. JULIAN (1972), Further evidence of global-scale, 5-day pressure waves, J. Atmos. Sci., 29, 1464-1469.

MADDEN, R. A. and P. JULIAN (1972), Reply, J. Atmos. Sci., 30, 935-940.

MAEHLUM, B. (1967), On the 'winter anomaly' in the midlatitude D region, J. Geophys. Res., 72, 2287-2299.

MANSON, A. H. (1971), The concentration and transport of minor constituents in the mesosphere and lower thermosphere (70 - 110 km) during periods of anomalous absorption, J. Atmos. Terr. Phys., 33, 715-721.

MANSON, A. H. (1976), Stratospheric-ionospheric-magnetospheric coupling at midlatitudes in the southern hemisphere, 1969-1974, J. Atmos. Terr. Phys., 38, 1017-1020.

MANSON, A. H., J. B. GREGORY and C. E. MEEK (1981), Atmospheric waves (10 min - 30 days) in the mesosphere and thermosphere at Saskatoon (52 N, 107 W), October 1978 - September 1979, Planet. Space Sci., 6, 615-625.

MANSON, A. H., J. B. GREGORY, C. E. MEEK and D. G. STEPHENSON (1978), Winds and wave motions to 110 km at midlatitudes. V. An analysis of data from September 1974 - April 1975, J. Atmos. Sci., 35, 592-599.

MATHEWS, J. D., J. H. SHAPIRO and B. S. TANENBAUM (1973), Evidence for distributed scattering in D region partial-reflection processes, J. Geophys. Res., 78, 8266-8275.

MEEK, C. E. (1981), An efficient method for analysing ionospheric drifts, J. Atmos. Terr. Phys., 42, 835-839.

MEEK, C. E. and A. H. MANSON (1978), Comparisons between time variations in D-region winds and electron densities at Saskatoon, Canada (52 N, 106 W), J. Atmos. Terr. Phys., 40, 1267-1274.

MEEK, C. E., A. H. MANSON and J. B. GREGORY (1979), Internal consistence analysis for partial and total reflection drifts data, J. Atmos. Terr.

Phys., 41, 251-258.

MITRA, S. N. (1949), A radio method of measuring winds in the ionosphere, Proc. Instn. Elec. Engrs. III, 96, 441-446.

NEWMAN, D. B. (1974), Differential phase volume model and amplitude measurements of partial reflections, Penn. State Rep. 426, Ionospheric Res. Lab., Penn. State Univ., University Park, Penn.

OFFERMAN, D., P. CURTIN, J. M. CISNEROS, J. SATRUSTEGUI, H. LAUCHE, G. ROSE, and K. PETZOLDT (1979), Atmospheric temperature structure during the Western European Winter Anomaly Campaign 1975/76, J. Atmos. Terr. Phys., 41, 1051-1062.

OGAWA, T. and Y. KONDO (1977), Diurnal variability of thermospheric N and NO, Planet. Space Sci., 25, 735-742.

PANOFSKY, H. A. and G. W. BRIER (1958), Some applications of statistics to meteorology, The Pennsylvania State University Press, University Park.

PFISTER, W. (1971), The wave-like nature of inhomogeneities in the E-region, J. Atmos. Terr. Phys., 33, 999-1025.

PHELPS, A. V. and J. L. PACK (1959), Electron collision frequencies in nitrogen and in the lower ionosphere, Phys. Rev. Lett., 3, 340-342.

PIRNAT, C. R. and S. A. BOWHILL (1968), Electron densities in the lower ionospherge deduced from partial reflection measurements, Aeron. Rep. No. 29, Aeron. Lab., Dep. Elec. Eng., Univ. Ill., Urbana-Champaign.

PITTEWAY, M. L. V., J. W. WRIGHT and L. S. FEDOR (1971), The interpretation of ionospheric radio drift measurements - III. Validation of correlation analysis by computer simulation, J. Atmos. Terr. Phys., 33, 635-660.

REES, D., A. F. D. SCOTT, J. M. CISNEROS, J. M. SATRUSTEGUI, H. WIDDEL and G. ROSE (1979), Relationships between the local dynamical structure of the atmosphere and ionospheric absorption during the Western European

Winter Anomaly Campaign 1975/76, J. Atmos. Terr. Phys., 41, 1063-1074.

RODGERS, C. D. (1976), Evidence for the five-day wave in the upper stratosphere, J. Atmos. Sci., 33, 710-711.

ROSE, G. and H. WIDDEL (1977), An experimental contribution to the question of transient couplings of tropospheric planetary pressure waves and changes in the short wave radio wave absorption in the D-region of the ionosphere, J. Atmos. Terr. Phys., 39, 51-56.

SALBY, M. L. and R. G. ROPER (1980), Long-period oscillations in the meteor region, J. Atmos. Sci., 37, 237-244.

SCHANING, B. (1973), Results of ship-borne ionospheric absorption measurements on the North Atlantic during winter, J. Atmos. Terr. Phys., 35, 1003-1008.

SCHWENTEK, H. (1976), Ionospheric absorption between 53 N and 53 S observed on board ship, J. Atmos. Terr. Phys., 38, 89-92.

SECHRIST, C. F., JR. (1967), A theory of the winter absorption anomaly at middle latitudes, J. Atmos. Terr. Phys., 29, 113-136.

SECHRIST, C. F., JR. (1970), Interpretation of D-region electron densities, Radio Sci., 5, 663-671.

SECHRIST, C. F., JR., E. A. MECHTLY and J. S. SHIRKE (1969), Coordinated rocket measurements on the D-region winter anomaly - I. Experimental results, J. Atmos. Terr. Phys., 31, 145-153.

SEN, H. K. and A. A. WYLLER (1960), On the generalization of the Appleton-Hartree magnetoionic formulas, J. Geophys. Res., 65, 3931-3950.

SPRENGER, K. and R. SCHMINDER (1969), On some relationships between correlation analysis and similar-fade analysis results of drift measurements in the lower ionosphere, J. Atmos. Terr. Phys., 31, 1085-1098.

STROBEL, D. F. (1971), Odd nitrogen in the mesosphere, J. Geophys. Res.,

76, 8384-8393.

STUBBS, T. J. (1973), The measurement of winds in the D-region of the ionosphere by the use of partially reflected radio waves, J. Atmos. Terr. Phys., 35, 909-919.

VAN LOON, H., R. L. JENNE and K. LABITZKE (1973), Zonal harmonic standing waves, J. Geophys. Res., 78, 4463-4471.

VINCENT, R. A. and T. J. STUBBS (1977), A study of motions in the winter mesosphere using the partial reflection drift technique, Planet. Space Sci., 25, 441-455.

VINCENT, R. A., T J. STUBBS, P. H. O. PEARSON, K. H. LLOYD and C. H. LOW (1977), A comparison of partial reflection drifts with winds determined by rocket techniques - I., J. Atmos. Terr. Phys., 39, 813-821.

VON BIEL, H. A. (1971), Determination of D-region electron densities within the scattering region, J. Geophys. Res., 76, 5365-5367.

VOSS, H. D. and L. G. SMITH (1977), Energetic particles and ionization in the nighttime middle and low latitude ionosphere, Aeron. Rep. No. 78, Aeron. Lab., Dep. Elec. Eng., Univ. Ill., Urbana-Champaign.

WEILAND, R. M. and S. A. BOHWILL (1978), D-region differential-phase measurements and ionization variability studies, Aeron. Rep. No. 81, Aeron Lab., Dep. Elec. Eng., Univ. Ill., Urbana-Champaign.

WHITTEN, R. C. and I. G. POPPOFF (1971), Fundamentals of Aeronomy, John Wiley and Sons, New York.

WRATT, D. S. (1974), Atmospheric physics: Electron density variations in the mesosphere, Ph.D. Thesis, Univ. Canterbury, Christchurch, New Zealand.

WRIGHT, J. W. (1972), The interpretation of ionospheric radio drift measurements - V. Demonstration of the point effect in the time-averaged

correlations and drifts calculations, J. Atmos. Terr. Phys., 34, 1365-1378.

WRIGHT, J. W. (1974), The interpretation of ionospheric radio drift measurements - VII. Diffraction methods applied to E-region echo fading: Evidence of a focusing model, J. Atmos. Terr. Phys., 36, 721-740.

ZIMMERMAN, S. P. and R. S. NARCISI (1970), The winter anomaly and related transport phenomena, J. Atmos. Terr. Phys., 32, 1305-1308.